ISSN 0021-9673

VOL. 463 NO. 2 FEBRUARY 3, 1989

THIS ISSUE COMPLETES VOL. 463

JOURNAL OF CHROMATOGRAPHY

INTERNATIONAL JOURNAL ON CHROMATOGRAPHY, ELECTROPHORESIS AND RELATED METHODS

ELSEVIER

JOURNAL OF CHROMATOGRAPHY

Scope. The *Journal of Chromatography* publishes papers on all aspects of chromatography, electrophoresis and related methods. Contributions consist mainly of research papers dealing with chromatographic theory, instrumental development and their applications. The section *Biomedical Applications*, which is under separate editorship, deals with the following aspects: developments in and applications of chromatographic and electrophoretic techniques related to clinical diagnosis or alterations during medical treatment; screening and profiling of body fluids or tissues with special reference to metabolic disorders; results from basic medical research with direct consequences in clinical practice; drug level monitoring and pharmacokinetic studies; clinical toxicology; analytical studies in occupational medicine.

Submission of Papers. Papers in English, French and German may be submitted, in three copies. Manuscripts should be submitted to: The Editor of *Journal of Chromatography*, P.O. Box 681, 1000 AR Amsterdam, The Netherlands, or to: The Editor of *Journal of Chromatography, Biomedical Applications*, P.O. Box 681, 1000 AR Amsterdam, The Netherlands. Review articles are invited or proposed by letter to the Editors. An outline of the proposed review should first be forwarded to the Editors for preliminary discussion prior to preparation. Submission of an article is understood to imply that the article is original and unpublished and is not being considered for publication elsewhere. For copyright regulations, see below.

Subscription Orders. Subscription orders should be sent to: Elsevier Science Publishers B.V., P.O. Box 211, 1000 AE Amsterdam, The Netherlands, Tel. 5803 911, Telex 18582 ESPA NL. The *Journal of Chromatography* and the *Biomedical Applications* section can be subscribed to separately.

Publication. The *Journal of Chromatography* (incl. *Biomedical Applications*) has 37 volumes in 1989. The subscription prices for 1989 are:

J. Chromatogr. + *Biomed. Appl.* (Vols. 461–497):
Dfl. 6475.00 plus Dfl. 999.00 (p.p.h.) (total *ca.* US$ 3933.75)

J. Chromatogr. only (Vols. 461–486):
Dfl. 5200.00 plus Dfl. 702.00 (p.p.h.) (total *ca.* US$ 3106.25)

Biomed. Appl. only (Vols. 487–497):
Dfl. 2200.00 plus Dfl. 297.00 (p.p.h.) (total *ca.* US$ 1314.25).

Our p.p.h. (postage, package and handling) charge includes surface delivery of all issues, except to subscribers in Argentina, Australia, Brasil, Canada, China, Hong Kong, India, Israel, Malaysia, Mexico, New Zealand, Pakistan, Singapore, South Africa, South Korea, Taiwan, Thailand and the U.S.A. who receive all issues by air delivery (S.A.L. — Surface Air Lifted) at no extra cost. For Japan, air delivery requires 50% additional charge; for all other countries airmail and S.A.L. charges are available upon request. Back volumes of the *Journal of Chromatography* (Vols. 1–460)are available at Dfl. 230.00 (plus postage). Claims for missing issues will be honoured, free of charge, within three months after publication of the issue. Customers in the U.S.A. and Canada wishing information on this and other Elsevier journals, please contact Journal Information Center, Elsevier Science Publishing Co. Inc., 655 Avenue of the Americas, New York, NY 10010. Tel. (212) 989-5800.

Abstracts/Contents Lists published in Analytical Abstracts, ASCA, Biochemical Abstracts, Biological Abstracts, Chemical Abstracts, Chemical Titles, Chromatography Abstracts, Current Contents/Physical, Chemical & Earth Sciences, Current Contents/Life Sciences, Deep-Sea Research/Part B: Oceanographic Literature Review, Excerpta Medica, Index Medicus, Mass Spectrometry Bulletin, PASCAL-CNRS, Referativnyi Zhurnal and Science Citation Index.

See inside back cover for Publication Schedule, Information for Authors and information on Advertisements.

0021-9673/89/$03.50

Printed in The Netherlands

CONTENTS

(Abstracts/Contents Lists published in Analytical Abstracts, ASCA, Biochemical Abstracts, Biological Abstracts, Chemical Abstracts, Chemical Titles, Chromatography Abstracts, Current Contents/Physical, Chemical & Earth Sciences, Current Contents/Life Sciences, Deep Sea Research/Part B: Oceanographic Literature Review, Excerpta Medica, Index Medicus, Mass Spectrometry Bulletin, PASCAL-CNRS, Referativnyi Zhurnal and Science Citation Index)

(Continued overleaf)

In articles with more than one author, the name of the author to whom correspondence should be addressed is indicated in the article heading by a 6-pointed asterisk (*)

Here's the solution to ten common HPLC problems

1. Eliminate the nuisance and expense of continuous sparging. This gradient programmer degasses the mobile phase as it's blended.

2. The single-piston pump requires less maintenance, primes easily, and doesn't lose its prime if a bubble enters the inlet.

3. Programmable flow control cuts separation and equilibration times, saves solvents, and keeps the pump from running dry.

4. Available inert construction is biocompatible and impervious to buffers.

5. Self-diagnostics in the pump and gradient programmer speed maintenance and cut downtime.

6. You probably won't need an auxiliary detector for special jobs. This variable gives great results even on carbohydrates at 190-200 nm and other samples such as metalloproteins at up to 750 nm. Slip-in flow cells adapt it for microbore LC, prep LC, and SFC.

7. Typical deuterium lamp life of over 10,000 hours can give you substantial savings in lamp replacement cost.

8. You don't have to be a computer enthusiast to quickly master the optional data management software.

9. Comprehensive manuals include complete operation, instrument theory, and troubleshooting sections with circuit diagrams.

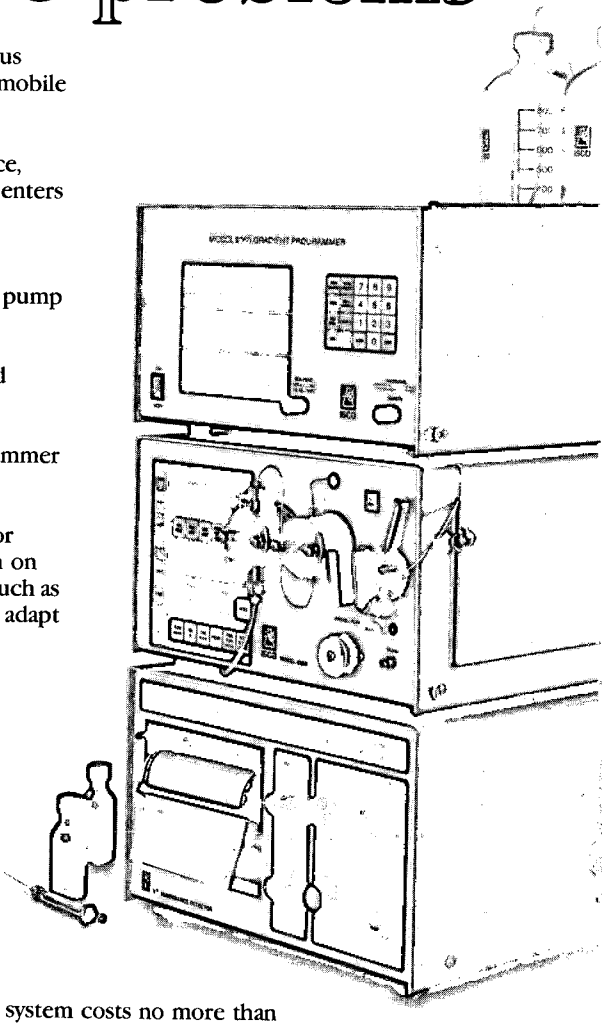

10. The price is very affordable. A complete gradient system costs no more than many competing systems lacking these features.

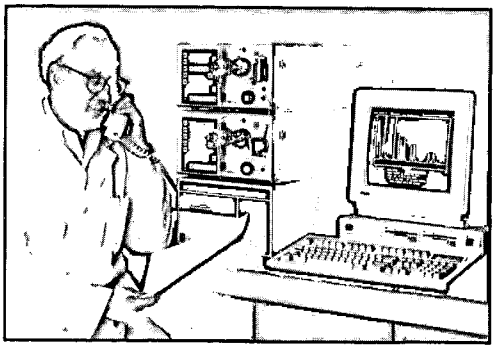

For more solutions, contact your distributor listed below for a free Isco catalog.

Isco, Inc.
4700 Superior
Lincoln, NE 68504
USA

ISCO

Totally automated HPLC .....Hands off chromatography

Robust chromatography for analytes in "real world" samples, and no operator intervention! ASTED®, a new robotic system developed by Gilson, uses dialysis and trace enrichment. ASTED automates sample pretreatment, permitting chromatographic analysis of virtually any sample type.

ASTED mixes raw sample with standards and reagents, separates low molecular weight analytes from biological or industrial matrices, then injects into the analytical column. The system is on-line, requires no guard column and ensures a long lifetime for the column. Cycle time is typically 5 minutes, with one sample being prepared while the previous one elutes.

Compatibility? ASTED is compatible with most HPLC systems, with practically any existing HPLC method, with most data processors. No need to change your protocol or modify your system.

Flexibility? ASTED offers prechromatographic chemistry, dialysis, trace enrichment, and injection, as combined or separate functions for method development.

Savings? With low running costs and high sample throughput, ASTED is highly competitive for quantitative or fingerprint routines.

Validation? ASTED has been fully validated for various applications: amino acids and metabolites in biological fluids; total theophylline and xanthines, anticonvulsant drugs, cortisol and glucocorticoids in plasma or serum; free catecholamines in urine. Other applications are being developed in food quality control, pharmaceuticals, environmental analysis.

For more information about ASTED, please contact your nearest Gilson representative.

Selected references:
D.C. Turnell and J.D.H. Cooper, J. Chromatogr., 395 (1987) 613-621.
J.D.H. Cooper, D.C. Turnell, B. Green and F. Vérillon, J. Chromatogr., 456 (1988) 53-69.

ASTED® (Automated Sequential Trace Enrichment of Dialysates)
Original Patent : U.K. 2 124 370 and Registered Trademark of Coventry Health Authority, U.K.

Journal of Chromatography, 463 (1989) 235–242
Elsevier Science Publishers B.V., Amsterdam — Printed in The Netherlands

CHROM. 21 061

OPTIMIZATION OF BASIC PARAMETERS IN TEMPERATURE-PROGRAMMED GAS CHROMATOGRAPHIC SEPARATIONS OF MULTI-COMPONENT SAMPLES WITHIN A GIVEN TIME

D. REPKA, J. KRUPČÍK and A. BRUNOVSKÁ

Slovak Technical University, Faculty of Chemistry, Department of Analytical Chemistry, Radlinského 9, 812 37 Bratislava (Czechoslovakia)

and

P. A. LECLERCQ and J. A. RIJKS*

Eindhoven University of Technology, Department of Chemical Engineering, Laboratory of Instrumental Analysis, P.O. Box 513, 5600 MB Eindhoven (The Netherlands)

(First received June 27th, 1988; revised manuscript received October 18th, 1988)

SUMMARY

A new procedure is introduced for the optimization of column peak capacity in a given time. The optimization focuses on temperature-programmed operating conditions, notably the initial temperature and hold time, and the programming rate. Based conceptually upon Lagrange functions, experiments were carried out along simplex sequential and central composite design procedures. The validity of the theory was demonstrated by separations of some crude oil distillation fractions.

INTRODUCTION

The separation of complex mixtures in capillary gas chromatography (GC) can be improved by the optimization of a combination of column selectivity and/or efficiency and/or analysis time. The approach to this optimization will greatly depend upon the number of components present in the sample, and upon the differences in polarity and volatility of the sample constituents.

Optimization of the column temperature in isothermal and temperature-programmed operation has been studied by many authors[1–15]. Simplex sequential methods have been applied for the optimization of the initial temperature and temperature gradient[5–8]. A different approach, called "experimental design", was used for the optimization of the temperature gradient and carrier gas velocity[9,10]. In some recent publications, isothermal retention data were used for the optimization of multi-ramp temperature-programmed GC separations[11–15]. Recently, reports appeared on selectivity optimization in isothermal capillary GC, by tuning the column temperature(s) in series-coupled capillary columns in single- or dual-oven GC systems[16,17]. In all of these studies, optimization of the initial isothermal hold time was not included.

0021-9673/89/$03.50

In this paper the optimization of the peak capacity in temperature-programmed capillary GC in a given time is discussed. This optimization is performed by tuning the initial temperature and hold time, as well as the programming rate in a single-oven GC instrument. The theory is outlined, and its applicability is demonstrated by separations of aliphatic and aromatic crude oil distillation fractions.

THEORETICAL

Optimization criteria

For the exploitation of statistical optimization methods in chromatography, proper criteria are required. Unfortunately, all criteria dealt with up till now[18,19] fail whenever the number of peaks in the chromatogram is not constant during optimization.

For multi-component samples, with more than a few hundred components, optimization of the peak capacity according to Grushka[20] can give a significant improvement of the separation. The peak capacity (PC) can be calculated in isothermal as well as temperature-programmed separations[21] from

$$\mathrm{PC} = 1.18 \sum_{i=m}^{n-1} (\mathrm{TZ}_i + 1) \tag{1}$$

where TZ_i is the "Trennzahl" or separation number[21] for the ith pair of adjacent n-alkanes, and m and n are the lowest and highest carbon numbers, respectively, of the n-alkanes in the range considered.

The position of any peak in temperature-programmed GC will depend upon the initial temperature, T_0, and hold time, t_0, and the programming rate, r. Therefore, optimization of the peak capacity within a given time can be realized by simultaneous tuning of these parameters.

Fundamental approach

A Lagrange function, F (ref. 22), was used for the optimization, so that a time constraint can be included

$$\mathrm{F} = \mathrm{PC} - \lambda(t_{\mathrm{R},n} - t_{\mathrm{R},n,\max}) \tag{2}$$

where λ = Lagrange multiplier, $t_{\mathrm{R},n}$ = retention time of the last eluting n-alkane of interest and $t_{\mathrm{R},n,\max}$ = the required or maximum analysis time.

Because both PC and $t_{\mathrm{R},n}$ are functions of T_0, t_0 and r, the Lagrange function $\mathrm{F} = \mathrm{F}(T_0, t_0, r, \lambda, t_{\mathrm{R},n,\max})$. For optimum separation conditions (maximum PC in a given analysis time), F should be maximized. Hence, the partial derivatives of F should be equal to zero:

$$\partial \mathrm{F}(T_0, t_0, r, \lambda)/\partial T_0 = 0 \tag{3a}$$

$$\partial \mathrm{F}(T_0, t_0, r, \lambda)/\partial t_0 = 0 \tag{3b}$$

$$\partial \mathrm{F}(T_0, t_0, r, \lambda)/\partial r = 0 \tag{3c}$$

$$\partial \mathrm{F}(T_0, t_0, r, \lambda)/\partial \lambda = 0 \tag{3d}$$

EXPERIMENTAL

A 4180 gas chromatograph (Carlo Erba, Milan, Italy) with a Grob-type cold on-column injection port and flame ionization detection (FID) was used. The oven temperature was controlled by a temperature programmer LT 410 (Carlo Erba). Retention times and half height peak widths were measured by a computing integrator C-R3A (Shimadzu, Kyoto, Japan).

The capillary column was made of soft soda-lime glass (91 m × 0.3 mm I.D.). The inner wall of the column was etched with gaseous hydrogen chloride at 330°C during 24 h. The stationary phase was coated statically, using a 1% solution of SE-30 in dichloromethane. Hydrogen was used as the carrier gas at constant inlet pressure; the linear gas velocity was 25 cm/s at 80°C. All calculations were performed on an HP-85B microcomputer connected to a HP 9121 disc drive. A matrix ROM, advanced programming ROM and printer/plotter ROM were used additionally (all from Hewlett-Packard, Palo Alto, CA, U.S.A.).

A model mixture was prepared by mixing C_8–C_{14} *n*-alkanes in dichloromethane (10 ng/μl per component). A sample of light petroleum was dissolved in dichloromethane (1 μg/μl). Aromatic hydrocarbons were isolated from the light petroleum by column liquid chromatography on silica, and successively diluted in dichloromethane (1 μg/μl)[23].

In all cases 1 μl was injected into the column.

RESULTS AND DISCUSSION

Assuming a time constraint of 120 min ($= t_{R,n,max}$), a simplex sequential approach was selected for the optimization of the peak capacity for a crude oil distillation fraction, ranging from *n*-octane (*n*-C_8) to *n*-tetradecane (*n*-C_{14}). The range of parameter values to be optimized was chosen between 40 and 230°C for the initial temperature, T_0, 0–120 min for the initial hold time, t_0, and 0–20°C /min for the programming rate, r. The corresponding interval steps were 1°C, 1 min and 0.1°C/min, respectively.

The results of this approach are summarized in Table I, where peak capacities calculated from eqn. 1 and measured tetradecane retention times are given for the operating conditions resulting from the simplex procedure. In cases where the time constraint was not met, no retention times or peak capacities for *n*-C_{14} are given. Obviously, the region of maximum peak capacity within a maximum acceptable retention time is reached at experiment 28.

The dependence of the column peak capacity (PC) and the analysis time, $t_{R,n}$, upon the initial temperature, the time of the initial isothermal temperature and the temperature gradient is described by the following set of quadratic equations[22]:

$$PC = a_0 + a_1T_0 + a_2r + a_3t_0 + a_{1,1}T_0^2 + a_{2,2}r^2 + a_{3,3}t_0^2 + a_{1,2}T_0r + a_{1,3}T_0t_0 + a_{2,3}rt_0 \quad (4)$$

$$t_{R,n} = b_0 + b_1T_0 + b_2r + b_3t_0 + b_{1,1}T_0^2 + b_{2,2}r^2 + b_{3,3}t_0^2 + b_{1,2}T_0r + b_{1,3}T_0t_0 + b_{2,3}rt_0 \quad (5)$$

TABLE I

EXPERIMENTAL CONDITIONS AND RESULTS IN THE COURSE OF THE SIMPLEX SEQUENTIAL OPTIMIZATION

Exp. No.	T_0 (°C)	r (°C/min)	t_0 (min)	*PC*	$t_{R,n}$ (min)
1	80	3.0	10	232	52.9
2	90	3.0	10	217	49.6
3	80	5.0	10	198	41.4
4	80	3.0	20	251	62.8
5	87	1.0	17	286	97.0
6	92	0.1	22	–	–
7	74	1.7	21	289	86.3
8	63	0.7	30	–	–
9	81	0.8	29	–	–
10	80	2.2	16	260	68.3
11	81	0.3	16	–	–
12	80	2.0	19	272	74.5
13	81	0.9	21	300	112.9
14	81	0.1	25	–	–
15	81	0.3	21	–	–
16	80	1.4	19	281	88.2
17	81	0.9	20	308	111.9
18	81	0.5	20	–	–
19	71	1.3	25	307	105.2
20	80	0.5	23	–	–
21	76	1.2	22	306	107.6
22	71	1.4	23	300	99.4
23	77	1.1	22	308	106.5
24	76	1.0	23	311	113.9
25	75	0.8	23	–	–
26	85	0.7	18	312	120.0
27	96	0.2	13	–	–
28	78	0.9	22	323	117.4
29	77	0.9	23	318	119.3
30	83	0.6	20	–	–
31	79	0.9	21	306	115.3

The coefficients of these equations were calculated by multiple linear regression analysis. The experimental conditions for this approach, which are given in Table II, were selected by a central composite design around the optimum found by the simplex procedure[22].

Differences in peak capacity under similar experimental conditions, for instance experiment 28 in Table I and experiment 9 in Table II, are not only caused by random variations in experimental conditions, *e.g.*, column temperatures or temperature programs, etc. or measurements (peak widths, etc.), but also by column ageing. (The data from Table II were acquired several months after collecting the data in Table I.) The reliability of the PC values in both tables corresponds to a standard deviation of about four units. However, the PC values in Table II are systematically lower than those in Table I.

TABLE II

EXPERIMENTAL CONDITIONS AND RESULTS OF THE CENTRAL COMPOSITE DESIGN AROUND THE OPTIMUM DERIVED BY THE SIMPLEX STRATEGY

Exp. No.	T_0 (°C)	r (°C/min)	t_0 (min)	*PC*	$t_{R,n}$ (min)
1	74	0.6	18	342	136.1
2	82	0.6	18	319	135.6
3	74	1.1	18	308	105.3
4	82	1.1	18	302	98.0
5	74	0.6	26	349	157.4
6	82	0.6	26	319	143.0
7	74	1.1	26	320	113.3
3	82	1.1	26	313	105.8
9	78	0.9	22	307	116.8
10	83	0.9	22	305	111.3
11	73	0.9	22	324	122.5
12	78	1.2	22	302	100.7
13	78	0.6	22	324	145.4
14	78	0.9	27	314	121.0
15	78	0.9	17	318	112.1

Requiring an analysis time of 120 min, the Lagrande function, eqn. 2, can be expressed as

$$F = a_0 + a_1T_0 + a_2r + a_3t_0 + a_{1,1}T_0^2 + a_{2,2}r^2 + a_{3,3}t_0^2 + a_{1,2}T_0r + \\ + a_{1,3}T_0t_0 + a_{2,3}rt_0 - \lambda(b_0 + b_1T_0 + b_2r + b_3t_0 + b_{1,1}T_0^2 + \\ + b_{2,2}r^2 + b_{3,3}t_0^2 + b_{1,2}T_0r + b_{1,3}T_0t_0 + b_{2,3}rt_0 - 120) \quad (6)$$

where use was made of eqns. 4 and 5. It also follows from eqns. 3, that the parameters T_0, t_0, r and λ, corresponding to the maximum value of the column peak capacity in an analysis time of 120 min must be fitted by the following equations:

$$\partial F/\partial T_0 = a_1 + 2a_{1,1}T_0 + a_{1,2}r + a_{1,3}t_0 - \lambda(b_1 + 2b_{1,1}T_0 + \\ + b_{1,2}r + b_{1,3}t_0) = 0 \quad (7a)$$

$$\partial F/\partial t_0 = a_3 + 2a_{3,3}t_0 + a_{1,3}T_0 + a_{2,3}r - \lambda(b_3 + 2b_{3,3}t_0 + \\ + b_{1,3}T_0 + b_{2,3}r) = 0 \quad (7b)$$

$$\partial F/\partial r = a_2 + 2a_{2,2}r + a_{1,2}T_0 + a_{2,3}t_0 - \lambda(b_2 + 2b_{2,2}r + \\ + b_{1,2}T_0 + b_{2,3}t_0) = 0 \quad (7c)$$

$$\partial F/\partial\lambda = -(b_0 + b_1T_0 + b_2r + b_3t_0 + b_{1,1}T_0^2 + b_{2,2}r^2 + b_{3,3}t_0^2 + b_{1,2}T_0r + b_{1,3}T_0t_0 + b_{2,3}rt_0 - 120) = 0 \quad (7d)$$

Substituting the a and b coefficients as computed before, these non-linear equations were solved numerically by a Newton method[24]. Due to random experimental errors, causing noisy response surfaces for the optimum operating conditions and the calculated peak capacity, more than one solution can be obtained by this numerical approach. In this particular case, two optima were observed, corresponding to the optimum parameters as shown in Table III. The peak capacities in Table III were calculated with eqn. 4.

TABLE III

MAXIMUM PEAK CAPACITIES AND THE CORRESPONDING OPTIMUM EXPERIMENTAL PARAMETERS FOR A REQUIRED ANALYSIS TIME OF 120 min

Determined by solving the Lagrange function.

PC	T_0 (°C)	t_0 (min)	r (°C/min)	λ
306	81.7	22.3	0.82	0.332
316	71.9	14.5	2.05	0.549

The optimized separation of a crude oil distillation fraction is shown in Fig. 1. The first set of optimum conditions in Table III was used. The retention time of tetradecane, $t_{R,n}$= 119.7 min, matches the required analysis time very well.

A chromatogram under identical conditions of the aromatic fraction of this sample, after removal of the saturated hydrocarbons by liquid–solid chromatography

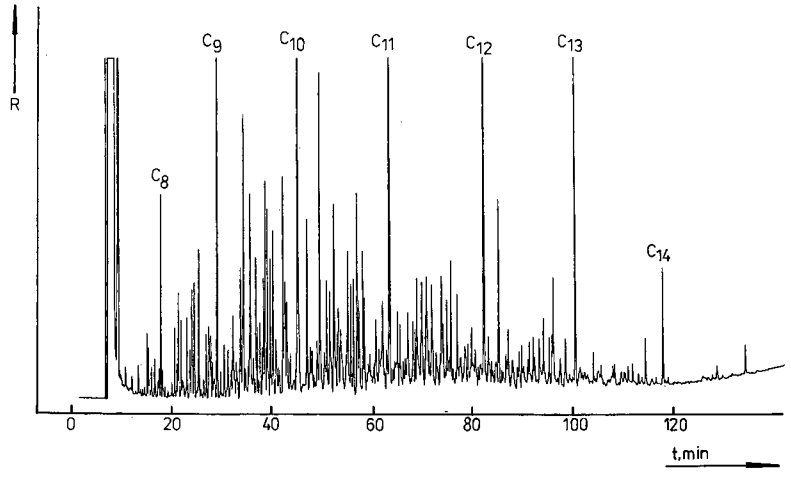

Fig. 1. Chromatogram of a crude oil distillation fraction at optimum temperature-programmed operating conditions. Time constraint 120 min.

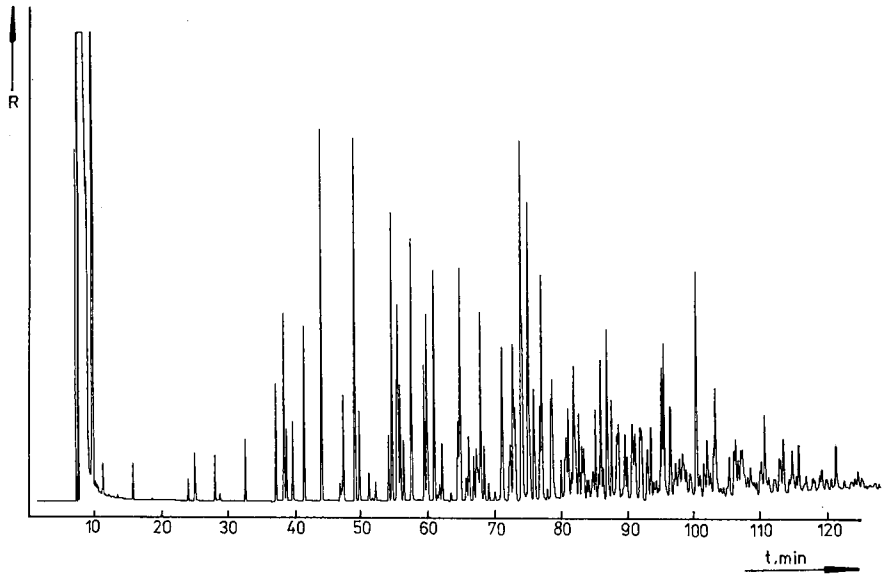

Fig. 2. Chromatogram of the aromatic fraction of the crude oil distillation fraction of Fig. 1.

(*cf.*, Experimental), is given in Fig. 2. Obviously, the number of peaks in the sample considerably exceeds the maximum peak capacity. When the saturated alkanes are removed off-line, prior to GC separation, the approach would be expected to be more efficient, if the optimization had been tuned to the range *n*-C_9 through *n*-C_{14}. With the latter sample much better results are expected with a more selective stationary phase for aromatics with the same procedure.

CONCLUSIONS

Simplex optimization of the peak capacity within a given analysis time can be used for a first approximation. Fine tuning by a (14-point) central composite design around this optimum yields the conditions for (at least 10) experiments, needed to compute the 20 coefficients of the Lagrange function used. After insertion of the required analysis time, this function can then be solved numerically to yield the experimental conditions leading to the maximum peak capacity in the given time. From the experimental results of this particular study, it is not evident that the Lagrange method yields better results than the simplex method. Whether it is necessary to apply a simplex procedure prior to a central composite design is a subject of further investigation.

REFERENCES

1 D. W. Grant and M. G. Hollis, *J. Chromatogr.*, 158 (1978) 3.
2 L. A. Jones, S. L. Kirby, C. L. Garganta, T. M. Gerig and J. D. Mulik, *Anal. Chem.*, 55 (1983) 1354.
3 N. W. Davies, *Anal. Chem.*, 56 (1984) 2600.
4 E. M. Sibley, C. Eon and B. L. Karger, *J. Chromatogr. Sci.*, 11 (1973) 309.

5 J. Holderith, T. Toth and A. Váradi, *Magy. Kem. Foly.*, 81 (1975) 162.
6 J. Holderith, T. Tóth and A. Váradi, *J. Chromatogr.*, 119 (1976) 215.
7 M. Šingliar and L. Koudelka, *Chem. Prum.*, 29 (1979) 134.
8 F. H. Walters and S. N. Deming, *Anal. Lett.*, 17 (1984) 2197.
9 J. P. Zajcev and V. A. Zazhigalov, *Tezisy Dokl. Ukr. Resp. Kont. Fiz. Khim.*, 12 (1977) 175; *C.A.*, 92 (1978) 208 545 p.
10 W. Witkowski and J. Lüthe, *Chem. Technol.*, 35 (1983) 419.
11 V. Bártů and S. Wičar, *Anal. Chim. Acta*, 150 (1983) 245.
12 V. Bártů, S. Wičar, G.-J. Scherpenzeel and P. A. Leclercq, *J. Chromatogr.*, 370 (1986) 219.
13 V. Bártů, S. Wičar, G.-J. Scherpenzeel and P. A. Leclercq, *J. Chromatogr.*, 370 (1986) 235.
14 Lu Peichang, Lin Bingcheng, Chu Xinhua, Luo Chunrog, Lai Guangda and Li Haochun, *J. High Resolut. Chromatogr. Chromatogr. Commun.*, 9 (1986) 702.
15 H.-J. Stan and B. Steinbach, *J. Chromatogr.*, 290 (1984) 311.
16 J. Krupčík, J. Garaj, P. Čellar and G. Guiochon, *J. Chromatogr.*, 312 (1984) 1.
17 D. Repka, J. Krupčík, E. Benická, P. A. Leclercq and J. A. Rijks, *J. Chromatogr.*, 463 (1989) 243.
18 H. J. G. Debets, B. L. Bajema and D. A. Doornbos, *Anal. Chim. Acta*, 151 (1983) 131.
19 P. J. Schoenmakers, *Optimization of Chromatographic Selectivity*, Elsevier, Amsterdam, 1986.
20 E. Grushka, *Anal. Chem.*, 42 (1970) 1142.
21 J. Krupčík, J. Garaj, G. Guiochon and J. M. Schmitter, *Chromatographia*, 14 (1981) 501.
22 G. S. G. Beveridge and R. S. Schetter, *Optimization, Theory and Practice*, McGraw-Hill, New York, 1970.
23 Z. Hricová-Nayová, *Graduation thesis*, Technical University of Bratislava, Bratislava, 1984.
24 M. Kubíček, *Numerical Algorithms for Solving Chemical Engineering Problems* (in Czech), State Publishing Company of Technical Literature/ALFA, Prague, 1983.

Journal of Chromatography, 463 (1989) 243–251
Elsevier Science Publishers B.V., Amsterdam — Printed in The Netherlands

CHROM. 21 064

OPTIMIZATION OF SELECTIVITY BY TUNING COLUMN TEMPERATURES FOR SERIES-COUPLED CAPILLARY COLUMNS IN DUAL-OVEN GAS CHROMATOGRAPHIC SYSTEMS

D. REPKA, J. KRUPČÍK and E. BENICKÁ

Slovak Technical University, Faculty of Chemistry, Department of Analytical Chemistry, Radlinského 9, 812 37 Bratislava (Czechoslovakia)

and

P. A. LECLERCQ and J. A. RIJKS*

Eindhoven University of Technology, Department of Chemical Engineering, Laboratory of Instrumental Analysis, P.O. Box 513, 5600 MB Eindhoven (The Netherlands)

(First received June 27th, 1988; revised manuscript received October 24th, 1988)

SUMMARY

A method has been developed and evaluated for optimization of the selectivity of series-coupled capillary columns in a twin-oven gas chromatographic system in the shortest possible analysis time. The temperatures of either one or both columns were varied independently (partial optimization) or simultaneously (overall optimization), in order to separate the maximum number of sample components. The method is based upon computer-aided calculation of Kováts indices of the coupled columns by means of second and third order (polynomial)functions of the temperatures of the individual columns. The applicability and limitations of the method are discussed and illustrated with the separations of a synthetic hydrocarbon mixture of 33 components.

INTRODUCTION

Although high resolution gas chromatography (GC) is the method of choice for the separation of complex mixtures, the frequency of peak overlap is appreciable. There is increasing interest in the development of mathematical models and methods that do allow the prediction of the probable number of peaks that can maximally be distinguished in a given range of a chromatogram.

Obviously it would be highly desirable to reach the ultimate aim of capillary GC separation: maximum resolution and separation efficiency within the shortest time. Unfortunately, general optimization procedures aiming at these goals are rather complex, tedious and time consuming, particularly for complex samples. Therefore, in most optimization procedures only a limited number of these variables is included. In daily laboratory practice, the optimization of the separation temperature is an attractive and simple approach for tuning of columns with an appropriate selectivity and efficiency in isothermal GC. The column temperature has an effect on both efficiency and selectivity, as well as on solute retention. The effect of temperature on

0021-9673/89/$03.50

selectivity is significant, particularly for polar phases and compounds. Therefore, the selectivity can be tuned by temperature control of series-coupled non-polar and polar capillary columns, whether they are coupled in a single[1–3] or a dual-oven GC system[1,4,5].

The algorithms for temperature optimization of single and series-coupled columns in a one-oven GC system are fundamentally similar. Recently introduced procedures[6–8] for the optimization of the selectivity by selection of the best column temperature can be applied to both single as well as for series-coupled columns in a one-oven system. While these procedures are based upon Kováts retention indices, obviously literature data can be used for this purpose.

For selectivity tuning with series-coupled columns in different GC ovens, so far no procedures are available, although the potential of this approach has been recognized[2–5]. In this paper, a computer-aided method is introduced for the optimization of the selectivity of series-coupled columns in a twin-oven GC instrument. This method is based on tuning the temperatures of the individual columns with the aim to separate the maximum number of solutes in the shortest possible time.

THEORETICAL

As was previously shown[7], the optimization of the column temperature for series-coupled columns in a single-oven system appears rather simple. This procedure is based upon Kováts retention indices, I, which are considered[9] to depend linearly on column temperature, T.

$$I_{i,T} = A_i + B_i T \tag{1}$$

where A_i and B_i are constants and i is the solute under investigation.

For the difference in retention indices, $\delta I_{j,i}$, between two adjacent peaks j and i, it follows from eqn. 1:

$$\delta I_{j,i} = A_j - A_i + (B_j - B_i)T \tag{2}$$

This difference is related to the resolution, $R_{j,i}$, according to[7]

$$\delta I_{j,i} = \frac{400\ R_{j,i}}{\sqrt{N_j} \cdot \ln \alpha} \tag{3}$$

where N_j is the effective plate number for peak j, and α the relative retention of two consecutive n-alkanes.

The number of peaks, m, that can be distinguished in the range of interest in the chromatogram is the main criterion for optimization. Whether peaks are considered separated depends on a minimum difference in Kováts indices, $\delta_{\min} = \delta I_{j,i,\min}$, compatible with the required (desired) resolution. The column temperature (one-oven system) or combination of column temperatures (twin-oven system), corresponding to the maximum number of peaks, $m_{\max}$, is considered optimal. If more than one (partial) optimum is observed, the one corresponding to the shortest retention time is considered to be the best choice. As expected, and according to recently published

papers[2,4,5,10], the temperature dependence of Kováts retention indices of series-coupled columns in a twin-oven GC system is not linear. The separation of a given sample can be optimized, in the sense described above, by trial-and-error or simplex sequential methods. However, many experiments are needed. Therefore, and for reasons of efficiency, suitable polynomial equations with empirically determined constants were selected, in order to calculate overall retention indices of the series-coupled columns at any temperature or combination of temperatures of the individual columns. These polynomials can be used to predict the number of peaks in a defined region of the temperature ranges of the individual columns.

EXPERIMENTAL

Instrumentation

The GC system with two independently controlled ovens consisted of two instruments, a Fractovap 2350 and a Fractovap 4180 respectively (Carlo Erba Instrumentazione, Milan, Italy). They were interfaced using a separately heated stainless-steel tube (150 mm × 1.5 mm I.D., wall thickness 0.3 mm), inserted in a glass tube (120 mm × 2.5 mm I.D., wall thickness 1.0). The column inlet of the first column (column A, placed in the Fractovap 2350 gas chromatograph) was connected to an all-glass inlet stream splitter injection port. The outlet of column A was led through the interface to the Fractovap 4180 gas chromatograph, where it was coupled to the inlet of column B using PTFE shrinkable tubing. The outlet of column B was inserted into the jet of the Fractovap 4180 flame ionization detector. The detector signal was fed to an electrometer model EL 480 (Carlo Erba), and recorded by a computing integrator Chromatopac C-R3A (Shimadzu, Kyoto, Japan). Nitrogen was used as the carrier gas with a constant inlet pressure of 170 kPa (absolute).

The inlet splitter was operated with a splitting ratio of 1:100. A sample of hydrocarbons (see Table I) was diluted in acetone to 0.2% (w/w) per compound. A 1-μl volume of the diluted sample was injected. The gas hold-up time was measured by injecting methane.

Curve fitting and optimization calculations were performed on an HP 85B microcomputer (Hewlett-Packard, Palo Alto, CA, U.S.A.). The facilities of the BASIC language were enlarged using a Matrix ROM, an Advanced Programming ROM and a Printer/Plotter ROM (all from Hewlett-Packard).

Columns

Two glass capillary columns were used, both made of soda lime glass (Unihost, Teplice, Czechoslovakia). The inner glass surface was etched with gaseous hydrogen chloride at 330°C during 24 h, prior to coating. Column A (40 m × 0.3 mm I.D.) was statically coated with a 0.2% solution of SE-30 in dichloromethane. Column B (50 m × 0.3 mm I.D.) was coated dynamically with a 5% solution of Carbowax 20M in dichloromethane, using a mercury plug forced by compressed nitrogen.

RESULTS AND DISCUSSION

Generally there are three modes for the optimization of the selectivity of double-oven tandem capillary GC columns by variation of the column temperatures of

TABLE I

COMPOSITION OF THE HYDROCARBON MIXTURE USED

Peak No.	*Name*
1	2,3,4-Trimethylpentane
2	2,2,5-Trimethylhexane
3	*n*-Octane
4	2,3,5-Trimethylhexane
5	2,4-Dimethylheptane
6	4,4-Dimethylheptane
7	3,5-Dimethylheptane (α,β)
8	3,3-Dimethylheptane
9	2,3-Dimethylheptane
10	3,4-Dimethylheptane (α)
11	3,4-Dimethylheptane (β)
12	3,3-Diethylpentane
13	Isopropylbenzene
14	*n*-Nonane
15	4,4-Dimethyloctane
16	*n*-Propylbenzene
17	2,6-Dimethyloctane
18	3,3-Dimethyloctane
19	3,4-Diethylhexane
20	2-Methyl-3-ethylpentane
21	1,3,5-Trimethylbenzene
22	1,2,4-Trimethylbenzene
23	*tert.*-Butylcyclohexane
24	1,2,3-Trimethylbenzene
25	*n*-Decane
26	*sec.*-Butylcyclohexane
27	1,3-Diethylbenzene
28	*n*-Butylbenzene
29	*n*-Butylcyclohexane
30	1,4-Diethylbenzene
31	1,2-Diethylbenzene
32	1,3-Dimethyl-4-ethylbenzene
33	*n*-Undecane

one or both columns: (1) varying only the second column temperature; (2) varying only the first column temperature; (3) simultaneous variation of both column temperatures. For the first two modes, the dependences of Kováts indices, I_{AB}, upon temperatures, T_A or T_B, have been reported[4,5]. The last mode had not been presented. All these possibilities are discussed in the following.

Optimization by varying only the second column temperature

Keeping the first column temperature constant, $T_A = 60°C$, the temperature of the second column was varied between 50 and 150°C in 10°C steps. Kováts indices, $I_{AB,i}$, of the hydrocarbons of the synthetic mixture (33 components) were measured on the coupled columns at any temperature of the second column. The experimental results are presented in Fig. 1.

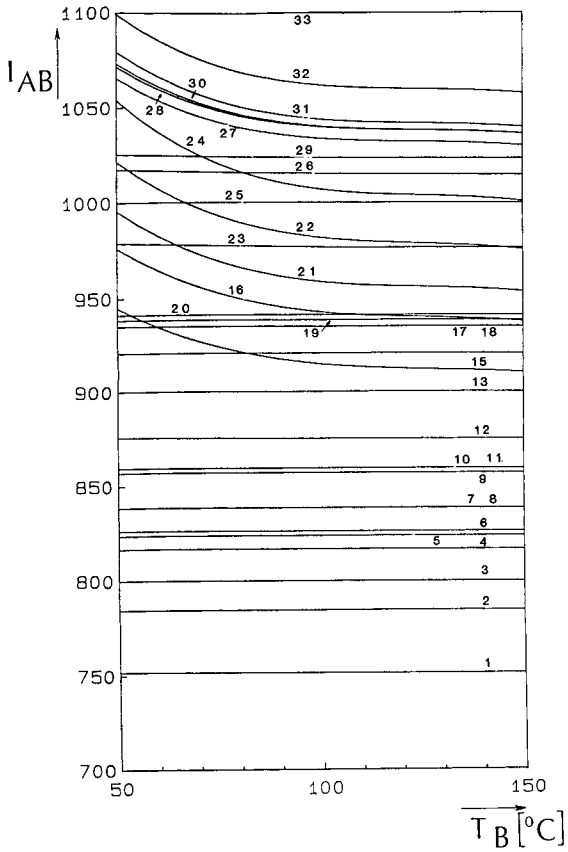

Fig. 1. Plot of Kováts retention indices of series-coupled columns in a twin-oven GC system *versus* column temperature of the second (polar) column at a constant (T_A = 60°C) temperature of the first (non-polar) column. The line numbers correspond to the component numbers given in Table I.

Regression analysis has shown that each curve in Fig. 1 can be described by the following polynomial:

$$I_{AB,i}(T_B, 60°C) = A_{0,i} + A_{1,i}T_B + A_{2,i}T_B^2 + A_{3,i}T_B^3 \quad (4)$$

The coefficients were determined, for each compound i, by fitting eqn. 4 to the experimental results. Subsequently, retention indices were calculated for all the sample constituents in the range of 50–150°C in 1°C steps for column B. The number of peaks that can be distinguished was also calculated, using a threshold, $\delta_{min} = \delta I_{j,i,min}$ (60°C, T_B), corresponding to a resolution, $R_{j,i,req} = 1.0$. The average δ_{min} value used for the determination of the number of peaks separated appeared to be about 2 I.u. for capacity factors larger than 2. The maximum number of peaks that can be separated at different temperatures of the second column is shown in Fig. 2. Obviously, according to the main criterion given in the Theoretical, more than one optimum is observed. Taking into account the second criterion, *i.e.*, minimum separation time, the optimum

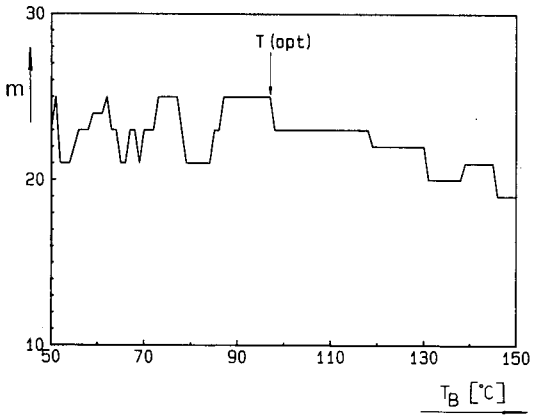

Fig. 2. Number of separated peaks, *m*, *versus* temperature of the second column, T_B, at constant temperature (T_A = 60°C) of the first column.

temperature, $T_{B,opt}$, in this case is 97°C. The chromatogram obtained under these conditions is depicted in Fig. 3.

Optimization by varying only the first column temperature

Following a similar procedure to that described above, the temperature of the first column, T_A, was varied from 60 to 130°C in 10°C steps at a constant temperature, T_B = 50°C, of the second column. An equation similar to eqn. 4 was fitted to the experimental results. Calculated Kováts indices [$I_{AB}(T_A, 50°C)$] at 1°C intervals are plotted *versus* the second column temperature in Fig. 4. The maximum number of peaks for different temperatures of the first column is presented in Fig. 5. Also in this case different optima are observed. The criterion of the shortest analysis time shows T_A = 80°C to be the optimum temperature for the first column. The chromatogram

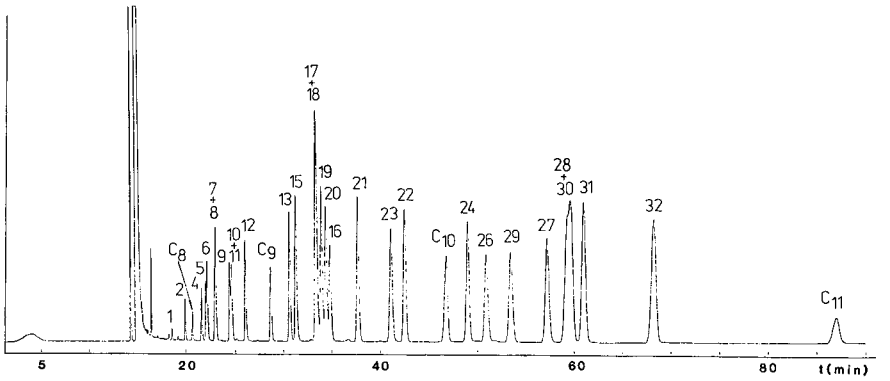

Fig. 3. Separation of the hydrocarbon sample in tandem capillary columns at the optimum temperature of the polar column, $T_{B,opt}$ = 97°C, at a constant temperature of the non-polar column (T_A = 60°C). For peak numbers see Table I.

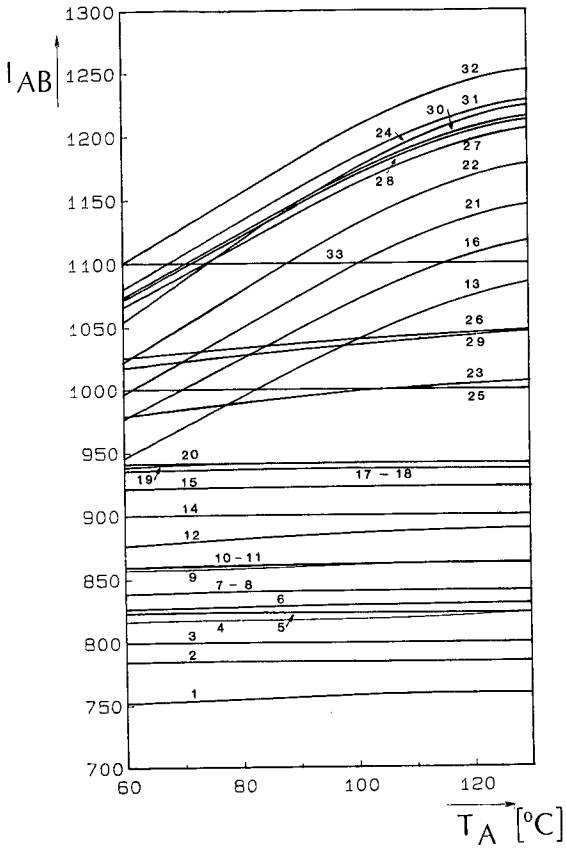

Fig. 4. Plot of Kováts retention indices of series-coupled columns in a twin-oven GC system *versus* column temperature of the first (non-polar) column at a constant temperature (T_B = 50°C) of the second (polar) column. The line numbers correspond to the component numbers given in Table I.

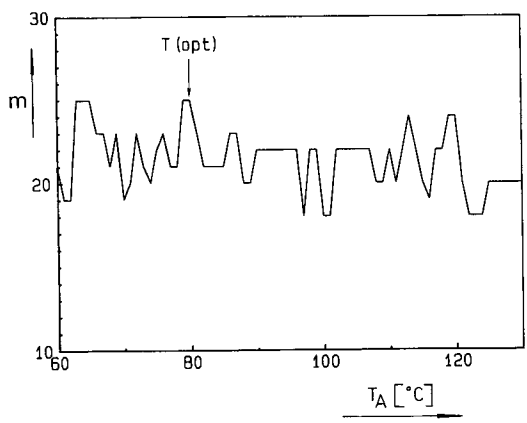

Fig. 5. Number of separated peaks, m, *versus* temperature of the first column, T_A, at a constant temperature of the second column, T_B = 50°C.

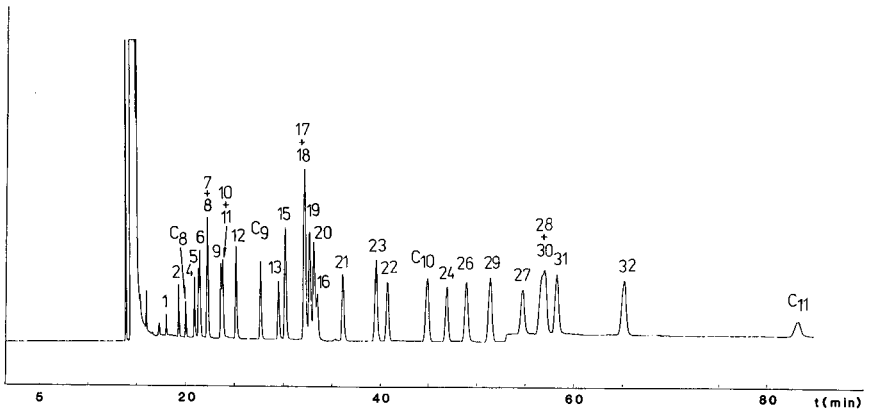

Fig. 6. Chromatogram of the hydrocarbon mixture at the optimum temperature of the non-polar column, $T_A = 80°C$, at a constant temperature of the second column, $T_B = 50°C$. Peak numbers correspond to the numbers given in Table I.

corresponding to this optimum is given in Fig. 6. Comparing the chromatograms under optimum conditions, Figs. 3 and 6 show that obviously 25 peaks are separated in both cases. However, different peak pairs are considered separated according to the criteria given in the Theoretical, in both cases.

Optimization by simultaneous variation of both column temperatures

In order to limit the number of experiments, in this case both column temperatures were varied in the interval 60–100°C according to a three level orthogonal design as shown in Table II. For the calculation of the Kováts indices the following equation was used to approximate the experimental data:

$$I_{AB,i}(T_A,T_B) = A_{0,i} + A_{1,i}T_A + A_{2,i}T_A^2 + B_{1,i}T_B + B_{2,i}T_B^2 + C_iT_AT_B \quad (5)$$

In the same way as discussed above, optimum temperatures calculated for the first and

TABLE II

TEMPERATURES OF THE FIRST (T_A) AND THE SECOND (T_B) COLUMNS AS PROPOSED BY A THREE LEVEL ORTHOGONAL DESIGN

Exp. No.	T_A (°C)	T_B (°C)
1	80	80
2	100	100
3	100	60
4	60	100
5	60	60
6	80	100
7	80	60
8	100	80
9	60	80

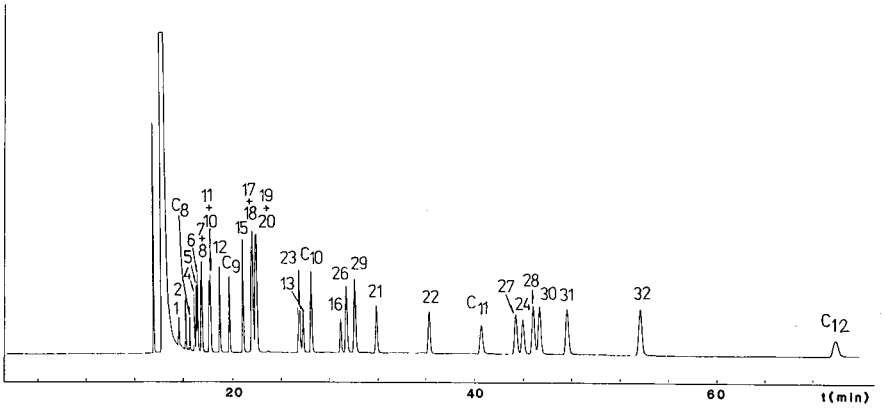

Fig. 7. Separation of the hydrocarbon sample in tandem capillary columns at the optimum selectivity tuned by simultaneous optimization of the temperatures of the non-polar column, $T_{A,opt}$ = 62°C, and the polar column, $T_{B,opt}$ = 100°C. Peak numbers correspond with the numbers given in Table I.

second columns appeared to be 62°C ($T_{A,opt}$) and 100°C ($T_{B,opt}$). The separation of the hydrocarbon mixture under these conditions is shown in Fig. 7.

As with the foregoing methods, optimization procedure 3 accidentally also yields an optimum where 25 hydrocarbons were separated with $R_{j,i,req}$ = 1.00 or better, but the analysis time was shorter. The equations presented proved to be very useful to approximate Kováts retention indices; the agreement between calculated and experimental indices in all instances appeared to be within ± 1 I.u. From Figs. 3, 6 and 7, changes in peak retention order at the respective optimum temperatures are obvious, *cf.*, peak pairs 19–20 and 28–30.

REFERENCES

1 P. Sandra, F. David, M. Proot, G. Diricks, M. Verstappe and M. Verzele, *J. High Resolut. Chromatogr. Chromatogr. Commun.*, 8 (1985) 782.
2 J. V. Hinshaw, Jr. and L. S. Ettre, *Chromatographia*, 21 (1986) 561.
3 J. V. Hinshaw, Jr. and L. S. Ettre, *Chromatographia*, 21 (1986) 669.
4 T. Tóth, H. van Cruchten and J. A. Rijks, in P. Sandra (Editor), *Proc. VIth Int. Symp. on Capillary Chromatography*, Hüthig, Heidelberg, 1985, p. 769.
5 T. Tóth and F. Garay, in P. Sandra (Editor), *Proc. VIIIth Int. Symp. on Capillary Chromatography*, Hüthig, Heidelberg, 1987, p. 585.
6 P. J. Schoenmakers, *Optimization of Chromatographic Selectivity*, Elsevier, Amsterdam, 1986.
7 J. Krupčík, J. Mocák, A. Šimová, J. Garaj and G. Guiochon, *J. Chromatogr.*, 238 (1982) 1.
8 J. Krupčík, D. Repka, T. Hevesi, J. Mocák and G. Kraus, *J. Chromatogr.*, 355 (1986) 99.
9 L. S. Ettre, *Chromatographia*, 6 (1973) 489.
10 R. E. Kaiser and R. I. Rieder, *J. High Resolut. Chromatogr. Chromatogr. Commun.*, 2 (1979) 416.

Journal of Chromatography, 463 (1989) 253–260
Elsevier Science Publishers B.V., Amsterdam — Printed in The Netherlands

CHROM. 21 067

MULTIDIMENSIONAL GAS CHROMATOGRAPHIC DETERMINATION OF COTININE AS A MARKER COMPOUND FOR PARTICULATE-PHASE ENVIRONMENTAL TOBACCO SMOKE*

STANLEY L. KOPCZYNSKI

Environmental Monitoring Systems Laboratory, Environmental Research Center, U.S. Environmental Protection Agency, Research Triangle Park, NC 27711 (U.S.A.)

(First received July 27th, 1988; revised manuscript received October 24th, 1988)

SUMMARY

Multidimensional gas chromatographic analysis of air particles for the tobacco alkaloid cotinine is described. The analytical procedure requires little sample preparation. Unambiguous identification of cotinine and nicotine in cigarette smoke and indoor air samples was achieved by precise, reproducible retention times observed with two parallel analytical columns of different polarities and a nitrogen-specific detector. Further investigation of smoking and environmental variables is needed to validate the use of cotinine as a marker compound for environmental tobacco smoke particulate matter.

INTRODUCTION

Much concern has been expressed regarding the health effects of environmental tobacco smoke (ETS) on non-smokers, particularly the children of smoking parents[1,2]. Tobacco smoke contains many toxic compounds, which are distributed between the gas phase and the particulate phase[3–6]. ETS is an important source of total suspended particulate matter in homes and other indoor environments[7]. A strong correlation has been found between the mutagenicity associated with the particulate concentration in various homes and the number of cigarettes smoked[8].

Body fluids have been analyzed for nicotine and cotinine content as a means to assess personal exposure to ETS[9]. Personal air monitoring is an alternative approach to exposure assessment that is more direct and less intrusive than the analysis of body fluids. Moreover, it can be employed to assess exposures to ETS gases and particles separately.

To identify and quantitate the contribution of ETS to the total particulate mass in indoor environments, suitable marker (surrogate) compounds are required. Nico-

* This article has not been subjected to Agency review and does not necessarily reflect the views of the Agency. Mention of trade names or commercial products does not constitue endorsement or recommendation for use.

0021-9673/89/$03.50

tine has been used as a marker for ETS because it is unique to tobacco and is major component of tobacco smoke[10-12]. However, the suitability of nicotine as a marker for ETS particulate matter is uncertain because of unresolved questions regarding its reactivity and volatility and ambiguities regarding its phase distribution[13].

In the study reported here, another tobacco alkaloid, cotinine, was investigated as a potential marker compound for ETS particulate-phase exposure. Cotinine is less volatile than nicotine, occurs pimarily in the particulate phase, and can be measured with a nitrogen-specific detector for enhanced discrimination from other components of ETS. A literature search revealed no environmental applications of this compound. Raw extracts of particulate samples were analyzed by multidimensional gas chromatography (MDGC). By employing heart-cutting techniques and multiple columns of different polarities, MDGC provides enhanced GC separations and increased information content for the identification of cotinine and other analytes.

MATERIALS AND PROCEDURES

Equipment

Analyses were performed with a Siemens SiChromat-2 MDGC system containing two ovens operated with independent temperature programs and equipped with a flame ionization detection (FID) and a nitrogen-specific detection (NSD) system, also from Siemens. Sample injections were made with a Varian Model 1095 on-column capillary injector. Computing integrators (Perkin-Elmer, Model LC1-100) were employed to collect and process the data.

The sample pathway consisted of a retention gap/guard column, a pre-column, a short trapping column, and two parallel analytical columns connected to a single NSD system (Fig. 1). The pre-column effluents were switched automatically to either the FID or the trapping column by means of a Deans-type column-switching device. Effluents in the trapping column entered the two analytical columns through a glass-lined, stainless-steel splitter union (Alltech).

The MDGC system was fitted with fused-silica, open tubular capillary columns.

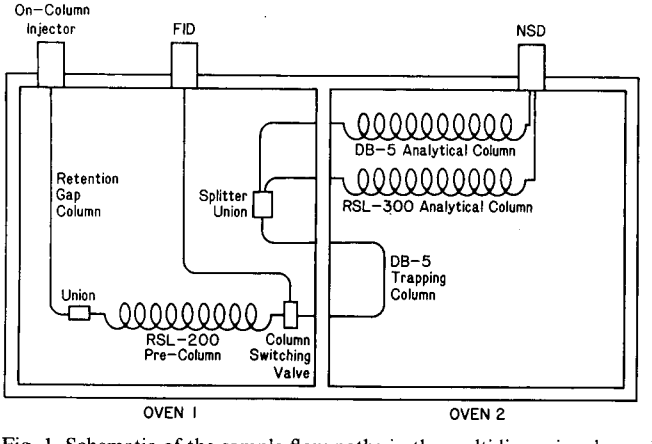

Fig. 1. Schematic of the sample flow paths in the multidimensional gas chromatograph.

A length of uncoated, deactivated, fused-silica tubing (1 m × 0.32 mm I.D., J&W Scientific) served as a retention gap and protected the pre-column from any non-volatile compounds present in sample injections. The pre-column was an RSL-200 column, 15 m × 0.32 mm I.D. with 0.5 μm film thickness (Alltech). The trapping column was a short section of DB-5 column, 0.75 m × 0.32 mm I.D. with 1.0 μm film thickness. The analytical columns were (1) a DB-5 column, 12 m × 0.32 mm I.D. with 1.0 μm film thickness (J&W Scientific) and (2) an RSL-300 column, 15 m × 0.32 mm I.D. with 0.5 μm thickness (Alltech).

Materials

Nicotine calibration solutions were prepared from a reference standard solution obtained from Supelco and the cotinine solutions from 98% purity cotinine obtained from Aldrich. Calibration solutions were prepared in ACS-grade benzene (Fisher Scientific). Particulate extractions were carried out with chromatographic-grade methylene chloride (Burdick and Jackson).

Cigarette smoke particulate samples collected on 37-mm tetrafluoroethylene filters were obtained from the John B. Pierce Foundation. The samples had been collected from an environmental chamber containing several active smokers and were stored in a freezer until extracted. Blank samples were obtained from the chamber while it contained non-smokers.

Indoor air samples were obtained from Battelle-Columbus as concentrated extracts in ethyl acetate[14]. The samples were collected in private homes with a prototype indoor air sampler containing an XAD-4 sorbent bed and a105-mm quartz fiber filter in tandem.

Sample preparation

The cigarette smoke particulate sample filters were cut into strips and extracted in 30 ml methylene chloride with an ultrasonic probe (Heat Systems-Ultrasonics, Model W185). Extractions were carried out for 30 min at 30 watts. Extraction solutions were evaporated under a gentle stream of charcoal-filtered helium to approximate 1 ml, reconstituted with 1 ml benzene, and then evaporated to 0.5 ml. The concentrated solutions were mixed in an ultrasonic bath and centrifuged (*ca.* 400 *g*) prior to analysis.

The indoor air samples were received from Battelle-Columbus as concentrated extracts in ethyl acetate. The filter and XAD-4 samples had been combined and Soxhlet extracted with methylene chloride for 16 h and then further extracted with ethyl acetate for an additional 8 h. The two extracts were combined and concentrated by Kuderna–Danish evaporation. The concentrated solutions were analyzed as received.

Gas chromatography

High carrier gas flow-rates were used in the MDGC analyses to reduce retention times an minimize peak tailing. The linear flow-rate through the analytical columns was 29.6 cm/s at the initial programmed temperature settings. The NSD current was set at 800 mA to achieve maximum sensitivity. The nicotine and cotinine cuts from the pre-column were obtained over intervals of 0.35 min and 0.70 min, respectively. The two cuts were collected together on the trapping column with the oven set

at 50°C. The on-column injector was programmed from 60°C to 280°C at 100°C/min, the pre-column oven from 90°C to 280°C at 15°C/min, and the analytical oven from 50°C to 280°C at 15°C/min. The MDGC was programmed to reset automatically at the end of an analysis (30 min). It was ready for the next sample as soon as the injector had cooled (25 min). Sample injection volumes ranged from 1 μl to 3 μl. To reduce analyte losses to any active sites present in the injector or the retention gap column, 1 μl ammoniated benzene was co-injected with each sample.

Nicotine and cotinine were identified by their retention times on the two analytical columns. Confirmation was obtained by GC–matrix isolation–Fourier transform IR spectroscopic (FT-IR) analysis. Quantitation was based on peak height measurements of the chromatogram obtained with the DB-5 column.

RESULTS AND DISCUSSION

Validation of procedures

High cotinine recoveries were obtained in the extraction and concentration procedures. A 98% extraction efficiency was obtained for cotinine based on re-extractions of two ETS particulate samples. A 90% recovery (relative standard deviation, R.S.D. = 11%, n = 7) was obtained for cotinine from evaporated solutions of methylene chloride and benzene. The recovery of the more volatile nicotine was poorer (53%) and more variable (R.S.D. = 32%, n = 4).

Ammoniated benzene, produced by bubbling ammonia through the solvent, was co-injected with all samples to reduce losses of basic analytes in the MDGC system. NSD area responses for cotinine and nicotine obtained with co-injections of 1 μl benzene were compared to responses obtained with co-injections of 1 μl ammoniated benzene (Table I). Injections contained 0.9–2.0 ng of the analyte. Although co-injected ammoniated benzene had little effect on the cotinine response with new columns, it produced a substantial increase in response when employed with used columns (23% with both the DB-5 and the RSL-300 columns). A comparison of the results for cotinine and nicotine indicates that nicotine is more susceptible to adsorption losses in both new and used columns. Thus, some sample cleanup prior to analysis may be indicated to minimize buildup of active sites in the GC system.

Identification of analytes by chromatographic retention times requires precise and reproducible measurements. Replicate injections of solutions of cotinine at loadings between 0.5 and 4 ng yielded highly reproducible retention times on both the DB-5 and the RSL-300 columns. The standard deviations (S.D.) for six injections were 0.003 min and 0.004 min on the DB-5 and RSL-300 columns, respectively.

TABLE I

PERCENT INCREASE IN DETECTOR RESPONSES FOR COTININE AND NICOTINE RESULTING FROM CO-INJECTIONS OF 1 μl AMMONIATED BENZENE

Condition of guard column and pre-column	*Cotinine*		*Nicotine*	
	DB-5	*RSL-300*	*DB-5*	*RSL-300*
Used	23	23	722	679
New	2.4	1.7	6.6	9.2

In this study the retention times observed for unknown sample peaks were compared directly with the retention times obtained on the same day with standard samples yielding similar peak intensities. As a result, the identification of cotinine for all cigarette smoke and room air samples on both columns was based on retention times which agreed with a standard mixture to within 0.008 min. The agreements in retention times obtained on both columns, together with the quality of the NSD chromatogram (Fig. 2), permit unambiguous identification of the analyte peaks.

The NSD calibration data between 0.2 and 3.7 ng cotinine on the DB-5 column fit a linear regression line and showed a small non-zero intercept (Fig. 3). Further investigation revealed that the linearity did not extend below 0.2 ng. Calibrations conducted between 0 and 0.2 ng cotinine indicated a limit of detection (at three times noise) of 15 pg.The calibration curve with the more polar RSL-300 became non-linear below 1 ng, and the limit of detection was somewhat higher than that obtained with the DB-5 column. Consequently, the DB-5 chromatogram was selected for quantitation. Replicate sample injections yielded very reproducible peak heights for cotinine in the DB-5 chromatogram (R.S.D. = 1.3%, n = 8). As a result of the high reproducibility of the cotinine measurements, the high cotinine recoveries obtained in the sample extraction and concentration procedures, and the use of daily calibration standards, internal standards were not employed in this study.

Sample analysis

The NSD chromatograms of the combined cotinine and nicotine heart-cuts of the cigarette smoke particulate samples show that the analyte peak signals are well

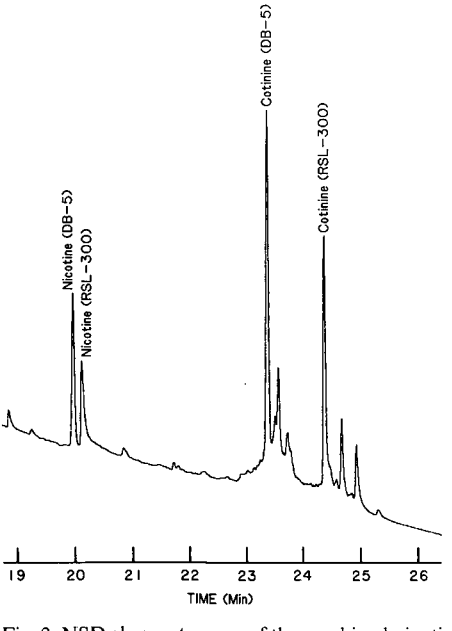

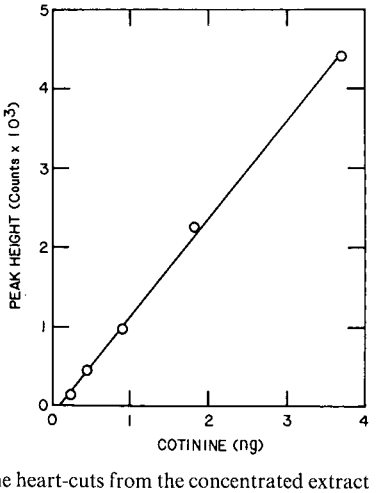

Fig. 2. NSD chromatogram of the combined nicotine and cotinine heart-cuts from the concentrated extract of an ETS particulate sample.

Fig. 3. Cotinine calibration for the DB-5 column with the nitrogen-specific detector.

TABLE II
ANALYSIS OF FILTER AND XAD-4 COMBINED EXTRACTS FROM THE LIVING ROOMS OF PRIVATE RESIDENCES

Sample	*Smoking rate (cigarettes/h)*	*Concentration in room air (ng/m³)*	
		Cotinine	*Nicotine**
4-L	1.9	316	29 000
3-L	1.3	21	1 700
8-L	0	5	60

* Nicotine analyses performed by the Battelle-Columbus laboratory[14].

separated and easily distinguished on both the DB-5 and RSL-300 columns (Fig. 2). Moreover, the analytical procedure requires only one detector for both analytical columns. The particulate-phase concentration of cotinine was determined in samples from two chamber studies conducted two years apart, in which five popular brands of cigarettes were smoked. The average concentration of cotinine in the six ETS particulate samples was 732 ng/μg. The consistency of this value (S.D. = 83) suggests that cotinine may be a suitable candidate marker compound for cigarette smoke particulate mass. No cotinine was detected in a filter blank obtained with the environmental

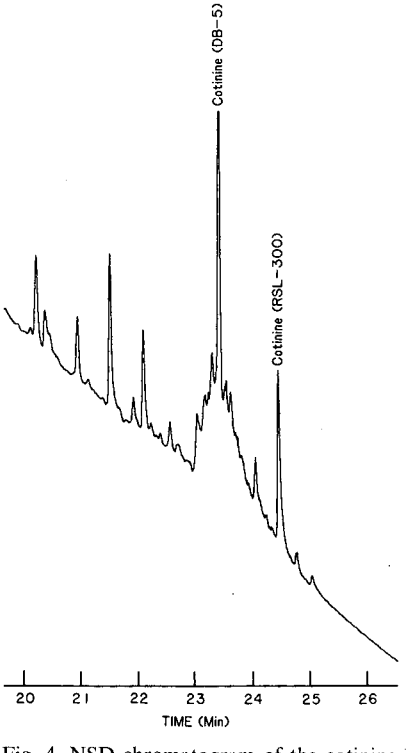

Fig. 4. NSD chromatogram of the cotinine heart-cut from the concentrated extract of living room air sample 3-L. The baseline drift is apparently the result of the rising temperature of oven 2. The unmarked peaks have not been identified.

chamber occupied by several non-smokers. Although nicotine was found in all of the samples, volatility losses precluded meaningful quantitative measurements. However, previous nicotine results were consistent for cigarette smoke samples collected on sodium bisulfate-treated filters[11].

Data for air samples from the living rooms of three homes that were analyzed for cotinine are shown in Table II and Fig. 4. Although these samples are composed of both the vapor-phase and particulate-phase cotinine, studies have shown that cotinine occurs mainly in the particulate phase[15,16]. The cotinine peaks illustrated in Fig. 4 were obtained from a sample collected in the home reporting a smoking rate of only 1.3 cigarettes/h. The injected sample contained 371 pg cotinine. Since the limit of detection of cotinine with the MDGC is 15 pg, it appears that the detection and measurement of cotinine in indoor particulate matter can be accomplished for smoking rates about one order of magnitude less than that represented in sample 3-L.

Although the cotinine concentration was found to increase with smoking rate, the increase is not proportional. Since the nicotine and cotinine concentrations are fairly proportional to one another, the cotinine results do not appear to be artifacts of the MDGC analysis. The large difference in concentration between samples 4-L and 3-L probably reflects differences in the ventilation rates of the two homes during sampling. The presence of cotinine and nicotine in homes reporting no smoking (8-L) suggests the possible presence of residue from smoking sometime previous to the sampling.

ACKNOWLEDGEMENTS

I am indebted to Rick Tosun, formerly of the John B. Pierce Foundation, for the cigarette smoke particulate samples and to Jane C. Chuang of Battelle-Columbus for the combined extracts from the living room air samples. I am also grateful to Ruth Barbour of EPA and Jeffrey Childers of NSI-Environmental Sciences for the GC–matrix isolation–FT-IR analyses.

REFERENCES

1 WHO Expert Committee on Smoking Control, *Controlling the Smoking Epidemic, Report of the WHO Expert Committee on Smoking Control*, WHO Technical Report Series 636, World Health Organization, Geneva, 1979.
2 Surgeon General, *The Health Consequences of Involuntary Smoking, A Report of the Surgean General*, Publication No. CDC 87-8398, U.S. Department of Health and Human Services, 1986.
3 K. Grob and J. A. Voellmin, *J. Chromatogr. Sci.*, 8 (1970) 218.
4 J. N. Schumacher, C. R. Green, F. W. Best and M. P. Newell, *J. Agric. Food Chem.*, 25 (1977) 310.
5 I. Schmeltz and D. Hoffmann, *Chem. Rev.*, 77 (1977) 295.
6 Surgeon General, *Smoking and Health, A Report of the Surgean General*, Publication No. (PHS) 79-50066, U.S. Department of Health, Education, and Welfare, Washington, DC, 1979.
7 J. D. Spengler, D. W. Dockery, W. A. Turner, J. M. Wolfson and B. G. Ferris, Jr., *Atmos. Environ.*, 15 (1981) 23.
8 J. Lewtas, S. Goto, K. Williams, J. C. Chuang, B. A. Peterson and N. K. Wilson, *Atmos. Environ.*, 21 (1987) 443.
9 R. A. Greenberg, N. J. Haley, R. A. Etzel and F. A. Loda, *N. Engl. J. Med.*, 310 (1984) 1075.
10 M. Muramatsu, S. Umemura, T. Okada and H. Tomita, *Environ. Res.*, 35 (1984) 218.
11 S. K. Hammond, B. P. Leaderer, A. C. Roche and M. Schenker, *Atmos. Environ.*, 21 (1987) 457.

12 G. B. Oldaker III and F. C. Conrad, Jr., *Environ. Sci. Technol.*, 21 (1987) 994.
13 National Research Council, *Environmental Tobacco Smoke. Measuring Exposures and Assessing Health Effects*, National Academy Press, Washington, DC, 1986.
14 J. C. Chuang and N. K. Wilson, presentation at the *11th International Symposium on Polynuclear Aromatic Hydrocarbons, Gaithersburg, MD, Sept. 23–25, 1987.*
15 D. J. Eatough, C. L. Benner, J. M. Bayona, F. M. Caka, R. L. Mooney, J. D. Lamb, M.L. Lewis, L. D. Hansen and N. E. Eatough, in B. Seifert, H. Esdorn, M. Fisher. H. Ruden and J. Wegner (Editors), *Indoor Air '87, Proceedings of the 4th International Conference on Indoor Air Quality and Climate*, Vol. 2, Institute for Water, Soil, and Air Hygiene, Berlin, 1987.
16 S. L. Kopczynski, *Proceedings of the 1988 EPA/APCA International Symposium: Measurement of Toxic and Related Air Pollutants*, APCA Publication VIP-10, EPA Report No. 600/9-88-015, Air Pollution Control Association, Pittsburgh, PA, 1988.

Journal of Chromatography, 463 (1989) 261–270
Elsevier Science Publishers B.V., Amsterdam — Printed in The Netherlands

CHROM. 21 070

CHROMATOGRAPHIC EVALUATION OF SORPTION AND DIFFUSION CHARACTERISTICS OF GLUCOSE, MALTOSE AND MALTOTRIOSE IN SILICA GELS

C. B. CHING*, K. HIDAJAT and M. N. RATHOR
Department of Chemical Engineering, National University of Singapore, 10 Kent Ridge Crescent, Singapore 0511 (Singapore)
(First received June 21st, 1988; revised manuscript received October 25th, 1988)

SUMMARY

Liquid chromatographic techniques were employed to evaluate the sorption and diffusion characteristics of glucose, maltose and maltotriose in silica gel. The equilibrium constants were found to decrease with increasing molecular size. The determined diffusion coefficient of glucose is comparable to that in the literature. The pore diffusivities decrease with increasing size of the carbohydrates at all temperatures.

INTRODUCTION

Gel permeation chromatography is a separation technique based mainly on differences in the pore diffusion rates of individual substances eluted through a porous packing. The pore diffusion rate is controlled by the molecular size and steric arrangement of a compound. Hence, in order to design large-scale processes, accurate data on pore diffusivity must be available.

In the past, chromatography techniques have been used successfully to evaluate mass transport and sorption rate constants in packed beds, but these mostly involved gas–solid systems[1] and much less work has been carried out on liquid–solid systems.

In this study, the pulse and response method was used to determine sorption kinetics and equilibrium parameters for a monosaccharide (glucose), disaccharide (maltose) and trisaccharide (maltotriose) in a column packed with silica gel. The reason for selecting these carbohydrates is that the effect of a gradual increase in molecular size on pore diffusivities and equilibrium constants can be systematically evaluated.

THEORETICAL

The chromatographic response curves were analysed by method of moments. For a column packed with silica gel, the first and second moments of the pulse response are related to the adsorption equilibrium constant (K) and the macropore diffusional time constant (D_p/R_p^2) by[2]

0021-9673/89/$03.50

$$\mu = \frac{\int_0^\infty ct\,dt}{\int_0^\infty c\,dt} = \frac{L}{\varepsilon v}[\varepsilon + (1 - \varepsilon)K] \tag{1}$$

$$\frac{\sigma^2}{\mu^2} \cdot L = \text{HETP} = \frac{2D_L}{v} + \frac{2\varepsilon V}{(1-\varepsilon)}\left(\frac{R_p}{3k_f} + \frac{{R_p}^2}{15\varepsilon_p D_p}\right)\left[1 + \frac{\varepsilon}{(1-\varepsilon)K}\right]^{-2} \tag{2}$$

where

$$\sigma^2 = \int_0^\infty c(t-\mu)^2 dt / \int_0^\infty c\,dt$$

In a liquid phase system the contribution to the height equivalent to a theoretical plate (HETP) arising from axial dispersion ($2D_L/v$) is essentially independent of fluid velocity. It follows from eqn. 2 that a plot of HETP *versus* fluid velocity should be linear with an intercept corresponding to axial dispersion $2D_L/v$ and the slope giving the overall mass transfer resistance.

Within the low Reynold's number range considered in this study, the external mass transfer coefficient may be calculated from either Wakao and Funazkri's[3] or Wilso and Geankoplis'[4] correlation. If the term $R_p/3k_f$ in eqn. 2 is much less than the term ${R_p}^2/15\varepsilon_p D_p$, the slope of the plot of HETP *versus* velocity will represent mass transfer resistance for macropore diffusion.

In the calculation of the moments of the experimental response curves, small corrections were applied to allow for the hold-up and dispersion in the detector (volume *ca.* 2.3 cm^3). These corrections were determined directly from pulse response measurements with the column removed from the system.

EXPERIMENTAL

The apparatus used included a Pharmacia jacketed column (I.D. 1.6 cm) packed with silica gel to a height of 11.3 cm. The effluent from the column was monitored continuously by a Waters Assoc. refractive index detector. The analogue signal from the detector was sent via a pre-amplifier to a Philips (IBM compatibe) AT computer data logging system. The eluent (water) was supplied to the column via a Rheodyne Type 7125 sample injection valve with a 100-μl loop by a Varian HPLC pump. Both the column and the refractive index detector were maintained at the same temperature by recirculating water through the column jacket and the flow cell bath.

Commercial silica gel particles supplied by Sigma were used. The gel particles were sieved to have an average diameter of 509 μm. The gel has the following properties: specific pore volume 0.468 cm^3/g; mean pore diameter 27 Å; specific surface area 680 m^2/g; and particle density 1.09 g/cm^3. These properties were determined with a Quantarsorb instrument.

RESULT AND DISCUSSIONS

Determination of ε *and* $D_L/\varepsilon v$

A typical chromatogram of the three species considered here is shown in Fig. 1. Fig. 2 shows the plot of the first moment of the response *vs.* reciprocal superficial

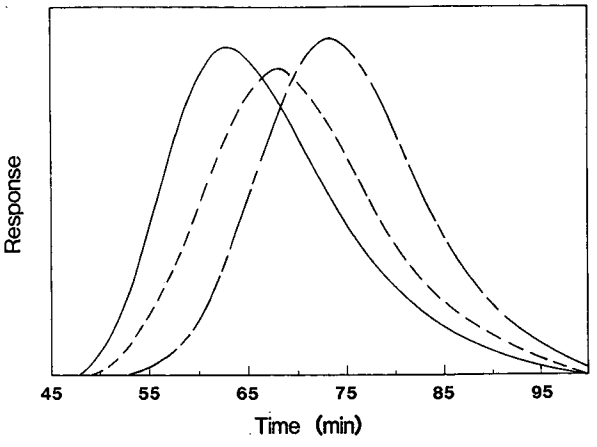

Fig. 1. Typical chromatograms of sugars: ---, glucose; – – –, maltose; ———, maltotriose.

velocity for a starch pulse. As the starch molecule is too large to penetrate the pores of the silica gel particles, the equilibrium value of K in eqn. 1 is zero and the slope of the plot of μ *vs.* $1/\varepsilon v$ will be equal to $L\varepsilon$, whereby the bed voidage ε is calculated to be 0.47.

^2H_2O penetrates the pores of the silica gel particles fully and easily, which means that no resistance to mass transfer exists for ^2H_2O and axial dispersion is the only controlling factor[5]. The axial dispersion in liquids is more pronounced than that in gases. This is due to the effect of the greater hold-up of liquid in the laminar boundary layer surrounding the particles, wich, combined with small random fluctuations in the flow, can lead to greater axial mixing. Fig. 3 shows the HETP data for ^2H_2O plotted against the interstitial velocity. It shows that the HETP is approximately constant ($2D_L/v \approx 0.24$ cm), independent of fluid velocity. It can also be concluded that because in a liquid system axial mixing is determined by the flow pattern in the bed rather than by molecular diffusion[6], this value of the HETP shoud be approximately the same for all other sorbates eluting through the same column under similar conditions.

Equilibrium data

Figs. 4–6 show the plots of first moment *vs.* reciprocal superficial velocity. The plots are essentially linear, and the data can be well represented by single straight lines for the temperature range 278–333 K, implying that the heat of adsorption is zero for all three sugars (Fig. 7). This also implies that no adsorption takes place and the K values correspond simply to the equilibrium distribution of the carbohydrates between the fluid phase and the pores.

Values of K calculated according to eqn. 1 are given in Table I. The data show that the equilibrium constant decreases with increasing molecular size, confirming that the larger molecular size hinders the sugars from penetrating the pores and attaining equilibrium.

Diffusivity data

Plots of HETP *vs.* interstitial liquid velocity are shown in Figs. 8–10. According to eqn. 2, when macropore diffusion is the controlling factor and the axial dispersion

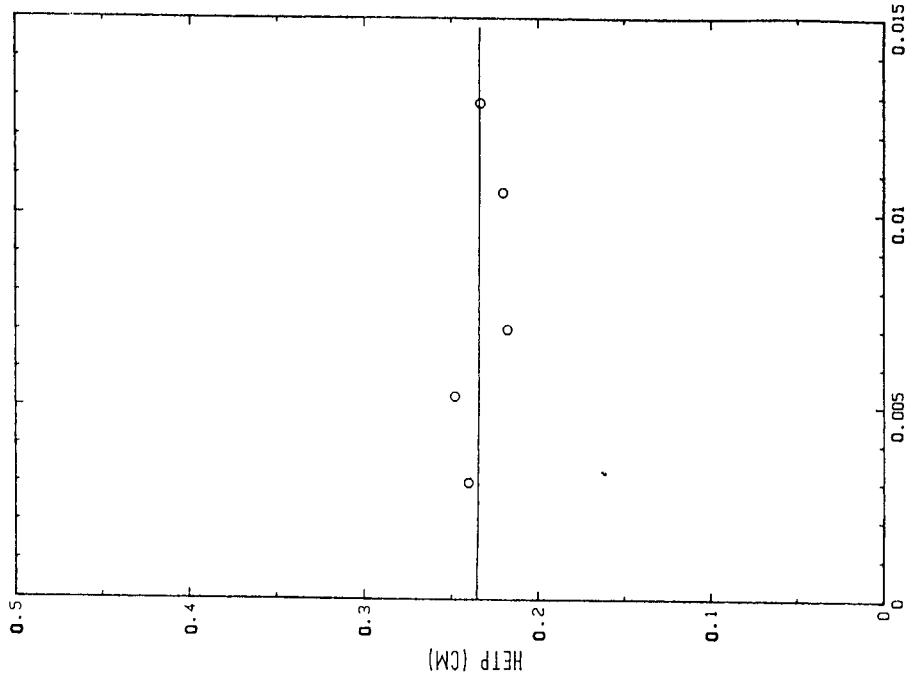

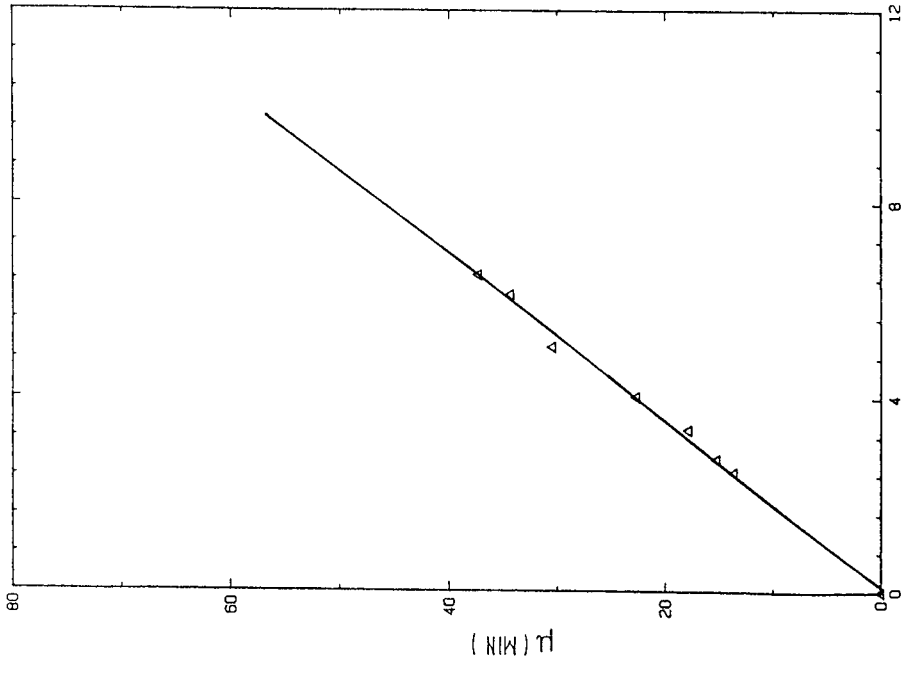

Fig. 2. First moment *versus* inverse of superficial velocity for starch.
Fig. 3. HETP *versus* interstitial velocities for ^2H_2O.

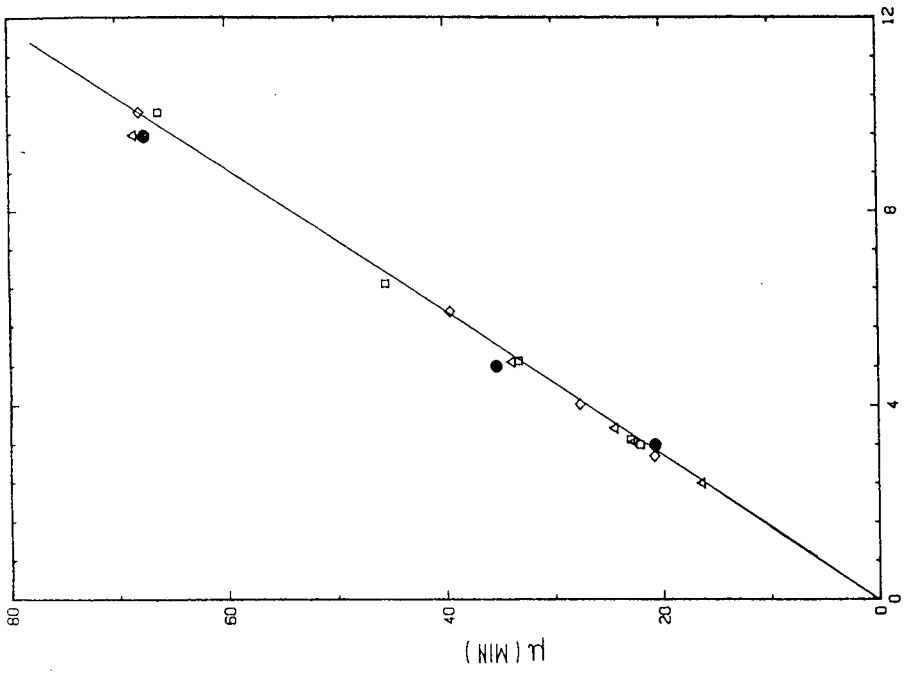

Fig. 4. First moment *versus* inverse of superficial velocity for glucose. ● = 278 K; △ = 303 K; □ = 333 K.

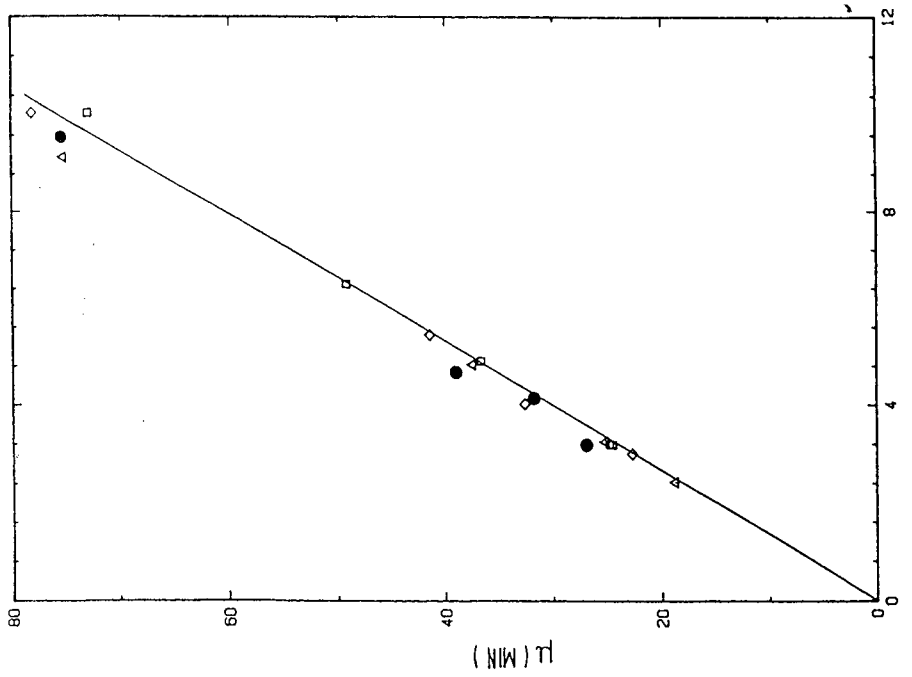

Fig. 5. First moment *versus* inverse of superficial velocity for maltose. ● = 278 K; △ = 303 K; □ = 333 K.

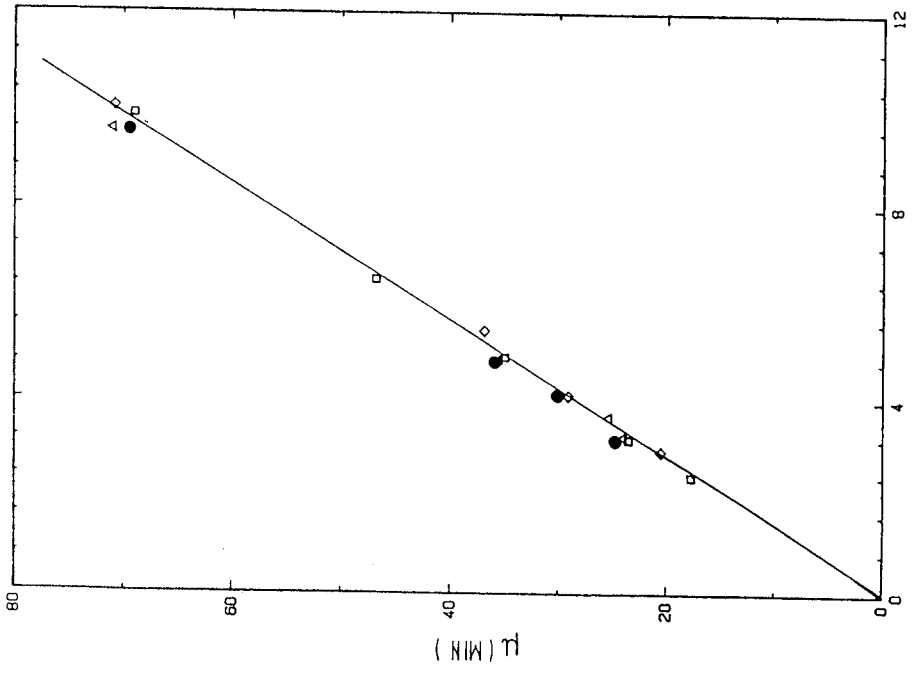

Fig. 6. First moment *versus* inverse of superficial velocity for maltotriose. ● = 278 K; △ = 303 K; □ = 333 K.

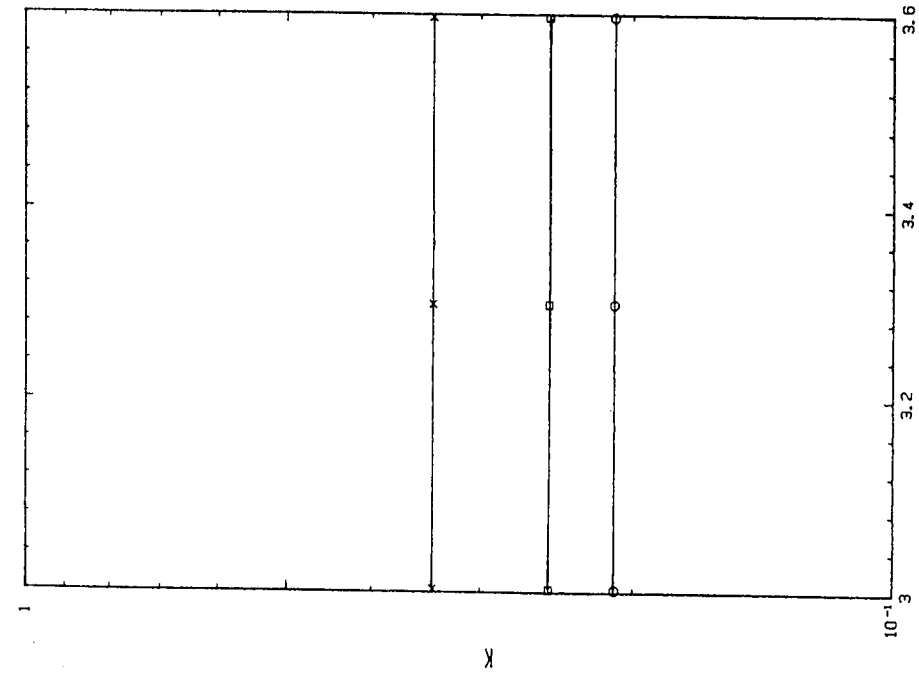

Fig. 7. Equilibrium constant *versus* inverse of temperature. × = Glucose; □ = maltose; ○ = maltotriose.

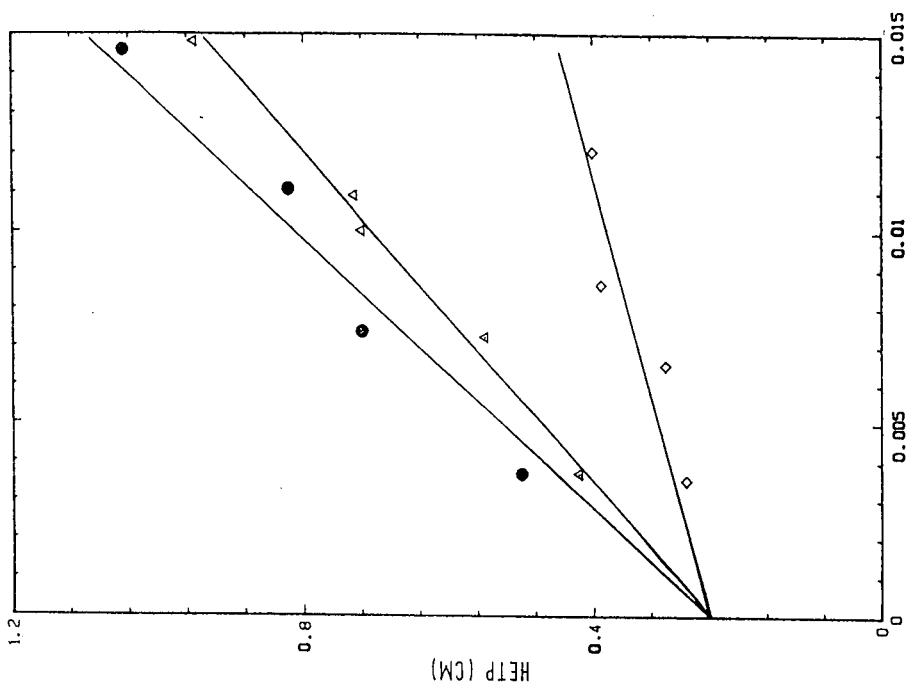

Fig. 8. HETP *versus* interstitial velocity for glucose. ● = 278 K; △ = 303 K; ◇ = 333 K.

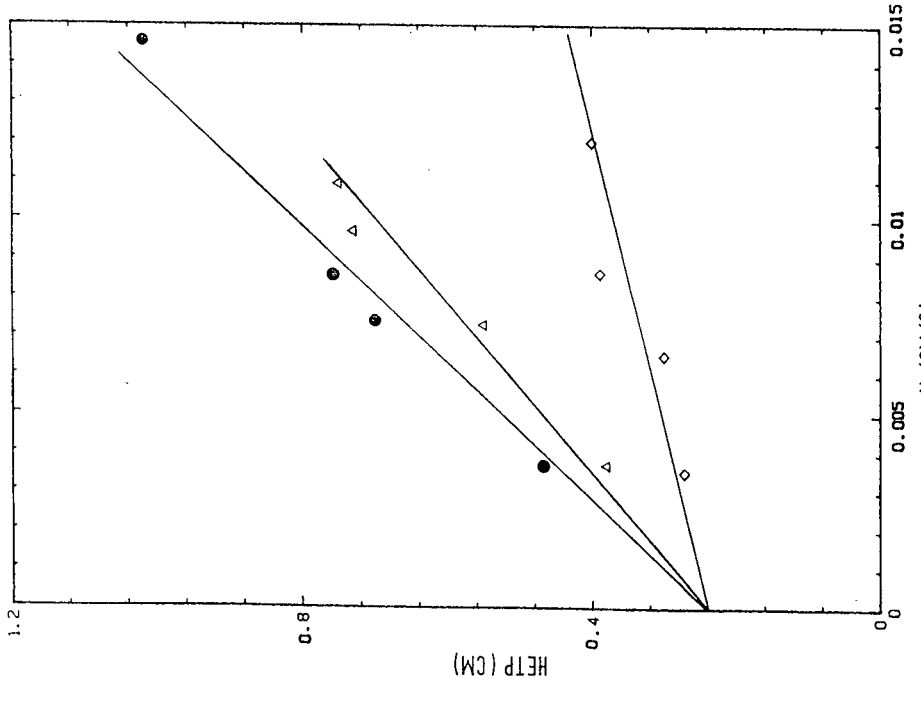

Fig. 9. HETP *versus* interstitial velocity for maltose. ● = 278 K; △ = 303 K; ◇ = 333 K.

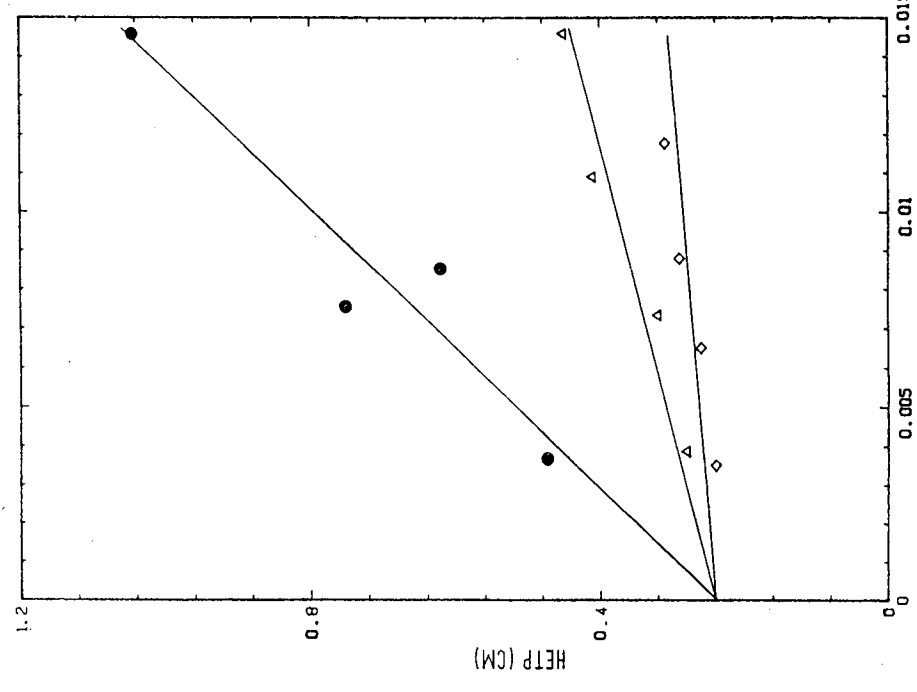

Fig. 10. HETP *versus* intersitial velocity for maltotriose. ● = 278 K; △ = 303 K; ◇ = 333 K.

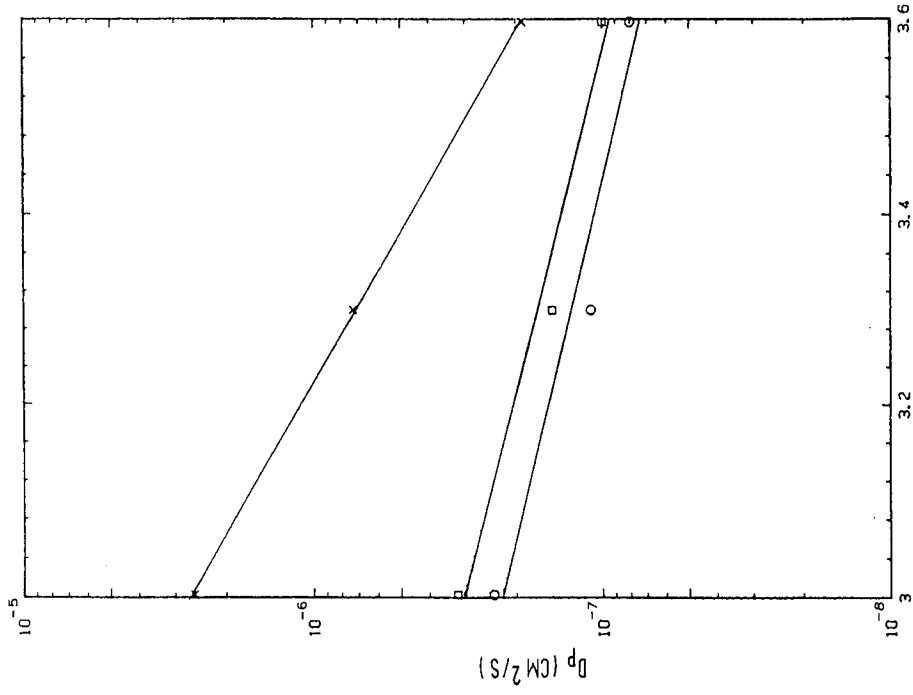

Fig. 11. D_p *versus* inverse of temperature. × = Glucose; □ = maltose; ○ = maltotriose.

TABLE I
EQUILIBRIUM CONSTANTS AND DIFFUSIVITY VALUES

Sugar	*K*	D_p (10^{-6} cm^2/s)		
		278 K	*303 K*	*333 K*
Glucose	0.34	0.19	0.73	2.58
Maltose	0.25	0.10	0.15	0.32
Maltotriose	0.21	0.08	0.11	0.24

term is constant, the plot should be linear with a slope equal to

$$\left(\frac{2\varepsilon}{1-\varepsilon}\right)\left(\frac{R_p}{3k_f}+\frac{R_p^2}{15\varepsilon_p D_p}\right)\left[1+\frac{\varepsilon}{(1-\varepsilon)K}\right]^{-2}$$

and a y-intercept of $2D_L/v$. The data conform more or less to this pattern, despite the presence of some scatter. As it was established in the experiments with ^2H_2O that the value of $2D_L/v$ is 0.24 cm, the straight lines were best fitted with the intercept fixed at 0.24 cm. The values of D_p were then calculated from the slopes of these lines and the results are summarized in Table I. To confirm the assumption that $R_p/3k_f \ll R_p^2/15\varepsilon_p D_p$, k_f values were calculated using the correlation of Wilson and Geankoplis[4]:

$$k_f = \frac{1.09}{\varepsilon} \cdot Re^{0.3} Sc^{0.33} \tag{3}$$

where $Sc = \mu/\rho_f D_m$, for $0.0015 < Re < 55$. The D_m values were obtained from the correlation of Wilke and Chang[7]. For illustrative purposes, for glucose at 303 K, $R_p/3k_f = 8.0$ and $R_p^2/15\varepsilon_p D_p = 116.0$. Hence the former assumption that the mass transfer contribution is mainly due to pore diffusion is valid.

The pore diffusivity of glucose obtained in this experiment at 303 K is $0.73 \cdot 10^{-6}$ cm^2/s (with a mean pore diameter of 27 Å). This value is comparable to the result obtained by Satterfield *et al.*[8], of $1.01 \cdot 10^{-6}$ cm^2/s at 298 K with a mean pore diameter of 32 Å. The pore diffusivities decrease with increasing size of the carbohydrates at all temperatures. This again illustrates the fact that size and molecular weight serve as hindrances to the easy diffusion of the molecules into the pores.

The D_p values increased with increase in temperature for each of the sugars. The plot of log D_p *vs.* $1/T$ is shown in Fig. 11. The activation energies, E, were calculated from the slopes of the lines and were 5.2, 2.54 and 1.58 kcal/mol for glucose, maltose and maltotriose, respectively.

CONCLUSION

Moment analysis on the output curves generally provided a good estimate of the dimensionless equilibrium constant, K, and other parameters such as HETP and pore diffusivity. The K and D_p values decreased with increase in molecular size, the D_p

values increased with increase in temperature and the K values were independent of temperature.

These experiments serve only as a preliminary investigation of the mass transfer characteristics of sugars in a packed column. They were conducted under conditions such that the resistances offered by certain transport phenomena are negligible. This study has indicated that separation based on size is possible with this packing material.

SYMBOLS

c fluid phase concentration (mol/cm^3)
D_c intracrystalline diffusivity (cm^2/s)
D_L axial dispersion
D_m moleular diffusivity (cm^2/s)
D_p pore diffusivity (cm^2/s)
E diffusional activation energy (cal/mol)
k_f external film mass transfer coefficient (cm/s)
K adsorption equilibrium constant [(mol/cm^3 in particle)/(mol/cm^3 in solution)]
L length of packed column (cm)
R_p pellet radius (cm)
t time (s)
V interstitial liquid velocity (cm/s)
v superficial velocity (cm/s)
μ mean response of curve (cm)
σ^2 variance of response curve (cm^2)
ε voidage of bed
ε_p porosity of adsorbent particle
ΔH enthalpy change for sorption
Re Reynolds number
Sc Schmidt nuber
T Temperature (K)

REFERENCES

1 P. Schneider and J. M.Smith, *AIChE J.*, 14 (1968) 762.
2 H. W. Haynes and P. N. Sarma, *AIChE J.*, 19 (1973) 1043.
3 N. Wakao and T. Funazkri, *Chem. Eng. Sci.*, 33 (1978) 1375.
4 E. J. Wilson and C. J. Geankoplis, *Ind. Eng. Chem. Fundam.*, 5 (1966) 9.
5 C. B. Ching and D.M. Ruthven, *Zeolite*, 8 (1988) 68.
6 D. M. Ruthven, *Principles of Adsorption and Adsorption Processes*, Wiley-Interscience, New York, 1984.
7 C. R. Wilke and Chang, *AIChE J.*, 1 (1955) 264.
8 C. N. Satterfield, C. K. Colton and W. H. Pitcher, *AIChE J.*, 19 (1973) 628.

Journal of Chromatography, 463 (1989) 271–280
Elsevier Science Publishers B.V., Amsterdam — Printed in The Netherlands

CHROM. 21 081

CALCULATION OF PROGRAMMED TEMPERATURE GAS CHROMATOGRAPHY CHARACTERISTICS FROM ISOTHERMAL DATA

II. PREDICTED RETENTION TIMES AND ELUTION TEMPERATURES

E. E. AKPORHONOR*, S. LE VENT* and D. R. TAYLOR
Department of Chemistry, University of Manchester Institute of Science and Technology, Manchester M60 1QD (U.K.)
(First received August 3rd, 1988; revised manuscript received November 1st, 1988)

SUMMARY

Theoretical procedures, described in Part I, *J. Chromatogr.*, 405 (1987) 67–76, for predicting retention times and elution temperatures in programmed temperature gas chromatography from isothermal data are experimentally tested for a number of compounds under a range of experimental conditions. In general, and taking into full consideration random error predictions, agreement is reasonably satisfactory.

INTRODUCTION

Part I[1] describes theoretical and computational procedures for predicting programmed-temperature gas chromatography (PTGC) characteristics using, as input information, experimental data for the same column and carrier gas pressure differential but obtained under isothermal gas chromatographic (IGC) conditions. Of the various types of PTGC data, perhaps the most important (for reasons presented in Part I[1]) are retention times and elution temperatures. These have been predicted for a range of organic compounds (*n*-alkanes, monocyclic aromatic hydrocarbons and ketones) on a capillary column under a variety of programmed-temperature conditions. The present paper describes the comparison of theoretical and experimental results for several values of (a) column temperature at sample injection (initial temperature), and (b) rate of column heating (heating rate); the temperature programme corresponds in each case to a linear increase of temperature with time (single linear ramp). Random error in (isothermal) input data (in some cases derived by standard statistical methodology from graphical plots, in others based on manufacturer's specifications, in others estimated) has been incorporated into the calculations to make comparison of theory and experiment more meaningful.

A further manuscript[2], to be submitted for publication, will make similar comparisons for retention indices and will compare two kinds of equivalent

* Present address: Chemistry Department, Bendel State University, Ekpoma, Bendel State, Nigeria.

0021-9673/89/$03.50

temperatures[1] with various averages of initial and elution temperatures and with the Giddings significant temperature[3].

EXPERIMENTAL

The gas chromatograph used was a Hewlett-Packard (HP) Model 5792A (with facilities for both IGC and PTGC operation) fitted with an HP 7671A automatic sampler. It was operated with an HP Ultra 2 capillary column (25 m × 0.2 mm I.D. fused-silica coated with a 0.33-μm layer of crossed-linked 5% phenylmethylsilicone) with split mode injection (0.5% of the sample entering the column) and a hydrogen flame ionisation detector. The flow of nitrogen carrier gas was controlled by a constant mass-flow device and a column pressure regulator; column flow-rate was of the order of 1 cm^3 min^{-1}, but this varied with column temperature.

Compounds studied were purchased from Aldrich, Eastman-Kodak, BDH or Fluka; they were of high purity (98–99.9%) and used without further purification. For chromatographic purposes, solutions were made by dissolving 50 mm^3 of each compound in 25 cm^3 of dichloromethane, and preset volumes of 1 mm^3 were injected, either manually or via the automatic sampler, into the chromatograph. A list of compounds studied is given in the first column of Table I.

Twelve replicate isothermal runs were performed for each compound at 393.16, 403.16, 413.16 and 423.16 K. Programmed temperature runs were conducted under a variety of combinations of initial absolute temperature, T_i (oven temperature at sample injection), and oven heating rate, k_3 (the symbolism corresponds to that used in

TABLE I

LIST OF COMPOUNDS STUDIED AND THEIR ISOTHERMAL RETENTION TIMES

Values in parenthesis are 95% confidence deviations.

Compound	*Retention time/s at temperature/K*			
	393.16	*403.16*	*413.16*	*423.16*
n-Nonane	136.6 (0.0)	126.7 (0.0)	119.5 (0.0)	114.7 (0.0)
n-Decane	177.8 (0.0)	156.4 (0.1)	141.8 (0.0)	131.2 (0.0)
n-Undecane	250.9 (0.1)	207.8 (0.1)	178.3 (0.0)	158.1 (0.0)
n-Dodecane	379.4 (0.1)	295.5 (0.1)	239.3 (0.0)	201.5 (0.0)
n-Tridecane	609.1 (0.0)	447.4 (0.2)	342.2 (0.0)	272.8 (0.0)
n-Tetradecane	1011.5 (0.1)	706.2 (0.4)	512.4 (0.2)	387.7 (0.1)
n-Pentadecane	1720.6 (0.1)	1147.6 (0.1)	795.0 (0.0)	573.4 (0.2)
Nonan-5-one	228.9 (0.0)	192.8 (0.1)	168.1 (0.1)	151.0 (0.1)
Propiophenone	344.6 (0.1)	275.8 (0.1)	228.6 (0.0)	196.3 (0.1)
Butyrophenone	505.6 (0.1)	385.9 (0.1)	305.4 (0.1)	250.7 (0.1)
Valerophenone	827.3 (0.0)	599.3 (0.2)	450.3 (0.1)	351.5 (0.1)
Hexanophenone	1393.1 (0.2)	963.8 (0.3)	690.3 (0.2)	513.7 (0.1)
Isopropyl benzoate	405.9 (0.1)	316.6 (0.1)	256.1 (0.1)	215.2 (0.1)
2-Phenylpropane	151.3 (0.1)	138.2 (0.0)	128.8 (0.0)	122.2 (0.0)
1-Phenylpropane	163.6 (0.1)	147.3 (0.0)	135.6 (0.0)	127.4 (0.1)
1-Phenylbutane	224.9 (0.0)	191.6 (0.1)	168.1 (0.1)	151.8 (0.0)
1-Phenylpentane	330.7 (0.1)	265.8 (0.1)	221.0 (0.1)	190.4 (0.0)
1-Phenyloctane	1430.5 (0.0)	984.9 (0.1)	701.9 (0.2)	519.9 (0.1)

TABLE II

INTERCEPTS ($\ln k_1$) AND GRADIENTS (k_2) OF LEAST SQUARES PLOTS OF $\ln k'$ AGAINST T^{-1}

Values in parenthesis are standard deviations.

Compound	*ln* k_1	k_2/K	*Covariance*
n-Nonane	−11.12 (0.06)	4190 (40)	−2.4
n-Decane	−11.80 (0.06)	4690 (20)	−1.2
n-Undecane	−12.39 (0.03)	5140 (10)	−0.3
n-Dodecane	−13.08 (0.02)	5640 (10)	−0.2
n-Tridecane	−13.62 (0.10)	6070 (50)	−5.0
n-Tetradecane	−15.44 (0.60)	7040 (200)	−120
n-Pentadecane	−15.01 (0.08)	7070 (30)	−2.4
Nonan-5-one	−12.09 (0.02)	5000 (10)	−0.2
Propiophenone	−12.07 (0.04)	5190 (20)	−0.8
Butyrophenone	−12.56 (0.04)	5570 (20)	−0.8
Valerophenone	−13.26 (0.04)	6070 (20)	−0.8
Hexanophenone	−14.00 (0.05)	6580 (20)	−1.0
Isopropyl benzoate	−12.58 (0.02)	5470 (10)	−0.2
2-Phenylpropane	−10.76 (0.07)	4150 (30)	−2.1
1-Phenylpropane	−10.89 (0.04)	4260 (20)	−0.8
1-Phenylbutane	−11.46 (0.08)	4710 (30)	−2.4
1-Phenylpentane	−12.13 (0.09)	5190 (30)	−2.7
1-Phenyloctane	−13.98 (0.05)	6580 (20)	−1.0

TABLE III

COMPARISON OF OBSERVED AND PREDICTED PTGC RETENTION TIMES AT A HEATING RATE OF 2.00 K min^{-1}

Compound	*Retention time/K*					
	Initial temperature 333.16 K			*Initial temperature 393.16 K*		
	*Predicted**		*Observed***	*Predicted**		*Observed***
	(1)	*(2)*		*(1)*	*(2)*	
n-Nonane	334 (13)	332 (13)	360.0 (0.2)	133 (2)	133 (2)	133.2 (0.1)
n-Decane	567 (2)	564 (3)	594.0 (0.1)	170 (1)	171 (1)	169.8 (0.1)
n-Undecane	875 (3)	872 (2)	900.4 (0.1)	229 (1)	230 (1)	230.4 (0.1)
n-Dodecane	1270 (6)	1268 (6)	1296.4 (0.1)	327 (1)	329 (1)	326.4 (0.1)
n-Tridecane	1666 (23)	1666 (23)	1680.4 (0.1)	466 (8)	468 (8)	468.6 (0.1)
n-Tetradecane	2149 (52)	2150 (51)	2087.9 (0.1)	677 (45)	679 (44)	661.2 (0.1)
n-Pentadecane	2480 (9)	2483 (9)	2466.4 (0.1)	906 (4)	910 (4)	901.2 (0.1)
Nonan-5-one	826 (5)	823 (4)	828.4 (0.1)	222 (1)	223 (1)	213.0 (0.1)
Propiophenone	1124 (10)	1122 (10)	1140.2 (0.1)	303 (2)	304 (2)	303.6 (0.1)
Butyrophenone	1471 (11)	1470 (10)	1500.3 (0.0)	411 (3)	413 (3)	414.0 (0.1)
Valerophenone	1904 (11)	1905 (11)	1911.8 (0.0)	591 (4)	593 (4)	589.2 (0.1)
Hexanophenone	2314 (8)	2317 (8)	2321.9 (0.1)	814 (2)	818 (1)	816.2 (0.1)
Isopropyl benzoate	1286 (6)	1284 (6)	1320.4 (0.1)	344 (1)	345 (1)	345.8 (0.0)
2-Phenylpropane	394 (5)	392 (5)	413.8 (0.2)	147 (1)	148 (0)	146.6 (0.1)
1-Phenylpropane	450 (6)	447 (6)	480.3 (0.2)	157 (1)	158 (1)	157.8 (0.0)
1-Phenylbutane	730 (4)	727 (4)	774.2 (0.1)	210 (1)	211 (1)	210.6 (0.1)
1-Phenylpentane	1089 (5)	1087 (4)	1134.4 (0.1)	291 (3)	293 (3)	293.4 (0.1)
1-Phenyloctane	2328 (8)	2331 (8)	2340.1 (0.1)	824 (2)	827 (1)	829.2 (0.1)

* Columns (1) and (2) refer to calculations using eqns. 1 and 2, respectively, for the column dead time dependence upon temperature. Values in parentheses are estimated standard deviations.

** Values in parentheses are 95% confidence deviations.

Part I[1]); the assumption is made in this work that the column temperature exactly matches that of the oven. All combinations of T_i of 333.16, 353.16, 373.16 and 393.16 K, and k_3 of 1.00, 2.00, 3.00, 5.00, 7.00, 10.00, 12.00 and 15.00 K min^{-1} have been used for each of twelve replicate runs on each compound.

Data acquisition was accomplished by a Trivector Trilab 2500 data system connected to the chromatograph via an A/D converter. A BBC Model B microcomputer, interfaced to the data system, was used to perform calculations on the acquired data via BASIC programs.

EXPERIMENTAL AND PREDICTED RESULTS

Mean retention times t_R for isothermal runs are presented in Table I, together with 95% confidence deviations (in parentheses). Times for the seven *n*-alkanes have been used to evaluate column dead times, t_0, at the four temperatures, on the BBC Computer, by the method of Al-Thamir *et al.*[4]. These column dead times were then used to (a) calculate capacity factors, k', from the isothermal retention times ($k' =$

TABLE IV

COMPARISON OF OBSERVED AND PREDICTED PTGC RETENTION TIMES AT A HEATING RATE OF 7.00 K min^{-1}

Compound	*Retention time/s*					
	Initial temperature 333.16 K			*Initial temperature 393.16 K*		
	*Predicted**		*Observed***	*Predicted**		*Observed***
	(1)	*(2)*		*(1)*	*(2)*	
n-Nonane	263 (7)	262 (7)	270.0 (0.0)	128 (2)	128 (2)	127.4 (0.1)
n-Decane	379 (1)	378 (1)	378.0 (0.0)	158 (1)	158 (1)	155.9 (0.1)
n-Undecane	503 (1)	503 (1)	508.0 (0.1)	200 (1)	201 (0)	199.4 (0.1)
n-Dodecane	639 (2)	640 (2)	636.0 (0.1)	261 (1)	263 (1)	259.2 (0.1)
n-Tridecane	765 (6)	766 (6)	763.8 (0.1)	335 (3)	337 (4)	333.6 (0.1)
n-Tetradecane	894 (24)	896 (24)	884.4 (0.1)	421 (23)	423 (23)	421.8 (0.0)
n-Pentadecane	1004 (2)	1005 (2)	999.0 (0.1)	516 (2)	518 (2)	516.0 (0.1)
Nonan-5-one	487 (2)	487 (2)	474.0 (0.2)	196 (1)	197 (0)	187.4 (0.1)
Propiophenone	600 (3)	601 (3)	603.6 (0.1)	250 (1)	251 (1)	247.8 (0.1)
Butyrophenone	715 (3)	716 (3)	717.0 (0.1)	312 (2)	313 (1)	312.0 (0.1)
Valerophenone	847 (3)	849 (2)	845.4 (0.1)	398 (2)	400 (2)	396.0 (0.1)
Hexanophenone	966 (1)	968 (1)	966.0 (0.2)	489 (1)	491 (1)	492.0 (0.0)
Isopropyl benzoate	651 (2)	652 (1)	654.0 (0.0)	273 (1)	274 (1)	273.0 (0.1)
2-Phenylpropane	298 (3)	297 (2)	304.2 (0.0)	140 (0)	140 (0)	139.2 (0.1)
1-Phenylpropane	327 (3)	327 (3)	336.0 (0.0)	148 (1)	148 (1)	147.8 (0.1)
1-Phenylbutane	454 (1)	454 (1)	456.0 (0.0)	188 (1)	189 (1)	187.2 (0.1)
1-Phenylpentane	587 (3)	587 (2)	589.8 (0.0)	242 (2)	243 (2)	241.8 (0.1)
1-Phenyloctane	971 (1)	973 (1)	968.4 (0.1)	493 (1)	495 (1)	495.0 (0.1)

* Columns (1) and (2) refer to calculations using eqns. 1 and 2, respectively, for the column dead time dependence upon temperature. Values in parentheses are estimated standard deviations.

** Values in parentheses are 95% confidence deviations.

TABLE V

COMPARISON OF OBSERVED AND PREDICTED PTGC RETENTION TIMES AT A HEATING RATE OF 15.00 K min^{-1}

Compound	*Retention time/s*					
	Initial temperature 333.16 K			*Initial temperature 393.16 K*		
	*Predicted**		*Observed***	*Predicted**		*Observed***
	(1)	*(2)*		*(1)*	*(2)*	
n-Nonane	211 (4)	211 (4)	212.8 (0.1)	122 (1)	123 (1)	121.0 (0.1)
n-Decane	276 (1)	277 (1)	274.7 (0.1)	145 (1)	145 (1)	142.2 (0.1)
n-Undecane	341 (1)	342 (0)	339.6 (0.0)	174 (1)	175 (1)	171.6 (0.1)
n-Dodecane	408 (1)	409 (1)	403.7 (0.1)	212 (1)	213 (0)	209.1 (0.1)
n-Tridecane	469 (3)	470 (3)	465.5 (0.1)	255 (2)	256 (2)	252.7 (0.1)
n-Tetradecane	525 (14)	526 (14)	524.1 (0.1)	297 (14)	298 (14)	298.3 (0.1)
n-Pentadecane	581 (2)	582 (2)	579.8 (0.1)	349 (2)	350 (1)	349.1 (0.1)
Nonan-5-one	334 (1)	334 (1)	323.5 (0.1)	171 (1)	172 (0)	164.2 (0.1)
Propiophenone	393 (1)	394 (1)	390.4 (0.0)	207 (1)	208 (1)	204.4 (0.1)
Butyrophenone	449 (1)	450 (1)	446.0 (0.2)	244 (1)	245 (1)	241.5 (0.1)
Valerophenone	512 (1)	513 (1)	508.8 (0.1)	292 (1)	293 (1)	289.7 (0.1)
Hexanophenone	567 (1)	569 (1)	568.2 (0.0)	338 (1)	340 (1)	340.3 (0.0)
Isopropyl benzoate	417 (1)	418 (1)	414.2 (0.1)	221 (1)	222 (0)	218.4 (0.1)
2-Phenylpropane	234 (1)	233 (1)	233.3 (0.2)	132 (0)	133 (0)	128.8 (0.1)
1-Phenylpropane	250 (2)	250 (2)	251.7 (0.1)	138 (1)	139 (0)	135.3 (0.1)
1-Phenylbutane	319 (1)	319 (0)	317.8 (0.0)	167 (1)	168 (0)	163.0 (0.1)
1-Phenylpentane	386 (2)	387 (2)	383.6 (0.1)	202 (2)	203 (1)	198.3 (0.1)
1-Phenyloctane	570 (1)	571 (1)	569.4 (0.0)	341 (1)	342 (1)	339.1 (0.1)

* Columns (1) and (2) refer to calculations using eqns. 1 and 2, respectively, for the column dead time dependence upon temperature. Values in parentheses are estimated standard deviations.

** Values in parentheses are 95% confidence deviations.

$t_R/t_0 - 1$), and (b) determine least squares linear relationships between t_0 and absolute temperature T (assumed free of measurement error) and between t_0 and the square root of T (together with the standard deviation of the pairs of coefficients and their covariances). The equations obtained for (b) were

$$t/\mathrm{s} = 22.96\ (1.86) + 0.1525\ (0.0046)T/\mathrm{K}; \qquad \text{covariance } -0.0085 \qquad (1)$$

$$t/\mathrm{s} = -46.4\ (3.6) + 6.54\ (0.179)\sqrt{T/\mathrm{K}}; \qquad \text{covariance } -0.64 \qquad (2)$$

(statistical deviations, standard or 95% confidence, are given in parentheses throughout the paper). On the basis of an expectation that ln k' is a linear function of T^{-1} (see Part I[1]), least squares methodology was used to obtain regression coefficients for each of the compounds studied, together with standard deviations and covariance. These values are presented in Table II; in conformation with the notation used in Part I, the constant and the multiplier of T^{-1} are designated ln k_1 and k_2.

TABLE VI

COMPARISON OF OBSERVED AND PREDICTED PTGC ELUTION TEMPERATURES AT A HEATING RATE OF 2.00 K min^{-1}

Compound	*Elution temperature/K*					
	Initial temperature 333.16 K			*Initial temperature 393.16 K*		
	*Predicted**		*Observed***	*Predicted**		*Observed***
	(1)	*(2)*		*(1)*	*(2)*	
n-Nonane	344.3 (0.5)	344.2 (0.4)	345.0	397.6 (0.1)	397.6 (0.1)	397.4
n-Decane	352.1 (0.1)	352.0 (0.1)	353.0	398.8 (0.1)	398.9 (0.1)	398.7
n-Undecane	362.3 (0,1)	362.2 (0.1)	363.8	400.8 (0.1)	400.8 (0.1)	400.7
n-Dodecane	375.5 (0.2)	375.4 (0.2)	376.4	404.1 (0.1)	404.1 (0.1)	403.9
n-Tridecane	388.7 (0.8)	388.7 (0.8)	389.6	408.7 (0.3)	408.8 (0.3)	408.6
n-Tetradecane	404.8 (1.7)	404.8 (1.7)	402.7	415.7 (1.5)	415.8 (1.5)	415.0
n-Pentadecane	415.8 (0.2)	415.9 (0.1)	415.4	423.4 (0.2)	423.5 (0.2)	423.0
Nonan-5-one	360.7 (0.2)	360.6 (0.2)	360.6	400.6 (0.1)	400.6 (0.1)	400.1
Propiophenone	370.6 (0.3)	370.5 (0.3)	371.7	403.3 (0.1)	403.3 (0.1)	403.0
Butyrophenone	382.2 (0.4)	382.2 (0.3)	383.1	406.9 (0.1)	406.9 (0.1)	406.7
Valerophenone	396.6 (0.3)	396.7 (0.3)	396.9	412.8 (0.2)	412.9 (0.2)	412.6
Hexanophenone	410.3 (0.1)	410.3 (0.1)	410.3	420.3 (0.1)	420.4 (0.1)	420.2
Isopropyl benzoate	376.0 (0.2)	376.0 (0.2)	377.3	404.6 (0.1)	404.7 (0.1)	404.5
2-Phenylpropane	346.3 (0.2)	346.3 (0.2)	346.9	398.1 (0.0)	398.1 (0.0)	397.9
1-Phenylpropane	348.2 (0.2)	348.1 (0.2)	349.1	398.4 (0.1)	398.4 (0.0)	398.2
1-Phenylbutane	357.5 (0.2)	357.4 (0.2)	358.8	400.2 (0.1)	400.2 (0.1)	400.0
1-Phenylpentane	369.5 (0.2)	369.4 (0.2)	370.8	402.9 (0.1)	402.9 (0.1)	402.7
1-Phenyloctane	410.8 (0.1)	410.8 (0.1)	411.0	420.6 (0.1)	420.7 (0.1)	420.6

* Columns (1) and (2) refer to calculations using eqns. 1 and 2, respectively, for the column dead time dependence upon temperature. Values in parentheses are estimated standard deviations.

** 95% Confidence deviations are all less than 0.1.

Using the theoretical and computational techniques described in Part I, retention times, t_R, and elution temperatures, T_e (with their standard deviations) have been calculated for the various programmed temperature conditions given above; initial temperature standard deviations have been taken as 0.03 K (in accordance with manufacturer's specifications) and heating rate standard deviations have been estimated as 0.01 K min^{-1}. Comparison of these predictions and corresponding values obtained by experiment (with 95% confidence deviations for retention times) are shown in Tables III–VIII for a selection of PTGC experimental conditions; a comprehensive set of tables covering all 32 combinations of experimental conditions may be obtained from the authors.

The effect of *individual* random errors in the input data for the calculations has been analysed. Four separate factors have been considered (a) standard deviations and covariances of the pairs of coefficients in the column dead time *vs.* temperature relationships, (b) initial temperature standard deviation, (c) heating rate standard deviation, (d) standard deviations and covariance of the pair of coefficients in the $\ln k'$ *vs.* T^{-1} relationship. *Individual* resultant contributions to predicted standard devia-

TABLE VII

COMPARISON OF OBSERVED AND PREDICTED PTGC ELUTION TEMPERATURES AT A HEATING RATE OF 7.00 K min^{-1}

Compound	*Elution temperature/K*					
	Initial temperature 333.16 K			*Initial temperature 393.16 K*		
	*Predicted**		*Observed***	*Predicted**		*Observed***
	(1)	*(2)*		*(1)*	*(2)*	
n-Nonane	363.8 (0.9)	363.7 (0.9)	364.8	408.1 (0.2)	408.1 (0.2)	407.9
n-Decane	377.4 (0.1)	377.3 (0.2)	377.8	411.6 (0.1)	411.6 (0.1)	411.2
n-Undecane	391.9 (0.1)	391.9 (0.1)	392.3	416.5 (0.1)	416.6 (0.1)	416.2
n-Dodecane	407.7 (0.2)	407.8 (0.2)	407.5	423.6 (0.1)	423.8 (0.1)	423.1
n-Tridecane	422.4 (0.7)	422.5 (0.7)	422.1	432.3 (0.4)	432.5 (0.4)	431.9
n-Tetradecane	437.5 (2.8)	437.7 (2.8)	436.2	442.3 (2.6)	442.5 (2.6)	442.0
n-Pentadecane	450.2 (0.2)	450.5 (0.2)	449.6	453.4 (0.3)	453.6 (0.2)	453.0
Nonan-5-one	390.0 (0.2)	390.0 (0.2)	388.7	416.0 (0.1)	416.1 (0.1)	414.9
Propiophenone	403.2 (0.4)	403.2 (0.4)	403.3	422.3 (0.2)	422.4 (0.1)	421.9
Butyrophenone	416.6 (0.3)	416.7 (0.3)	416.4	429.5 (0.2)	429.7 (0.2)	429.1
Valerophenone	432.0 (0.3)	432.2 (0.3)	431.3	439.6 (0.2)	439.8 (0.2)	439.2
Hexanophenone	445.9 (0.1)	446.1 (0.0)	445.6	450.2 (0.1)	450.0 (0.1)	450.3
Isopropyl benzoate	409.1 (0.2)	409.2 (0.2)	409.3	425.0 (0.1)	425.1 (0.1)	424.8
2-Phenylpropane	368.0 (0.3)	367.9 (0.3)	368.5	409.5 (0.1)	409.5 (0.0)	409.2
1-Phenylpropane	371.4 (0.3)	371.3 (0.4)	372.3	410.4 (0.1)	410.5 (0.1)	410.2
1-Phenylbutane	386.1 (0.1)	386.1 (0.1)	386.8	415.1 (0.1)	415.2 (0.1)	414.8
1-Phenylpentane	401.6 (0.3)	401.7 (0.3)	401.9	421.4 (0.2)	421.5 (0.2)	421.2
1-Phenyloctane	446.4 (0.1)	446.7 (0.1)	446.1	450.7 (0.1)	450.9 (0.1)	450.7

* Columns (1) and (2) refer to calculations using eqns. 1 and 2, respectively, for the column dead time dependence upon temperature. Values in parentheses are estimated standard deviations.

** 95% Confidence deviations are all less than 0.1.

tions of retention times and elution temperatures (together with total standard deviations) are presented in Tables IX and X for two compounds *n*-decane and *n*-tetradecane, using the column dead time eqn. 1 (results for eqn. 2 are very similar) and four PTGC experimental conditions. The latter compound has very large contributions to (d), as indicated in Table II; the former is much more "typical" of the compounds studied here.

DISCUSSION

The results presented in Tables IX and X indicate the possibility of a substantial prediction error contribution from the assumption of a linear relationship between ln k' and T^{-1}, but the case of *n*-tetradecane is exceptional (as Table II indicates) in the compounds studied here. Generally, there is no clear general predominance of one particular contributions to overall predicted error, although there may be some uncertainty about the chosen standard deviations for initial temperature and heating rate, particularly for the latter. The overall fractional errors for predicted elution

TABLE VIII

COMPARISON OF OBSERVED AND PREDICTED PTGC ELUTION TEMPERATURES AT A HEATING RATE OF 15.00 K min^{-1}

Compound	*Elution temperature/K*					
	Initial temperature 333.16 K			*Initial temperature 393.16 K*		
	*Predicted**		*Observed***	*Predicted**		*Observed***
	(1)	*(2)*		*(1)*	*(2)*	
n-Nonane	385.9 (1.1)	385.8 (1.1)	386.2	423.6 (0.3)	423.8 (0.3)	423.2
n-Decane	402.2 (0.2)	402.3 (0.2)	401.7	429.3 (0.2)	429.5 (0.1)	428.5
n-Undecane	418.4 (0.2)	418.6 (0.1)	417.9	436.6 (0.1)	436.9 (0.1)	435.9
n-Dodecane	435.1 (0.2)	435.4 (0.1)	433.9	446.2 (0.1)	446.5 (0.1)	445.3
n-Tridecane	450.3 (0.6)	450.6 (0.6)	449.4	457.0 (0.4)	457.3 (0.4)	456.2
n-Tetradecane	464.3 (3.6)	464.6 (3.6)	464.0	467.5 (3.5)	467.8 (3.4)	467.8
n-Pentadecane	478.3 (0.4)	478.7 (0.3)	477.9	480.4 (0.4)	480.7 (0.4)	480.3
Nonan-5-one	416.6 (0.2)	416.7 (0.2)	413.9	436.0 (0.1)	436.2 (0.1)	434.2
Propiophenone	431.4 (0.4)	431.6 (0.3)	430.6	444.9 (0.2)	445.2 (0.2)	444.3
Butyrophenone	445.4 (0.3)	445.7 (0.3)	444.5	454.2 (0.2)	454.5 (0.2)	453.6
Valerophenone	461.1 (0.3)	461.4 (0.2)	460.2	466.1 (0.2)	466.4 (0.2)	465.6
Hexanophenone	475.0 (0.2)	475.3 (0.1)	475.1	477.8 (0.2)	478.1 (0.2)	478.3
Isopropyl benzoate	437.3 (0.2)	437.5 (0.1)	436.6	448.3 (0.1)	448.6 (0.1)	447.6
2-Phenylpropane	391.6 (0.3)	391.5 (0.3)	391.3	426.1 (0.1)	426.3 (0.0)	425.3
1-Phenylpropane	395.8 (0.4)	395.7 (0.4)	395.9	427.6 (0.1)	427.8 (0.1)	427.0
1-Phenylbutane	412.9 (0.1)	413.0 (0.0)	412.6	434.8 (0.2)	435.1 (0.2)	433.9
1-Phenylpentane	429.6 (0.4)	429.8 (0.4)	429.0	443.7 (0.4)	444.0 (0.4)	442.7
1-Phenyloctane	475.6 (0.2)	475.9 (0.1)	475.4	478.3 (0.2)	478.7 (0.1)	478.0

* Columns (1) and (2) refer to calculations using eqns. 1 and 2, respectively, for the column dead time dependence upon temperature. Values in parentheses are estimated standard deviations.

** 95% Confidence deviations are all less than 0.1.

temperatures are considerably smaller than those for predicted retention times, but this is as expected on the basis of the interrelationship between these two quantities, *viz.*, $T_e - T_i = k_3 t_R$. On the basis of error-free k_3, the fractional errors in t_R and $T_e - T_i$ will be equal, and the fractional error in T_e will be a fraction $(1 - T_i/T_e)$ of this.

The agreement between predicted and experimental parameters as indicated by the selected data of Tables III–VIII (and by the more comprehensive data available to the authors) is generally reasonably satisfactory (particularly bearing in mind the predicted standard errors; generally, errors in the experimental PTGC parameters can be discounted in comparison). In some cases, *absolute* differences are substantial but these normally apply to high retention times; *fractional* differences [(experimental − predicted)/experimental] are probably a more realistic indicator of the quality of the predictions. Two generalisations have been made: (a) where there is a substantial difference, observed parameters are usually larger than predicted ones; (b) fractional differences generally decrease with increasing initial temperature and with increasing heating rate.

The difference in pairs of predictions for the two column dead time formulae

TABLE IX

INDIVIDUAL CONTRIBUTIONS TO STANDARD DEVIATIONS OF RETENTION TIMES

Compound	*Heating rate/ K min*$^{-1}$	*Retention time error/s**									
		T_i = 333.16 K					T_i = 393.16 K				
		a	*b*	*c*	*d*	*Total*	*a*	*b*	*c*	*d*	*Total*
n-Decane	2.00	1.8	0.4	0.7	0.7	2.1	0.4	0.1	0.0	0.8	0.9
n-Decane	10.00	0.6	0.1	0.1	0.7	1.0	0.3	0.0	0.0	0.6	0.7
n-Tetradecane	2.00	1.9	0.9	7.3	51.0	51.6	1.2	0.5	1.0	45.4	45.4
n-Tetradecane	10.00	0.6	0.2	0.5	18.3	18.3	0.6	0.1	0.2	18.5	18.5

* Standard error contributions from: (a) column dead time–temperature relationship, (b) initial temperature, (c) heating rate, (d) ln(capacity factor)–temperature relationship.

(eqns. 1 and 2) is generally small, never more than 4 s for retention times, and well within predictive error, suggesting that two-coefficient formulae are adequate. On the other hand, the formulae have been obtained (because of the experimental necessity of obtaining reasonably short IGC retention times) over a rather different temperature range (393–423 K) than those covered in PTGC experiments; the same point in fact applies to coefficients in the ln k' *vs.* T^{-1} linear relationships. This might well be a contributory factor to the differences between experimental and predicted parameters. Other contributory factors might be: (a) inadequacy of the methodology used[4] to determine column dead times, this being formally dependent upon a linear relationship between molar Gibbs energy of solution in the stationary phase and carbon number of the *n*-alkanes; (b) variation of molar enthalpies and entropies of solution with temperature, causing some deviation from linearity of ln k' and T^{-1} (such a temperature dependence has in fact been considered by others[5]); (c) a temperature time lag between column and oven (see, *e.g.*, ref. 6), although this factor will clearly be more significant for packed columns; (d) non-instantaneous transfer of solute from injection port to column and non-instantaneous cooling from port to initial column temperature.

TABLE X

INDIVIDUAL CONTRIBUTIONS TO STANDARD DEVIATIONS OF ELUTION TEMPERATURES

Compound	*Heating rate/ K min*$^{-1}$	*Elution temperature error/K**									
		T_i = 333.16 K					T_i = 393.16 K				
		a	*b*	*c*	*d*	*Total*	*a*	*b*	*c*	*d*	*Total*
n-Decane	2.00	0.06	0.02	0.07	0.02	0.10	0.01	0.03	0.03	0.03	0.05
n-Decane	10.00	0.11	0.01	0.03	0.12	0.16	0.06	0.02	0.02	0.11	0.12
n-Tetradecane	2.00	0.06	0.00	0.11	1.70	1.70	0.04	0.01	0.08	1.51	1.52
n-Tetradecane	10.00	0.09	0.00	0.03	3.05	3.05	0.11	0.01	0.03	3.08	3.08

* Standard error contributions from: (a) column dead time–temperature relationship, (b) initial temperature, (c) heating rate, (d) ln(capacity factor)–temperature relationship.

REFERENCES

1 E. E. Akporhonor, S. Le Vent and D. R. Taylor, *J. Chromatogr.*, 405 (1987) 67.
2 E. E. Akporhonor, S. Le Vent and D. R. Taylor, in preparation.
3 J. C. Giddings, in N. Brenner, J. E. Callen and M. D. Weiss (Editors), *Gas Chromatography (Third International Symposium held under the auspices of the Analysis Instrumentation Division of the Instrument Society of America, June 13–16, 1961)*, Academic Press, New York, 1962, pp. 57–77.
4 W. K. Al-Thamir, J. H. Purnell, C. A. Wellington and R. J. Laub, *J. Chromatogr.*, 173 (1979) 388.
5 J. Curvers, J. Rijks, C. Cramers, K. Knauss and P. Larson, *J. High Resolut. Chromatogr. Chromatogr. Commun.*, 8 (1985) 607, 611.
6 P. Y. Shrotri, A. Mokashi and D. Mukesh, *J. Chromatogr.*, 387 (1987) 399.

Journal of Chromatography, 463 (1989) 281–295
Elsevier Science Publishers B.V., Amsterdam — Printed in The Netherlands

CHROM. 21 062

THERMODYNAMICS OF ADSORPTION OF ORGANICS ON A COBALT-MODIFIED SOLID OBTAINED FROM COLLOIDAL SILICA

M. M. MARKOVIĆ*, M. M. KOPEČNI and S. K. MILONJIĆ
Chemical Dynamics Laboratory, The Boris Kidrič Institute of Nuclear Sciences, P.O. Box 522, 11001 Belgrade (Yugoslavia)
and
T. S. ĆERANIĆ
Faculty of Science, University of Belgrade, P.O. Box 550, 11001 Belgrade (Yugoslavia)
(First received April 18th, 1988; revised manuscript received October 19th, 1988)

SUMMARY

Adsorption of various organics, including *n*-alkanes, cyclohexane, benzene and halomethanes, on the solid surface obtained from colloidal silica was studied by gas–solid chromatography (GSC). Adsorption experiments, ranging from zero surface coverage and to finite concentration, were performed in the temperature region from 333 to 443 K. In order to reduce surface inhomogeneity, a modified material was prepared by controlled surface silanol proton–Co^{2+} ion exchange and its adsorption properties were also investigated by GSC. Comparing the values for the standard free energy change for adsorption at zero coverage for all absorbates used, it can be deduced that the modification procedure diminished the intensity of adsorption and so enhanced the homogeneity of the solid surface. Adsorption isotherms were obtained using the elution by characteristic point technique and the data were fitted to the BET equation. Thermodynamic parameters for adsorption in the finite concentration region were determined and are discussed in terms of the surface coverage.

INTRODUCTION

Silica is one of the most frequently used adsorbents in gas–solid chromatography (GSC), no matter whether selective separation of gases and low boiling organic compounds are concerned, or the determination of thermodynamic parameters in order to get a better insight into the adsorption process. The main disadvantage of a polar adsorbent is its surface inhomogeneity, resulting in peak asymmetry, too long retention times and reduced column efficiency. The available literature indicates that both thermal treatment[1–3] and different sorts of chemical modifications[4–7] of silica reduce or eliminate some of the active adsorption sites and result in a more uniform surface.

Rowan, Jr. and Sorrell[4] have shown that a modified adsorbent enabling increased resolution and reduced peak asymmetry can be produced by the reaction of an alcohol or a chlorosilane with the surface hydroxyls of the silica gel. Coating of

0021-9673/89/$03.50

porous silica beads (Porasil C) with different inorganic salts was performed[5] in order to establish optimum conditions for selective separations. The most effective separation of aliphatic compounds was obtained with either sodium sulphate or sodium phosphate as the coating salt, while for benzenes cobalt(II) sulphate was found to be superior to all other salts studied. Cooke *et al.*[6] modified the silica surface by coating it with chlorides of Ca^{2+}, Mn^{2+}, Co^{2+} and Zn^{2+}. The modified adsorbents yield more symmetrical elution peaks and decreased retention times, which reduces analysis times and provides more accurate thermodynamic adsorption data.

A quite different modification treatment has been reported from this Laboratory[7]. The surface of the solid material obtained from colloidal silica of very high purity has been altered by ion exchange of alkali-metal ions, resulting in reduced retention times of the organics investigated.

Continuing previous investigations on the adsorption process occurring at the surface of silica, a new adsorbent was prepared by controlled surface silanol proton–Co^{2+} ion exchange applied to the solid obtained from colloidal silica. The adsorption properties of both the modified and the unmodified adsorbents were investigated by GSC. The modification was performed in order to reduce the surface inhomogeneity of the starting material, and Co^{2+} was selected as a modifying agent because of its very important catalytic properties.

EXPERIMENTAL

Colloidal silica was obtained from liquid glass by an ion-exchange procedure described previously[8]. Coagulation of the colloidal material was carried out by adding to it 0.5 *M* sodium chloride at pH 10.4. Disperse phases were separated by filtration. The solid phase was then transferred to a polyethylene bottle containing 0.1 *M* hydrochloric acid solution and allowed to equilibrate for 24 h. The washing procedure was repeated and the pH of the solution after equilibration was 2.2, corresponding to the pH at the point of zero charge of fully protonated silica. The solid phase was separated by filtration and washed with doubly distilled water until no further reaction with chloride ions was observed. The material was dried, first in air and afterwards in an air oven at 383 K for 24 h. It was crushed, then sieved and a 0.149–0.210 mm fraction was used as an unmodified adsorbent (SiO_2-H) for column packing and, also, as a starting material for the modification procedure.

To exchange Co^{2+} for silanol protons, 2.5 g of the solid unmodified material were allowed to equilibrate with 25 ml of 0.01 *M* solution of $CoSO_4 \cdot 7H_2O$ for 2 h. In order to avoid formation of hydrolytic species of Co^{2+}, the pH of the prepared solution was 6.9. The equilibration procedure was repeated three times with a fresh portion of the solution. The solid phase was then separated by filtration, washed with doubly distilled water until no further reaction with sulphate ions was observed and dried in air. The modified adsorbent obtained, SiO_2-Co, was used as a column packing.

Bound Co^{2+} was extracted with a 2 *M* nitric acid solution at room temperature. Measurement of the concentration of the Co^{2+} in the nitric acid solution was carried out by atomic absorption spectrometry (AAS) using a Perkin-Elmer Model 6500 ICP. A value of 11.2 μmol Co^{2+} per g SiO_2 was obtained.

The specific surface area of each adsorbent was determined using the three-point

nitrogen adsorption method with a BET calculation. Values found were 214 and 234 m^2/g for SiO_2-H and SiO_2-Co samples, respectively. The amorphous structure of the materials was established by the X-ray method, using a Siemens Kristalloflex 4 instrument with CuK_α radiation.

The adsorption properties of the materials were examined using a Spectra Physics model 7100 research gas chromatograph with flame ionization detection (FID). Dry nitrogen was employed as the carrier gas. The column inlet pressure was measured by a mercury manometer, and the outlet pressure, assumed to be atmospheric, was measured by a precise barometer. All the other relevant parameters were measured and controlled with the precision required for physico-chemical measurements. Stainless-steel columns, 77 cm × 2.2 mm I.D., were cleaned with both polar and non-polar solvents prior to packing. After packing each column was conditioned overnight under a nitrogen flow at 523 K.

The organic adsorbates, obtained from various commercial sources, were of analytical grade and injected with a 10-μl Hamilton syringe. The system dead-time was assumed to be equal to the retention time of methane at the column temperature. Experiments were performed in the temperature region from 333 to 443 K.

The mass of the column packing, measured after the GSC experiments, was 1.490 and 1.610 g for the SiO_2-H and SiO_2-Co adsorbents, respectively.

RESULTS AND DISCUSSION

Zero surface coverage region

The adsorption of different organics on both the modified and the unmodified adsorbents was investigated in the linear part of the adsorption isotherms (Henry's law region), where lateral interactions between the adsorbed molecules on the surface can be neglected and the thermodynamic functions depend only on the adsorbate–adsorbent interactions. The attainment of the Henry's law region was indicated by the symmetry of the chromatographic peaks and by the constancy of the retention times measured over a significant range of sample sizes. Hence, the net retention volumes for a given adsorbate are independent of its gas phase concentration.

The distribution coefficient, K_s, in the Henry's law region is given by[9]

$$K_s = V_n/A_s \ (\mathrm{cm^3\ m^{-2}}) \tag{1}$$

where V_n (cm^3) is the adsorbate net retention volume and A_s (m^2) denotes the total surface area of the adsorbent in the column. Distribution coefficients for all the experimental temperatures and adsorbates used on the two adsorbents are given in Tables I and II.

The standard free energy change for adsorption under zero coverage conditions, $-\Delta G_a^0$, may be derived from[9]

$$-\Delta G_a^0 = RT \cdot \ln(p_{s.g.} K_s/\pi_s) \ (\mathrm{kJ\ mol^{-1}}) \tag{2}$$

where $p_{s.g.}$ is the absorbate vapour pressure in the gaseous standard state (101 kPa) and π_s is the spreading pressure of the chosen surface standard state. Introducing a widely used definition for the surface standard state proposed by De Boer[10], π_s becomes 0.338 $mN\ m^{-1}$.

TABLE I

DISTRIBUTION COEFFICIENTS, K_s ($cm^3\ m^{-2}$), OF ADSORBATES ON SiO_2-H ADSORBENT

Adsorbate	*T(K)*									
	333	*353*	*363*	*373*	*383*	*393*	*413*	*423*	*433*	*443*
n-Hexane	1.552	0.579		0.271		0.133				
n-Heptane			1.124	0.694	0.444	0.297				
Cyclohexane	1.224	0.499		0.249		0.127				
Benzene							0.465	0.318	0.225	0.159
Dichloromethane	1.224	0.579		0.297		0.155				
Chloroform		0.983	0.643	0.482		0.206				
Carbon tetrachloride		0.736	0.491	0.369		0.162				

At zero surface coverage, the standard ethalpy change for adsorption, $-\Delta H_a^0$, can be identified[10] with the differential heat of adsorption, q_d^0, and may be obtained from the temperature dependence of K_s according to:

$$\mathrm{d}(\ln K_s)/\mathrm{d}(1/T) = q_d^0/R = -\Delta H_a^0/R \tag{3}$$

Provided that $-\Delta H_a^0$ is temperature independent over the temperature region studied, eqn. 3 predicts a linear relationship between $\ln K_s$ and $1/T$. The $-\Delta H_a^0$ values were obtained using the method of least squares.

The standard entropy change for adsorption, ΔS_a^0, may be calculated from the expression:

$$\Delta S_a^0 = (\Delta H_a^0 - \Delta G_a^0)/T\ (\mathrm{J\ mol^{-1}\ K^{-1}}) \tag{4}$$

Thermodynamic parameters for adsorption of all the adsorbates examined under zero coverage conditions are presented in Tables III and IV. According to the K_s values listed in Tables I and II, or more exactly from the corresponding $-\Delta G_a^0$ values (Tables

TABLE II

DISTRIBUTION COEFFICIENTS, K_s ($cm^3\ m^{-2}$), OF ADSORBATES ON SiO_2-Co ADSORBENT

Adsorbate	*T(K)*									
	333	*353*	*363*	*373*	*383*	*393*	*413*	*423*	*433*	*443*
n-Hexane	1.243	0.490		0.217		0.106				
n-Heptane			0.965	0.607	0.389	0.254				
Cyclohexane	1.048	0.425		0.199		0.097				
Benzene							0.352	0.225	0.168	0.130
Dichloromethane	0.986	0.442		0.216		0.115				
Chloroform		0.768	0.509	0.355		0.173				
Carbon tetrachloride		0.563	0.400	0.294		0.143				

TABLE III

STANDARD THERMODYNAMIC ADSORPTION PARAMETERS OF ADSORBATES UNDER ZERO COVERAGE CONDITIONS ON SiO_2-H

Adsorbate	*T(K)*	$-\Delta G_a^0$ *(kJ mol^{-1})*	$-\Delta H_a^0$ *(kJ mol^{-1})*	$-\Delta S_a^0$ *(J mol^{-1} K^{-1})*
n-Hexane	333	17.00	44.2 ± 0.1	82.1 ± 0.3
	353	15.13		
	373	13.62		
	393	12.03		
n-Heptane	363	17.56	52.7 ± 0.2	97.0 ± 0.1
	373	16.55		
	383	15.57		
	393	14.66		
Cyclohexane	333	16.34	40.7 ± 0.1	73.5 ± 0.5
	353	14.69		
	373	13.36		
	393	11.89		
Benzene	413	16.94	55.9 ± 0.1	94.1 ± 0.1
	423	16.02		
	433	15.15		
	443	14.23		
Dichloromethane	333	16.34	37.9 ± 0.0	65.5 ± 0.2
	353	15.13		
	373	13.92		
	393	12.54		
Chloroform	353	16.68	44.5 ± 0.3	78.7 ± 0.5
	363	15.87		
	373	15.41		
	393	13.47		
Carbon tetrachloride	353	15.83	43.2 ± 0.3	77.3 ± 0.4
	363	15.06		
	373	14.58		
	393	12.69		

III and IV), *n*-heptane exhibits more intensive interactions with both adsorbents investigated than does *n*-hexane. This is a consequence of the additional CH_2 group in the molecule of *n*-heptane, available for non-specific interaction with the surface. The increment in the standard free energy change of adsorption, $-\Delta G(-CH_2-)$, contributed by this extra CH_2 group, at 373 K is 2.93 and 3.19 kJ mol^{-1} for the SiO_2-H and SiO_2-Co adsorbents, respectively. The value of 2.93 kJ mol^{-1} for the unmodified adsorbent is in a good agreement with the values of 2.39 kJ mol^{-1} at 433 K (see ref. 7) and 3.12 kJ mol^{-1} at 373 K (see ref. 11) obtained previously for a similar silica adsorbent (unmodified material).

Cyclohexane is less strongly retained than the corresponding *n*-alkane with the same number of carbon atoms (*n*-hexane) on both adsorbents used (Tables III and IV), which can probably be explained by the existence of a "boat" structural isomer in addition to the "chair" configuration, preventing maximum adsorption.

TABLE IV

STANDARD THERMODYNAMIC ADSORPTION PARAMETERS OF ADSORBATES UNDER ZERO COVERAGE CONDITIONS ON SiO_2-Co

Adsorbate	*T(K)*	$-\Delta G_a^0$ *(kJ mol^{-1})*	$-\Delta H_a^0$ *(kJ mol^{-1})*	$-\Delta S_a^0$ *(J mol^{-1} K^{-1})*
n-Hexane	333	16.39	44.6 ± 0.1	84.7 ± 0.1
	353	14.64		
	373	12.94		
	393	11.29		
n-Heptane	363	17.10	52.8 ± 0.1	98.4 ± 0.0
	373	16.13		
	383	15.14		
	393	14.14		
Cyclohexane	333	15.91	42.9 ± 0.0	81.3 ± 0.1
	353	14.22		
	373	12.67		
	393	11.00		
Benzene	413	15.99	51.7 ± 0.4	86.6 ± 0.4
	423	14.80		
	433	14.10		
	443	13.48		
Dichloromethane	333	15.74	38.9 ± 0.0	69.7 ± 0.0
	353	14.33		
	373	12.93		
	393	11.56		
Chloroform	353	15.96	42.7 ± 0.0	75.8 ± 0.1
	363	15.17		
	373	14.47		
	393	12.89		
Carbon tetrachloride	353	15.04	39.7 ± 0.1	69.3 ± 0.5
	363	14.44		
	373	13.88		
	393	12.70		

Since benzene retention times in the temperature range 333–393 K exceed 1 h, its adsorption was studied in the temperature range 413–443 K. However, although the standard enthalpy change for adsorption of *n*-hexane was determined in different temperature regions, it can be supposed that a linear relationship between ln K_s and $1/T$ is valid for the extended region from 333 to 443 K, allowing a comparison of the interactions of *n*-hexane and benzene with the adsorbent surface. The higher negative $-\Delta H_a^0$ value for benzene, compared with *n*-hexane, and hence the more intensive interaction with the surfaces of both adsorbents, is a consequence of the π-electron bonds existing in the aromatic molecule of benzene. Specific interaction between the π-electrons of benzene and the surface hydroxyl groups is to a certain extent similar to an hydrogen bond[12]. The rôle of the specific part of the interaction can be evaluated by considering the differential standard free energy of adsorption, $-\Delta(\Delta G^0)$[11]

$$-\Delta(\Delta G^0) = RT \cdot \ln[K_s(C_6H_6)/K_s(nC_6)] \text{ (kJ mol}^{-1}) \quad (5)$$

where $K_s(nC_6)$ is the distribution coefficient for *n*-hexane at the temperature T, and $K_s(C_6H_6)$ is that for benzene, extrapolated to the same temperature. The $-\Delta(\Delta G^0)$ values obtained are 6.78 and 6.21 kJ mol^{-1} for SiO_2-H and SiO_2-Co, respectively.

Concerning the data obtained for halomethanes, it is clear that chloroform interacts more strongly with the surface of the adsorbent than does carbon tetrachloride or dichloromethane. For silica as well as for other adsorbents[13–15], the intensity of adsorption does not follow the trend normally expected on the basis of the number of chlorine atoms, boiling point or dipole moment. Chloroform exhibits a certain specific interaction not only because of its dipole moment ($\mu = 3.33 \cdot 10^{-30}$ C m) but also due to its extreme asymmetry, in contrast to the symmetrical molecules of dichloromethane ($\mu = 5.33 \cdot 10^{-30}$ C m) and carbon tetrachloride ($\mu = 0.00$ C m).

From the data obtained (Tables I–IV) it can be concluded that for all adsorbates used the adsorption process is less intensive on the modified than on the unmodified adsorbent. This result was expected since, in the process of cobalt-modification, active protons from surface silanol groups were exchanged with Co^{2+} (ref. 16), reducing the number of surface hydroxyls that can act as active adsorption centres. The reduction in the intensity of the interactions with the modified silica, in combination with a significant reduction in the asymmetry of the chromatographic peak shape, implies a reduction in the heterogeneity of this material.

Finite coverage region

At finite coverages the surface adsorption results in non-linear isotherms where the distribution coefficients are dependent on the adsorbate concentration in the gas phase.

Adsorption isotherms for all the adsorbates investigated were obtained using the elution by characteristic point (ECP) technique detailed elsewhere[17]. In ECP measurements it is important to assure that the effect of non-ideality is small in comparison with non-linearity[17]. It is checked by noting that the self-sharpening side of the peak is vertical and that, when peaks of different sizes are superimposed, the peak maxima lie on the common envelope of the diffuse sides.

The amount of probe adsorbed, a, at the temperature T, according to the ECP procedure, can be obtained from[17]

$$a = (jp_oF_{jy_o}S_ay_o)/(hvRTm) \text{ (mol g}^{-1}\text{)} \tag{6}$$

where j is the James-Martin compressibility factor, p_o (Pa) the outlet column pressure, y_o the mole fraction of the adsorbate in the gas phase at the column outlet, S_a (cm^2) the chart area bounded by the GS adsorption envelope of the peak maxima and by the axis at time $t = t_M$, where t_M is the system dead time, h (cm) the peak height, v (cm min^{-1}) the chart speed, R the gas constant, T (K) the experimental temperature and m (g) is the total weight of adsorbent in the column. The term F_{jy_o}, representing the total volume flow-rate, measured at the column outlet, through a zone containing a mole fraction y_0, can be expressed by[18]

$$F_{jy_o} = F_o(1 + k)/[1 + k(1 - jy_o)] \text{ (ml min}^{-1}\text{)} \tag{7}$$

where F_o (ml min^{-1}) is the total volume flow-rate at $y_o = 0$, measured at the column

outlet, and k is the mass distribution coefficient of the adsorbate. Using F_{jy_0}, a correction for the sorption effect was introduced. It cannot be neglected because the mole fraction, for all adsorbates used, in the gas phase exceeds 0.01 (ref. 17).

The vapour pressure, p (in Pa), corresponding to the amount of the probe adsorbed, a, is given by[19]

$$p = (m_a \nu RTh)/(SF_c) \tag{8}$$

where m_a (mol) is the known amount of sample injected, S (cm^2) is the peak area and F_c is the column flow-rate at the column temperature, T, corrected for pressure drop and for the presence of water in the soap-bubble flowmeter.

The correction for gas phase imperfection can be neglected because in this work the mean column pressure did not exceed $1.01 \cdot 10^6$ Pa (10 atm)[20]. The adsorption isotherms obtained are represented in the form $a = f(p/p_a)$, where p_a is the vapour pressure of the sorbate liquid calculated by the Antoine equation[21].

Experimental adsorption isotherms were fitted to the BET equation[22]

$$a = \frac{a_m C(p/p_a)}{(1 - p/p_a)[1 + (C - 1)(p/p_a)]} \tag{9}$$

where a_m (mol g^{-1}) is the monolayer capacity, and C is a constant correlated with the heat of adsorption. In order to determine a_m and C, each experimental isotherm was

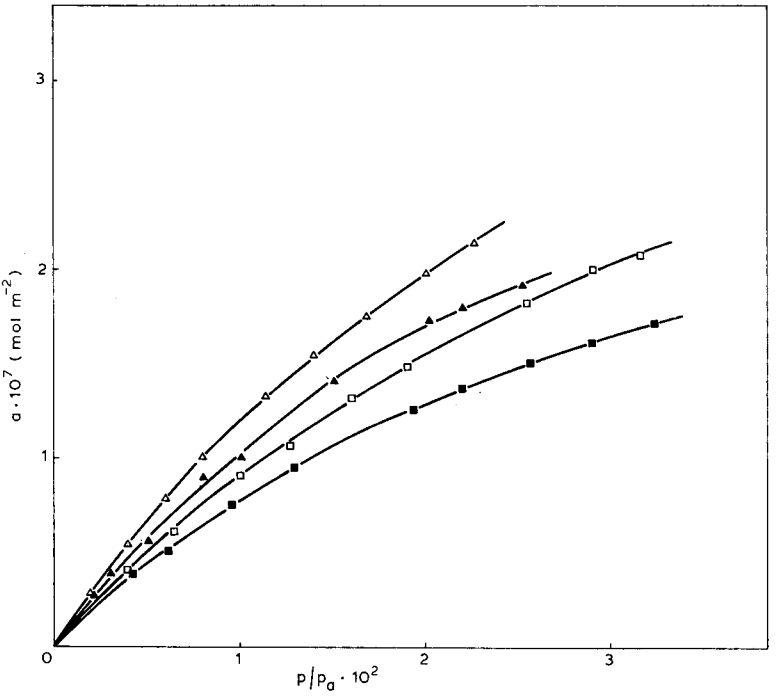

Fig. 1. Adsorption isotherms for *n*-hexane on the SiO_2-H adsorbent. The solid lines represent BET fits. T (K): 333 (△); 353 (▲); 373 (□); 393 (■).

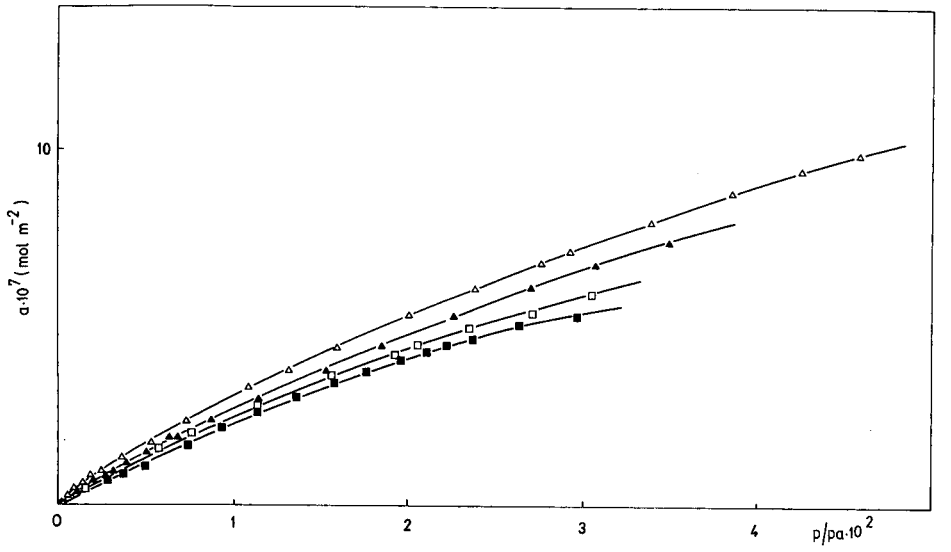

Fig. 2. Adsorption isotherms for chloroform on the SiO_2-H adsorbent. The solid lines represent BET fits. T (K): 353 (△); 363 (▲); 373 (□); 393 (■).

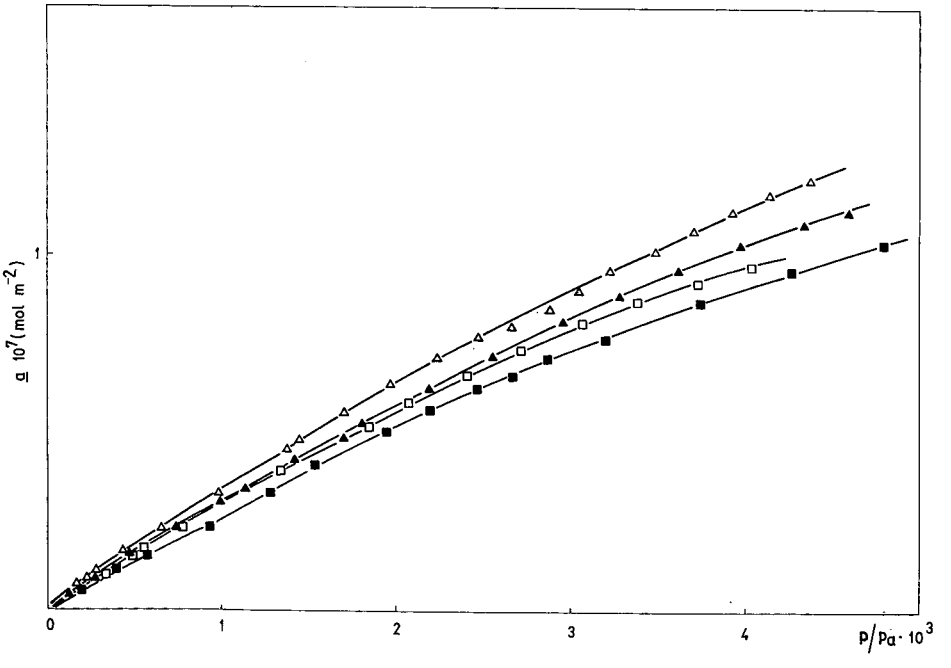

Fig. 3. Adsorption isotherms for benzene on the SiO_2-H adsorbent. The solid lines represent BET fits. T (K): 413 (△); 423 (▲); 433 (□); 443 (■).

reduced to the linear form of the BET equation applied to the whole p/p_a range experimentally utilized. The constants a_m and C were obtained using the least squares method.

Figs. 1–3 present examples of the isotherms computed for *n*-hexane, chloroform and benzene, each representing a class of organics, on the SiO_2-H adsorbent. Similar patterns are obtained for the cobalt-modified variety. The BET fit is represented by the solid line. The BET constants, a_m and C, for all systems studied are compiled in Table V. It is obvious (Figs. 1–3) that the adsorption process for *n*-hexane, chloroform and benzene for the given coverage range can be very well described by the BET model. Due to non-coincidence in the diffuse sides of the peaks at higher coverages, the ECP technique cannot be used to obtain multilayer adsorption data.

In order to get a better insight into the adsorption process in the finite coverage

TABLE V

BET CONSTANTS, a_m (mol m^{-2}) AND C, FOR ADSORBATES ON SiO_2-H AND SiO_2-Co

Adsorbate	*T(K)*	*SiO_2-H*		*SiO_2-Co*	
		$a_m \cdot 10^7$	C	$a_m \cdot 10^7$	C
n-Hexane	333	5.19	29.35	1.45	149.11
	353	3.70	40.05	1.96	73.89
	373	4.55	24.55	2.52	42.73
	393	3.23	31.61	2.44	38.60
n-Heptane	363	7.59	13.52	1.71	85.08
	373	7.14	13.08	1.91	65.25
	383	6.19	14.21	1.79	37.35
	393	3.84	22.32	2.23	41.00
Cyclohexane	333	6.69	12.41	2.28	45.51
	353	5.23	14.85	2.54	31.53
	373	5.12	13.02	3.16	21.30
	393	4.59	12.31	–	–
Benzene	413	3.88	99.84	8.68	18.61
	423	3.49	101.35	9.04	16.51
	433	3.02	115.28	11.65	11.33
	443	3.52	84.88	8.89	15.55
Dichloromethane	333	10.30	36.14	6.39	54.21
	353	16.31	18.09	3.94	99.60
	373	–	–	5.39	51.92
	393	11.08	22.51	5.23	47.39
Chloroform	353	23.9	13.50	4.56	66.21
	363	19.5	15.77	5.71	40.79
	373	15.7	18.68	5.70	37.14
	393	13.0	22.79	6.10	30.62
Carbon tetrachloride	353	9.41	9.48	2.97	43.21
	363	8.85	10.31	3.64	29.93
	373	–	–	3.32	32.70
	393	13.69	4.52	4.96	16.96

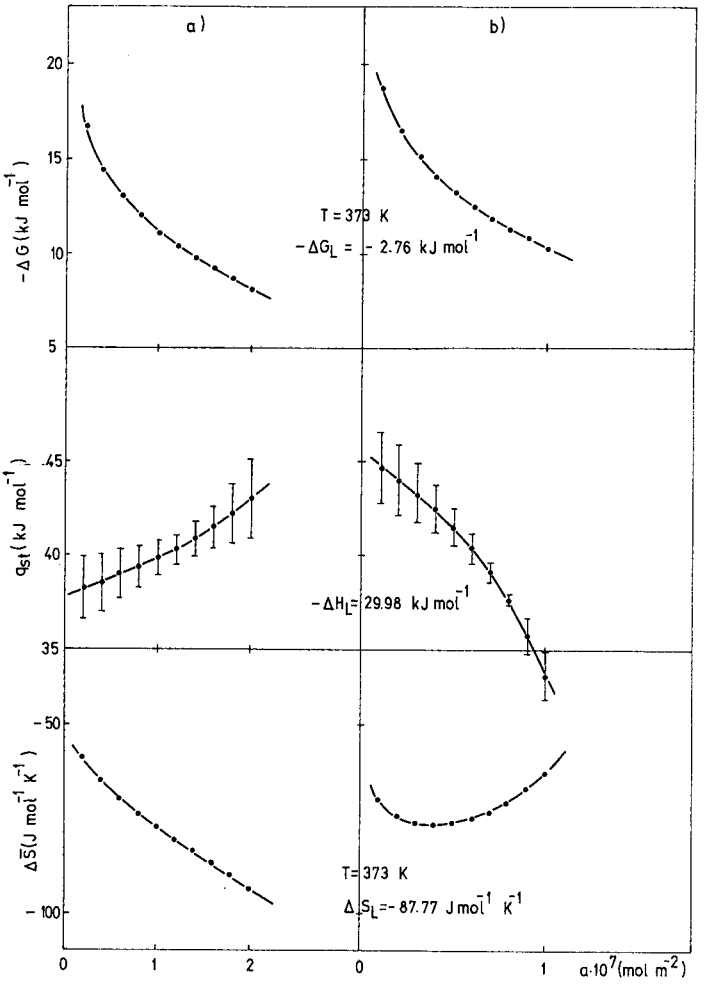

Fig. 4. Dependence of thermodynamic adsorption parameters of *n*-hexane on the surface coverage for: (a) SiO_2-H adsorbent and (b) SiO_2-Co adsorbent; $-\Delta G_L$, $-\Delta H_L$ and ΔS_L are the corresponding parameters for pure liquid *n*-hexane.

region, thermodynamic parameters of adsorption were determined. Assuming ideal gas behaviour, the partial molar free energy of adsorption was determined from each isotherm at the given amount of probe sorbed, a, from[23]

$$\Delta\bar{G} = RT \cdot \ln(p/p_{s.g.})\,(\text{kJ mol}^{-1}) \tag{10}$$

using linear interpolation to calculate the vapour pressure, p, at the coverage in question. Here, $\Delta\bar{G}$ represents the change in free energy of adsorption as 1 mol of adsorbate passes from the vapour at unit fugacity to the surface at the coverage in question[23].

The isosteric heat of adsorption, q_{st}, for the given a can be calculated from[23]

$$q_{st} = -[\partial(\Delta\bar{G}/T)/\partial(1/T)]_a\,(\text{kJ mol}^{-1}) \tag{11}$$

by fitting the values of $(\Delta\bar{G}/T)$ at the given a to a linear least squares function in $1/T$. The partial molar entropy change for adsorption was obtained in the usual way:

$$\Delta\bar{S} = -(q_{st} + \Delta\bar{G})/T \text{ (J mol}^{-1}\text{ K}^{-1}) \tag{12}$$

Figs. 4–6 present the thermodynamic parameters of adsorption of *n*-hexane, chloroform and benzene on the SiO_2-H and SiO_2-Co adsorbents as a function of the surface coverage. The values of $-\Delta G_L$, $-\Delta H_L$ and ΔS_L are the corresponding parameters for pure liquid adsorbate.

The decrease of $-\Delta\bar{G}$ (Figs. 4–6) with increasing surface coverage indicates that

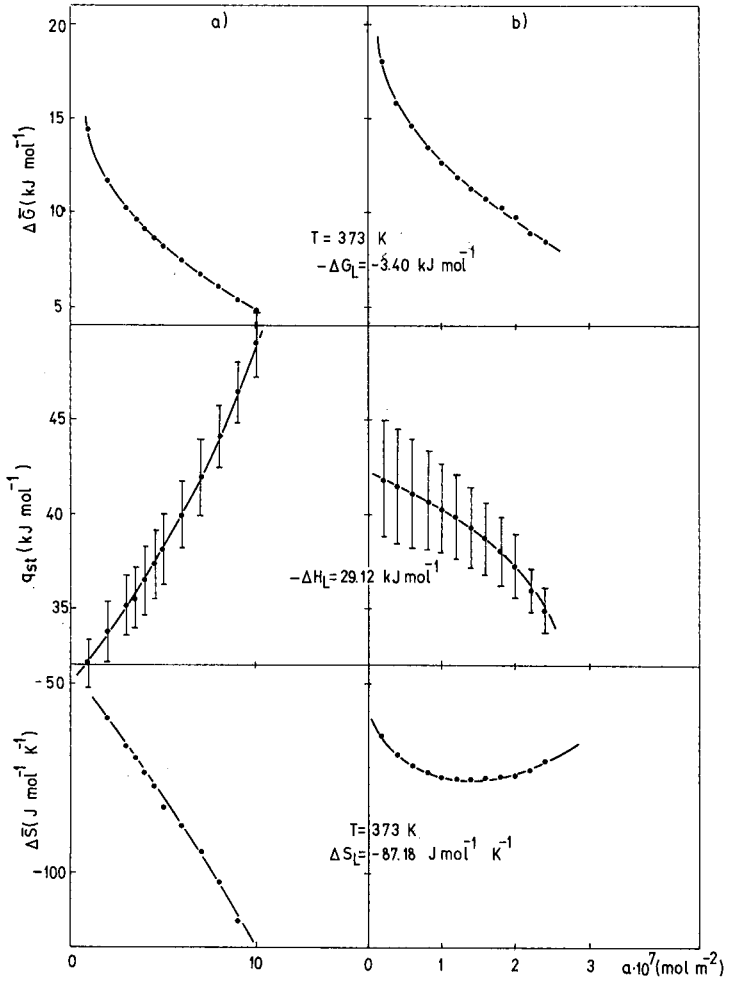

Fig. 5. Dependence of thermodynamic adsorption parameters of chloroform on the surface coverage for: (a) SiO_2-H adsorbent and (b) SiO_2-Co adsorbent; $-\Delta G_L$, $-\Delta H_L$ and ΔS_L are the corresponding parameters for pure liquid chloroform.

low surface coverages are preferred from the energy point of view. Also, as expected, all adsorbates presented show a non-liquid-like structure for the range of surface coverage studied. Errors (as standard deviations) in the q_{st} values were calculated and represented by the error bars in Figs. 4–6. The errors are of the usual order of magnitude for least squares treatment of eqn. 11. Due to somewhat larger errors at the initial part of the q_{st} plots (from 1.5 kJ mol^{-1} for chloroform on the SiO_2-H adsorbent to 3.3 kJ mol^{-1} for benzene on the SiO_2-Co adsorbent), the shape of these curves at low surface coverages is not quite certain. It can be concluded, however, from Figs. 4–6 that the trend in q_{st} is different for the modified and the unmodified adsorbents. Further, Figs. 4–6 indicate that for adsorption on the unmodified adsorbent there is an increase in q_{st} which may possibly yield a maximum corresponding to the coverage at

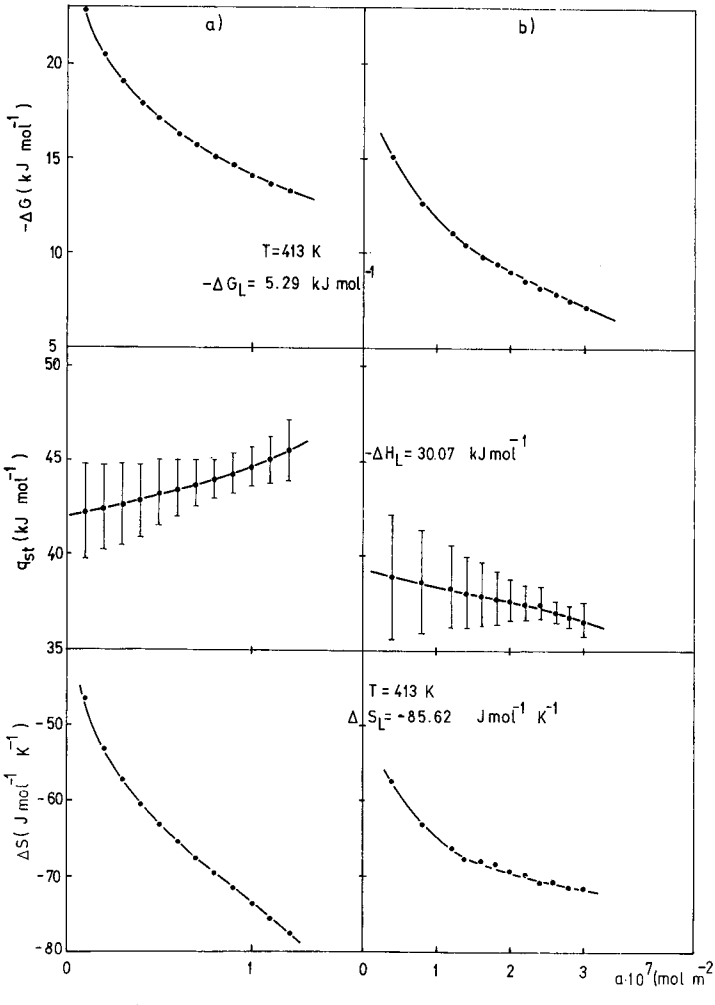

Fig. 6. Dependence of thermodynamic adsorption parameters of benzene on the surface coverage for: (a) SiO_2-H adsorbent and (b) SiO_2-Co adsorbent; $-\Delta G_L$, $-\Delta H_L$ and ΔS_L are the corresponding parameters for pure liquid benzene.

which the most energetically favourable sites, probably originating from strong, localized sorbate–sorbent interactions[23], are created. Similar behaviour was observed in the case of adsorption of hexan-1-ol and butan-1-ol on cotton cellulose, which can be explained by the ability of cellulose to form strong localized sorbate–sorbent interactions through hydrogen bonding[23]. However, the increase in q_{st} with increasing surface coverage for the adsorption of alkan-1-ols on graphitized carbon black was attributed to the creation of energetically favourable sites by sorbate–sorbent interactions[24]. At the same time, the minimum in $\Delta\bar{S}$, for the case of adsorption on the unmodified adsorbent, may be due to a decrease in configurational entropy[23]. In the case of adsorption on the modified adsorbent, the minimum in $\Delta\bar{S}$ is quite obvious, showing that the modification procedure applied reduces the number of active adsorption sites, yielding a more homogeneous surface.

The lack of a maximum in q_{st} on the cobalt-modified solid may be ascribed to the reduced number of high energy adsorptive sites, which upon modification are converted into less active cobalt-form sites.

The dependence of the thermodynamic parameters in the finite concentration region on the surface coverage for all other adsorbates used has the same pattern as in Figs. 4–6.

Further increase in the surface coverage and, hence, a better insight into the adsorption process in the finite coverage region on both the modified and the unmodified adsorbents could not be attained due to the effects of non-ideality. Nevertheless, the thermodynamic results presented show that the modification procedure applied here to the fully protonated silica, using Co^{2+} to exchange the active protons from the surface silanol groups, leads to a less active adsorbent with a more homogeneous surface.

ACKNOWLEDGEMENTS

The authors are grateful to Professor S. Kondo, Osaka University of Education, for specific area measurements, and the Scientific Research Fund of SR Serbia (Belgrade, Yugoslavia) for partial financial support.

REFERENCES

1 L. Feltl, P. Lutovský, L. Sosnová and E. Smolková, *J. Chromatogr.*, 91 (1974) 321.
2 S. K. Milonjić and M. M. Kopečni, *Chromatographia*, 19 (1984) 342.
3 M. M. Kopečni, S. K. Milonjić, W. Rudzinski and J. Jagiello, *Collect. Czech. Chem. Commun.*, 52 (1987) 572.
4 R. Rowan, Jr. and J. B. Sorrell, *Anal. Chem.*, 42 (1970) 1716.
5 A. F. Isbell, Jr. and D. T. Sawyer, *Anal. Chem.*, 41 (1969) 1381.
6 N. H. C. Cooke, E. F. Barry and B. S. Solomon, *J. Chromatogr.*, 109 (1975) 57.
7 M. M. Kopečni, R. J. Laub and S. K. Milonjić, *Anal. Chem.*, 52 (1980) 1032.
8 S. K. Milonjić, M. M. Kopečni and Z. E. Ilić, *Bull. Soc. Chim., Beograd*, 48 (1983) 351.
9 G. M. Dorris and D. G. Gray, *J. Colloid. Interface Sci.*, 77 (1980) 353.
10 J. H. De Boer, *The Dynamical Character of Adsorption*, Oxford University Press (Clarendon), London, 1953, p. 115.
11 S. K. Milonjić, *Ph.D. Thesis*, University of Belgrade, Belgrade, 1981.
12 J. A. Gerasimov, V. Dreving, E. Eremin, A. Kiselev, V. Lebedev, G. Panchenkov and A. Shlygin, *Physical Chemistry*, Mir, Moscow, 1974, p. 476.
13 J. P. Okamura and D. T. Sawyer, *Anal. Chem.*, 43 (1971) 1730.

14 A. G. Datar, P. S. Ramanathan and M. S. Das, *J. Chromatogr.*, 93 (1974) 217.
15 S. K. Milonjić and M. M. Kopečni, *J. Chromatogr.*, 172 (1979) 357.
16 V. L. Razin, S. K. Milonjić and Ju. G. Frolov, Presentation at *Euchem Conference on Silica, Le Bischenberg-Obernai, September 22–24, 1986.*
17 J. R. Conder and C. L. Young, *Physical Measurement by Gas Chromatography*, Wiley, New York, 1979, pp. 390, 393, 374.
18 J. R. Conder and J. H. Purnell, *Trans. Faraday Soc.*, 65 (1969) 824.
19 S. Katz and D. G. Gray, *J. Colloid. Interface Sci.*, 82 (1981) 326.
20 J. R. Conder and J. H. Purnell, *Trans. Faraday Soc.*, 64 (1968) 1505.
21 R. R. Dreisbach, *Physical Properties of Chemical Compounds*, American Chemical Society, Washington, DC, 1959.
22 P. R. Tremaine and D. G. Gray, *Anal. Chem.*, 48 (1976) 380.
23 P. R. Tremaine and D. G. Gray, *J. Chem. Soc., Faraday Trans. 1*, 71 (1975) 2170.
24 G. I. Berezin, A. V. Kiselev and I. V. Kleshnina, *Zh. Fiz. Khim.*, 73 (1969) 1657.

Journal of Chromatography, 463 (1989) 297–304
Elsevier Science Publishers B.V., Amsterdam — Printed in The Netherlands

CHROM. 21 082

RELATIONSHIPS BETWEEN STRUCTURE AND RETENTION INDEX FOR N-SUBSTITUTED AMIDES OF ALIPHATIC ACIDS ON A NON-POLAR COLUMN

WALDEMAR KRAWCZYK* and GRZEGORZ T. PIOTROWSKI
Department of Chemistry, Warsaw University, Pasteura 1, 02-093 Warsaw (Poland)
(First received July 18th, 1988; revised manuscript received November 2nd, 1988)

SUMMARY

The retention indices of 100 amides of aliphatic acids (R^1–CO–NHR^2) divided into ten series depending on the substituent R^1 at the carboxylic carbon atom or the substituent R^2 at the nitrogen atom, each containing the same set of ten substituents at the second site, have been measured on a non-polar GE SE-30 column. A relationship between the retention index of the amide and the number of primary, secondary, tertiary and quaternary carbon atoms in the molecule has been found. The retention indices obtained were correlated with those of corresponding simple model compounds, such as substituted hydrocarbons (R^1–H and R^2–H) and amines (R^2–NH_2). The good linear correlations obtained indicate that, for prediction of retention indices of amides the correlation method should be used instead of the additivity rule. Retention indices of amides were found to obey a two-parameter linear equation with the retention indices of corresponding model compounds as independent variables.

INTRODUCTION

The possibility of fairly accurate prediction of retention indices plays a very important rôle in the synthesis and analysis of organic compounds.

There are several methods for the prediction of retention indices. Most of them consider the retention index as an additive function, and the simplest ones assume that the retention indices of compounds containing a certain functional group can be calculated by addition of a specific retention increment for this group to the retention indices of the corresponding hydrocarbons[1,2]. These methods, although not very precise, are commonly used because of their simplicity.

Recently Oszczapowicz *et al.*[3–8] have shown that retention indices of compounds, I(Cpd), correlate very well with the retention indices of the corresponding model compounds, I(Std), taken as standards:

$$I(\text{Cpd}) = a \cdot I(\text{Std}) + b \quad (1)$$

They have pointed out[3] that the additivity rule, used for prediction of retention indices

0021-9673/89/$03.50

TABLE I

RETENTION INDICES OF AMIDES (R^1CONHR^2) ON A GE SE-30 NON-POLAR COLUMN AT 180°C

No.	R^1	R^2									
		CH_3	*C_2H_5*	*n-C_3H_7*	*iso-C_3H_7*	*n-C_4H_9*	*iso-C_4H_9*	*tert.-C_4H_9*	*n-C_6H_{13}*	*Cyclohexyl*	*Phenyl*
1	H	793 ± 6	794 ± 6	934 ± 4	911 ± 6	1067 ± 5	1014 ± 6	915 ± 3	1274 ± 2	1306 ± 4	1386 ± 8
2	CH_3	857 ± 8	890 ± 5	974 ± 4	895 ± 3	1090 ± 3	1013 ± 2	900 ± 4	1292 ± 4	1313 ± 3	1429 ± 9
3	C_2H_5	921 ± 4	950 ± 4	1040 ± 2	979 ± 4	1140 ± 4	1091 ± 3	969 ± 0	1353 ± 5	1378 ± 1	1480 ± 2
4	*n*-C_3H_7	1005 ± 3	1044 ± 6	1127 ± 3	1042 ± 4	1228 ± 3	1167 ± 1	1048 ± 2	1434 ± 2	1459 ± 4	1531 ± 5
5	iso-C_3H_7	940 ± 5	1002 ± 3	1090 ± 2	987 ± 2	1169 ± 4	1116 ± 3	983 ± 0	1352 ± 3	1392 ± 1	1484 ± 3
6	Cyclopropyl	1056 ± 5	1089 ± 6	1197 ± 5	1107 ± 3	1293 ± 4	1249 ± 2	1104 ± 4	1471 ± 3	1512 ± 4	1616 ± 6
7	*n*-C_4H_9	1105 ± 3	1141 ± 5	1237 ± 4	1152 ± 5	1338 ± 3	1281 ± 1	1156 ± 3	1516 ± 4	1551 ± 5	1642 ± 3
8	iso-C_4H_9	1069 ± 3	1103 ± 4	1165 ± 2	1088 ± 3	1261 ± 1	1218 ± 2	1101 ± 1	1469 ± 4	1496 ± 4	1571 ± 4
9	*tert.*-C_4H_9	959 ± 6	1000 ± 5	1077 ± 2	1016 ± 4	1181 ± 1	1136 ± 2	1002 ± 2	1386 ± 5	1398 ± 3	1465 ± 3
10	*n*-C_5H_{11}	1123 ± 2	1216 ± 2	1319 ± 3	1258 ± 3	1425 ± 3	1372 ± 1	1246 ± 1	1642 ± 4	1645 ± 3	1743 ± 4

of organic compounds, should be regarded as a very special case of linear regression, where the slope, a, of the correlation line is by definition equal to unity. It has been found that in many cases this coefficient is considerably different from unity and it was concluded that the use of the additivity rule for prediction of retention indices of some compounds may cause discernible errors and that the correlation method should be used instead.

It has been shown that for compounds containing two variable substituents the best results are obtained when dual parameter regression is used[4,5,7,8]:

$$I(\text{Cpd}) = a_1 \cdot I(\text{Std}_1) + a_2 \cdot I(\text{Std}_2) + b \qquad (2)$$

Thus the question arose as to how far the additivity rule can be applied for prediction of retention indices of monosubstituted amides and whether the methods presented above will provide better results in this case too.

In this work the Kováts retention indices[9,10] for 100 amides of aliphatic carboxylic acids (R^1–CO–NHR^2) have been measured on a non-polar GE SE-30 column. The compounds investigated can be divided into ten series depending on the substituent R^1 at the carboxylic carbon atom or the substituents R^2 at the nitrogen atom. Each series contained the same set of ten variable substituents at the second site. The substituents R^1 and R^2 are listed in Table I.

EXPERIMENTAL

Materials

All amides studied were synthesized in our laboratory by treating a primary amine with an equimolar amount of the corresponding acyl chloride. The amines were commercial samples from Merck or Fluka. Acyl chlorides were prepared by reaction of the corresponding carboxylic acids with oxalyl chloride. *n*-Alkanes C_{10}–C_{15} were obtained from Applied Science Labs.

Gas chromatography

A Chromatron Model GCHF 18.3.4 gas chromatograph with a flame ionization detector, connected on line with a microcomputer and equipped with a 1 m × 3 mm I.D. column packed with 15% GE SE-30 silicone gum rubber on Chromosorb W AW (60–80 mesh), was used. The column temperature was maintained at 180°C. The carrier gas was nitrogen at a flow-rate of 25 ml/min. Samples of 0.5 μl of solutions in pyridine or quinoline were injected by means of a 10-μl Hamilton syringe.

Retention indices and dead times were determined by regression analysis by the method of Grobler and Bálizs[11] as improved by Haken *et al.*[12] using the series of six C_{10}–C_{15} *n*-alkanes, each time under the same conditions as used for the sample studied.

RESULTS AND DISCUSSION

The retention indices obtained with confidence intervals at a significance level of 0.05, calculated from at least five measurements, are listed in Table I.

Searching for relationships between the retention indices and the structures of

the amides, our attention was drawn to the possibility of calculation of retention indices on the basis of the number of primary, secondary, tertiary and quaternary carbon atoms in the alkyl substituents R^1 and R^2 according to

$$I(\text{Cpd}) = \sum_{i=1}^{4} n^i I^i + I^0 \tag{3}$$

where n^i = number of primary, secondary, tertiary and quaternary carbon atoms respectively, I^i = increment of primary, secondary, tertiary and quaternary carbon atom respectively and I^0 = increment characteristic for monosubstituted amides. All calculations were made by means of the least-squares method. The confidence intervals were calculated at a significance level of 0.05.

The regression coefficients, R, obtained and Exner's Ψ^* function[13], as well as increments for carbon atoms calculated on the basis of eqn. 3, are presented in Table II.

The results indicated that for amides containing aliphatic substituents R^1 and R^2, the retention index depends on the number of carbon atoms, on whether these atoms are primary, secondary, tertiary or quaternary, and may also depend on the site of attachment to the functional group

$$I(\text{Cpd}) = \sum_{i=1}^{4} n^i(R^1) \cdot I^i(R^1) + \sum_{i=1}^{4} n^i(R^2) \cdot I^i(R^2) + I^0 \tag{4}$$

where $n^i(R^1), n^i(R^2)$ = number of primary, secondary, tertiary and quaternary carbon atoms in substituents R^1 and R^2, respectively and $I^i(R^1)$, $I^i(R^2)$ = increment of primary, secondary, tertiary and quaternary carbon atoms in substituents R^1 and R^2, respectively. The parameters obtained given in Table II (eight parameter scheme)

TABLE II

INCREMENTS FOR CALCULATION OF RETENTION INDICES

Without R^1–CO–$NHCH_3$ series. n represents the number of retention indices considered.

Four parameters (eqn. 3)	*Eight parameters (eqn. 4)*
I^I = 38.8 ± 6.6	$I^I(R^1)$ = 33.1 ± 6.6
I^{II} = 93.5 ± 2.5	$I^{II}(R^1)$ = 88.0 ± 2.5
I^{III} = 79.5 ± 6.8	$I^{III}(R^1)$ = 78.1 ± 8.2
I^{IV} = 35.9 ± 14.4	$I^{IV}(R^1)$ = 51.5 ± 17.1
–	$I^I(R^2)$ = 52.1 ± 9.4
–	$I^{II}(R^2)$ = 98.7 ± 3.2
–	$I^{III}(R^2)$ = 76.5 ± 7.7
–	$I^{IV}(R^2)$ = 9.9 ± 17.2
I^0 = 698.1	I^0 = 687.4
R = 0.9956	R = 0.9972
Ψ = 0.0973	Ψ = 0.0799
n = 72	n = 72

* $\Psi = [n(1 - r^2)/f]^{1/2}$, where r is the correlation coefficient, n the number of experimental points and f the number of degrees of freedom.

shows that indeed for primary and quaternary carbon atoms the increment depends on the site of attachment whereas for secondary and tertiary atoms it seems independent.

Searching for the best methods of prediction of retention indices of amides with substituents of any type, we have calculated the linear regression between the retention indices of amides of each series and those of appropriate model compounds. For each series containing a constant substituent R^2 at the nitrogen atom, we have correlated the retention indices of amides with those of corresponding hydrocarbons (R^1–H or R^1–CH_3). The regression coefficients, *a* and *b* (eqn. 1), and the estimators of correlation, *i.e.*, the correlation coefficient, *r*, and Exner's Ψ function are given in Table III. For each series the slope, *a*, of the regression lines is markedly different from unity and application of the additivity rule, instead of this method, may result in considerable errors. The regressions obtained indicate that, for all the series studied, the correlations with the retention indices of hydrocarbons R^1–H are very good, whereas the correlations with the retention indices of hydrocarbons R^1-CH_3 are very good for the first three series but for the other series are only satisfactory. The results presented show that, as model compounds for the prediction of retention indices of amides, hydrocarbons R^1–H should be used.

For series with an invariant substituent R^1 at the carboxylic group, we have

TABLE III

REGRESSION PARAMETERS OF RETENTION INDICES OF AMIDES (R^1CONHR^2) CONTAINING A CONSTANT SUBSTITUENT, R^2, AT THE NITROGEN ATOM *vs.* RETENTION INDICES OF CORRESPONDING HYDROCARBONS A (R^1H) AND B (R^1CH_3) (EQN. 1)

No.	R^2	*Type*	*a*	*b*	*r*	Ψ	*n*
1	CH_3	A	0.716 ± 0.231	787.4	0.9849	0.2232	5
		B	0.708 ± 0.132	719.5	0.9910	0.1636	6
2	C_2H_5	A	0.843 ± 0.115	795.3	0.9973	0.0956	5
		B	0.845 ± 0.066	710.1	0.9984	0.0686	6
3	*n*-C_3H_7	A	0.887 ± 0.129	873.3	0.9969	0.1022	5
		B	0.800 ± 0.157	825.1	0.9901	0.1718	6
4	iso-C_3H_7	A	0.899 ± 0.167	795.5	0.9949	0.1296	5
		B	0.734 ± 0.281	782.6	0.9640	0.3257	6
5	*n*-C_4H_9	A	0.868 ± 0.188	983.8	0.9932	0.1508	5
		B	0.749 ± 0.219	952.5	0.9786	0.2519	6
6	iso-C_4H_9	A	0.908 ± 0.128	912.4	0.9971	0.0985	5
		B	0.763 ± 0.244	899.3	0.9745	0.2748	6
7	*tert.*-C_4H_9	A	0.879 ± 0.130	800.1	0.9968	0.1036	5
		B	0.715 ± 0.273	788.8	0.9641	0.3253	6
8	*n*-C_6H_{13}	A	0.863 ± 0.213	1188.5	0.9911	0.1715	5
		B	0.741 ± 0.230	1159.2	0.9758	0.2677	6
9	Cyclohexyl	A	0.837 ± 0.110	1218.1	0.9974	0.0923	5
		B	0.711 ± 0.211	1193.0	0.9780	0.2558	6
10	Phenyl	A	0.790 ± 0.265	1328.0	0.9837	0.2319	5
		B	0.707 ± 0.201	1287.7	0.9796	0.2461	6

TABLE IV

REGRESSION PARAMETERS OF RETENTION INDICES OF AMIDES (R^1CONHR^2) CONTAINING A CONSTANT SUBSTITUENT, R^1, AT THE CARBOXYLIC GROUP *vs.* RETENTION INDICES OF CORRESPONDING HYDROCARBONS (R^2H) (EQN. 1)

No.	R^1	*a*	*b*	*r*	Ψ	*n*
1	H	1.057 ± 0.175	635.4	0.9898	0.1688	7
2	CH_3	0.962 ± 0.181	716.9	0.9868	0.1916	7
3	C_2H_5	0.953 ± 0.170	780.1	0.9881	0.1817	7
4	*n*-C_3H_7	0.914 ± 0.125	877.2	0.9930	0.1400	7
5	iso-C_3H_7	0.892 ± 0.125	829.8	0.9927	0.1431	7
6	Cyclopropyl	0.932 ± 0.157	928.0	0.9895	0.1712	7
7	*n*-C_4H_9	0.905 ± 0.136	981.4	0.9915	0.1537	7
8	iso-C_4H_9	0.874 ± 0.153	938.0	0.9886	0.1780	7
9	*tert.*-C_4H_9	0.886 ± 0.119	837.4	0.9932	0.1377	7
10	*n*-C_5H_{11}	1.022 ± 0.112	1015.7	0.9955	0.1124	7

correlated the retention indices of amides with those of corresponding hydrocarbons (R^2–H) or primary amines[3] (R^2–NH_2), to determine whether the slopes are different from unity for both correlations and which of the standards tested ensure higher accuracy of prediction. The results obtained are presented in Tables IV and V, respectively. The regressions indicate that for all series studied the correlations with the retention indices of primary amines are of the highest quality and the correlation with the retention indices of hydrocarbons are still good.

It should be mentioned that we have found very good correlations of the retention indices of amides, containing a constant substituent R^1 at the carboxylic group, with those of the corresponding acetamides (Table VI).

The regression coefficients, *a*, for the series of amides studied containing a constant substituent R^1 at the carboxylic group were identical within the confidence intervals. The same was observed for the series of amides with a constant substituent

TABLE V

REGRESSION PARAMETERS OF RETENTION INDICES OF AMIDES (R^1CONHR^2) CONTAINING A CONSTANT SUBSTITUENT, R^1, AT THE CARBOXYLIC GROUP *vs.* RETENTION INDICES OF CORRESPONDING PRIMARY AMINES (R^2NH_2)* (EQN. 1)

No.	R^1	*a*	*b*	*r*	Ψ	*n*
1	H	0.966 ± 0.089	448.5	0.9957	0.1066	8
2	CH_3	1.028 ± 0.087	419.0	0.9964	0.0973	8
3	C_2H_5	0.991 ± 0.072	509.6	0.9974	0.0840	8
4	*n*-C_3H_7	0.968 ± 0.115	600.9	0.9931	0.1358	8
5	iso-C_3H_7	0.949 ± 0.119	555.9	0.9922	0.1438	8
6	Cyclopropyl	0.965 ± 0.100	667.3	0.9947	0.1187	8
7	*n*-C_4H_9	0.940 ± 0.095	724.3	0.9949	0.1165	8
8	iso-C_4H_9	0.949 ± 0.091	655.6	0.9954	0.1103	8
9	*tert.*-C_4H_9	0.917 ± 0.112	588.4	0.9926	0.1402	8
10	*n*-C_5H_{11}	0.971 ± 0.086	800.8	0.9961	0.1025	8

* According to ref. 3; the retention index of *tert.*-butylamine is 483 ± 6.

TABLE VI

REGRESSION PARAMETERS OF RETENTION INDICES OF AMIDES (R^1CONHR^2) CONTAINING A CONSTANT SUBSTITUENT, R^1, AT THE CARBOXYLIC GROUP *vs.* RETENTION INDICES OF CORRESPONDING ACETAMIDES (CH_3CONHR^2) (Eqn. 1)

No.	R^1	*a*	*b*	*r*	Ψ	*n*
1	H	1.017 ± 0.139	−43.9	0.9861	0.1855	10
2	C_2H_5	0.974 ± 0.036	92.2	0.9990	0.0506	10
3	*n*-C_3H_7	0.947 ± 0.042	199.6	0.9985	0.0611	10
4	iso-C_3H_7	0.930 ± 0.055	160.9	0.9974	0.0806	10
5	Cyclopropyl	0.959 ± 0.055	248.0	0.9975	0.0789	10
6	*n*-C_4H_9	0.932 ± 0.038	319.4	0.9987	0.0563	10
7	iso-C_4H_9	0.911 ± 0.045	283.5	0.9982	0.0675	10
8	*tert.*-C_4H_9	0.907 ± 0.059	196.1	0.9968	0.0893	10
9	*n*-C_5H_{11}	1.006 ± 0.110	327.5	0.9911	0.1488	10

R^2 at the nitrogen atom. This leads to the conclusion that, for the prediction of their retention indices, a two-parameter linear regression (eqn. 2) may be used. As a first standard series, for substituents at the nitrogen atom, we have chosen hydrocarbons R^2–H. As the second one (for substituents at the carboxylic carbon atom) we have used hydrocarbons R^1–H. Because the linear correlations with hydrocarbons R^2–H (Table IV) were of good quality, but not as good as for primary amines R^2–NH_2 (Table V), we have also calculated dual-parameter correlations using primary amines R^2–NH_2 and hydrocarbons R^1–H as standards. The results obtained are collected in Table VII. The correlations with both types of standards are of very good quality as indicated by both the correlation coefficient, *R*, and Exner's Ψ function.

CONCLUSION

We have compared the retention indices calculated on the basis of eqns. 2, 3 and 4 with the experimental values. The distribution of errors (Table VIII) indicates that, in the prediction of retention indices of aliphatic acid amides containing alkyl substituents at the nitrogen atom, the best results are obtained on the basis of eqn. 4. However, for amides containing other type of substituents, dual-parameter regression (eqn. 2) should be used.

TABLE VII

MULTIPLE REGRESSION PARAMETERS OF RETENTION INDICES OF AMIDES *vs.* RETENTION INDICES OF STANDARDS (EQN. 2)

Standards	a_1	a_2	*b*	*R*	Ψ	*n*
R^1H R^2H	0.829 ± 0.078	0.951 ± 0.051	625.5	0.9917	0.1346	35
R^1H R^2NH_2	0.866 ± 0.050	0.980 ± 0.038	351.0	0.9953	0.1011	40

TABLE VIII

DISTRIBUTION (%) OF ERRORS OF PREDICTIONS OF RETENTION INDICES BASED ON EQNS. 2, 3 AND 4

I(calc.) − I(exptl.)	*Equation*			
	*2**	*2***	*3*	*4*
0–10	25.7	30.0	41.7	52.8
10–20	17.1	27.5	34.7	33.3
20–30	11.4	27.5	16.7	11.1
30–40	28.6	12.5	5.6	2.8
40–50	5.7	–	1.3	–
50–60	8.6	2.5	–	–
60–70	–	–	–	–
70–80	2.9	–	–	–
Mean accuracy of prediction***	25 ± 6	18 ± 4	14 ± 3	11 ± 2

* R^1H and R^2H as the standards.
** R^1H and R^2NH_2 as the standards.
*** In retention index units.

ACKNOWLEDGEMENT

We should like to express our gratitude to Professor J. Oszczapowicz whose kind discussions made it possible to obtain the results presented.

REFERENCES

1 L. S. Ettre, *Chromatographia*, 7 (1974) 39.
2 J. N. Tejedor, *J. Chromatogr.*, 177 (1979) 279.
3 J. Oszczapowicz, J. Osek and E. Dolecka, *J. Chromatogr.*, 315 (1984) 95.
4 J. Oszczapowicz, J. Osek, K. Ciszkowski, W. Krawczyk and M. Ostrowski, *J. Chromatogr.*, 330 (1985) 79.
5 J. Osek, J. Oszczapowicz and W. Drzewiński, *J. Chromatogr.*, 351 (1986) 177.
6 J. Oszczapowicz, J. Osek, W. Krawczyk and B. Kielak, *J. Chromatogr.*, 357 (1986) 93.
7 J. Oszczapowicz, K. Ciszkowski and J. Osek, *J. Chromatogr.*, 362 (1986) 383.
8 J. Osek, J. Jaroszewska-Manaj, W. Krawczyk and J. Oszczapowicz, *J. Chromatogr.*, 369 (1986) 398.
9 E. Kováts, *Helv. Chim. Acta*, 41 (1958) 1915.
10 L. S. Ettre, *Chromatographia*, 6 (1973) 489.
11 A. Grobler and G. Bálizs, *J. Chromatogr. Sci.*, 12 (1974) 57.
12 J. K. Haken, M. S. Wainwright and R. J. Smith, *J. Chromatogr.*, 133 (1977) 1.
13 O. Exner, *Collect. Czech. Chem. Commun.*, 31 (1966) 3222.

Journal of Chromatography, 463 (1989) 305–316
Elsevier Science Publishers B.V., Amsterdam — Printed in The Netherlands

CHROM. 21 114

IMPROVED CROSS-AXIS SYNCHRONOUS FLOW-THROUGH COIL PLANET CENTRIFUGE FOR PERFORMING COUNTER-CURRENT CHROMATOGRAPHY

I. DESIGN OF THE APPARATUS AND ANALYSIS OF ACCELERATION

YOICHIRO ITO*, HISAO OKA* and JIMMIE L. SLEMP
Laboratory of Technical Development, National Heart, Lung, and Blood Institute, National Institutes of Health, Building 10, Room 5D12, 9000 Rockville Pike, Bethesda, MD 20892 (U.S.A.)
(Received October 3rd, 1988)

SUMMARY

A novel design of the cross-axis synchronous flow-through coil planet centrifuge is introduced. The apparatus holds a pair of large coil holders symmetrically, one on each side of the rotary frame, at a lateral position 12.5 cm from the center of the holder shaft held 10 cm from the centrifuge axis. Mathematical analysis of acceleration generated by the planetary motion of the apparatus revealed a unique centrifugal force field which promises high retention of the stationary phase in the multilayer coil to perform efficient preparative-scale counter-current chromatography.

INTRODUCTION

Counter-current chromatography (CCC) is a true liquid–liquid partition chromatography which totally eliminates the use of a solid support[1]. Being a support-free system, the method offers a number of advantages over other chromatographic methods by minimizing various problems arising from the use of solid supports such as adsorptive loss and deactivation of samples, tailing of solute peaks, contamination, etc. In practice, CCC provides its greatest advantage in preparative-scale separations where high-performance liquid chromatography (HPLC) suffers loss of partition efficiency and high expenditure of the solvents and solid support materials.

Recently, partition efficiency of preparative CCC has been remarkably improved by development of a new centrifuge system called the cross-axis synchronous flow-through coil planet centrifuge (X-axis CPC) which performs multigram separations at a high partition efficiency[2–7]. A series of previous studies has shown that in the X-axis CPC the position of the coil on the rotary frame and helical diameter of the coil play a vital role in both stationary phase retention and partition efficiency. The experimental data obtained from the most recent model of the X-axis CPC with a 20-cm revolutional radius[4,5] further indicated that the column performance can be

* Visiting scientist from Aichi Prefectural Institute of Public Health, Nagoya, Japan.

0021-9673/89/$03.50

improved by (1) increasing the helical diameter of the coiled column and (2) lateral shift of the coil holder along the holder shaft.

In the present studies, a new model of the X-axis CPC is designed to accommodate a pair of large column holders each at a lateral location 12.5 cm from the center of the holder shafts. In Part I, principle and design of the apparatus are described in detail, and unique hydrodynamic effects produced by the present model are discussed in the light of the acceleration analysis together with the experimental results obtained from the existing X-axis CPC instruments.

PRINCIPLE AND DESIGN OF THE APPARATUS

Fig. 1 illustrates a set of rotary-seal-free flow-through centrifuge systems developed for performing CCC. In each diagram, a cylindrical coil holder with a bundle of flow tubes revolves around the main axis of the centrifuge and simultaneously rotates about its own axis at the same angular velocity, as indicated by a pair of arrows. The bundle of flow tubes with one end tightly supported at the central axis above the centrifuge does not twist because the synchronous planetary motion of the holder steadily unwinds the twist of the tube bundle caused by revolution. Consequently, all these systems permit continuous elution through the rotating column without the use of the rotary seal device which would become a potential source of various complications such as leakage, contamination, etc.

Type I shown at the top of the figure has a vertical orientation of the holder which can be modified in two different ways: in the left column, the holder is tilted toward the

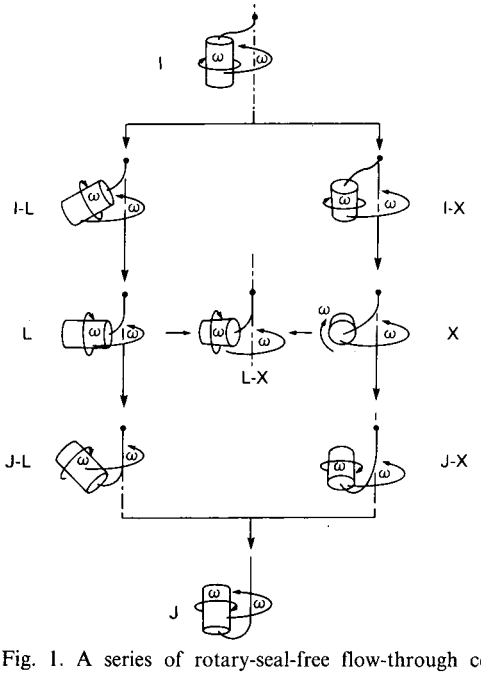

Fig. 1. A series of rotary-seal-free flow-through coil planet centrifuge systems for counter-current chromatography.

central axis of the centrifuge to form types L and J and their hybrids, whereas in the right colum the holder is rotated sideways to form types X and J and their hybrids. In the past, most of those centrifuge systems (except for types I–X and J–X) were constructed for performing CCC. Among those, types J and X were found to be most useful because of their unique capability to form unilateral distribution of the two solvent phases in the coiled column which is in turn utilized for performing high-speed CCC[8]. Type J is ideal for semipreparative to analytical-scale separations, while type X is most suitable for preparative-scale separations.

The original X-axis CPC was derived from type X as described elsewhere[2]. In the present apparatus, type X is further modified by shifting the position of the holder along its axis to form a hybrid between types L and X or type L–X as indicated at the center of Fig. 1. As described later, this new orientation of the holder can produce remarkable improvement in the retention of the stationary phase in the coiled column under the proper mode of elution and planetary motion.

The design of the present apparatus is illustrated in Fig. 2, where A shows a side view of the apparatus and B, a cross-sectional view through the central axis of the coil holders in a horizontal plane. The motor (1) (Fig. 2A, bottom) drives the central shaft (2) and the rotary frame around the central axis of the centrifuge. (In the actual design, the motor drives the rotor via a pair of toothed pulleys coupled with a toothed belt.) The rotary frame consists of four side-plates, a pair of inner plates (3) and a pair of outer plates (4), all rigidly bridged together with multiple aluminum links (not shown in the figure). A pair of horizontal plates, the upper (5) and the lower (6) plates (Fig. 2A), connects the pair of inner side-plates to the central shaft. The inner and the outer side-plates horizontally hold a coil holder shaft (7) symmetrically on each side of the rotary frame at a distance of 10 cm from the central axis of the centrifuge. A pair of identical coil holders (8) is mounted around the holder shafts symmetrically, one on each side of the rotary frame between the inner and the outer side-plates at a location about 12.5 cm from the center of the holder shaft as shown in Fig. 2B.

The planetary motion of each coil holder is established by the use of a set of miter gears and toothed pulleys as follows: A stationary miter gear (45°) (9) is rigidly mounted on the bottom plate of the centrifuge coaxially around the central shaft (2). This stationary sun gear is coupled to a pair of identical planetary gears (10) each attached to the proximal end of a countershaft (11) which radially extends toward the periphery of the rotary frame through the lower portion of the inner side-plate. This gear arrangement produces synchronous rotation of each countershaft on the rotating rotary frame. This motion is further conveyed to each coil holder by coupling a toothed pulley (12) mounted at the peripheral end of the countershaft to the identical pulley (13) on the respective coil holder shaft with a toothed belt (14). Consequently, each coil holder undergoes the desired planetary motion, *i.e.*, revolution around the central axis of the centrifuge and rotation about its own axis at the same angular velocity.

In the actual design of our prototype, each coil holder is made from three portions, *i.e.*, a main holder shaft supporting the coil holder and the toothed pulley, an auxiliary shaft placed on the opposite side, and a central pipe connecting these two shafts where the positions of the main holder shaft and the auxiliary shaft are mutually exchangeable on each side of the rotary frame. Each shaft is removable from the rotary frame by loosening the screws on each bearing block. Three pairs of spool-shaped coil holders were fabricated each with hub diameter of 10, 15, or 20 cm and equipped with

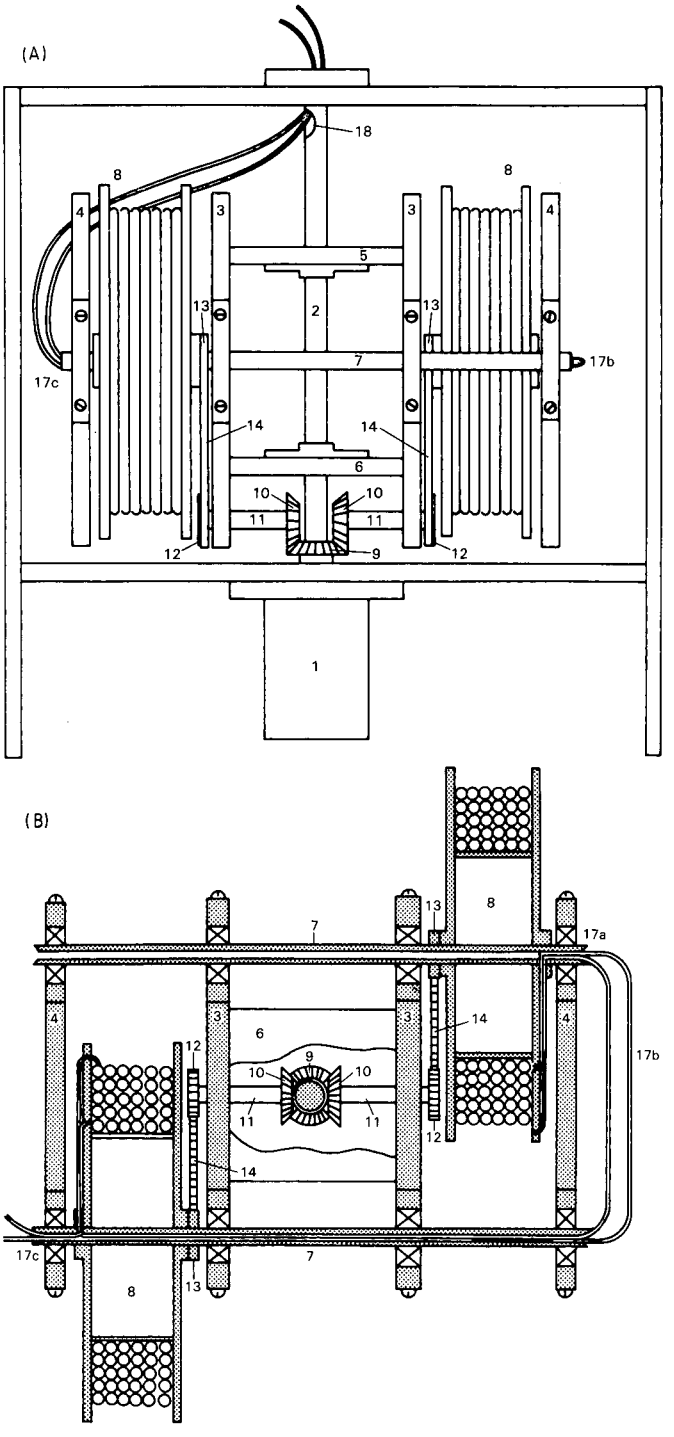

Fig. 2. The design of the present cross-axis synchronous flow-through coil planet centrifuge. (A) Side view of the apparatus. (B) Cross sectional view through the holder axis in the horizontal plane: 1 = motor; 2 = central shaft; 3 = inner side-plate; 4 = outer side-plate; 5 = upper plate; 6 = lower plate; 7 = coil holder shaft; 8 = coil holder; 9 = stationary miter gear; 10 = planetary miter gear; 11 = countershaft; 12 and 13 = toothed pulleys; 14 = toothed belt; 17a–c = flow tubes; 18 = side hole of the central shaft.

a pair of flanges of 24 cm in diameter, spaced 5 cm apart. The coiled column was prepared by winding a piece of PTFE (polytetrafluoroethylene) tubing (Zeus Industrial Products, Raritan, NJ, U.S.A.) directly around the holder hub, making either a single layer or multiple layers of coil as described in detail in Part II[9]. Here should be noted the advantages of the present design of the apparatus over that of the original X-axis CPC with the central coil position[2]. The lateral shift of the coil holder permits accommodation of a larger diameter coil holder which can extend in space beyond the center line of the rotary frame. This lateral coil position further provides a favorable hydrodynamic condition for most of the two-phase solvent systems in retention of the stationary phase, as discussed later in detail.

The pair of coiled columns on the rotary frame is connected in series to double the column capacity. The layout of the flow tubes (0.85 mm I.D. PTFE) is illustrated in Fig. 2A and B. A pair of flow tubes (17a) from the second column (Fig. 2B, right) first passes through the center hole of the holder shaft and, by making a loop (17b), enters the opening of the other holder shaft to reach the first column holder (Fig. 2B, left), where one flow tube (interconnecting tube) joins one end of the first column while the other bypasses the column. The flow tube from the other end of the first column and the latter flow tube from the second column exit the holder shaft together (17c) and then enter the side hole (18) (Fig. 2B) of the central shaft to reach the stationary tube-guide projecting down from the top plate of the centrifuge. These flow tubes are lubricated with grease and protected with a sheath of tygon tubing to prevent direct contact with metal parts. Under ordinary conditions, the flow tubes can maintain their integrity for many months of operation. As described earlier, these tubes are free from twisting and, therefore, serve for the continuous elution through the rotating coils without complications such as leakage and contamination.

Revolutional speed of the apparatus can be regulated up to 1000 rpm with a speed control unit (Bodine Electric Co., Chicago, IL, U.S.A.). In our laboratory the solvents are pumped with a Milton Roy metering pump while the effluent is continuously monitored with an LKB Uvicord S and fractionated with an LKB fraction collector.

ANALYSIS OF ACCELERATION GENERATED BY L–X PLANETARY MOTION

Analysis of the acceleration field produced by the original X-axis CPC at the central and lateral positions on the holder shaft has been reported earlier[2]. In order to discuss the hydrodynamics involved in the present system, it is desirable to briefly review the analysis of acceleration in the lateral position which can be directly applied to the L–X planetary motion illustrated in Fig. 1.

Fig. 3A shows planetary motion of an X-axis CPC where a cylindrical coil holder with radius r revolves around the central axis of the centrifuge system and simultaneously rotates about its own axis at the same angular velocity, ω, in the indicated directions. While doing so, the cylinder maintains the axial orientation perpendicular to and at a distance R from the central axis of the centrifuge. An arbitrary point, P, is located at the periphery of the cylinder at a distance l from point M on the central plane, as illustrated. Then, we observe the motion of point P as the cylinder undergoes the planetary motion described above.

In the reference x–y–z coordinate system for analysis, illustrated in Fig. 3B, the

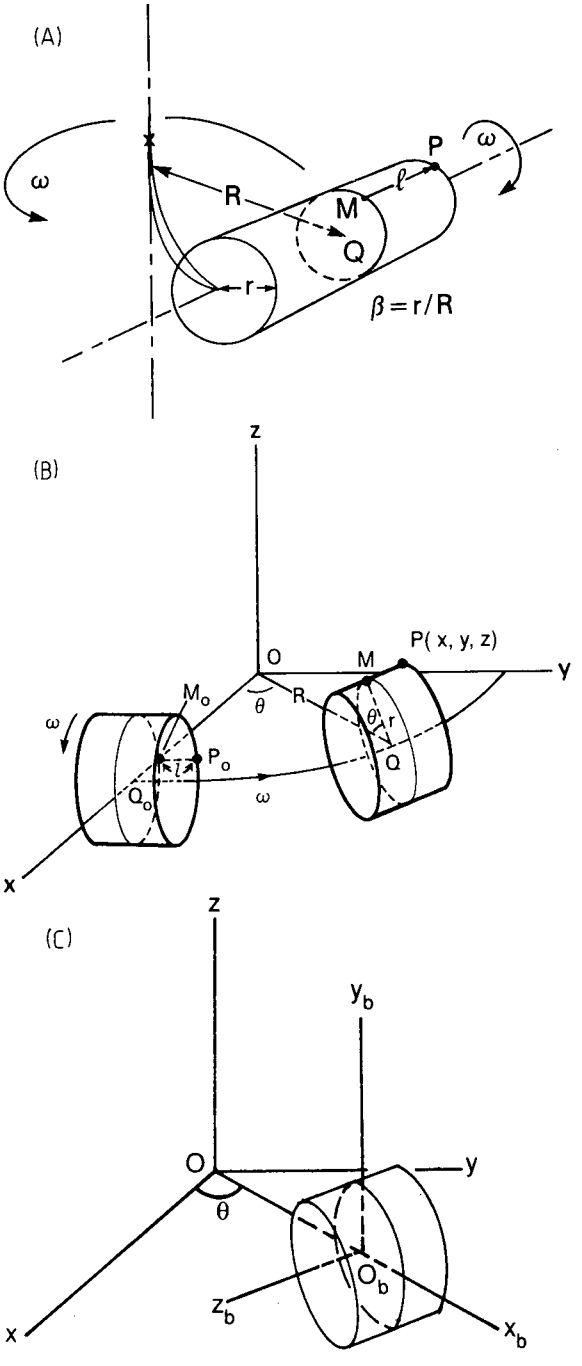

Fig. 3. Analysis of acceleration. (A) Mode of planetary motion. (B) Reference x–y–z coordinate system for analysis. (C) Relationship between the reference x–y–z coordinate system and x_b–y_b–z_b body coordinate system.

cylinder revolves around the z-axis at angular velocity ω and simultaneously rotates about its own axis at the same angular velocity in the indicated directions. The arbitrary point to be analyzed initially locates at point P_0 $(R-r,l,0)$ and, after a lapse of time t, moves to point P (x, y, z) which can be expressed in the following equations:

$$x = R\cos\theta - r\cos^2\theta - l\sin\theta \tag{1}$$

$$y = R\sin\theta - r\sin\theta\cos\theta + l\cos\theta \tag{2}$$

$$z = r\sin\theta \tag{3}$$

The acceleration acting on the arbitrary point is then obtained from the second derivatives of these equations as follows:

$$d^2x/dt^2 = -R\omega^2(\cos\theta - 2\beta\cos 2\theta) + l\omega^2\sin\theta \tag{4}$$

$$d^2y/dt^2 = -R\omega^2(\sin\theta - 2\beta\sin 2\theta) - l\omega^2\cos\theta \tag{5}$$

$$d^2z/dt^2 = -R\omega^2\beta\sin\theta \tag{6}$$

where $\beta = r/R$.

In order to visualize the effects of acceleration on the objects rotating with the cylinder, it is more appropriate to express the acceleration vectors with respect to the body frame or the x_b–y_b–z_b coordinate system illustrated in Fig. 3C. Transformation of the vectors from the original reference coordinate system to the body coordinate system may be performed according to the following equations:

$$\alpha_{x_b} = (d^2x/dt^2)\cos\theta + (d^2y/dt^2)\sin\theta = -R\omega^2(1 - 2\beta\cos\theta) \tag{7}$$

$$\alpha_{y_b} = d^2z/dt^2 = -R\omega^2\beta\sin\theta \tag{8}$$

$$\alpha_{z_b} = (d^2x/dt^2)\sin\theta - (d^2y/dt^2)\cos\theta = -R\omega^2 2\beta\sin\theta + l\omega^2 \tag{9}$$

where α_{x_b}, α_{y_b}, and α_{z_b} indicate the acceleration vectors acting along the corresponding coordinate axes. Eqns. 7–9, thus obtained, may serve as general formulae of acceleration generated by three types of synchronous planetary motion, illustrated in Fig. 1, by designating two parameters, R and l, where $l/R = \pm 1$ for type L–X (the present scheme), $l = 0$ for type X, and $R = 0$ for type L.

From these equations, the centrifugal force vectors (same magnitude with the acceleration but acting in the opposite direction) at various points on the cylinder are computed for three types of planetary motion, *i.e.*, type L ($R = 0$), type L–X ($l/R = -1$) and type X ($l = 0$), and diagrammatically illustrated in Fig. 4A–C. In order to express three-dimensional pattern of the centrifugal force vectors on a two-dimensional diagram, two force vectors, $-\alpha_{x_b}$ and $-\alpha_{y_b}$, are combined into a single arrow forming various angles from the x_b-axis, whereas the third force vector, $-\alpha_{z_b}$, which acts perpendicularly to the x_b–y_b plane, is drawn as a vertical column along the y_b-axis. The ascending column indicates the force acting upward ($z_b > 0$) and the descending

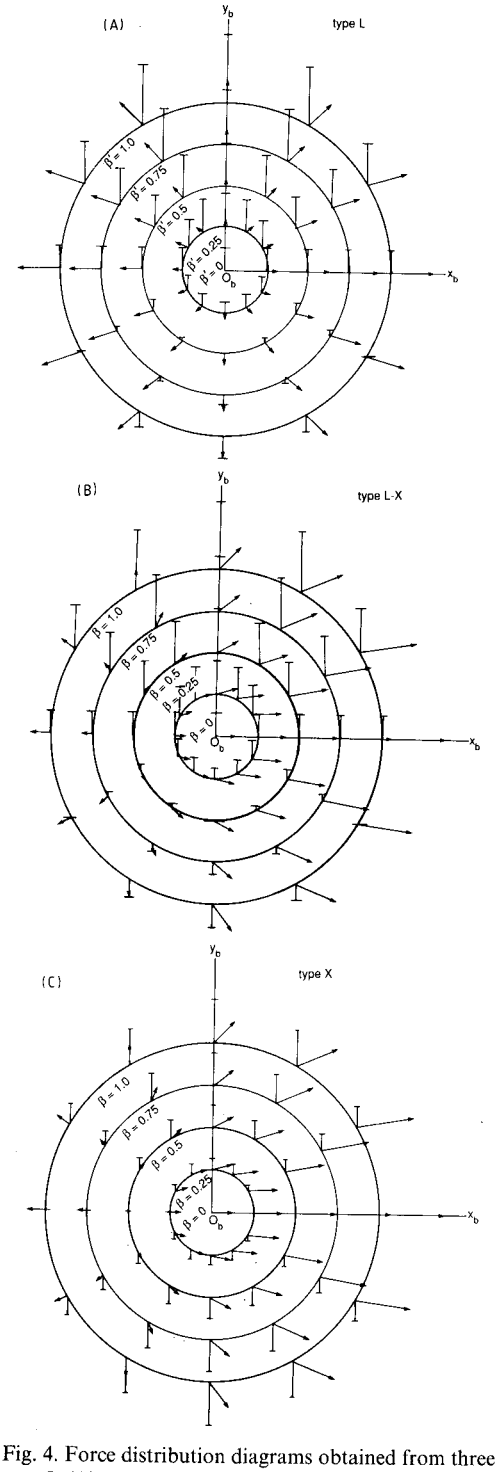

Fig. 4. Force distribution diagrams obtained from three mutually related synchronous planetary motions, type L (A), type L–X (B), and type X (C).

column, the force acting downward ($z_b < 0$). Several concentric circles around point O_b (the axis of the cylinder) indicate locations on the cylinder corresponding to parameter β or β' ($\beta' = r/l$ for type L planetary motion) indicated in the diagram. The distribution of the centrifugal force vectors in each diagram is fixed to the x_b–y_b–z_b body coordinate system and every point on the cylinder rotates around point O_b (z_b-axis) in either clockwise or counterclockwise direction as determined by the planetary motion of the cylinder.

As shown in these diagrams, the arbitrary point on the cylinder is subjected to a highly complex three-dimensional fluctuation of the centrifugal force field which varies in both magnitude and direction during each revolutional cycle. Force distribution pattern also changes with the location of the point on the cylinder where force vectors tend to increase their magnitude in the remote location from the axis of the cylinder. Each planetary motion generates a characteristic distribution of the centrifugal force vectors: type L planetary motion (Fig. 4A) forms a symmetrical distribution of outwardly radiating arrows around all circles and an asymmetric distribution of columns along the y_b-axis on the diagram. On the other hand, type X planetary motion (Fig. 4C) forms a contrasting pattern of the force distribution which consists of an asymmetric distribution of arrows along the x_b-axis and a symmetric distribution of column around point O_b. Interestingly enough, the hybrid type L–X (Fig. 4B) inherits asymmetric features from the parents forming asymmetric distributions of both arrows and columns each identical to that of the respective parent.

The effects of the above centrifugal force field to the hydrodynamic distribution and motion of two immiscible solvent phases in the coiled column is extremely complex and hardly predictable on the theoretical basis. However, it may be worthwhile to consider some possible hydrodynamic effects produced by the present L–X planetary motion in the light of the experimental results obtained from the various other types of planetary motions previously applied to CCC.

SPECULATION OF HYDRODYNAMIC EFFECTS OF L–X PLANETARY MOTION

Slow rotation of a coil around the axis laid horizontally in the gravitational field generates an Archimedean screw force which drives all objects of different density toward one end of the coil, which is conventionally called the head and the other end, the tail. When such a coil contains two mutually immiscible solvent phases, each phase is competitively pushed toward the head of the coil and the end result is that the two phases establish a hydrodynamic equilibrium where each phase occupies nearly equal space in each helical turn on the head side[10]. As the rotational speed of the coil is increased, the centrifugal force field produced by the rotation is superimposed on the gravitational field resulting in an asymmetrical distribution of the force field between the upper and the lower halves of the coil (Fig. 5A). This in turn alters the hydrodynamic equilibrium state in such a way that one of the phases (head phase), generally the heavier phase in this case, dominates the head of the coil. When the rotational speed reaches the critical range, the two solvent phases are completely separated along the length of the coil, the heavier phase entirely occupying the head side and the lighter phase on the tail side of the coil[10]. This unilateral hydrodynamic distribution of the two solvent phases, when combined with a strong centrifugal force field, provides the basis for the high-speed CCC[11].

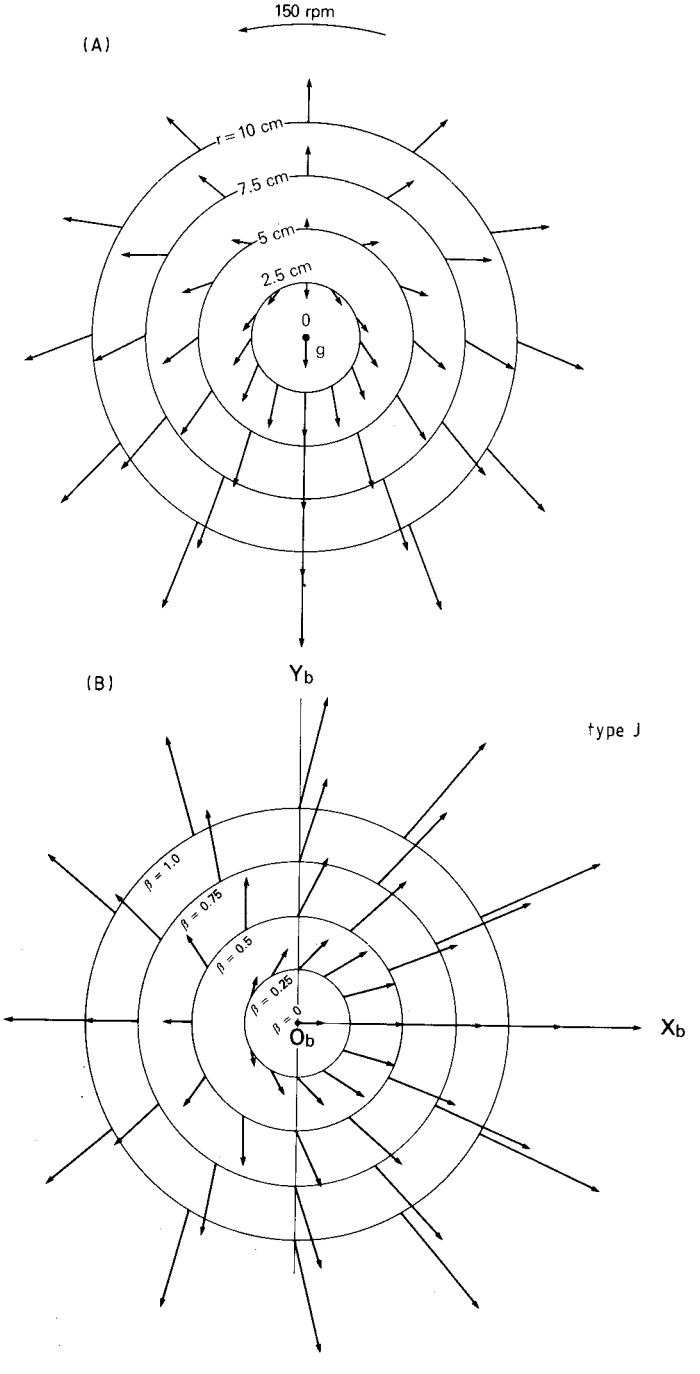

Fig. 5. Force distribution diagrams obtained from two different motions. (A) Combined force field of gravity and centrifugal force in simple rotation. (B) Centrifugal force field in type J synchronous planetary motion. Note the striking resemblance between the two.

Similar unilateral phase distribution is observed in the coil subjected to various types of planetary motion such as type J, type X and their hybrids, all of which generate an asymmetrical centrifugal force field between the proximal and distal position of the rotating coil. However, in these centrifuge systems, the mode of unilateral phase distribution varies according to the physical properties of the solvent system or, in a more convenient term, the settling time of the two solvent phases in the gravitational field[12]. In hydrophobic binary solvent systems with short settling times of 3–10 s, the lighter phase is always the head phase, whereas in hydrophilic butanol solvent systems with long settling times of 30–60 s, the heavier phase becomes the head phase. In the rest of the solvent systems with an intermediate range of settling times of 10–30 s, the head phase is determined by the mode of the planetary motion and further modified by the location of the coil on the holder expressed by β.

The type J planetary motion (Fig. 5B), which generates a strong two-dimensional centrifugal force field, usually distributes the lighter phase of the intermediate solvent systems toward the head of the coil[13]. This tendency is further enhanced in the remote location (large β value) on the holder where the magnitude of the radiating force vectors are increased in all directions. In the type X planetary motion (Fig. 4C), which generates a three-dimensional centrifugal force field, the magnitude of the main centrifugal force vectors is substantially reduced due to the formation of the lateral components. Subsequently, the intermediate solvent systems generally distribute the heavier phase toward the head[3]. However, it has been recently discovered that the hydrodynamic phase distribution in the type X planetary motion is significantly altered by shifting the position of the coil along the axis of the holder[5].

As shown in Fig. 4C, the type X planetary motion generates a lateral force field (columns) symmetrically on the upper and the lower segments of the coil. This symmetrical distribution of the lateral force vectors is altered by lateral shift of the coil position along the holder axis, while the main force field (arrows) remains unchanged. When this shift is applied toward the left, the lateral force component acting toward the left is added in all portions of the coil, resulting in an enhanced force field in the upper portion and a decreased force field in the lower portion of the coil as illustrated in Fig. 4B. According to the previous observation[5], hydrodynamic effects of this asymmetrical lateral force field may be divided into the following two categories: one on the head–tail phase distribution and the other on the retention of the stationary phase with respect to the direction of the planetary motion of the coil holder.

The lateral shift of the coil along the holder shaft adds a lateral force vector at the proximal and distal portions of the coil which may create an effect similar to that of an increased β value. In this situation, the intermediate solvent systems generate an inverse hydrodynamic trend to distribute the lighter phase toward the head as in the hydrophobic solvent systems. This effect becomes greater as the deviation ($\pm l$) of the coil position from the center of the holder shaft increases. Consequently, all intermediate solvent systems would eventually distribute the lighter phase toward the head of the coil as in the type J planetary motion.

The lateral shift of the coil further produces a peculiar effect on the retention of the stationary phase, particularly in the intermediate solvent group. In the type X planetary motion ($l = 0$), where the laterally acting force vectors display a symmetrical arrangement between the upper and the lower halves of the coil, retention of the stationary phase is not affected by direction of the planetary motion,

whether it is counterclockwise (P_I) or clockwise (P_{II}) revolution, as far as the proper mode of the head–tail elution is applied to the coil. However, in the lateral coil position where the laterally acting force field becomes asymmetrical, the retention of the stationary phase is determined by combination of the head–tail elution mode and the planetary motion. Among four possible combinations, *i.e.*, head–tail/P_I, head–tail/P_{II}, tail–head/P_I, and tail–head/P_{II}, one particular condition yields the highest level of stationary phase retention which in most cases substantially exceeds that obtained from the type X planetary motion ($l = 0$).

The above description about the effect of lateral coil shift is mostly based on the findings previously obtained from the X-axis CPC with a large revolutional radius ($R = 20$ cm) equipped with a 25-cm wide coil holder where the ratio of the lateral shift (l) to the revolutional radius or l/R is limited to $\pm$ 0.625 (ref. 4). The present X-axis CPC model with a 10-cm revolutional radius holds the coil holder in the lateral positions to provide $l/R = -1.25 \pm 0.25$ and, therefore, will significantly enhance the above effects to improve the retention of the stationary phase in the coil.

REFERENCES

1 Y. Ito, in N. B. Mandava and Y. Ito (Editors), *Countercurrent Chromatography: Theory and Practice*, Marcel Dekker, New York, 1988, Ch. 3, p. 79.
2 Y. Ito, *Sep. Sci. Technol.*, 22 (1987) 1971.
3 Y. Ito, *Sep. Sci. Technol.*, 22 (1987) 1989.
4 Y. Ito and T.-Y. Zhang, *J. Chromatogr.*, 449 (1988) 135.
5 Y. Ito and T.-Y. Zhang, *J. Chromatogr.*, 449 (1988) 153.
6 T. Y. Zhang, Y.-W. Lee, Q. C. Fang, R. Xiao and Y. Ito, *J. Chromatogr.*, 454 (1988) 185.
7 Y. Ito and T. Y. Zhang, *J. Chromatogr.*, 455 (1988) 151.
8 Y. Ito, *CRC Crit. Rev. Anal Chem.*, 17 (1986) 65.
9 M. Bhatnagar, H. Oka and Y. Ito, *J. Chromatogr.*, (1989) in press.
10 Y. Ito, *J. Liq. Chromatogr.*, 11 (1988) 55.
11 Y. Ito, *Adv. Chromatogr.*, (1984) 181.
12 Y. Ito and W. D. Conway, *J. Chromatogr.*, 301 (1984) 405.
13 Y. Ito, *J. Chromatogr.*, 301 (1984) 387.

Journal of Chromatography, 463 (1989) 317–328
Elsevier Science Publishers B.V., Amsterdam — Printed in The Netherlands

CHROM. 21 115

IMPROVED CROSS-AXIS SYNCHRONOUS FLOW-THROUGH COIL PLANET CENTRIFUGE FOR PERFORMING COUNTER-CURRENT CHROMATOGRAPHY

II. STUDIES ON RETENTION OF STATIONARY PHASE IN SHORT COILS AND PREPARATIVE SEPARATIONS IN MULTILAYER COILS

MOLINA BHATNAGAR, HISAO OKA* and YOICHIRO ITO*
Laboratory of Technical Development, National Heart, Lung, and Blood Institute, National Institutes of Health, Building 10, Room 5D12, 9000 Rockville Pike, Bethesda, MD 20892 (U.S.A.)
(Received October 3rd, 1988)

SUMMARY

Performance of the apparatus was evaluated in terms of stationary phase retention, partition efficiency and sample loading capacity. Preliminary studies with short coils revealed high retention of the stationary phase under a proper combination of the head–tail elution and planetary motion. Preparative capability of the apparatus was successfully demonstrated on efficient multigram separations of 2,4-dinitrophenyl amino acids, indole auxins, and bacitracin in a pair of large multilayer coils with a total capacity of 1.5 l.

INTRODUCTION

As described in Part I[1], the present design of the cross-axis synchronous flow-through coil planet centrifuge (X-axis CPC) generates a characteristic centrifugal force field which will permit high retention of the stationary phase in the coiled column.

In this paper, perfomance of the present apparatus was studied in terms of stationary phase retention, partition efficiency, sample loading capacity, etc. A series of systematic studies was conducted to measure retention of the stationary phase in short single-layer coils mounted on two column holders with different hub diameters. Using the optimal experimental conditions determined by the preliminary studies, the preparative capability of the present apparatus was demonstrated on gram-quantity separations of various biological samples in a pair of large multilayer coils connected in series with a total capacity of 1.5 l.

* Visiting scientist from Aichi Prefectural Institute of Public Health, Nagoya, Japan.

0021-9673/89/$03.50

EXPERIMENTAL

Apparatus

The design of the apparatus used in the present studies is described in detail in Part I[1]. Briefly, the present X-axis CPC symmetrically holds a pair of multilayer coils on the rotaty frame 10 cm from the center of the holder shaft (Fig. 1). This lateral position of the columns allows for the use of larger multilayer coils and also yields higher retention of the stationary phase.

Separation columns

Present studies were performed with two different types of coiled columns: single-layer short coils for preliminary phase retention studies and long multilayer coils for preparative separation studies.

Short coils were prepared with a 5 m × 2.6 mm I.D., and 28 ml capacity PTFE (polytetrafluoroethylene) tubing (Zeus Industrial Products, Raritan, NJ, U.S.A.) by manually winding a single layer onto the holder hub of either 10 or 20 cm diameter. The column was mounted at a lateral position 10 cm left from the center of the holder shaft. A counterweight was mounted on the opposite side of the rotary frame symmetrically in the lateral position. Each coil was securely affixed onto the holder hub with fiberglass reinforced adhesive tape. Each end of the coil was connected to a flow tube, measuring *ca.* 1 m × 0.85 mm I.D. These flow tubes were directed to the outside of the centrifuge as described in Part I[1].

Each multilayer coil was prepared from one piece of 2.6 mm I.D. PTFE tubing by winding it in a spool-type fashion onto the holder of 15 cm diameter, thus making multiple layers between a pair of flanges spaced 5 cm apart. The column consisted of 15 layers of coiled tubing with a capacity of about 750 ml. The β value varied from 0.75 at the internal terminal to 1.15 at the external terminal. As described in Part I[1], β is the

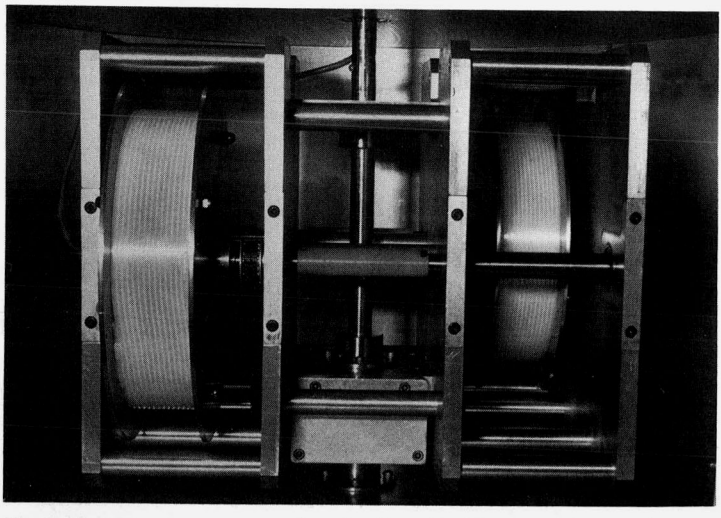

Fig. 1. The present apparatus equipped with a pair of large multilayer coil separation columns in the lateral position.

ratio of the radius of rotation (distance from the central axis of the holder to the coil) to the radius of revolution (distance from the central axis of the centrifuge to the axis of the holder). A similar second multilayer coil was laterally placed in a symmetrical position, on the opposite side of the rotary frame (thus making the total column capacity about 1.5 l). These two columns were connected in series with a flow tube on the rotary frame in such a way that the external terminal of the first column and the internal terminal of the second column were joined. In this way, mechanical balance of the centrifuge system was ensured and the two columns had identical elution modes. Fig. 1 shows the present apparatus equipped with a pair of multilayer coils in the lateral position of the holder shaft. This column location is of great importance as it allows for the utilization of large columns with greater volume capacities and improved stationary phase retention.

Reagents

Organic solvents used for the preparation of the two-phase solvent systems include *n*-hexane, ethyl acetate, chloroform, *n*-butanol, *sec.*-butanol, ethanol, methanol, hydrochloric acid, and acetic acid. Among these, acetic acid and ethanol were of reagent grade and obtained from J. T. Baker (Phillipsburg, NJ, U.S.A.); and Midwest Solvents Co. (Pekin, IL, U.S.A.); respectively, while hydrochloric acid (1 *M*), and all test samples such as 2,4-dinitrophenyl amino acids (DNP-L-leucine, DNP-L-proline, DNP-β-alanine, DNP-DL-glutamic acid, diDNP-L-cystine, DNP-Δ-L-ornithine, DNP-L-aspartic acid, and DNP-L-alanine), indole auxins (indole-3-acetamide, indole-3-acetic acid, indole-3-butyric acid), and bacitracin were obtained from Sigma (St. Louis, MO, U.S.A.). All other solvents were glass-distilled chromatographic grade and purchased from Burdick & Jackson Labs. (Muskegon, MI, U.S.A.).

Preparation of two-phase solvent systems and sample solutions

Using the solvents mentioned above, the following volatile two-phase solvent systems were prepared for preliminary studies on retention of the stationary phase: *n*-hexane–water; *n*-hexane–methanol; *n*-hexane–ethyl acetate–methanol–water (1:1:1:1); ethyl acetate–water; ethyl acetate–acetic acid–water (4:1:4); chloroform–water; chloroform–acetic acid–water (2:2:1); *n*-butanol–water; *n*-butanol–acetic acid–water (4:1:5); and *sec.*-butanol–water. The solvent systems of chloroform–acetic acid–0.1 *M* hydrochloric acid (2:2:1); *n*-hexane–ethyl acetate–methanol–water (3:7:5:5); and chloroform–95% ethanol–water (5:4:3) were prepared for the preparative separations with multilayer coils. Each solvent system was carefully equilibrated in a separatory funnel at room temperature by vigorously shaking and repeatedly degassing the mixture and by allowing the mixture to completely separate before its use.

Sample solutions for DNP amino acid separations were prepared in the following manner: two sets of sample mixtures were prepared, one for the lower phase elution and the other for the upper phase elution, both with the same solvent system of chloroform–acetic acid–0.1 *M* hydrochloric acid (2:2:1). The sample for the lower phase elution consisted of DNP-Leu (400 mg), DNP-Pro (800 mg), DNP-β-Ala (800 mg), diDNP-$(Cys)_2$ (400 mg), and DNP-Glu (1600 mg) dissolved in equal volumes of upper and lower phases totaling 100 ml of solvent. The second set of the sample for the upper phase elution consisted of DNP-Orn (400 mg), DNP-Asp (800 mg), DNP-Glu

TABLE I

SUMMARY OF EXPERIMENTAL CONDITIONS FOR PREPARATIVE CCC

A = Chloroform–acetic acid–0.1 *M* hydrochloric acid (2:2:1); B = *n*-hexane–ethyl acetate–methanol–water (3:7:5:5); C = chloroform–95% ethanol–water (5:4:3).

Experiment No.	*Sample*	*Sample volume (ml)*	*Settling time (s)*	*Solvent system*	*Mobile phase*	*Flow-rate (ml/h)*	*Planetary* motion*	*Elution mode*	*Revolution speed (rpm)*
1	DNP amino acid mixture DNP-L-leucine 400 mg DNP-L-proline 800 mg DNP-β-alanine 800 mg diDNP-L-cystine 400 mg DNP-DL-glutamic acid 1600 mg	100	37	A	Lower phase	120	P_I	Head-to-tail	600
2	DNP amino acid mixture DNP-L-ornithine 400 mg DNP-L-aspartic acid 800 mg DNP-DL-glutamic acid 800 mg diDNP-L-cystine 400 mg DNP-L-alanine 1600 mg	100	37	A	Upper phase	120	P_I	Tail-to-head	600
3	Indole auxins Indole-3-acetamide 1 g Indole-3-acetic acid 1 g Indole-3-butyric acid 1 g	140	36	B	Lower phase	120	P_I	Head-to-tail	600
4	Bacitracin 5 g	120	100	C	Lower phase	120	P_I	Head-to-tail	600

* Planetary motion P_I: 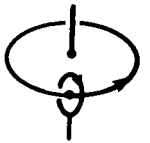 ; P_{II}: 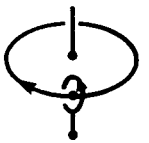 Large circles indicate revolution around the central axis of the centrifuge and small circles rotation around the holder axis.

(800 mg), diDNP-$(Cys)_2$ (400 mg), and DNP-Ala (1600 mg). The 4-g sample was similary dissolved in 100 ml of solvent, again using equal volumes of upper and lower phases. Indole-3-acetamide, indole-3-acetic acid, and indole-3-butyric acid, each 1 g, were dissolved in 140 ml solvent mixture consisting of equal volumes of the two phases. Bacitracin (5 g) was dissolved in 120 ml of solvent consisting of 30 ml water, 40 ml ethanol (95%), and 50 ml chloroform which were added in the above order and amounts.

Measurement of settling time of sample solution

The settling time of the sample solutions used in the preparative separations were measured by using the following procedures as described elsewhere[2]. First, the two-phase solvent system was equilibrated with the desired sample. Then, 2 ml of each phase were delivered into a 5-ml capacity graduated cylinder equipped with a glass stopper. The cylinder was gently shaken by carefully turning it upside down and returning it to its upright position five times. The cylinder was then placed on a horizontal surface, and the time required for the solvent mixture to form two clear layers was measured with a stopwatch. The measurement of the settling time was repeated several times for each sample solution to obtain the mean value. The settling times thus obtained are listed in Table I.

Procedures for preliminary studies on stationary phase retention in short coils

For each experiment, the short coil was first entirely filled with the stationary phase. Then the apparatus was run at the desired revolutional speed while the mobile phase was continuously eluted through the coil at a flow-rate of about 120 ml/h. The effluent from the outlet was collected in a 25-ml capacity graduated cylinder. After 20 ml were eluted, results were recorded by simply observing the amount of upper and lower phases comprising the total volume of the effluent. The apparatus was then flushed out by allowing nitrogen gas to push out the material in the column while rotating the apparatus at 100–200 rpm in the tail-to-head elution mode to facilitate the process. The experiments were performed by varying experimental conditions such as revolutional speeds (200, 400, 600, 800 rpm), planetary motions (P_I and P_{II}), elution modes (head-to-tail or tail-to-head), and the use of upper and lower phases as the mobile phase.

Construction of phase distribution diagram

From the volume of the stationary phase eluted from the column (V_s), the percentage retention of the stationary phase relative to the total column capacity was computed according to the expression, $100(V_c + V_f - V_s)/V_c$, where V_c and V_f are the total column capacity and the dead space volume in the flow tubes, respectively. Using these retention data, a set of phase distribution diagrams was prepared by plotting the percentage retention of the stationary phase against the applied revolutional speed in rpm. The retention curves obtained from the different elution modes of head–tail elution and planetary motion, but otherwise identical experimental conditions, were drawn in the same diagram to facilitate comparison. In order to distinguish the applied elution mode, each retention curve was drawn with a specific symbolic design as indicated in Table II.

TABLE II

FOUR DIFFERENT ELUTION MODES AT LATERAL COIL POSITION ($l = -10$ cm)

*Planetary motion**	*Head-tail elution mode*	*Combined elution mode**	*Symbolic designs in PDD***
P_I	Head-to-tail	P_I–H	○———○
	Tail-to-head	P_I–T	○-----○
P_{II}	Head-to-tail	P_{II}–H	△———△
	Tail-to-head	P_{II}–T	△-----△

* H = Head-to-tail; T = tail-to-head.
** PDD = Phase distribution diagram (Fig. 2).

Procedures for preparative separations with multilayer coils

Using the optimum conditions determined by the preliminary experiments with the short coils, preparative-scale counter-current chromatography (CCC) separations were performed with a pair of multilayer coils symmetrically mounted, one on each side of the centrifuge rotor, at the lateral positions on the holder shaft.

Each preparative separation was performed as follows: the entire column (the pair of multilayer coils connected in series) was first filled with the stationary phase. This was followed by the introduction of the sample solution through the sample port. Then, the apparatus was run at 600 rpm in planetary motion P_I while the mobile phase was pumped into the column at a constant flow-rate of 120 ml/h in the suitable head–tail elution mode. The effluent from the outlet of the column was continuously monitored with an LKB Uvicord S at 278 nm and fractionated with an LKB fraction collector to obtain approximately 15 ml of fraction in each tube (during a 7.5-min interval). An aliquot of fraction, 50 μl for the DNP amino acid and indole auxin separations and 0.5 ml for the bacitracin separation, was mixed with 3 ml methanol, and, using a Zeiss PM6 spectrophotometer, the absorbance of these samples was measured at suitable wavelengths of 430 nm for DNP amino acids, 280 nm for indole auxins, and 250 nm for bacitracin.

After each separation was completed, retention of the stationary phase was measured by collecting the column contents by forcing them out of the column with pressured nitrogen gas combined with the slow rotation of the coil in the tail-to-head elution mode.

High-performance liquid chromatographic (HPLC) analysis of bacitracin

Both the original sample solution and the peak fraction of bacitracin obtained by the CCC separation were analyzed with a Shimadzu HPLC system consisting of a Model LC-6A pump, a manual injector kit, a Model SPD-6A detector, and a Model C-R5A recording data processor. HPLC analysis was performed on a Capcell Pak C_{18} column (15 × 0.46 cm I.D., type AG, Shiseido, Tokyo, Japan) by using a solvent composed of methanol and 0.04 *M* Na_2HPO_4 (pH 9.4) at a volume ratio of 62:38. At a flow-rate of 1 ml/min, the chromatogram was isocratically obtained by monitoring the absorbance at 234 nm.

RESULTS AND DISCUSSION

Model studies on retention in short coils

In the series of preliminary studies, ten different two-phase solvent systems were used to investigate the retention of the two solvent phases in the short coils mounted on a set of holders laterally located on the holder shaft. The results obtained clearly show that the degree of stationary phase retention is significantly affected by the direction of the planetary motion as well as the head–tail elution modes.

The results of the stationary phase retention studies are summarized in Fig. 2A. In this figure, each column consists of phase distribution diagrams obtained from the solvent systems labeled at the top of each column. These columns are arranged from left to right in the order of hydrophobicity of the major organic solvents (*i.e.*, *n*-hexane, ethyl acetate, chloroform, *n*-butanol, and *sec.*-butanol). The top two rows of the figure show retention of the lower phase obtained by the elution of the upper mobile phase, while the bottom two rows show the retention of the upper phase by the elution of the lower phase. Within each stationary phase group, the first row shows results obtained from a 10-cm holder diameter (or $\beta = 0.5$) and the second row shows results from a 20-cm holder diameter (or $\beta = 1.0$). Parameter β determines both the direction and magnitude of the centrifugal force field acting on various locations of the holder as described in Part I[1]. The two different elution modes are represented in Table II as the following: the solid line indicates the head-to-tail elution and the dotted or broken line the tail-to-head elution. The direction of the planetary motion is displayed as well: circles represent planetary motion P_I while triangles show the opposite planetary motion P_{II}.

Hydrophobic binary solvent systems, including *n*-hexane–water, ethyl acetate–water, and chloroform–water, show high stationary phase retention when the upper phase is eluted from tail to head (broken lines in the upper half of the figure) with planetary motion P_I or when the lower phase is eluted in the opposite elution mode of head-to-tail in planetary motion P_I (solid lines in the bottom half of the figure). These facts suggest that the upper phase tends to move toward the head and the lower phase toward the tail. The hydrophilic solvent systems such as *n*-butanol–acetic acid–water (4:1:5) and *sec.*-butanol–water, however, display an opposite hydrodynamic behavior. Planetary motion P_I, along with the head-to-tail elution of the upper mobile phase, brings about satisfactory retention levels (about 50%) for the lower phase. In observing upper phase retention levels, planetary motion P_{II} with the head-to-tail elution also produces similar retention levels of the stationary phase. The rest of the solvent systems with intermediate degrees of hydrophobicity generally show a hydrodynamic trend similar to that of the hydrophobic binary solvent systems with high retention levels.

The overall results of the above retention studies on the present apparatus indicated significant improvement of retention over those obtained from the central coil position in the original X-axis CPC[3,4]. Intermediate solvent systems used in the original apparatus with the central coil position show reversed hydrodynamic trends from those found in the present studies. In the present apparatus, intermediate solvent systems such as *n*-hexane–methanol, ethyl acetate–acetic acid–water (4:1:4), and *n*-butanol–water, display excellent retention at $\beta = 0.5$ or 1.0 under the proper head-to-tail elution mode combined with planetary motion P_I. Tremendous improve-

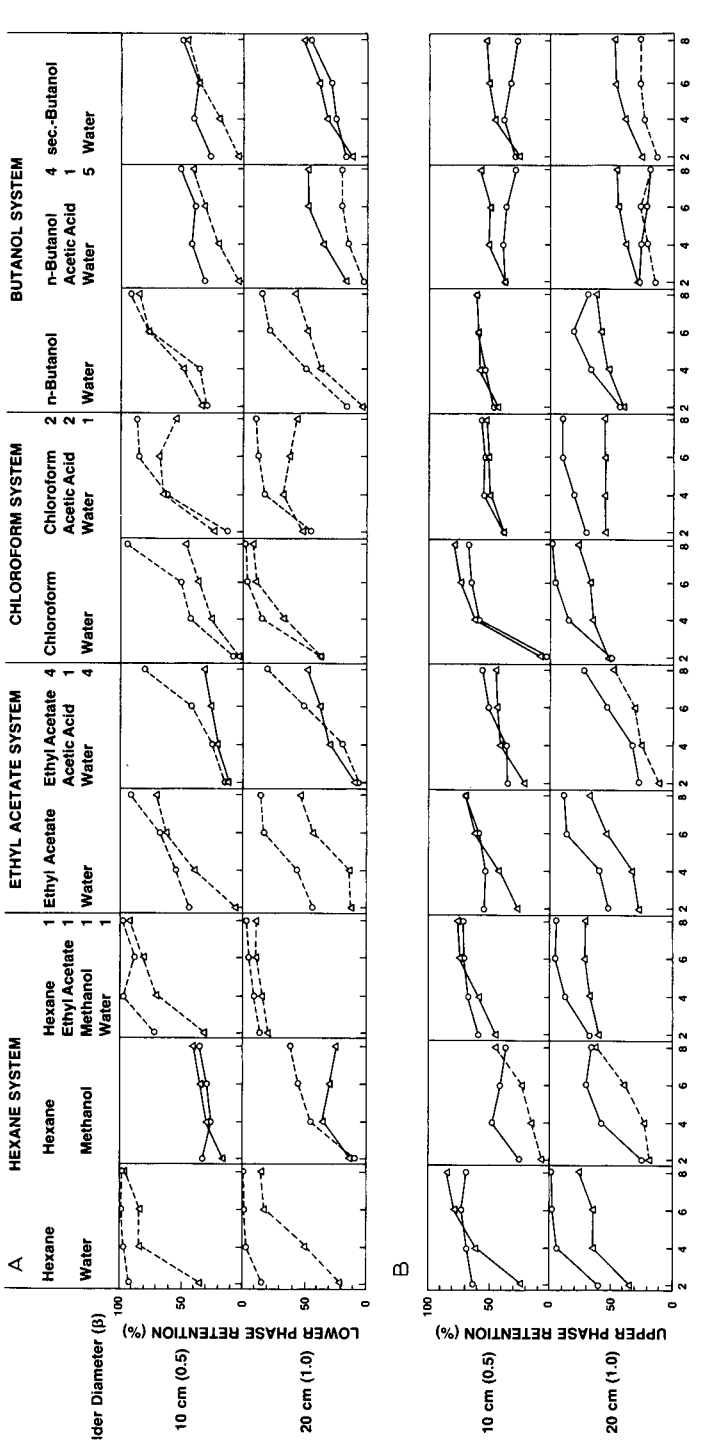

Fig. 2. Phase distribution diagrams obtained from the present X-axis CPC (type L–X, 10 cm revolution radius, $l = -10$ cm). See Table II for symbolic designs for phase distribution curves.

ment in retention with hydrophilic solvent systems was also observed. Retention values of *n*-butanol–acetic acid–water (4:1:5) and that of *sec.*-butanol–water reached approximately 50% at both β values. The above results clearly indicate that the present system, due to its lateral coil position, gives remarkable retention of the stationary phase in all the solvent systems examined, provided that the proper combination of planetary motion and head–tail elution mode is utilized. These results are consistent with the results of acceleration analysis described in Part I[1].

Preparative CCC with multilayer coils

Fig. 3A shows a chromatogram of the first set of DNP amino acid mixture with a solvent system composed of chloroform–acetic acid–0.1 *M* hydrochloric acid (2:2:1) using the lower non-aqueous phase as the mobile phase. The separation was performed at a flow-rate of 120 ml/h at 600 rpm (P_I). The 4-g quantity of the sample mixture was efficiently separated within 24 h. DNP-glutamic acid was eluted as a skewed peak, apparently due to the non-linear isotherm caused by its high concentration in the sample solution. Fig. 3B shows a similar chromatogram of the second set of DNP amino acid mixture by eluting with the upper aqueous phase but otherwise identical experimental conditions. All peaks were well resolved and eluted out in 21 h. The retention of the stationary phase in these separations was 78.5% in the first experiment and 70.3% in the second experiment.

Fig. 4 shows a chromatogram of indole auxins with a two-phase solvent system composed of *n*-hexane–ethyl acetate–methanol–water (3:7:5:5). The separation was performed by eluting the lower aqueous phase in the head-to-tail mode at a flow-rate of 120 ml/h at 600 rpm (P_I). Three components were well separated as discrete symmetrical peaks within 24 h. The partition efficiencies were computed according to the conventional gas chromatographic formula:

$$N = (4R/w)^2$$

where N denotes the partition efficiency expressed in terms of theoretical plate number, R, the retention time or volume of the peak maximum and w, the peak width expressed in the same unit as R. The present separation yielded high partition efficiencies ranging from 300 theoretical plates for the first peak to 700 theoretical plates for the second peak. The retention of the stationary phase was 70.8%.

The present method was applied to separation of commercial bacitracin sample using a solvent system composed of chloroform–95% ethanol–water (5:4:3). Bacitracin (5 g) was dissolved in 120 ml of solvent consisting of approximately equal volumes of the upper and the lower phases. The lower non-aqueous phase was used as the mobile phase and introduced through the head of the multilayer coil at a flow-rate of 120 ml/h at 600 rpm (P_I). In Fig. 5, a chromatogram of bacitracin thus obtained consists of three major peaks which include the second peak of bacitracin A as labeled.

Purity of the bacitracin A fraction obtained from the above separation was determined by a reversed-phase HPLC analysis. Fig. 6A shows the chromatogram obtained from the original sample solution which contains over 20 UV-absorbing peaks, including the main bacitracin A peak eluting at 11.8 min. Fig. 6B shows the chromatogram of the major peak fraction (fraction 85) obtained under the identical analytical condition which indicates high purity of bacitracin A with only few minor

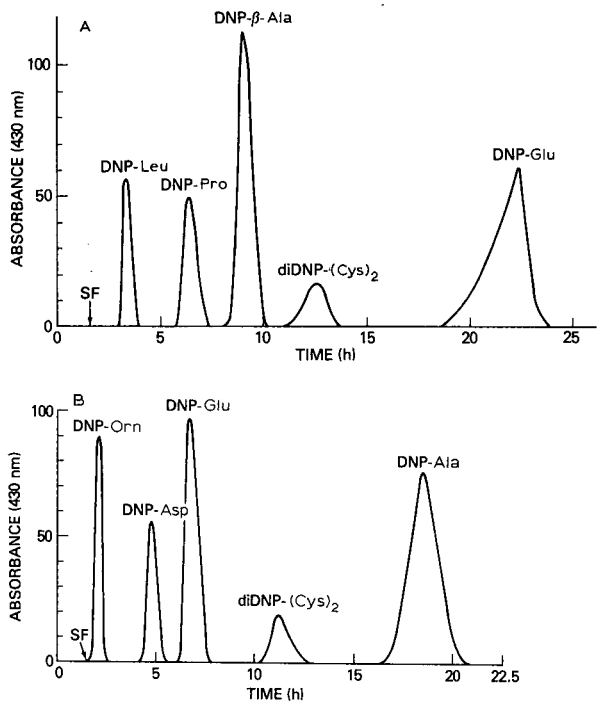

Fig. 3. Chromatograms of DNP amino acid mixture with chloroform–acetic acid–0.1 *M* hydrochloric acid (2:2:1). (A) Lower phase mobile; (B) upper phase mobile. See Table I for experimental conditions.

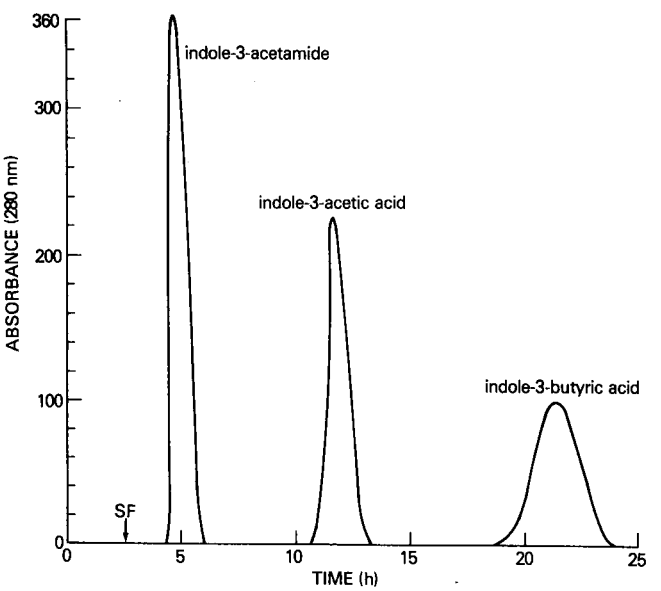

Fig. 4. Chromatogram of indole auxins with *n*-hexane–ethyl acetate–methanol–water (3:7:5:5). See Table I for experimental conditions.

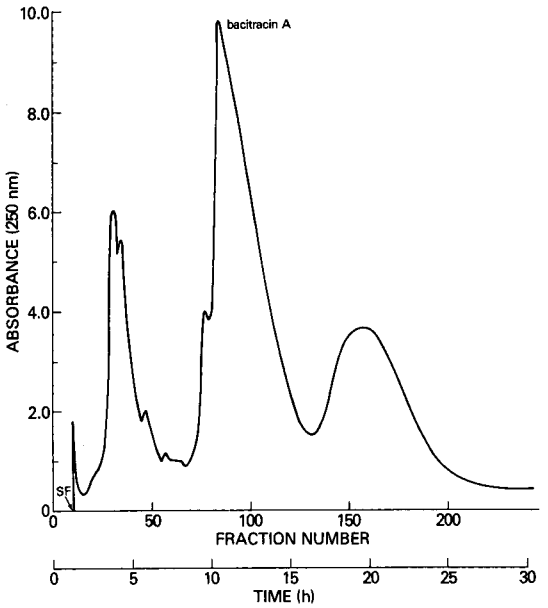

Fig. 5. Chromatogram of bacitracin with chloroform–95% ethanol–water (5:4:3). See Table I for experimental conditions.

peaks of impurity. The earlier eluted two peaks with retention times of 3.0 and 4.0 min were derived from chloroform and a possible impurity from ethanol used in the CCC separation.

In the above bacitracin separation, the retention of the stationary phase was found to be as high as 71%, which apparently produced excellent peak resolution in the present separation. Previously, it has been observed that heavy loading of sample solution with a long settling time of over 30 s tends to decrease retention of the

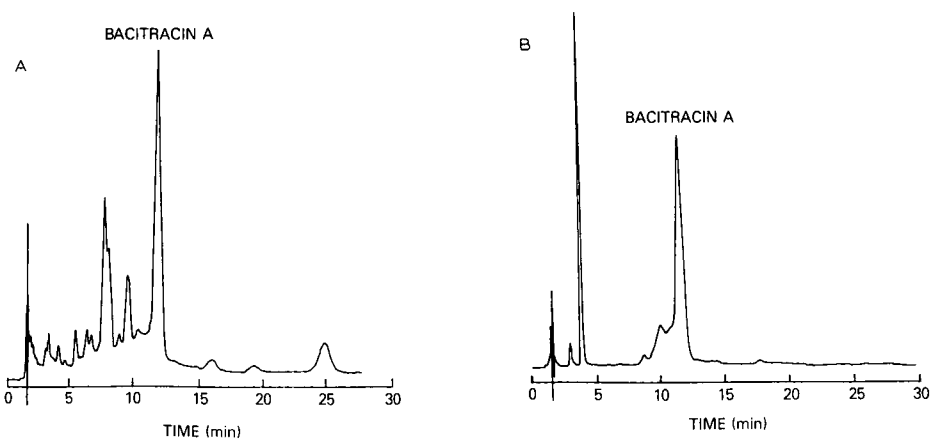

Fig. 6. HPLC analysis of bacitracin. (A) Chromatogram of original sample; (B) chromatogram of peak fraction 85 of bacitracin A. For experimental conditions, see Experimental section.

stationary phase resulting in poor peak resolution in the existing type J high-speed CCC instruments[2]. With the present apparatus, however, a 5-g quantity of bacitracin dissolved in 120 ml of solvent mixture with a long settling time of about 100 s was efficiently separated with a high retention value of over 70%. This unusual retention capability of the present X-axis CPC may be explained on the basis of the asymmetric lateral centrifugal force field resulted from lateral shift of the coil position as discussed in Part I[1].

The overall results of the above studies clearly indicate a great potential of the present apparatus for preparative-scale separations. The unique capability of the apparatus may be summarized as follows: (1) high retention of the stationary phase to yield excellent peak resolution; (2) high partition efficiency due to vigorous mixing; (3) universal choice of the two-phase solvent systems; (4) large column capacity and high sample loading capability; (5) stable balance of the centrifuge system without counterweight adjustment.

Because of these advantages, the present X-axis CPC will be extremely useful for preparative separations of a variety of natural and synthetic products in both research laboratories and industrial plants.

ACKNOWLEDGEMENTS

The authors are indebted to Shimadzu Scientific Co. (Columbia, MD, U.S.A.) and Shiseido (Tokyo, Japan) for lending a set of HPLC instruments free of charge.

REFERENCES

1 Y. Ito, H. Oka and J. L. Slemp, *J. Chromatogr.*, (1989) in press.
2 Y. Ito and W. D. Conway, *J. Chromatogr.*, 301 (1984) 405.
3 Y. Ito, *Sep. Sci. Technol.*, 22 (1987) 1971.
4 Y. Ito, *Sep. Sci. Technol.*, 22 (1987) 1989.

Journal of Chromatography, 463 (1989) 329–344
Elsevier Science Publishers B.V., Amsterdam — Printed in The Netherlands

CHROM. 21 030

HIGH-PERFORMANCE ANION-EXCHANGE CHROMATOGRAPHY OF PROTEINS USING AZA-ETHER BONDED SILICA-BASED PHASES

N. T. MILLER* and CHIA-HUI SHIEH**,*
CAA Separations, 1106 Commonwealth Avenue, Boston, MA 02215 (U.S.A.)
(First received March 1st, 1988; revised manuscript received October 4th, 1988)

SUMMARY

The use of wide-pore silica-based hydrophilic aza-ether bonded phases for the chromatographic separation of proteins under anion-exchange conditions was studied. Polyether silanes containing terminal morpholine or piperazine derivatives are synthesized for attachment to the silica surface and provide a flexible approach to bonded phase design. In one instance, a quaternized amine support may be prepared by further derivatization of the methylpiperazine bonded phase. The supports provide high-performance anion-exchange chromatographic separations of proteins using gradients of increasing salt content, *e.g.*, to 1.0 *M* sodium acetate at pH 7.0. The salt type and concentration can be varied to control protein retention while the buffer system used at pH 7.0 exerts a minimal influence on the separation. The anion exchangers may be reproducibly prepared and exhibit chromatographic retention stability at pH 7.5 for at least 2 months of operation. Acceptable capacity for protein on the bonded phase is demonstrated with high recovery of solute mass. The flexibility in anion exchanger design provides a probe of bonded ligand hydrophobic effects which can contribute in an undefined and deleterious manner to the desired ion-exchange separation. Taken together, these results provide a greater insight into the operating characteristics of anion exchangers, especially with regard to competing retention mechanisms.

INTRODUCTION

High-performance anion-exchange chromatography (AEC) continues to be a widely used technique in the analysis and purification of biopolymers. Bonded anion-exchange phases have usually incorporated a tertiary amine functionality attached to carbohydrate, silica or polymer supports[1]. Quaternary ammonium salts immobilized on supports demonstrate an advantageous pH-independent permanent charge, but phase characterization is more difficult as these strong anion exchangers are usually prepared directly from the bonded tertiary amine phases.

* Present address: The PQ Corporation, R&D Center, 280 Cedar Grove Rd., Lafayette Hill, PA 19444, U.S.A.
** Present address: Beckman Instruments, Inc., Altex Division, 2350 Camino Ramon, San Ramon, CA 94583-0701, U.S.A.

0021-9673/89/$03.50

Currently, two main approaches are taken in the design of bonded tertiary amine phases for anion-exchange high-performance liquid chromatography (HPLC) of biomacromolecules. First, in analogy with classical anion-exchange soft gel supports, the diethylaminoethyl (DEAE) ligand is attached to silica or hydrophilic polymers[2,3]. Several commercial columns of this type have been extensively used in life science applications[4–8].

A second more recent approach, developed by Alpert and Regnier[9], involves the adsorption and cross-linking of polyethyleneimine (PEI) polymers on microparticulate porous silicas. The synthetic procedure provides control of the number of surface polymeric layers and the degree of hydrophobicity (by virtue of the cross-linking agent used[10]). A variety of commercially available packings utilize this type of chemistry[11–14].

Recent work in this field has examined new applications[1], improved column stability[15,16] and the capability for faster (< 1 min) separations[17].

In this paper, we present results on new anion-exchange phases obtained by attaching a morpholine or piperazine functionality to a polyether silane followed by bonding to silica. The columns achieve high-performance protein separations and exhibit good reproducibility, stability and capacity for protein. In particular, this bonded phase approach allows a variety of amines to be attached to the ether ligand for a probe of both ionic and hydrophobic contributions by the attached amine to protein retention and separation. Hydrophobic retention of protein on the anion exchangers may be examined under high salt mobile phase conditions typically of use in hydrophobic interaction chromatography (HIC).

EXPERIMENTAL

Equipment

The gradient liquid chromatograph (Beckman, San Ramon, CA, U.S.A.) consisted of two Model 114M pumps, a Model 340 mixer and injector, a Model 165 variable-wavelength UV detector (set at 280 or 260 nm) and a Model 427 integrator. A gradient delay volume of 5.9 ml was measured and subtracted from all chromatographic data presented.

Chemicals and materials

Methyl iodide was obtained from Aldrich (Milwaukee, WI, U.S.A.). Analytical-reagent grade organic solvents were from J.T. Baker (Phillipsburg, NJ, U.S.A.) and HPLC-grade water was prepared in-house. α-Lactalbumin (α-LAC, Type III, from bovine milk), transferrin (TRANS, human), two grades of ovalbumin ("pure" OVA, grade VI, 99% pure; and "crude" OVA, grade III, 90% pure), soybean trypsin inhibitor (STI, Type I-S), cytochrome *c* (CYT, type VI, from horse heart), ribonuclease A (RNase, Type III-A, from bovine pancreas), lysozyme (LYS, grade I, from chicken egg white) and α-chymotrypsinogen A (CHTG, type II, from bovine pancreas) were obtained from Sigma (St. Louis, MO, U.S.A.). Adenosine, adenosine 5′-monophosphate (AMP), adenosine 5′-diphosphate (ADP), adenosine 5′-triphosphate (ATP) and adenosine 5′-tetraphosphate (ATeP) (all from equine muscle) and ammonium acetate, sodium acetate, sodium chloride, sodium sulfate, potassium orthophosphate, Tris, Bis-Tris and Bis-Tris-propane were also obtained from Sigma.

Column hardware (blanks, fittings, etc.) was supplied by Extrudehone (Irwin, PA, U.S.A.) and Valco Instruments (Houston, TX, U.S.A.). Vydac silica gel of particle diameter 5.5 μm, nominal pore size 300 Å and surface area 74 m^2/g (data obtained from the manufacturer) was obtained from Separations Group (Hesperia, CA, U.S.A.).

Analytical Spherogel CAA HIC columns (10 cm × 4.6 mm I.D.) containing 5-μm 300-Å pore diameter silica-based bonded ether packing for HIC were obtained from Beckman.

Synthesis

The anion-exchange silanes were synthesized in a three-step procedure representing a modification of the previously published polyether silane synthesis[18]. The quaternized amine phase was synthesized by reaction of the methylpiperazine bonded phase with methyl iodide in methanol following a published procedure[19]. Table I lists the anion-exchange ether-based stationary phases synthesized and used in this study. Bonding of the trialkoxysilanes to silica was accomplished in a manner similar to that used previously[18]. Elemental analysis for surface coverage was performed by Multi-Chem Labs. (Lowell, MA, U.S.A.). The precision of the percentage carbon data for a given phase was *ca.* 3% relative standard deviation (R.S.D.). A correction is made for 0.62% carbon found in the unbonded Vydac silica gel. Nitrogen analysis data proved less precise (*ca.* 10% R.S.D.), but were of some value in the interpretation of bonded phase coverage (the unbonded Vydac silica showed 0.05% nitrogen). In the calculation of surface coverage in Table I, we approximate an average reaction of all three ethoxy groups per silane molecule. The actual stoichiometry of bonding continues to be under investigation.

Chromatographic procedures

The anion-exchange phases were packed into 10 cm × 4.6 mm I.D. column tubes, following standard slurry procedures, using methanol as the driving solvent with a Model DSTV 122 air-driven pump (Haskel, Burbank, CA, U.S.A.). Mobile phases were prepared by adding the correct mass of salt and buffer to a volumetric flask containing HPLC-grade water, previously degassed by aspirator vacuum. The pH was adjusted to the desired value using phosphoric acid, glacial acetic acid, potassium hydroxide or ammonia solution, depending on the buffer system selection. Subsequently, a small amount of HPLC water was added to the mark. Using this procedure, mobile phase reproducibility in terms of the precision in protein peak elution volume on one column for the same sample mixture averaged 3.0% R.S.D.

RESULTS AND DISCUSSION

We describe here the successful separation of proteins by anion-exchange chromatography on bonded phases produced by reaction of any one of several aza-ether triethoxysilanes with the silica surface. Table I lists the variety of supports that were prepared in this work. In this approach, the aza-ether silanes, with one exception, were synthesized prior to bonding of the ligand to silica. This practice insures a high degree of bonded phase control and reproducibility. In one instance, a second reaction was performed on the bonded methylpiperazine (MP) phase with methyl iodide

TABLE I

CHARACTERISTICS OF ANION EXCHANGE PHASES, $\equiv Si(CH_2)_3(OCH_2CH_2)_nR$

Phase	*R*	*n*	*C(%)**	*Coverage** ($\mu mol/m^2$)*
MOR		2	4.17	4.7
MOEP	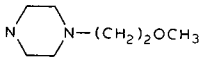	2	4.58	4.0
MP	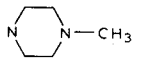	2	5.42	5.7
DMAEP	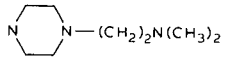	1	2.25	2.0
DEAEP	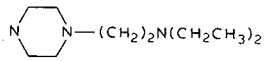	1	3.47	2.8
QMP	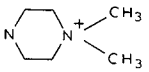	2	5.37	5.2

* Percentage of carbon in bonded phase determined by elemental analysis, corrected for unbonded silica.

** Coverage is calculated assuming an average reaction of three ethoxy groups per silane molecule.

(see Experimental) to prepare the quaternized support (QMP). The bonded phase coverage is high at about 4.9 μmol/m^2, with the exception of the DMAEP and DEAEP phases, which possess bulky ligands on shorter spacers, at about 2.4 μmol/m^2.

The bonded phase design permits an increase in the number of nitrogen atoms per bonded ligand from one (morpholine, phase MOR) to two (methylpiperazine, phase MP) to three atoms (dimethylaminoethylpiperazine, phase DMEAP), and also a quaternized methylpiperazine phase (QMP). Lastly, the methoxyethylpiperazine (MOEP) and diethylaminoethylpiperazine (DEAEP) phases were prepared in order to examine the role of increased hydrophobicity on the bonded amine.

Fig. 1 shows the high-performance separation of four standard proteins on the MP phase at 25°C by use of a 20-min increasing salt gradient from a 10 m*M* potassium phosphate solution at pH 7.0 to the buffer solution containing 1.0 *M* sodium acetate. The separation of transferrin (TRANS, p*I* 5.5, mol.wt. 77 000), α-lactalbumin (α-LAC, p*I* 5.2, mol.wt. 17 500), ovalbumin (OVA, p*I* 4.7, mol.wt. 44 000), and soybean trypsin inhibitor (STI, p*I* 4.0, mol.wt. 21 500) occurs in order of decreasing p*I*, as expected. Note that sharp peaks are obtained with the resolution of a number of minor components. The profile obtained for OVA is similar to that obtained by others on DEAE- of PEI-type anion exchangers[20,21]. In fact, Fig. 2 illustrates that the separation obtained for OVA on the MP column is indicative of the sample purity. Fig. 2A shows the chromatogram obtained for a commercial ovalbumin sample of relatively low purity (*ca.* 90% OVA) and Fig. 2B that of the higher grade of OVA used in the separation in Fig. 1. The main peaks overlap well and indicate that

Fig. 1. Separation of standard protein mixture on MP phase. Standard proteins (1 = transferrin, 2 = α-lactalbumin, 3 = ovalbumin, 4 = soybean trypsin inhibitor) were chromatographed on a 10 cm × 4.6 mm I.D. MP column at a flow-rate of 1.0 ml/min using a 20-min linear gradient at 25.0°C from 10 m*M* potassium phosphate (pH 7.0) to 10 m*M* potassium phosphate (pH 7.0)–1.0 *M* sodium acetate. Detection, 280 nm, 0.1 a.u.f.s.; injection volume, 5 μl. Protein amounts: transferrin, 100 μg; α-lactalbumin, 25 μg; ovalbumin, 50 μg; soybean trypsin inhibitor, 50 μg.

Fig. 2. Chromatography of two grades of ovalbumin on the MP phase. Chromatographic conditions as in Fig. 1. (A) Grade III, 90% protein, injection volume 5 μl, protein amount 50 μg; (B) grade VI, 99% pure protein, injection volume 5 μl, protein amount 50 μg.

TABLE II

COLUMN REPRODUCIBILITY OF MP PHASE

Mobile phase, A = 0.05 *M* ammonium acetate (pH 6.0), B = 0.05 *M* ammonium acetate (pH 6.0)–1.0 *M* sodium chloride, linear gradient from 0 to 100% B in 20 min; flow-rate 1.0 ml/min; detection at 280 nm, 0.1 a.u.f.s.; temperature, 25°C.

*Batch**	*C (%)*	V_g *(ml)***			
		TRANS	*α-LAC*	*OVA*	*STI*
1	4.87	2.8	4.9	6.6	8.6
2	5.09	3.3	5.2	7.2	9.1
3	5.39	3.4	5.2	7.2	9.0
4	5.42	3.5	5.5	7.6	9.3
Mean	5.19	3.3	5.2	7.2	9.0
R.S.D. (%)	5.0	9.6	4.7	5.8	3.3

* The four bonding batches were prepared separately using the same lot of silane and of silica.
** V_g = protein elution volume corrected for gradient delay volume.

the column will be of value in sample profiling and protein purification. Separate studies revealed that as much as 2 mg of protein may be loaded on to these columns with no indication of overloading (*i.e.*, no change in retention time)[22].

The column reproducibility and stability on any given aza-ether packing is good. For example, Table II presents column-to-column reproducibility data for the MP bonded phase. Each phase was prepared separately using the same batch of silane and Vydac silica and identical bonding reaction conditions. The carbon data show a precision of 5.0% R.S.D., which is an acceptable variation in the light of the 3% average precision of carbon analysis for one phase. The precision of the corrected (for gradient delay volume) protein chromatographic retention is found to agree from column to column within an average of *ca.* 5% for the well retained proteins, α-LAC, OVA and STI. The reproducibility of retention for TRANS is lower (*ca.* 10%), probably owing to the elution of this protein at the start of the gradient. Table III lists

TABLE III

STABILITY OF THE MP BONDED PHASE FOR PROTEIN AEC RETENTION

Conditions as in Table II.

*Volume of mobile phase passed (l)**	V_g *(ml)*		
	α-LAC	*OVA*	*STI*
0	5.5	7.6	9.3
8	5.0	7.3	9.1
16	4.4	6.7	8.8
20	5.0	6.6	8.7
Mean	5.0	7.1	9.0
R.S.D. (%)	9.0	6.8	3.1

* Mobile phase = 0.050 *M* ammonium acetate (pH 7.5)–0.2 *M* sodium chloride.

protein elution volumes on the MP phase as a function of use. The retention varies with an average precision of about 6% when 20 l of 50 m*M* ammonium acetate (pH 7.5)–0.2 *M* sodium chloride mobile phase are passed through the column. This column usage represents a 2-month period or *ca.* 500 samples injected. Fig. 3 shows chromatograms of the standard proteins obtained on a fresh MP column (Fig. 3A) and obtained after the passage of 20 l of pH 7.5 mobile phase (Fig. 3B). In Fig. 3B, less sample (4 μl) was injected than in Fig. 3A (6 μl). It can be seen that the two chromatograms are similar. Hence the aza-ether bonded phase chemistry is optimized for good column-to-column reproducibility and stability.

We next compared the relative chromatographic behavior of the four standard proteins used above on each of the anion-exchange supports listed in Table I. Table IV reveals a gradual increase in protein retention volume (V_g) in the bonded phase order MOR, MOEP, MP, DMAEP, DEAEP. The elution order of proteins on each column is as expected on the basis of anion exchange, *i.e.*, in order of decreasing p*I*. Interestingly, using the DMAEP bonded phase, the protein α-LAC failed to elute during the sodium acetate salt gradient, and neither α-LAC nor STI was recovered from the DEAEP column. Note that the quaternized anion-exchange QMP phase shows a similar retention to the DMAEP phase, but with elution of α-LAC.

The results in Table IV suggest that certain phases (DMAEP and DEAEP) exhibiting stronger anion-exchange protein retention may also show hydrophobic retention effects, resulting in poor recovery of α-LAC and STI. Recent studies have demonstrated the sensitivity of α-LAC retention to support hydrophobicity[23]. Moreover, the QMP phase, which is synthesized by addition of one methyl group to a nitrogen atom to form a permanent positive charge, exhibits anion-exchange reten-

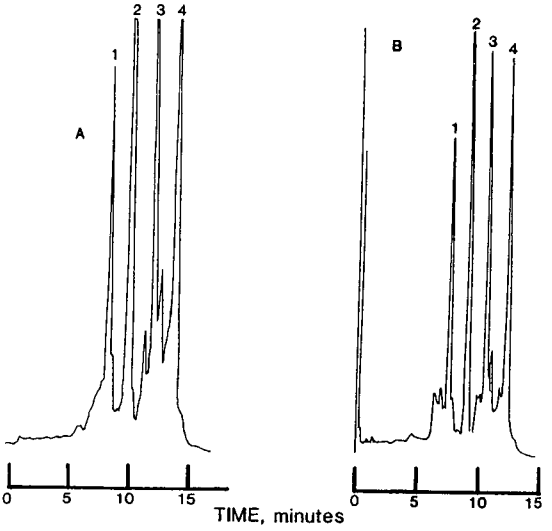

Fig. 3. Separation of standard protein mixture on the MP phase as a function of column usage. Chromatographic conditions as in Fig. 1, except the 20-min linear gradient was run from 50 m*M* ammonium acetate (pH 6.0) to the buffer plus 1.0 *M* sodium chloride. (A) Separation on a freshly prepared MP column, 6-μl injection of standard protein mixture. (B) Separation after 20 l of pH 7.5 mobile phase have passed through the column; 4 μl of standard protein mixture injected.

TABLE IV

COMPARISON OF AZA-ETHER BONDED PHASES FOR AEC OF PROTEINS

Mobile phase: A = 10 m*M* potassium dihydrogenphosphate (pH 7.0); B = 10 m*M* potassium dihydrogenphosphate (pH 7.0)–1.0 *M* sodium acetate. Other conditions as in Table II.

Phase	V_g *(ml)*			
	TRANS	*α-LAC*	*OVA*	*STI*
MOR	0	0	3.1	4.1
MOEP	2.2	3.0	4.7	6.5
MP	4.2	5.3	6.8	9.0
DMAEP	5.1	–*	7.5	11.9
DEAEP	6.7	–*	10.9	–*
QMP	5.2	6.5	7.5	11.3

* No elution observed.

tion as strong as the DMAEP phase but with good recovery of α-LAC. We have determined that all four of the standard proteins elute at V_0 (elution volume of unretained compound) on the ether HIC (with no bonded terminal amine) column under the ion-exchange conditions used in Fig. 1. Thus, phase hydrophobicity may arise from the terminal amine chosen. In the remaining sections of this paper, we examine in greater detail ion-exchange protein retention on these aza-ether columns and as the hydrophobic contribution of the terminal amine on the bonded phase to biopolymer retention.

ION-EXCHANGE EFFECTS

Although the protein chromatographic results in Table IV provide a ranking of the bonded phases in terms of anion-exchange strength, it is more valuable to have a quantitative measure such as the pK_a value of the bonded ligand. It was not possible to measure the pK_a of the bonded phase according to published methods[9] as slow equilibrium of the phase with the added titrant, even in 1.0 *M* sodium chloride solution, led to inconsistent results. We examined a chromatographic method using nucleotide retention following the procedures of El Rassi and Horvath[24]. Chromatographing the adenyl phosphate series on each of the aza-ether columns in Table I under isocratic conditions [10 m*M* potassium dihydrogenphosphate (pH 7.0)–0.1 *M* sodium acetate] yields a retention which is a function of the number of negative charges on the nucleotide. Fig. 4 shows a typical chromatogram of the series on the MP phase. The excellent performance achieved suggests that these columns may be of value in nucleic acid separations.

We had previously determined that on the uncharged ether bonded HIC column, all of the adenyl nucleotides elute at the void mark using these mobile phase conditions. Thus, a plot of log k' (k' = capacity factor) of the nucleotide *vs.* the charge on the solute can give a measure of the charge on each of the aza-ether bonded phases. Fig. 5 provides such a plot and Table V lists the slopes of the linear portions of the plots for each bonded phase. As may be observed, the ranking of the phases in order of increasing charge selectivity agrees well with the ranking of columns estab-

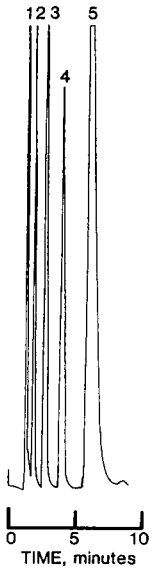

Fig. 4. Separation of adenyl nucleotides on the MP phase. Samples of nucleotides (1 = adenosine, 2 = AMP, 3 = ADP, 4 = ATP, 5 = ATeP) were chromatographed on the 10 cm × 4.6 mm I.D. MP column at a flow-rate of 1.0 ml/min using a mobile phase of 10 m*M* potassium phosphate (pH 7.0)–0.1 *M* sodium acetate at 25°C. Detection, 260 nm, 0.1 a.u.f.s.

lished previously for protein AEC retention (see Table IV), with the exception of the relative position of the QMP phase. The data in Table IV suggested that a significant hydrophobic contribution to protein retention existed on the DMAEP and DEAEP phases, which is not observed on the QMP phase. As may be seen in Fig. 5 and Table V, similar ion-exchange retention is obtained for sufficiently hydrophilic solutes, *i.e.*, nucleotides, on the QMP, DMAEP and DEAEP bonded phases.

For the columns that exhibit poor selectivity under these chromatographic conditions, a greater slope may be generated by the appropriate reduction in ionic strength, *e.g.*, MOR at 10 m*M* potassium dihydrogenphosphate with no sodium acetate present, or pH, *e.g.*, MOEP at pH 5.0 (see Fig. 5 and Table V).

Effect of pH

We next studied the influence of pH on the protein separations obtainable on the aza-ether columns. Table VI presents data for protein retention on the MP and QMP columns as a function of mobile phase pH. The phosphate buffer system employed has been shown to possess adequate buffer capacity for the pH range studied (6–8)[26]. In addition, all of the standard proteins should possess a net negative charge in this pH range. Similar retention values are noted at pH 6 and 7 on the MP column with a sharp decrease in retention at pH 8.0. The result suggests a loss of charge on the MP bonded ligand, i.e., $7 \leqslant pK_a \leqslant 8$. On the other hand, while retention on the QMP column fluctuates with pH, significant retention is still observed at pH 8.0. This relative independence of retention on pH is probably due to the permanent charge on the quaternized nitrogen of the QMP phase. The fluctuation in retention volume observed may indicate that only one nitrogen on the QMP phase is quaternized.

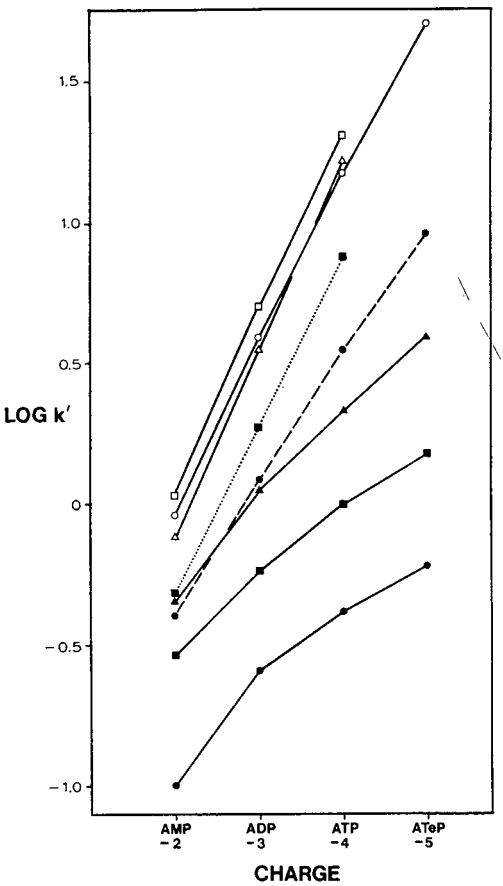

Fig. 5. Plot of log k' obtained on the aza-ether column *vs.* the charge number on the adenyl nucleotide series: adenosine 5'-monophosphate to adenosine 5'-tetraphosphate. Conditions as in Fig. 4 except (- - -) for MOR phase run in 10 m*M* potassium phosphate (pH 7.0) and (· · · ·) for MOEP phase run in 10 m*M* potassium phosphate (pH 5.0)–0.1 *M* sodium acetate. △ = QMP; □ = DEAEP; ○ = DMAEP; ▲ = MP; ■ = MOEP; ● = MOR.

TABLE V

SLOPE VALUES FOR LOG k' OF ADENYL NUCLEOTIDES *VS.* CHARGE NUMBER ON THE ADENYL NUCLEOTIDE AT pH 7.0

Mobile phase 10 m*M* potassium dihydrogenphosphate (pH 7.0)–0.1 *M* sodium acetate; flow-rate, 1.0 ml/min; temperature, 25°C; detection at 260 nm, 0.1 a.u.f.s.

Phase	*Slope*	*Phase*	*Slope*
MOR	0.18	DEAEP	0.641
MOEP	0.272	QMP	0.672
MP	0.270	MOR	0.453*
DMAEP	0.585	MOEP	0.60**

* Slope measured with an isocratic mobile phase of 10 m*M* potassium dihydrogenphosphate (pH 7.0).

** Slope measured with an isocratic mobile of 10 m*M* potassium dihydrogenphosphate (pH 5.0)–0.1 *M* sodium acetate.

TABLE VI

EFFECT OF MOBILE PHASE pH ON AEC OF PROTEINS

Mobile phase, A = 10 m*M* potassium dihydrogenphosphate (pH as indicated); B = 10 m*M* potassium dihydrogenphosphate (pH as indicated)–1.0 *M* sodium acetate. Other conditions as in Table IV.

Phase	*pH*	V_g *(ml)*			
		*TRANS (5.5)**	*α-LAC (5.2)**	*OVA (4.7)**	*STI (4.0)**
MP	6.0	2.7	4.3	6.2	8.9
	7.0	4.2	5.3	6.8	9.0
	8.0	0	0	0	1.9
QMP	6.0	3.2	4.4	6.0	9.9
	7.0	5.2	6.5	7.5	11.3
	8.0	3.6	5.3	5.7	9.9

* Values in parentheses are protein p*I* values from ref. 25.

The apparent loss of charge on the MP phase at pH 8.0 deserves discussion. Methylpiperazine has been found to possess pK_a values of 4.9 and 9.1 in aqueous solution[27]. The apparent reduction of the pK_a value of 9.1 by *ca.* 1.5 units in chromatographic practice may be explained in part by an examination of the bonded ligand structure. First, the methylpiperazine moiety is attached to the polyether "spacer" such that an oxygen atom is two atoms away from the ring nitrogen atom. pK_a values of 10.7 and 9.61 have been given[27] for ethylamine and 2-methoxyethylamine, respectively. Hence the influence of the added oxygen is to decrease the effective pK_a value, rendering the ligand less useful for anion exchange. In fact, the MOEP phase possesses ether side-chains on both piperazine nitrogens and exhibits less protein anion-exchange retention relative to the MP phase. The effect has also been noted for dextran-based DEAE phases[28] serving to decrease the pK_a value to 9.5.

Second, it is also possible that neighboring nitrogen atoms may have a significant influence on the pK_a of any one nitrogen as is observed for ethylamine (pK_a = 10.7) and ethylenediamine (pK_a = 9.9 and 6.8). Note, however, the influence of adding a third amine as in diethylenetriamine, with pK_a values of 9.0, 4.2 and 9.8, respectively. Finally, immobilization of the ligand on the silica surface may also influence its effective pK_a value.

Several routes exist to overcome this neighboring atom effect, including (1) the use of ligands with known high pK_a values, *e.g.*, DEAE; (2) increasing the distance between interacting atoms in the ligand chain and (3) quaternizing the amine to introduce a permanent positive charge. The second approach has been well studied by Alpert and Regnier[9] using PEI chemistry, *i.e.*, polymers with the repeating unit $(CH_2CH_2N)_n$. Insertion of nitrogen increases the bonded amine density and is preferable to longer alkyl chains between nitrogens, which increase the phase hydrophobicity. The DMAEP and DEAEP phases illustrate this approach. The use of quaternized ligands provides charge with less hydrophobicity as only a methyl group is added in the synthetic reaction. From the practical point of view, use of the MP phase at pH 8.0 would be preferable for the separation of strongly charged proteins, *e.g.*, p$I \leqslant 4.0$, while the QMP phase would effectively retain more weakly charged biopolymers.

Effect of salt

For the MP column, protein retention at pH 7.0 exhibited a minor dependence on any of several buffer salts chosen, including potassium phosphate, ammonium acetate, tris(hydroxymethyl)aminomethane (Tris), bis(2-hydroxyethyl)iminotris(hydroxymethyl)methane (Bis-Tris), and 1,3-bis[tris(hydroxymethyl)methylamino]propane (Bis-Tris-propane). With the exception of ammonium acetate, all of these buffers show good buffer capacity at pH 7.0. The selectivity does not appear to vary greatly from buffer to buffer. Table VII indicates the influence of the eluting salt on protein retention using the MP column and the same 20-min linear gradient to 1.0 *M* salt concentration. Protein retention is greatest for sodium chloride, intermediate with sodium acetate and least with sodium sulfate. This order correlates well with the typical displacing ability of anions on solute retention observed in anion-exchange chromatography[29,30]. The relative retention of proteins is not greatly affected in each of the three salt systems, indicating that the salts have a general modulating effect on protein elution, in contrast to other reports[31]. It should be noted that the effect of salt on protein AEC retention in these experiments is opposite to their lyotropic (salting-out) ability, according to the Hofmeister series[32]. This observation is further evidence that the aza-ether columns achieve protein separation via anion exchange under these chromatographic conditions. Although we have used sodium chloride gradients in several of the separations throughout this work, in general we do not recommend its long-term use owing to the well known deleterious effects on stainless-steel pump surfaces[33].

Evaluation of nucleotide selectivity, pH and ionic strength effects on protein separation all indicate that the predominant mode of operation for these columns is anion exchange. However, relative protein retention behavior, as shown in Table IV, indicated that an apparent hydrophobic contribution to protein retention can occur when an amine of relatively greater hydrophobicity (*i.e.*, DMAEP and DEAEP) is selected for use as the bonded phase. We next examined stationary phase hydrophobicity attributable to the amine selected as the "active" ligand by use of the anion-exchange column in the HIC separation mode.

Hydrophobic effects

Previously, we had studied protein HIC retention on uncharged ether columns under high salt conditions[18]. Table VIII gives retention data obtained on the un-

TABLE VII

EFFECT OF ELUTING SALT TYPE ON AEC OF PROTEINS

Mobile phase, A = 10 m*M* potassium dihydrogenphosphate (pH 7.0); B = 10 m*M* potassium dihydrogenphosphate (pH 7.0)–1.0 *M* indicated salt. Other conditions as in Table IV.

Eluting salt	V_g *(ml)*			
	TRANS	*α-LAC*	*OVA*	*STI*
Sodium sulfate	2.7	3.5	4.0	5.7
Sodium acetate	4.2	5.3	6.8	9.0
Sodium chloride	4.6	5.8	7.3	9.2

TABLE VIII

COMPARISON OF MP AND ETHER PHASES FOR PROTEIN HIC

Columns, 10 cm × 4.6 mm I.D. containing either MP or ether phase; mobile phase, A = 3.0 *M* ammonium sulfate–0.5 *M* ammonium acetate (pH 6.0), B = 0.5 *M* ammonium acetate (pH 6.0), linear gradient from 0 to 100% B in 20 min; flow-rate, 1.0 ml/min; temperature, 25°C; detection at 280 nm, 0.1 a.u.f.s. CYT = Cytochrome *c*; RNase = ribonuclease A; LYS = lysozyme; CHTG = α-chymotrypsinogen.

Phase	V_g *(ml)*			
	*TRANS (5.5)**	*α-LAC (5.2)**	*OVA (4.7)**	*STI (4.0)**
MP**	9.5	10.1	8.8	11.6
Ether***	13.1	12.6	12.1	15.0
	*CYT (10.6)**	*RNase (9.4)**	*LYS (11.0)**	*CHTG (9.5)**
MP**	0	3.8	8.4	11.6
Ether***	4.9	9.6	12.1	16.7

* Values in parentheses are protein p*I* values from ref. 25.

** Bonded ligand is ≡Si(CH$_2$)$_3$(OCH$_2$CH$_2$)$_2$N⟨⟩N—CH$_3$

*** Bonded ligand is ≡Si(CH$_2$)$_3$O(CH$_2$CH$_2$O)$_2$CH$_3$.

charged ether HIC column and the MP anion-exchange phase for eight proteins under HIC mobile phase and gradient conditions. Fig. 6 shows comparative chromatograms of the protein separations achieved on the two columns under HIC conditions. All of the proteins elute earlier on the MP phase relative to the ether HIC phase under the same mobile phase conditions. Thus, for all eight proteins, the MP phase is less hydrophobic than the uncharged ether column. Second, the elution order of

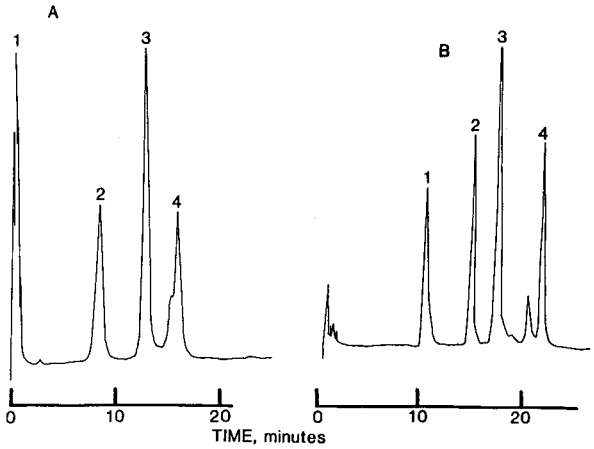

Fig. 6. Comparison of protein separation on MP and ether phases under HIC conditions. The sample of proteins (1 = cytochrome *c*, 2 = ribonuclease A, 3 = lysozyme, 4 = α chymotrypsinogen) were chromatographed on (A) the 10 cm × 4.6 mm I.D. MP column and (B) the 10 cm × 4.6 mm I.D. ether column [bonded ligand, ≡Si(CH$_2$)$_3$O(CH$_2$CH$_2$O)$_2$CH$_3$] at a flow-rate of 1.0 ml/min using a 20-min linear gradient at 25.0°C from 3.0 *M* ammonium sulfate–0.5 *M* ammonium acetate (pH 6.0) to 0.5 *M* ammonium acetate (pH 6.0). Detection, 280 nm, 0.1 a.u.f.s.; injection volume, 5 μl. Protein amounts: cytochrome *c*, lysozyme and α-chymotrypsinogen, each 30 μg; ribonuclease A, 90 μg.

proteins with p*I* 4–6 is similar on both the ether and MP columns, with the exception of α-LAC, indicating largely HIC retention. The anomalous retention of α-LAC on the MP column suggests that ion exchange is still occurring. Fig. 6 supports this contention in that the earlier eluting peaks on the MP phase are broader than those eluting later on the ether column. It is well known in the RPLC of small molecules that multiple equilibria for retention can lead to broad peaks[26]. For proteins of p*I*>9, the elution order is similar for the two bonded phases, indicating an HIC separation mode. However, selectivity differences are evident, particularly in the front of the chromatogram (*i.e.*, CYT/RNase), suggesting that ion exchange may contribute to separation even under high salt mobile phase conditions.

Table IX lists more retention data for the proteins CYT, RNase, LYS and CHTG under HIC conditions on all six bonded aza-ether phases synthesized in this work. First, note that the protein elution order on all aza-ether columns matches that on the uncharged ether column, indicating a predominantly HIC separation mode. Second, the columns may be ranked in order of increasing protein HIC retention: MOR < MP < QMP < MOEP < DMAEP < Ether < DEAEP. This ranking is similar to that in terms of increasing protein AEC retention (Table IV) and that based on increasing nucleotide selectivity (Table V). This correlation further relates bonded amine hydrophobicity and ionic character. Hence the diethylaminoethyl portion of the DEAEP phase provides relatively greater AEC retention of proteins, but also greater HIC retention. The greater phase hydrophobicity is probably due to the diethyl chains of the DEAE ligand and results in poor recovery of α-LAC and STI.

Recent work has shown that similar effects operate in reversed-phase LC separations of proteins, *i.e.*, increased surface hydrophobicity by virtue of longer alkyl bonded chains[34] or increased bonded ligand density[35] leads to decreased protein recovery. From this point of view, the QMP phase provides the permanent charge needed for strong anion exchange with a minimum of added carbon, *i.e.*, a methyl group.

Thus, in the separation of proteins by ion exchange or HIC using bonded phase approaches, one must be aware of the properties of the bonded ligand, *i.e.*, ionic, hydrophobic, etc., which may contribute in an undefined and deleterious manner to

TABLE IX

COMPARISON OF AZA-ETHER BONDED PHASES FOR PROTEIN HIC

Conditions as in Table VIII.

Phase	V_g *(ml)*			
	CYT	*RNase*	*LYS*	*CHTG*
Ether	4.9	9.6	12.1	16.7
MOR	0	2.5	6.7	10.6
MP	0	3.8	8.4	11.6
MOEP	0	8.0	12.0	13.7
DMAEP	3.5	8.3	12.0	15.4
DEAEP	10.2	13.3	17.7	21.9
QMP	0	5.0	9.4	11.7

the desired separation mode for each solute. The concern is of special relevance with regard to the recent development of dual separation columns designed to perform in distinct separation modes using different mobile phase conditions[30,36–38].

CONCLUSIONS

The use of aza-ether columns for the high-performance AEC separation of proteins has been demonstrated. Hydrophilic polyether silanes containing terminal morpholine and piperazine derivatives may be synthesized for attachment to silica to provide a variety of bonded anion-exchange phases with a range of ionic and hydrophobic properties. In one instance, a quaternized support may be produced by further derivatization of the methylpiperazine phase. These aza-ether bonded phases are reproducibly prepared and exhibit acceptable stability and capacity. Protein separation, nucleotide selectivity and pH and ionic strength effects provide a probe of anion-exchange character on these phases. Protein separation by hydrophobic interaction under high salt mobile phase conditions indicates the hydrophobic character of the bonded amine ligand. It can be shown using these approaches that bonded amine ligand hydrophobicity is probably responsible for recovery losses of some proteins during AEC operation.

ACKNOWLEDGEMENTS

The authors acknowledge valuable discussions with Professor B. L. Karger of Northeastern University. Dr. N. H. C. Cooke of Beckman Instruments is thanked for his examination of the manuscript. Steve Howard and Garrett Thurston are acknowledged for packing the columns and the initial chromatographic evaluation. The authors also thank Shu-mei Shieh and Machiko Hollifield for their skilful assistance in the preparation of the manuscript.

REFERENCES

1 H. G. Barth, W. E. Barber, C. H. Lochmuller, R. E. Majors and F. E. Regnier, *Anal. Chem.*, 60 (1988) 387R.
2 S. H. Chang, K. M. Gooding and F. E. Regnier, *J. Chromatogr.*, 125 (1976) 103.
3 W. Jost, K. K. Unger, R. Lipecky and H. G. Gassen, *J. Chromatogr.*, 185 (1979) 403.
4 Y. Kato, K. Nakamura and T. Hashimoto, *J. Chromatogr.*, 245 (1982) 193.
5 R. W. Stout, S. I. Sivakoff, R. D. Ricker, H. C. Palmer, M. A. Jackson and T. J. Odiorne, *J. Chromatogr.*, 352 (1986) 381.
6 M. Colpan and D. Riesner, *J. Chromatogr.*, 296 (1984) 339.
7 E. H. Cooper, R. Turner, J. R. Webb, H. Lindblom and L. Fagerstam, *J. Chromatogr.*, 327 (1985) 269.
8 M. P. Strickler and M. J. Gemski, *J. Liq. Chromatogr.*, 9 (1986) 1655.
9 A. J. Alpert and F. E. Regnier, *J. Chromatogr.*, 185 (1979) 375.
10 W. Kopaciewicz, M. A. Rounds and F. E. Regnier, *J. Chromatogr.*, 318 (1985) 157.
11 K. M. Gooding and M. N. Schmuck, *J. Chromatogr.*, 327 (1985) 139.
12 D. J. Burke, J. K. Duncan, L. C. Dunn, L. Cummings, C. Siebert and G. S. Ott, *J. Chromatogr.*, 353 (1986) 425.
13 M. Flaschner, H. Ramsden and L. J. Crane, *Anal. Biochem.*, 135 (1983) 340.
14 W. Kopaciewicz, S. Fulton and S. Y. Lee, *J. Chromatogr.*, 409 (1987) 111.
15 R. M. Chicz, Z. Shi and F. E. Regnier, *J. Chromatogr.*, 359 (1986) 121.
16 M. A. Rounds, W. D. Rounds and F. E. Regnier, *J. Chromatogr.*, 397 (1987) 25.

17 M. A. Rounds and F. E. Regnier, *J. Chromatogr.*, 443 (1988) 73.
18 N. T. Miller, B. Feibush and B. L. Karger, *J. Chromatogr.*, 316 (1984) 519.
19 H. Z. Sommer, H. I. Lipp and L. L. Jackson, *J. Org. Chem.*, 36 (1971) 824, 35 (1970) 1558.
20 Y. Kato, K. Komiya and T. Hashimoto, *J. Chromatogr.*, 246 (1982) 13.
21 M. N. Schmuck, D. L. Gooding and K. M. Gooding, *J. Chromatogr.*, 359 (1986) 323.
22 C. H. Shieh, unpublished results.
23 S. L. Wu, A. Figueroa and B. L. Karger, *J. Chromatogr.*, 371 (1986) 3.
24 Z. El Rassi and Cs. Horváth, *Chromatographia*, 19 (1984) 9.
25 P. G. Righetti, G. Tudor and K. Ek, *J. Chromatogr.*, 220 (1981) 115.
26 B. L. Karger, J. N. LePage and N. Tanaka, in Cs. Horváth, (Editor), *HPLC–Advances and Perspectives*, Vol. 1, Academic Press, New York, 1980, p. 113.
27 Z. Rappoport (Editor), *Handbook of Tables for Organic Compound Identification*, CRC Press, Cleveland, OH, 3rd ed., 1972, p. 436.
28 *Pharmacia Product Literature*, Pharmacia, Uppsala, Sweden, 1983.
29 L. R. Snyder and J. J. Kirkland, *Introduction to Modern Liquid Chromatography*, Wiley-Interscience, New York, 2nd ed., 1979, p. 421.
30 W. Kopaciewicz and F. E. Regnier, *Anal. Biochem.*, 133 (1983) 251.
31 M. L. Heinitz, L. Kennedy, W. Kopaciewicz and F. E. Regnier, *J. Chromatogr.*, 443 (1988) 173.
32 P. H. van Hippel and T. Schleich, in S. N. Timasheff and G. D. Fasman (Editors), *Structure and Stability of Biological Macromolecules*, Marcel Dekker, New York, 1969, p. 417.
33 J. Luiken, R. van der Zee and G. W. Welling, *J. Chromatogr.*, 284 (1984) 482.
34 K. A. Cohen, K. Schellenberg, K. Benedek, B. L. Karger, B. Grego and M. T. W. Hearn, *Anal. Biochem.*, 140 (1984) 223.
35 D. Wu and R. R. Walters, *Anal. Chem.*, 60 (1988) 1517.
36 L. A. Kennedy, W. Kopaciewicz and F. E. Regnier, *J. Chromatogr.*, 359 (1986) 73.
37 Cs. Horváth and Z. El Rassi, *Chromatogr. Forum*, 1 (1986) 49.
38 A. Figueroa, C. Corradini, B. Feibush and B. L. Karger, *J. Chromatogr.*, 371 (1986) 335.

Journal of Chromatography, 463 (1989) 345–354
Elsevier Science Publishers B.V., Amsterdam — Printed in The Netherlands

CHROM. 21 083

PREPARATION AND RETENTION CHARACTERISTICS OF DIFFERENT PHENYLPOLYSILOXANE PHASES FOR REVERSED-PHASE LIQUID CHROMATOGRAPHY

GYULA SZABÓ and EDIT CSATÓ*
"Frédéric Joliot-Curie" National Research Institute for Radiobiology and Radiohygiene, P.O. Box 101, H-1775 Budapest (Hungary)
and
PÉTER KERESZTES and J. PÉTER PALLOS
Bio-Separation Technologies Co., Beck str. 42, H-1222 Budapest (Hungary)
(First received June 14th, 1988; revised manuscript received November 2nd, 1988)

SUMMARY

Reversed-phase silicas prepared by treating silica with three different phenylpolysiloxanes were compared with monomeric phenyl silica, by determining the specific surface area, S_{BET}, carbon content and also their properties in liquid chromatography using methanol–water mixtures as the eluents. Relative to the monomeric phenyl silica, the phenylpolysiloxane modified silicas show no marked differences in the surface concentration of the organic groups, but their hydrophobic characteristic is significantly higher. This results in a different chromatographic behaviour for solutes with different polarities.

INTRODUCTION

In reversed-phase liquid chromatography, hydrophobic packing materials, produced by surface reaction of silica, are most often used. The chromatographic properties of a reversed-phase sorbent are dependent on the synthesis conditions of the bonded phase. The preparation and study of bonded phase materials have received considerable attention. Modifications can be accomplished with mono-, di- or trichlorosilane or alkoxysilane[1]. The choice of reagent together with the variation in type of silica (structure, pore volume and surface area) will result in packing materials having widely differing chromatographic properties. This has been well documented[2–6]. Much of this work has been concerned with monomeric bonded phases and has been reviewed[7].

Although much research has been performed on monomeric phases, relatively little effort has been expended in the study of polymeric phases. The synthesis and characterization of silicone polymers varying in structure and polarity were surveyed by Aue *et al.*[8], Novotny and Grushka[9] and Stewart and Perry[10]. Schmidt *et al.*[11] introduced a pellicular-type material, namely Zipax coated and bonded with 1% (w/w) of an high-molecular-weight polymer called ODS Permaphase. Majors and

0021-9673/89/$03.50

Hopper[12] studied in detail the reaction between silica and various polar and non-polar organochlorosilanes and alkoxysilanes. Direct polymerization was achieved by treating the silica with a di- or trifunctional organochlorosilane in the presence of water vapour. Kirkland and Yates[13,14] patented a procedure in which a pre-polymerized material representing an organofunctional siloxane was deposited on the silica support. The reluctance of researchers to accept polymeric phases is probably the result of difficulties reported with early pellicular phases. Problems have included low column efficiency due to mass transfer limitations[15,16], poor peak shape[17] and difficulties with the reproducibility of syntheses[18]. Recently, some researchers[19–22] synthesized and studied series of C_{18} polymeric phases on totally porous silica for separation of polycyclic aromatic hydrocarbons. They concluded that significant differences existed in the chromatographic properties of C_{18} bonded phases prepared in different ways. In general, the column selectivity was directly related to the bonded phase surface coverage, while the absolute retention was more closely related to the amount of carbon contained within the column (the phase ratio). Other kinds of polymeric phases have also been produced for use in size exclusion chromatography[23,24] and ligand exchange chromatography[25].

In comparison with the relatively extensive literature on the preparation of C_{18} polymer phases, only a limited number of papers have dealt with surface modification with phenylpolysiloxanes. Attempts to bind phenylpolysiloxane to the surface were made for capillary gas chromatography[26,27].

In our work, we intended to modify silica gels with three different phenylpolysiloxane. Namely, fully hydroxylated porous silica was treated with phenylmethylpolysiloxane, phenylpropylpolysiloxane and diphenylpolysiloxane. The retention behaviours of solutes on columns packed with these types of phenyl phases were examined and compared with those of monomeric phenylmethyl silica gel in reversed-phase liquid chromatography. The polar characters of the different phases were studied so that we could show the effects of the modifiers bonded to the surface.

EXPERIMENTAL

Equipment

Chromatographic separations were carried out with a Varian 8500 solvent delivery system, a Model 7125 sample injector (Rheodyne, Berkely, CA, U.S.A.) and a Varian Model 635 UV–VIS monitor. The columns were packed in 250 mm × 4.0 mm I.D. stainless-steel tubes (Bio-Separation Technologies, Budapest, Hungary). The thermal studies were performed with a Derivatograph-3427 (MOM, Budapest, Hungary). The BET surface area of silicas was determined by a sorptometer made at the Department for Physical Chemistry of the Technical University of Budapest (Hungary).

Chemicals and reagents

Separon SGX Si-100 5-μm was obtained from Laboratorní Přistroje (Prague, Czechoslovakia). Phenylmethyldichlorosilane, phenylmethylpolysiloxane (REN 50, molecular weight about 1500 g/mol), phenylpropylpolysiloxane (SY 308, molecular weight 1500 g/mol), diphenylpolysiloxane (SY 430, molecular weight about 1700 g/mol) (Wacker, München, F.R.G.) and trimethylchlorosilane (Merck, Darmstadt,

F.R.G.) were used as received. All other chemicals obtained from commercial sources were used without purification. The test solutes were dissolved in methanol at a concentration of 0.1 mg/ml by weight. Typically 10 μl were injected. The flow-rates were 1 ml/min as usual. Sample peaks were detected at 254 nm.

Preparation of phenylmethyl phase packing

The preparation of the phenylmethyl packing material was based on Unger's procedure[28]. A 10-g amount of dried silica gel was mixed with 5% phenylmethyldichlorosilane in anhydrous toluene and refluxed in a sealed flask. The reaction was completed within 8 h. The phenyl silica gel was filtered off and washed with toluene, methanol, water and methanol, respectively. The solid phase was then kept at 353 K for several hours under vacuum. Residual hydroxyl groups were deactivated by treating the solid material with a 10% solution of trimethylchlorosilane in toluene. This deactivated phenyl-bonded silica gel was high-pressure slurry packed into a 250 mm × 4.0 mm I.D. column by Bio-Separation Tech.

Preparation of phenylpolysiloxane phase packing

The preparation of phenylpolysiloxane packings was based on the procedure of Kirkland and Yates[13]. A 10-g amount of dried silica gel was mixed with 1% phenylpolysiloxane in toluene and refluxed gently under a condenser for 2 h. The volatile solvent was removed while stirring the mixture under vacuum. The resulting dry powder was then heated at 473 K for 2 h. After heating, the silica gel was washed with toluene, dioxane, methanol, water and methanol, respectively. The solid phase was then kept at 353 K for 4 h under vacuum. Residual hydroxyl groups were deactivated by treating the silica gel with a 10% solution of trimethylchlorosilane in toluene. These phenylpolysiloxane-bonded silica gels were high-pressure slurry packed into 250 mm × 4.0 mm I.D. columns by Bio-Separation Tech.

Analysis of stationary phase

The amount of organic moiety bound to the silica supports was determined from the thermogravimetric curves of the modified silica gels[29]. The specific surface areas of the gels, S_{BET}, were obtained from sorption measurements at 77 K.

RESULTS AND DISCUSSION

Analysis of stationary phase

The specific surface area, S_{BET}, was obtained from nitrogen sorption measurement at 77 K. It was assumed that the starting silica support had a surface area of 535 m^2/g (Laboratorni Přistroje). These measurements (see Table I) demonstrate a considerable reduction in S_{BET}. The decrease in S_{BET} values on different phenyl phases is about 25–40% of that of the starting silica gel. The amounts of organic moiety bound to the silica supports were determined from the weight losses of the modified gels and are given in Table I. It is seen that the carbon content of different phenyl phase silica gels is about the same.

Retention of test solutes

Retention data for the test solutes were obtained on three different phenyl-

TABLE I

CHARACTERISTICS OF SILICA GELS PREPARED

Material	*Particle size (μm)*	*Functional group bonded*	*Specific surface area S_{BET} (m^2/g)*	*Carbon content (%)*	*Surface concentration ($\mu mol/m^2$)*
A	5	Phenylmethylhydroxysilyl	397	13.0	2.92
B	5	Phenylmethylpolysiloxane	327	10.7	2.41
C	5	Phenylpropylpolysiloxane	325	12.7	2.23
D	5	Diphenylpolysiloxane	368	12.8	1.68

polysiloxane phases and on a monomeric phenylmethyl phase, using mixtures of methanol–water (60:40) as the mobile phase. Fig. 1 shows the separation of the test solutes on different phenyl stationary phases. The retention characteristics of the chromatographed substances are expressed in terms of their capacity factor, k', and their selectivity factor, α. In order to eliminate the influence of the specific surface area of the sorbents investigated, we used the k'/S_{BET} values. These data are in Table II. It is apparent that the value of k' for the highly hydrophobic substances (toluene, bromobenzene, *p*-xylene, propylbenzene) are higher on any polysiloxane phase; in contrast the value of k' increases for phenol, cresol acetophenone, anisole and methyl benzoate, more polar species, on the monomeric phenyl phase.

Again, the elution order is the same on every phenyl packing. After comparing the k'/S_{BET} values of test solutes on phases A–D, it is evident that any phenylpolysiloxane support is less polar than the monomeric phenyl phase. The polarity of phenylpolysiloxane silica gels increase in the sequence phenylmethyl-, phenylpropyl-, diphenylpolysiloxane. Polymeric phenyl-modified silica gels seem to be better stationary phases for non-polar aromatics than monomeric phenyl phases.

Comparison of monomeric and polymeric phenylmethyl phases

Monomeric and polymeric modified packings having the same functional group (phenylmethyl) were prepared. In this section, only a brief discussion will be given of the packing properties that influence the retention behaviour of solutes in reversed-phase chromatography. According to the generally accepted rules, the elution volumes of chromatographed substances on reversed-phase columns are mainly due to non-specific interactions between the solute molecules and the stationary phase. The character of this type of interactions may be evaluated by the relationship $\log k'$ *vs.* n_c where n_c represents the number of carbon atoms in the solute molecule[30,31]. This relationship is linear for solutes belonging to an homologous series[31]. In order to eliminate the influence of S_{BET} of the sorbents investigated, we used the $\log (k'/S_{BET})$ values, instead of $\log k'$. For these investigations the same mobile phase composition (methanol–water, 70:30) was used. The appropriate retention data are shown in Table III. Fig. 2 presents plots of $\log (k'/S_{BET})$ *vs.* n_c for the stationary phases investigated by us. It appears that the highest of k'were obtained for the polymeric phase. Also that the plots are not parallel for both packing materials, the slope of the plot for the monomeric phase being smaller. According to Colin and Guiochon[31], the slope of such plots increases with the degree of coverage of the support surface, but the surface coverage of both silica gels is the same (see Table I). The different slopes of the plots

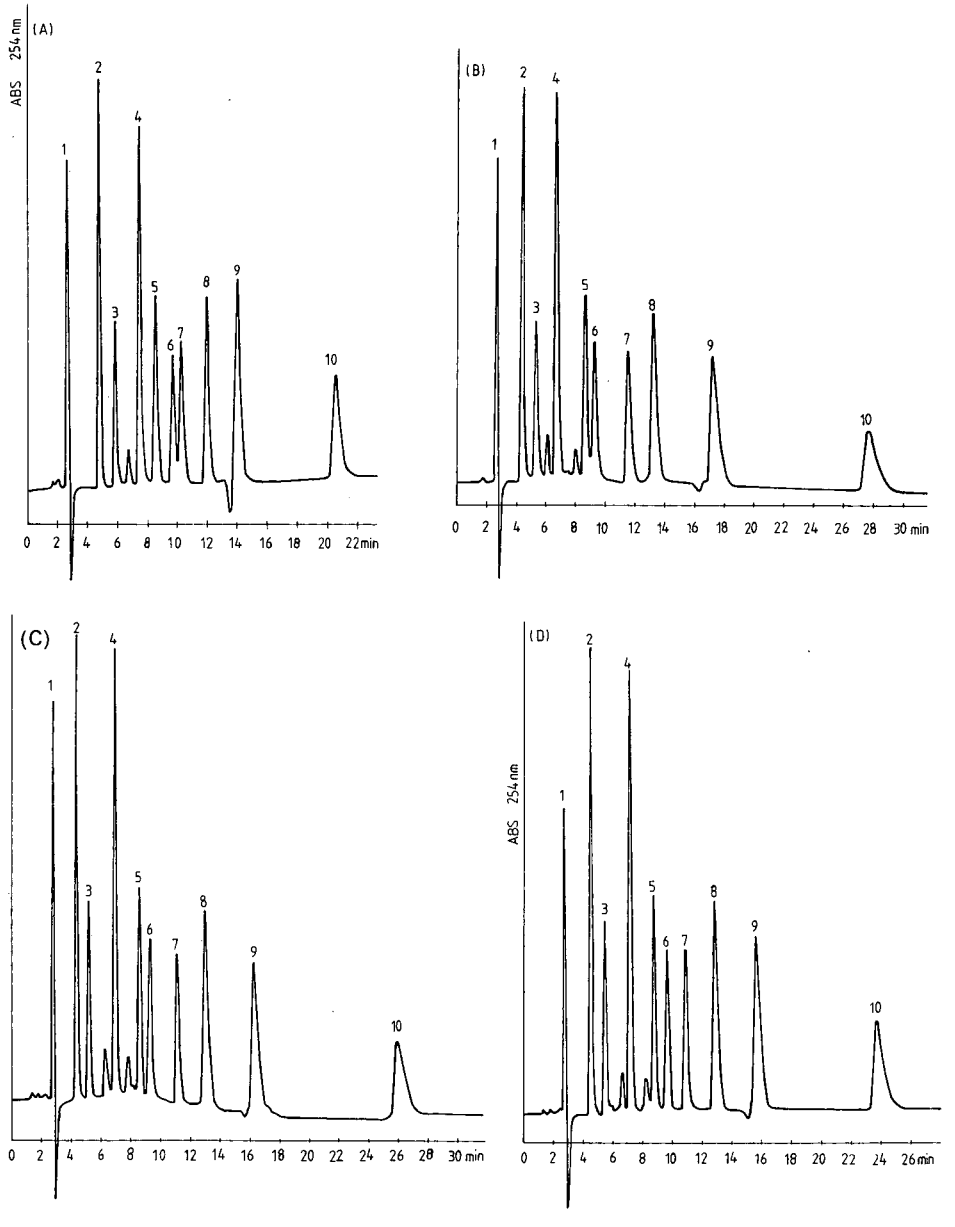

Fig. 1. Separation of test solutes on phenylmethyl (A), phenylmethylpolysiloxane (B), phenylpropylpolysiloxane (C) and diphenylpolysiloxane (D). Peak identitities: 1 = methanol; 2 = phenol; 3 = *o*-cresol; 4 = acetophenone; 5 = anisole; 6 = methyl benzoate; 7 = toluene; 8 = bromobenzene; 9 = *p*-xylene; 10 = propylbenzene. Mobile phase: methanol–water (60:40). Flow-rate: 1 ml/min. Detection: UV absorbance (ABS) at 254 nm. Temperature ambient.

TABLE II

CAPACITY AND SELECTIVITY FACTORS OF TEST SOLUTES ON DIFFERENT PHENYL PHASES

Eluent: methanol–water (60:40, v/v) Temperature: ambient. Columns:A, bonded group, phenylmethylsilyl; B, phenylmethylpolysiloxane; C, phenylpropylpolysiloxane; D, diphenylpolysiloxane.

Sample	*Column A*			*Column B*			*Column C*			*Column D*		
	k'	$k'/S_{BET}\cdot 10^3$	α	k'	$k'/S_{BET}\cdot 10^3$	α	k'	$k'/S_{BET}\cdot 10^3$	α	k'	$k'/S_{BET}\cdot 10^3$	α
Phenol	0.85	2.141		0.57	1.743		0.57	1.753		0.57	1.548	
			1.49			1.56			1.49			1.61
o-Cresol	1.27	3.190		0.89	2.721		0.85	2.615		0.92	2.500	
			1.48			1.56			1.76			1.71
Acetophenone	1.88	4.735		1.39	4.250		1.50	4.615		1.57	4.266	
			1.23			1.48			1.38			1.36
Anisole	2.30	5.793		2.07	6.331		2.07	6.369		2.14	5.815	
			1.18			1.12			1.12			1.13
Methyl benzoate	2.71	6.826		2.32	7.094		2.35	7.230		2.42	6.576	
			1.09			1.35			1.27			1.19
Toluene	2.96	7.455		3.14	9.602		3.00	9.231		2.89	7.053	
			1.23			1.18			1.21			1.23
Bromobenzene	3.62	9.110		3.71	11.345		3.64	11.200		3.57	9.701	
			1.22			1.30			1.32			1.28
p-Xylene	4.42	11.135		5.14	15.718		4.82	14.830		4.57	12.418	
			1.56			1.72			1.71			1.64
Propylbenzene	6.92	17.431		8.05	27.060		8.20	25.476		7.50	20.380	

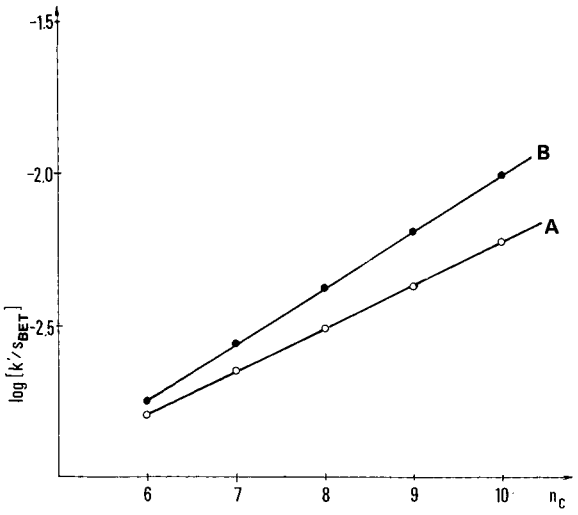

Fig. 2. Plots of log (k'/S_{BET}) *vs.* number of carbon atoms, n_c, for monomeric phenylmethyl silica gel (A) and polymeric phenylmethyl silica gel (B). Mobile phase: methanol–water (70:30).

for the two silica gels probably result from the different types of interaction between the solute molecules and the bonded film. It is not clear, when the surface coverage of these two silica gels is the same, whether this is caused by an additional hydrophobic interaction on the polymeric modified packing of the new surface site (siloxane bridges) with the solutes. Young[32] reported that siloxane bridges on the silica surface are essentially hydrophobic.

Separation of non-polar aromatics

Polymeric phenyl phases were supposed to be better stationary phases for non-polar solutes than monomeric phenyl packings. So we decided to examine the chromatographic behaviours of some polycyclic aromatic hydrocarbons on monomeric

TABLE III

CAPACITY AND SELECTIVITY FACTORS OF AROMATIC HOMOLOGOUS SOLUTES ON COLUMNS PACKED WITH MONOMERIC AND POLYMERIC PHENYLPROPYL MODIFIED SILICA

Columns: A, monomeric phenylmethyl silica gel; B, polymeric phenylmethyl silica gel. Eluent: methanol–water (70:30, v/v).

Sample	*Column A*			*Column B*		
	k'	$k'/S_{BET} \cdot 10^3$	α	k'	$k'/S_{BET} \cdot 10^3$	α
Benzene	0.63	1.62		0.58	1.77	
			1.36			1.55
Toluene	0.86	2.21		0.90	2.75	
			1.38			1.52
Ethylbenzene	1.19	3.05		1.37	4.19	
			1.37			1.53
Propylbenzene	1.63	4.18		2.10	6.42	
			1.41			1.53
Butylbenzene	2.31	5.92		3.22	9.85	

TABLE IV

CAPACITY AND SELECTIVITY FACTORS OF AROMATIC HYDROCARBONS ON COLUMNS PACKED WITH MONOMERIC AND POLYMERIC PHENYL MODIFIED SILICA GELS

Eluent: methanol–water (70:30, v/v) Temperature: ambient. Columns: A, phenylmethylsilyl; B, phenylmethylpolysiloxane; C, phenylpropylpolysiloxane; D, diphenylpolysiloxane.

Sample	*Column A*			*Column B*			*Column C*			*Column D*		
	k'	$k'/S_{BET}\cdot 10^3$	α	k'	$k'/S_{BET}\cdot 10^3$	α	k'	$k'/S_{BET}\cdot 10^3$	α	k'	$k'/S_{BET}\cdot 10^3$	α
Benzene	0.63	1.58		0.58	1.77		0.82	2.52		0.67	1.82	
			1.95			2.61			1.96			2.29
Naphthalene	1.23	3.09		1.51	4.62		1.62	4.95		1.54	4.18	
			1.85			2.12			1.07			2.02
Phenanthrene	2.20	5.74		3.21	9.82		3.01	9.26		3.11	8.45	
			1.03			1.09			1.07			1.09
Anthracene	2.35	5.92		3.52	10.76		3.23	9.94		3.40	9.24	
			1.22			1.34			1.25			1.33
Pyrene	2.88	7.25		4.72	14.43		4.05	12.46		4.52	12.28	
			1.53			1.55			1.39			1.40
Chrysene	4.43	11.16		7.31	22.35		5.65	17.38		6.33	17.20	
			1.03			1.04			1.08			1.03
Benz[*a*]anthracene	4.58	11.54		7.60	22.24		6.13	18.86		6.53	17.74	
			1.07			1.15			1.09			1.07
Benz[*b*]anthracene	4.92	12.39		8.74	26.74		6.70	20.62		7.01	19.05	
			1.18			1.29			1.24			0.94
Benzo[*a*]pyrene	5.81	14.63		11.27	34.46		8.35	25.69		6.64	18.04	
			1.07			0.87			0.92			1.34
Benzo[*e*]pyrene	6.27	15.79		9.80	29.97		7.73	23.78		8.88	24.13	
			1.25			1.48			1.43			1.44
Dibenz[*a,c*]anthracene	7.84	19.75		14.50	44.34		11.20	34.15		12.83	34.86	
			1.11			1.03			1.06			1.04
Dibenz[*a,b*]anthracene	8.74	22.02		14.09	45.56		11.79	36.27		13.32	36.19	

phenyl silica gel and polymeric phenyl supports. Retention data for solutes were obtained on three different phenylpolysiloxane phases and monomeric phenyl silica gel, using methanol–water (70:30) as the mobile phase. The retention of the chromatographed substances is expressed in terms of their capacity factors k'. In order to eliminate the influence of the surface area of the sorbents investigated, we used the k'/S_{BET} values. In Table IV these data are presented. It is seen that the values obtained from k' and k'/S_{BET} decrease in the sequence phenylmethylpolysiloxane phenylpropylpolysiloxane- > diphenylpolysiloxane > phenylmethyl phase. This illustrates that, with the same mobile phase, the retention will be weakest on the monomeric phenylmethyl phase and strongest on the phenylmethylpolysiloxane phase. After comparing columns B–D, it is evident that the phenylmethylpolysiloxane silica gel is the most hydrophobic and the diphenylpolysiloxane packing is the least. This fact confirms the conclusion obtained from reversed-phase high-performance liquid chromatography[33], namely that the hydrophobicity of monomeric phenyl phases increases in the sequence triphenyl < diphenyl < phenylmethyl.

It is easily seen from Table IV that the separation of the substances investigated is best on the phenylmethylpolysiloxane support (column B), but phenylpropylpolysiloxane (column C), diphenylpolysiloxane (column D) and phenylmethyl silica (column A) are well suited. The selectivity of the packings was observed for the chromatographic behaviour of benzanthracenes, benzopyrenes and dibenzanthracenes. The elution order of the benzanthracenes from all columns was benz[*a*]anthracene < benz[*b*]anthracene. The elution order of the dibenzanthracenes from all columns was dibenz[*a*,*c*]anthracene < dibenz[*a*,*h*]anthracene. The elution order of benzopyrenes from columns A and D was benzo[*a*]pyrene < benzo[*e*]pyrene and that from columns B and C was benzo[*e*]pyrene < benzo[*a*]pyrene, using methanol–water mixtures.

Stationary phases modified with different phenylpolysiloxane were shown to have some merit such as retentivity and different selectivity from the monomeric phenyl phase. They can be a good alternative for the monomeric type packings, and the complementary use of such stationary phases with the commercial phenyl silica gel will increase the capability of reversed-phase liquid chromatography.

ACKNOWLEDGEMENTS

We are grateful to Dr. R. M. Cassidy for helpful discussion and revision of the manuscript, to Wacker-Chemie for providing the different phenylpolysiloxanes and to Mrs. É. Szakács and Miss Zs. Horváth for their technical work.

REFERENCES

1 L. R. Snyder and J. J. Kirkland (Editors), *Introduction to Modern Liquid Chromatography*, Wiley, New York, 1979, p. 272.
2 P. Roumeliotis and K. K. Unger, *J. Chromatogr.*, 149 (1978) 211.
3 K. Karch, J. Sebestian and I. Halász, *J. Chromatogr.*, 122 (1976) 3.
4 G. E. Berendsen and L. de Galan, *J. Liq. Chromatogr.*, 1 (1978) 561.
5 G. E. Berendsen, K. A. Pikaart and L. de Galan, *J. Liq. Chromatogr.*, 3 (1980) 1437.
6 M. B. Evans, A. D. Dale and C. J. Little, *Chromatographia*, 13 (1980) 5.
7 H. Engelhardt and G. Ahr, *Chromatographia*, 14 (1981) 227.
8 W. A. Aue, Sh. Kapila and E. Grushka (Editors), *Bonded Stationary Phases in Chromatography*, Ann Arbor Sci. Publ., Ann Arbor, MI. 1974, p. 13.

9 M. Novotny and E. Grushka (Editors), *Bonded Stationary Phases in Chromatography*, Ann Arbor Sci. Publ., Ann Arbor, MI, 1974, p. 199.
10 H. N. M. Stewart and S. G. Perry, *J. Chromatogr.*, 37 (1968) 97.
11 J. A. Schmidt, R. A. Henry, R. C. Williams and J. F. Dieckman, *J. Chromatogr. Sci.*, 9 (1971) 645.
12 R. E. Majors and H. J. Hopper, *J. Chromatogr. Sci.*, 12 (1974) 726.
13 J. J. Kirkland and P. C. Yates, *U.S. Pat.*, 3 795 313 (1974).
14 J. J. Kirkland and P. C. Yates, *U.S. Pat.*, 3 722 181 (1973).
15 J. J. Kirkland and J. J. DeStefano, *J. Chromatogr. Sci.*, 8 (1970) 309.
16 R. E. Majors, *J. Chromatogr. Sci.*, 12 (1974) 767.
17 J. H. Knox and G. Vasvari, *J. Chromatogr.*, 83 (1973) 181.
18 M. Novotný, S. L. Bektesh and K. L. Grohmann, *J. Chromatogr.*, 83 (1973) 25.
19 S. A. Wise, L. C. Sander and W. E. May, *J. Liq. Chromatogr.*, 6 (1983) 2709.
20 M. Verzele and P. Mussche, *J. Chromatogr.*, 254 (1983) 117.
21 S. A. Wise and W. E. May, *Anal. Chem.*, 55 (1983) 1479.
22 L. C. Sander and S. A. Wise, *Anal. Chem.*, 56 (1984) 504.
23 D. P. Herman, L. R. Field and S. Abbott, *J. Chromatogr. Sci.*, 19 (1981) 470.
24 Gy. Szabó, K. Offenmüller and E. Csató, *Anal. Chem.*, 60 (1988) 213.
25 M. Ginpel and K. Unger, *Chromatographia*, 17 (1983) 200.
26 J. S. Bradshaw, N. W. Adams, R. S. Johnson, B. J. Tarbet, C. M. Scregenberger, M. A. Pulsiper, M. B. Aandrus, K. E. Markides and M. L. Lee, *J. High Resolut. Chromatogr. Chromatogr. Commun.*, 8 (1985) 678.
27 J. S. Bradshaw, R. S. Johnson, N. W. Adams, M. A. Pulsipher, K. E. Markides and M. L. Lee, *J. Chromatogr.*, 357 (1986) 69.
28 K. K. Unger, *Porous Silica* (*Journal of Chromatography Library*, Vol. 16), Elsevier, Amsterdam, 1979, p. 120.
29 C. Fulcher, M. A. Crowell, R. Bayliss, K. B. Holland and J. R. Jezorek, *Anal. Chim. Acta*, 129 (1981) 29.
30 H. Colin, N. Ward and G. Guiochon, *J. Chromatogr.*, 149 (1978) 169.
31 H. Colin and G. Guiochon, *J. Chromatogr.*, 141 (1977) 289.
32 G. J. Young, *J. Colloid Sci.*, 73 (1958) 67.
33 Gy. Szabó, E. Csató, M. Dévai, A. Borbély-Kuszmann and G. Liptay, *Anal. Chem.*, in press.

Journal of Chromatography, 463 (1989) 355–363
Elsevier Science Publishers B.V., Amsterdam — Printed in The Netherlands

CHROM. 21 080

REVERSED-PHASE HIGH-PERFORMANCE LIQUID CHROMATOGRAPHY–NUCLEAR MAGNETIC RESONANCE ON-LINE COUPLING WITH SOLVENT NON-EXCITATION

KLAUS ALBERT, MANUEL KUNST and ERNST BAYER*
Institut für Organische Chemie, Auf der Morgenstelle 18, D-7400 Tübingen (F.R.G.)
and
MANFRED SPRAUL and WOLFGANG BERMEL
Bruker Analytische Messtechnik GmbH, Silberstreifen, D-7512 Rheinstetten (F.R.G.)
(First received September 2nd, 1988; revised manuscript received October 31st, 1988)

SUMMARY

An improved type of continuous-flow nuclear magnetic resonance (NMR) probe showing excellent characteristics with respect to signal line shape and resolution is described. The stationary sensitivity in the continuous-flow cell is about 60% of that of rotating NMR tubes in a one-pulse experiment. An increase in sensitivity in the continuous-flow mode is obtained by pre-polarization of the solvent. Using the $1\bar{3}3\bar{1}$ solvent non-excitation technique a reversed-phase high-performance liquid chromatographic separation of an aromatic test mixture was demonstrated.

INTRODUCTION

Great progress has been made in recent years in the apparatus design used in high-performance liquid chromatography (HPLC). The instrument handling was simplified by the use of microprocessors, whilst automation procedures were successfully introduced by the development of autoinjection systems. On the detector side, more information as to the UV characteristics of the sample constituents were available by the introduction of variable-wavelength UV detectors. Nevertheless, the structural recognition of unknown compounds still requires a more structurally relevant detector. The superior stereochemical information available from nuclear magnetic resonance (NMR) spectroscopy justifies the current efforts at improving the sensitivity of continuous-flow NMR detection in reversed-phase separations[1–5]. In this respect, two problems must be solved: (1) improvement of the NMR characteristics such as signal line shape and signal-to-noise ratio of a continuous-flow cell of definite volume; (2) improvement of solvent suppression ratios in reversed-phase separations.

Our approach to overcome the problems is the design of a flow cell with optimum geometry together with a special detector coil which directly fits the cell. The benefit of such a development should be improved sensitivity as well as reduced signal

0021-9673/89/$03.50

linewidth. Because solvent suppression ratios depend especially on the linewidth at the base of the signal (at the height of the ^{13}C satellites) this feature is a prerequisite to overcome sensitivity problems in reversed-phase preparations. In an earlier publication[2] we have described the construction and application of 44- and 126-μl continuous-flow cells. In this work we deal with the characteristics of a new 120-μl flow cell suitable for direct HPLC–NMR coupling.

The pulse repetition time in an NMR experiment is dependent on the spin–lattice relaxation time, T_1, of the eluent. In the case of 90° pulse excitation, an equilibrium delay of $5T_1$ has to be used to obtain full equilibrium magnetization. It is shown that the solvent volume in an HPLC column may be used for pre-polarization of eluents leading to increased NMR sensitivity in the continuous-flow mode.

In reversed-phase separations the signals of protonated solvents lead to dynamic range problems. Efficient solvent suppression in the continuous-flow mode was performed by application of the $1\bar{3}3\bar{1}$ solvent non-excitation technique of Hore[6,7] in a separation of seven aromatic compounds.

EXPERIMENTAL

Continuous-flow probe design

A 3-mm I.D. glass tube tapering at both sides to the external diameters of the feed and drain PTFE tubings was silylated with dimethyldichlorosilane to avoid adsorption effects. A specially designed coil with an overall length of 18 mm was directly attached to the 4-mm O.D. glass tube resulting in a detector volume of 120 μl. PTFE tubings were attached to the glass tubing with the help of shrink-fit tubings. The cell was fixed in a glass dewar at the top of a standard narrow bore probe. The temperature was monitored by a thermocouple in the dewar. A schematic diagram of the flow cell design is shown in Fig. 1.

Apparatus

^1H NMR spectra were recorded on three NMR instruments of different magnetic field strengths: Bruker AC 300 (7.0 T), AM 400 widebore (9.4 T) and AM 500 (11.7 T). All instruments were controlled by the computer system Aspect 3000 with an array processor and hard disk. The 9.4-T instrument was equipped with a 12-bit analogue-to-digital converter (ADC), the other two instruments with a 16-bit ADC.

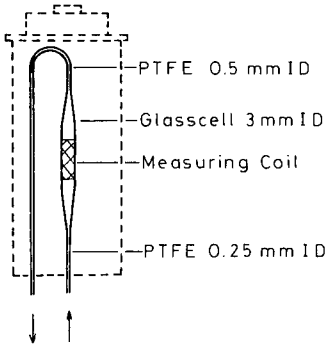

Fig. 1. Schematic diagram of the NMR flow cell design.

HPLC–NMR coupling

A stainless-steel HPLC column (ODS-Hypersil, 5 μm, 250 mm × 4.0 mm, Shandon) was fixed at the bottom of the 11.7-T magnet and connected to the continuous-flow probe by a stainless-steel capillary (Fig. 2). The injection system was fixed to one stand of the cryomagnet and connected to the HPLC column by a stainless-steel capillary. The HPLC instrument (Bruker LC 31) was located 1 m from the magnet.

Solvent systems

Test spectra were recorded of solutions of 10% chloroform in [$^2H_6$]acetone, of 0.1% ethylbenzene in deuteriochloroform and of a buffered mixture of acetonitrile–water (37.5:62.5) containing 0.15% of triethylamine at pH 3 (phosphoric acid). Solvents were circulated by the pump of the Bruker LC 31.

Separations on the ODS-Hypersil column were performed with acetonitrile–water (50:50). The distilled water in all experiments contained 3% deuterium oxide for field/frequency stabilization. All solvents were obtained from Merck (Darmstadt, F.R.G.).

Pre-polarization experiment

This experiment was performed using the decoupling coil of a dual 188.5-μl continuous-flow probe already described[3]. PTFE tubing (2 m × 1.1 mm I.D.) was coiled near the probe bottom of the 9.4-T instrument in a region of strong magnetic field, providing a pre-polarization volume of 2.0 ml. A peristaltic pump was used to circulate a 0.1% solution of ethanol in deuterium oxide. Magnetization curves were obtained by an inversion recovery sequence (180°–t–90°) with a variable delay, t, ranging between 0.1 and 2.0 s, a spectral width of 6000 Hz per 4 K and a 90° pulse of 20 μs.

Continuous-flow measurements using $1\bar{3}3\bar{1}$ solvent non-excitation

After recording a continuous-flow NMR spectrum of the pure solvent mixture of acetonitrile and water, the frequency difference between the two signals was determined. In the timing of the sequence (Fig. 3) a frequency difference of 965 Hz (AC 300) resulted in a delay, D_2, of 1 ms. The pulse carrier frequency was adjusted to the water resonance. The original 90° pulses (5.9 μs at the AC 300 and 6.0 μs at the AM

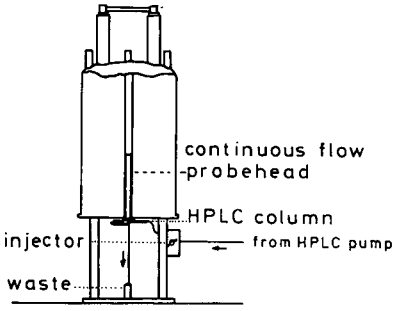

Fig. 2. Experimental arrangement for HPLC–NMR coupling.

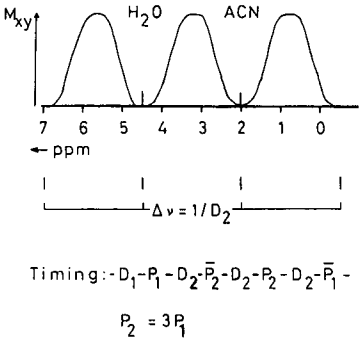

Fig. 3. Transverse magnetization excited by the $1\bar{3}3\bar{1}$ sequence as a function of the offset setting in acetonitrile–water mixtures. ACN = acetonitrile.

500) were attenuated with the help of an attenuator. According to the $1\bar{3}3\bar{1}$ solvent suppression technique, the resulting value was divided into four pulse lengths in the ratio 1:3:3:1. A spectral width of 4800 Hz (AC 300)/6000 Hz (AM 500) at a memory size of 8 K was used. For data acquisition at a flow-rate of 1 ml/min, the delay time, D_1, between scans was set to 0.1 s (AC 300) and 0.5 s (AM 500), therefore the total pulse repetition times were 0.9 s (AC 300) and 1.2 s (AM 500). In all experiments, eight scans were coadded resulting in time resolutions including the disc transfer time for data storage of 8 and 11 s. Up to 256 interferograms (files of eight scans) were recorded and stored on disk. In the data processing, magnitude calculation was performed after employing a sinebell or gaussian window function.

RESULTS AND DISCUSSION

NMR characteristics of the 120-μl continuous-flow probe

Test data for ^{1}H NMR probes are usually recorded by measuring the line shape of a chloroform signal and the signal-to-noise (S/N) ratio of a 0.1% solution of ethylbenzene. In the case of the 120-μl continuous-flow probe, tests were performed. Fig. 4 shows the spectrum of chloroform in [$^2H_6$]acetone at a flow-rate of 1 ml/min recorded on the 11.7-T instrument. The linewidth at the height of the ^{13}C satellites is 15.5 Hz, at 1/5 of this amplitude it is 23.5 Hz. In the case of the 7.0-T instrument the corresponding values are 14 and 30 Hz, whereas S/N of the CH_2 quartet of a 0.1% solution of ethylbenzene in deuteriochloroform is 75:1 (Fig. 5). In order to compare this value with sensitivity tests performed with conventional probes, one first has to consider different measuring volumes. In the case of a standard high resolution 5-mm probe at 7.0 T, a measuring volume of 250 μl yields a S/N value of 175:1. The correction factor for different volumes is[8] $\sqrt{V_2/V_1}$, therefore this value has to be corrected to 124:1. The sensitivity obtained with the present continuous-flow probe with a volume of 120 μl approaches 60% of that of the conventional probe. Nevertheless, keeping in mind that a non-rotating cell design is used, the sensitivity obtained is excellent. This is due to the increased filling factor of the measuring coil which is directly mounted around the glass containing the detection area.

The NMR cell volume employed is apparently larger than that used in routine

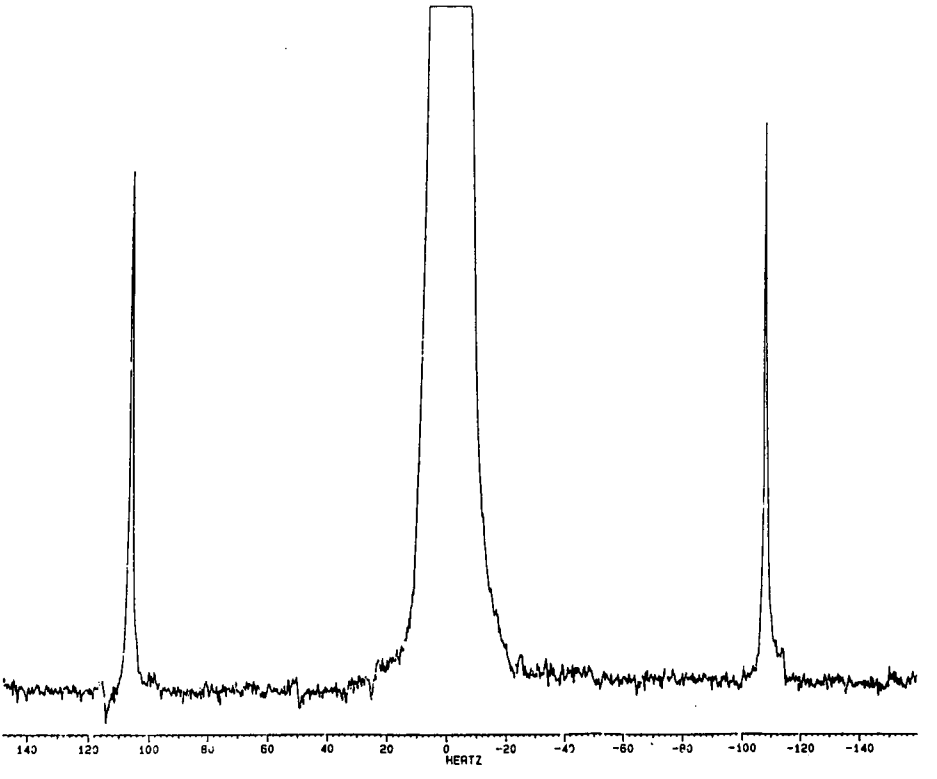

Fig. 4. ^{1}H NMR signal line shape of chloroform in [$^{2}H_6$]acetone (hump test), measured in a 120-μl continuous-flow probe (500 MHz) at a flow-rate of 1 ml/min.

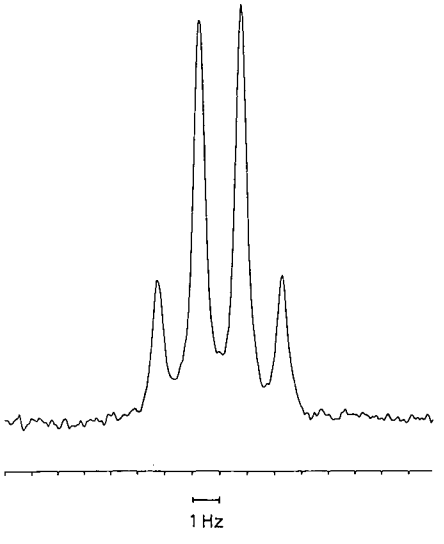

Fig. 5. ^{1}H NMR spectrum of the CH_2 protons of ethylbenzene (0.1% solution in deuteriochloroform), measured in a 120-μl continuous-flow probe (300 MHz, one scan, acquisition time 2.7 s).

UV detection. We have recently pointed out[3] that peak broadening effects due to increased NMR detection volumes are tolerable when long analytical columns (250 mm) are used. At the present state of NMR coil development, a detector volume of 40–120 μl is needed to yield good S/N values in the continuous-flow mode within a time resolution of the chromatogram of lower than 10 s.

Signal behaviour in continuous-flow NMR spectroscopy

An important feature of on-line HPLC–NMR coupling is the flow-rate dependency of NMR signals. Due to the decreased residence time, τ, of a nucleus in the flow cell, both the spin–lattice relaxation time, T_1, and the spin–spin relaxation time, T_2, are reduced[9,10]:

$$1/T_{1\ \text{flow}} = 1/T_{1\ \text{static}} + 1/\tau$$
$$1/T_{2\ \text{flow}} = 1/T_{2\ \text{static}} + 1/\tau$$

Therefore the NMR signal half width increases with increasing flow-rate[2]. On the other hand the signal intensity increases with increasing flow-rate if Boltzmann equilibrium is maintained before the nuclei enter the cell. Full polarization of nuclei may be achieved, allowing them to flow through a pre-polarization volume in the magnetic field for a time period that exceeds $5T_1$. Fig. 6 shows the magnetization curves of the CH_2 protons of ethanol at different flow-rates using a pre-polarization volume of 2 ml, equivalent to the total solvent volume in an HPLC column of 250 mm × 4 mm. The magnetization intensity, I, is plotted against the variable delay, t, between the 180° and the 90° pulse of the NMR inversion recovery sequence. The different slopes of magnetization are described by three relaxation times of 3.4 (stationary mode), 2.0 (flow-rate 2.4 ml/min) and 1.0 s (flow-rate 5.0 ml/min). Thus it is evident that a flow enhancement rate is possible, dependent on the ratio of the detector volume to the flow-rate and on the flip angle and pulse repetition time.

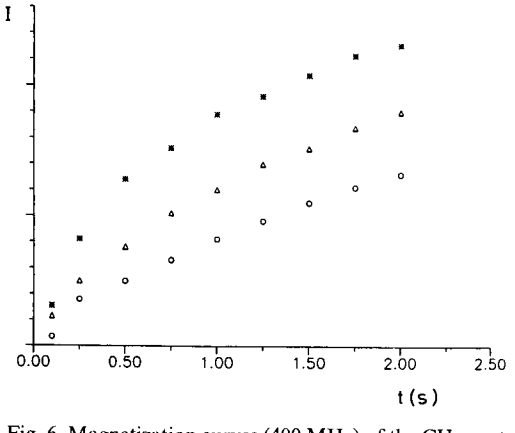

Fig. 6. Magnetization curves (400 MHz) of the CH_2 protons of ethanol in deuterium oxide at flow-rates of 0 (○), 2.4 (△) and 5.0 ml/min (*). Arbitrary intensity scale.

$1\bar{3}3\bar{1}$ Solvent non-excitation

The main problem in reversed-phase HPLC–NMR coupling is the suppression of solvent signals. Because of the time necessary for saturation of the solvent peak, the gated homodecoupling technique used in stopped-flow experiments[2] is not suitable for continuous-flow detection. Effective solvent suppression in continuous-flow acquisition is performed by application of the binomial solvent suppression techniques[6,7,11]. Laude and Wilkins[4,5] used the 11 technique of Clore *et al.*[11] whereas our group[3] takes advantage of the $1\bar{3}3\bar{1}$ technique of Hore[6,7].

Fig. 7 shows the spectrum of 0.15% triethylamine in a mixture of 62.5% water (pH 3) and 37.5% acetonitrile at a flow-rate of 1 ml/min with application of the $1\bar{3}3\bar{1}$ suppression technique. The intensity of the suppressed water signal is in the same range as those of the signals of the 0.15% triethylamine, indicating a solvent suppression ratio of three orders of magnitude. The disadvantage of this technique is that further nulls of the magnetization occur at intervals $1/D_2$ (Fig. 5) and that the signal phasing changes at every null. Therefore magnitude calculation has to be performed.

In Fig. 8 the contour plot of a separation of aromatic compounds (each 70 μg) at a flow-rate of 1 ml/min in acetonitrile–water (50:50) is shown. The chemical shift range between 2.6 and 10.3 ppm is plotted against the elution time between 0 and 40 min omitting the residual acetonitrile resonance at 2.0 ppm. Throughout the whole

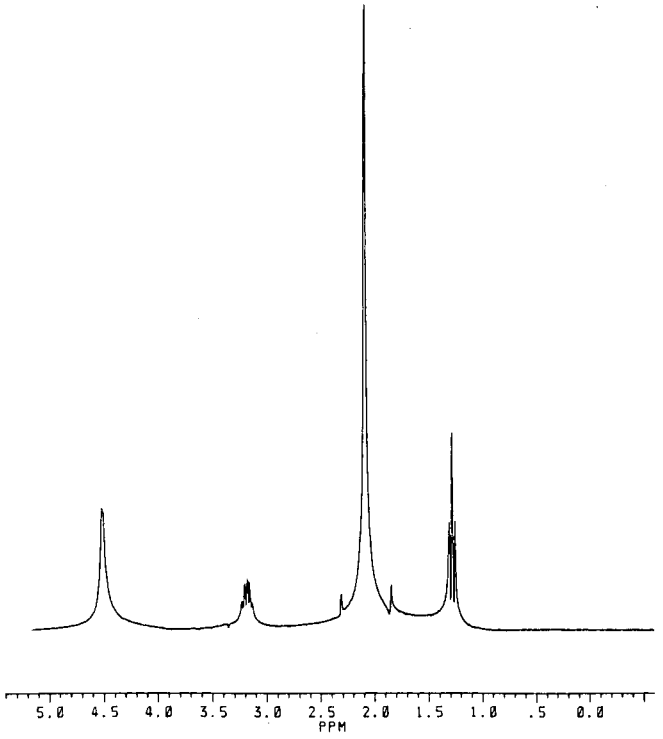

Fig. 7. ^{1}H NMR spectrum of a 0.15% solution of triethylamine in acetonitrile–water (37.5:62.5) at a flow-rate of 1 ml/min (300 MHz, eight scans, 4800 Hz per 8 K). $1\bar{3}3\bar{1}$ solvent non-excitation.

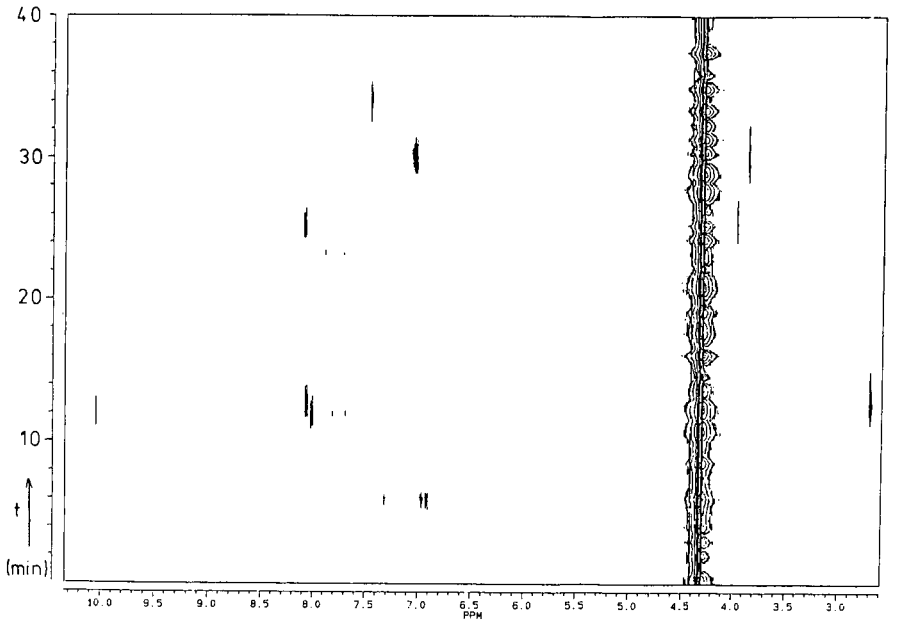

Fig. 8. ^{1}H NMR chromatogram (contour plot, 500 MHz) of a separation of phenol (t_R = 6 min), benzaldehyde (t_R = 12 min), acetophenone (t_R = 13 min), nitrobenzene (t_R = 23 min), methyl benzoate (t_R = 25 min), anisole (t_R = 30 min) and benzene (t_R = 34 min), each 70 μg, in acetonitrile–water (50:50). Flow-rate 1 ml/min. Eight scans per file; 6000 Hz per 8 K; 1$\bar{3}\bar{3}$T solvent non-excitation, column ODS-Hypersil 5 μm, 250 mm × 4.0 mm (Shandon).

separation the signal of the residual water is seen at 4.2–4.4 ppm. At a retention time, t_R, of 6 min the signals of phenol protons appear, followed by the signals of benzaldehyde at t_R = 12 min and of acetophenone at t_R = 13 min. The chemical shift values of the aldehyde and the alkoxy group in these compounds are strongly related to the structures of the substituents. The signals of nitrobenzene at t_R = 23 min are very weak, whereas the signal of methyl benzoate at t_R = 25 min can clearly be detected. The last two compounds are anisole at t_R = 30 min and benzene (t_R = 34 min). With the exception of nitrobenzene, the ^{1}H NMR peaks in this chromatogram reveal more structural information than any diode array detection.

CONCLUSIONS

The quality of NMR spectra obtained in continuous-flow systems is approaching more and more that of conventional stationary NMR spectra. In a one-pulse experiment, the stationary sensitivity is about 60% of that of rotating NMR tubes. In repeating multipulse experiments, the sensitivity may be equal or even better in the continuous-flow mode because of the advantage of rapid pulsing. Here pulse repetition rates are dependent on the T_1 values of the eluents.

Concerning the progress in sensitivity apparently available, another solution of the solvent problem seems to be possible. In microbore column separations, only a few ml of solvents are necessary for a separation, enabling the use of deuteriated

solvents. Using a special NMR coil arrangement, the sensitivity values reported in this paper should be obtained by continuous-flow cells using detector volumes in the range between 2 and 14 μl. Since, in microbore HPLC, flow-rates of 0.1 ml/min are used, flow broadening effects should be negligible. The application of such small cell volumes should also allow the development of solenoidal cells without changing the standard shimsystem, thus resulting in a two-fold sensitivity enhancement because of the perpendicular location of the cell relative to the magnetic field[8]. It is thus apparent that further enhancement of NMR sensitivity in the continuous-flow mode is expected within the next few years.

REFERENCES

1 H. C. Dorn, *Anal. Chem.*, 56 (1984) 747 A.
2 E. Bayer, K. Albert, M. Nieder, E. Grom, G. Wolff and M. Rindlisbacher, *Anal. Chem.*, 54 (1982) 1747.
3 K. Albert, M. Nieder, E. Bayer and M. Spraul, *J. Chromatogr.*, 346 (1985) 17.
4 D. A. Laude, Jr., R. W.-K. Lee and C. L. Wilkins, *Anal. Chem.*, 57 (1985) 1464.
5 D. A. Laude, Jr. and C. L. Wilkins, *Anal. Chem.*, 59 (1987) 546.
6 P. J. Hore, *J. Magn. Reson.*, 54 (1983) 539.
7 P. J. Hore, *J. Magn. Reson.*, 55 (1983) 283.
8 D. I. Hoult and R. E. Richards, *J. Magn. Reson.*, 24 (1976) 71.
9 A. I. Zhernovoi and G. D. Latyshev, *NMR in a Flowing Liquid*, Consultants Bureau, New York, 1956.
10 C. A. Fyfe, M. Cocivera and S. W. H. Damji, *Acc. Chem. Res.*, 11 (1978) 277.
11 G. M. Clore, B. J. Kimber and A. M. Gronenborn, *J. Magn. Reson.*, 54 (1983) 170.

Journal of Chromatography, 463 (1989) 365–374
Elsevier Science Publishers B.V., Amsterdam — Printed in The Netherlands

CHROM. 21 065

DETERMINATION OF WATER IN SOLID SAMPLES USING HEADSPACE GAS CHROMATOGRAPHY

JOSEPH M. LOEPER* and ROBERT L. GROB*
Chemistry Department, Villanova University, Villanova, PA 19085 (U.S.A.)
(First received July 17th, 1988; revised manuscript received October 24th, 1988)

SUMMARY

The research described herein concerns the use of the headspace technique coupled with gas chromatography for the quantitative determination of water in solid chemical compounds and pharmaceutical products. Samples were dissolved in alcohol and the water reacted with calcium carbide. The generated acetylene was measured with a flame ionization detector and related to the original amount of water in the sample. Samples were also analyzed by the Karl Fischer titration technique and the two sets of experimental data were subsequently compared.

INTRODUCTION

A method for the indirect determination of water by headspace gas chromatography (HSGC) was developed and shown to be effective for various organic solvents[1]. Samples containing water were transferred to dry vials containing calcium carbide and the water reacted with the calcium carbide to produce acetylene. This acetylene was then measured by HSGC and used to calculate the original concentration of water in the sample.

This article describes an investigation into the use of the same technique for the determination of water in solid sample materials. Some minor modifications to the sample preparation procedures and solvent systems have expanded the range of the technique to include various organic solids and pharmaceutical products.

EXPERIMENTAL

Apparatus

A Hewlett-Packard Model 5880A gas chromatograph and terminal, equipped with a flame ionization detector was used for the analysis. The separation was accomplished with a 6 ft. × 0.25 in. (4 mm I.D.) glass column with a packing of 5% SE-30 on Porapak Q (80–100 mesh) (Waters Chromatography Division, Millipore, Milford, MA, U.S.A.). The headspace samples were injected manually with a gas-tight precision sampling syringe (Series A-2, 2.0 ml) available from Precision Sam-

* Present address: Weston Analytics, Lionville, PA, U.S.A.

0021-9673/89/$03.50

pling Corp. (Baton Rouge, LA, U.S.A.). The sample reaction and subsequent headspace equilibration was completed in 50 ml glass reaction vials available from Supelco (Bellefonte, PA, U.S.A.). The vials were sealed with septa of brominated butyl rubber, obtained from The West Co. (Phoenixville, PA, U.S.A.), and aluminum seals from Wheaton Scientific (Millville, NJ, U.S.A.).

Reagents

Methanol, ethanol, 2-propanol, hydrated salts, and organic acids were purchased from J. T. Baker (Phillipsburg, NJ, U.S.A.). Calcium carbide (10–40 mesh) was obtained through Fisher Scientific (Fair Lawn, NJ, U.S.A.).

Analysis of solid materials

The percent water content of the solid materials was determined initially by the headspace calcium carbide procedure and then by Karl Fischer titration. Consequently, only compounds which would not interfere in a Karl Fischer titration were selected. The results from the Karl Fischer titrations could then be compared with those obtained with the headspace technique.

For the headspace analysis (HSA), samples were transferred to dry, 15 ml vials and capped. Transfers were done in a glovebag and the sample weight determined by difference. Methanol (10 ml) was then added to the vial to dissolve the sample. Solutions of methanol spiked with water and a blank were also prepared. The headspace vials were then prepared by adding 1.0 g calcium carbide (an excess) and 10.0 ml of 2-propanol to each. A 0.20-ml aliquot of the methanol solution was then transferred to a headspace vial (already containing 10.0 ml of 2-propanol). The vial was then sealed and equilibrated for the HSA.

For the Karl Fischer determinations, samples were titrated directly in methanol, with the end point determined potentiometrically.

Six individual samples were analyzed by each technique.

RESULTS AND DISCUSSION

Solvent considerations

The determination of water in a solid material requires that water comes into contact with the calcium carbide in the headspace vial. Dissolution of a compound into a appropriate solvent followed by the addition of the resulting solution into the headspace vial would be the most practical means of providing the contact. Under the proper conditions, one might also be able to extract the water present in some solids into a suitable solvent. Addition of this extract to the headspace vial should also prove to be adequate. Methanol is an excellent solvent for water determinations as demonstrated by its wide utility in Karl Fischer titrations, but it was eliminated from consideration due to its non-specific reaction with calcium carbide to produce acetylene.

$$2CH_3OH + CaC_2 \rightarrow C_2H_2 + Ca(OCH_3)_2$$

Investigations with ethanol also indicated that this solvent reacts with the calcium carbide, but the situation is not as severe as that encountered with methanol. With the

ethanol, some of the difficulties are probably from the reaction of methanol in the alcohol (5%), used for denaturation, as well as reaction of the ethanol itself. In ethanol, these non-specific reactions take place slowly, and reaction of the methanol is incomplete. Since the reaction of methanol in ethanol was slow, we felt that the same situation might exist with solutions of 2-propanol containing methanol. If this were true, then solid materials could be dissolved in methanol and diluted with 2-propanol before addition to the headspace vials.

Solutions of 2-propanol containing 2.0, 5.0, 7.5 and 10.0% (v/v) of methanol were prepared. Using these solutions as solvents for the calcium carbide technique, both blank solutions and solutions spiked with known amounts of water were prepared and used with the procedure. Eight vials were prepared for each of the solutions. After completion of the HSA, the average peak area was calculated for the blank solution of a given methanol concentration. This blank was then subtracted from the peak areas for individual vials containing the spiked solutions. The average net peak area for each of the spiked solutions was calculated, as well as the relative standard deviation (R.S.D.) of the spike determinations. These results are listed in Table I. The results indicate that levels of up to 5% methanol in 2-propanol can be tolerated. For solutions of 7.5 and 10.0%, however, the interferences from methanol caused poor precision.

Fig. 1 illustrates a plot of the change in peak areas for three of the blank solutions as a function of time. The plot illustrates the difficulties introduced by the presence of methanol. At the 5% level there is no significant change in the level of acetylene over a 3-h period. this increase in acetylene would account for the poor precision obtained with solutions containing the higher percentages of methanol.

Analysis of organic compounds and sodium salts of organic acids

Five hydrated compounds were chosen as test materials for use with the HSGC–calcium carbide technique and comparison with Karl Fischer titrations. The compounds are listed in Table II along with their percent purity and percent water content, corrected for purity.

The results of the water determinations for all of these compounds, except *p*-toluenesulfonic acid, are also listed in Table II. Some difficulties were encountered with this compound, and these results will be discussed separately.

The results obtained with the headspace technique are in good agreement with those obtained by Karl Fischer titration. The largest discrepancy is with the sodium diethyldithiocarbamate, with a relative difference of 4.86%. The headspace results are

TABLE I

REPRODUCIBILITY STUDIES WITH 2-PROPANOL–METHANOL SOLUTIONS

Methanol in 2-propanol (%)	*Spike, water concentration (ppm)*	*R.S.D. (%)*
2.0	250	3.28
5.0	300	3.34
7.5	300	8.13
10.0	300	5.29

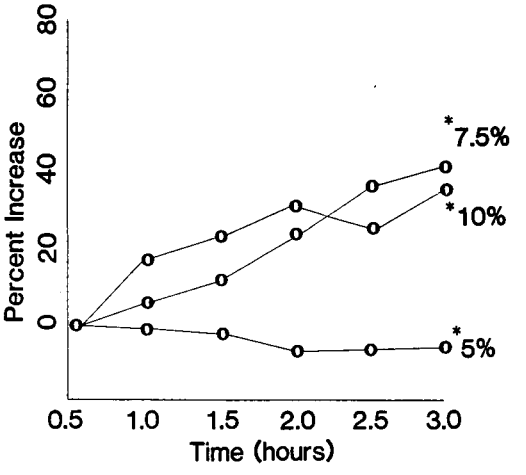

Fig. 1. Percent increase in acetylene *versus* time for solutions of methanol in 2-propanol. Percent methanol in 2-propanol is indicated by the asterisks.

also in agreement with the theoretical percentage of water for all of the compounds except citric acid. There were no difficulties encountered with the Karl Fischer titration of this compound and there are no anticipated interferences. Citric acid monohydrate is characterized as a compound which will begin to lose water in an anhydrous atmosphere[2] so it might be possible that it lost some of its water of hydration while in storage. It is interesting to note that the results obtained by the headspace technique for sodium diethyldithiocarbamate are actually in better agreement with the theoretical percentage of water than with the Karl Fischer results. It would be difficult to determine which of the experimental techniques was more accurate in this case, however. The percent purity of the material was listed as 98.4% on the label of the bottle, but the composition of the impurities was not specified.

TABLE II

PERCENT WATER CONTENT OF HYDRATED TEST MATERIALS

Compound	*Purity (%)*	*Water content (%)*		
		Theoretical	*HSGC (n = 6)*	*Karl Fischer (n = 6)*
Citric acid monohydrate	99.9	8.56	7.75 (2.69)*	7.84 (2.28)
Oxalic acid dihydrate	100.2	28.61	28.19 (3.36)	28.48 (0.25)
Sodium acetate trihydrate	99.8	39.60	39.70 (1.42)	38.33 (0.60)
Sodium diethyl-dithiocarbamate trihydrate	98.4	23.59	23.50 (4.00)	24.70 (0.72)
p-Toluenesulfonic acid monohydrate	99.6	9.42	–	–

* R.S.D. (%)

TABLE III

SPIKE RECOVERY EXPERIMENTS

Compound	*Recovery (%) (n = 6)*
Oxalic acid dihydrate	98.5 ± 3.3 (3.36)*
Sodium diethyldithiocarbamate trihydrate	98.8 ± 3.9 (3.90)

* R.S.D. (%)

Matrix spike recoveries were determined with oxalic acid and sodium diethyl dithiocarbamate. The results are listed in Table III. The quantitative recoveries obtained in both experiments would indicate that there is no change in the distribution coefficient of the acetylene in the presence of either of these compounds.

Some difficulties were encountered with the use of *p*-toluenesulfonic acid as a sample. Determination of the water content of this compound yielded results which were higher than the theoretical values and the results obtained by Karl Fischer titration. The vials containing the samples never achieved complete reaction, as the concentration of acetylene increased significantly with time, even after the usual 18-h reaction period. The *p*-toluenesulfonic acid was believed to be the cause of a non-specific reaction which resulted in the formation of acetylene. Since *p*-toluenesulfonic acid is a strong acid, there are several possible explanations which could account for the results which were obtained. One possibility would be reaction of the acid with an alcohol to produce an ester and water. Another possibility might be the neutralization of the acid with the calcium hydroxide in the system to produce the calcium salt of the acid and water. A final possibility is the direct reaction of the acid with the calcium carbide to produce acetylene.

$$2HA + CaC_2 \rightarrow C_2H_2 + CaA_2$$

where HA is *p*-toluensulfonic acid. Difficulties with ester formation in the presence of a strong acid are also encountered in Karl Fischer titrations[3,4]. To overcome this, one typically adds an amine to the solution which will increase the pH and inhibit ester formation. This same approach was applied to the HSGC–calcium carbide technique. A solution of 0.4% diethylamine in 2-propanol was prepared and tested with the calcium carbide technique. The presence of the amine caused no difficulties with the determination of water in the solvent. The solvent was then used for dissolution of the *p*-toluensulfonic acid for water determination with the HSGC–calcium carbide technique. The results which were obtained were still significantly higher than expected. All results of the determinations of the water content of *p*-toluensulfonic acid are listed in Table IV.

These results would indicate that the calcium carbide technique is not a very viable alternative for the determination of water in the presence of *p*-toluenesulfonic acid. Two other acidic compounds, oxalic acid (pK_a = 12.27 in water)[5] and citric acid (pK_a = 3.13 in water)[5] did not interfere with the determination of water, so certain acidic compounds can be handled by the technique. Thus, the success or failure

TABLE IV

DETERMINATION OF WATER IN *p*-TOLUENESULFONIC ACID

Solvent	*Water content (%)*		
	HSGC	*Theoretical*	*Karl Fischer*
2% Methanol in 2-propanol	15.82 (n = 3)	9.42	9.75
2-Propanol	13.21 (n = 3)	9.42	9.75
2% Methanol, 0.4% diethylamine in 2-propanol	13.76 (n = 6)	9.42	9.75

apparently is dependent on the strength of the acidic compounds present. If the pK_a, of oxalic acid in water were used as a general guide for the strength of acids which could be handled, this would leave a large range of organic acids which do not interfere with water determinations. There is no pK_a value for *p*-toluenesulfonic acid because aromatic sulfonic acids are strong acids and completely ionized in water[6].

Determination of water of hydration in transition metal salt

Seven hydrated transition metal salts were obtained for use as test materials. Most of the compounds were difficult to work with as received. They came in the form of fairly large chunks (1/4 × 1/2 in.). To facilitate ease of handling, most of the compounds were ground to a smaller particle size with a mortar and pestle and then placed in an oven at some predetermined temperature. Many of the higher hydrates of the transition metal salts are characterized as losing some of their water of hydration at a certain temperature[2], resulting in the formation of a stable, lower hydrate. To prepare a compound, a temperature was selected at which a stable, lower hydrate would form.

Three compounds were prepared in this manner and then subjected to thermogravimetric analysis (TGA) for determination of percent water content. The results of the TGA are shown in Table V, along with the theoretical percentage of water for each of the compounds. TGA of $Zn(NO_3)_2 \cdot 6H_2O$ was attempted, but this compound never reached constant mass. The melting point of this compound is listed as 36°C[2], but no reference is made as to the formation of the anhydrous salt above 36°C.

These same compounds were then used as sample materials with the HSGC–calcium carbide technique. Some serious difficulties were encountered in the application of the HSGC procedure to the determination of water in these compounds, however. The first compound investigated was cobalt dichloride dihydrate. The results obtained by the HSGC procedure were significantly higher than those expected from the information listed in Table V. Karl Fischer titration of the salt (in duplicate) yielded results which agreed with the data listed in Table V. The results are listed in Table VI.

There are two possible explanations for the discrepancy in the results obtained. One is that the cobalt dichloride changes the activity coefficient of the acetylene in the solvent, thereby changing the distribution coefficient of the acetylene in the system.

TABLE V

THERMOGRAVIMETRIC ANALYSIS

Compound	*Water content (%)*	
	TGA	*Theoretical*
$MnCl_2 \cdot H_2O$	12.48	12.51
$Cd(CH_3COO)_2 \cdot 2H_2O$	13.51	13.97
$CoCl_2 \cdot 2H_2O$	21.82	21.71

Since there was no cobalt dichloride present in the calibration solutions used in the analysis, a change in the distribution coefficient of acetylene caused by cobalt dichloride in the sample would result in an inaccurate quantitative determination of water in the sample. The other possibility is that some non-specific reaction through which acetylene is formed is taking place when the cobalt dichloride is present.

To investigate the possibility of a change in the distribution coefficient of the acetylene in the presence of a salt, some spike recovery experiments were preformed. The sample matrices investigated consisted of cobalt dichloride dihydrate, and the anhydrous forms of cobalt dichloride, manganese dichloride and cadmium acetate.

The recoveries from the experiments (Table VII) are all close to 100%, which would substantiate the premise that there is no change in the distribution coefficient of the acetylene in the various matrices investigated. Closer examination of the data reveals some other difficulties, however. For the three experiments with the anhydrous salts, the acetylene peak areas for the blank salt solutions are noticeably larger than the acetylene peak areas for the blank calibration solutions, indicating a higher than expected water concentration. This problem is the same as that encountered in the initial work with cobalt dichloride (Table VI). Upon examination of the individual peak areas obtained for each of the vials containing a particular salt solution, one also finds a distinct increase in the acetylene peak area with time (after overnight reaction), a situation that was not encountered with the vials containing no salt. If there is no change in the distribution coefficient of the acetylene in the presence of these transition metal salts, then the only other explanation for the higher than expected results would be that some non-specific reaction is taking place which also produces acetylene.

It seems unlikely that the transition metal salts would react directly with the calcium carbide to produce acetylene. In fact, reaction of cobalt dichloride or manganese dichloride in this manner would be impossible, since these salts do not possess any hydrogen atoms. Cadmium acetate does contain hydrogen, but these are methyl

TABLE VI

DETERMINATION OF WATER IN COBALT DICHLORIDE DIHYDRATE

	Water content (%)
HSGC (n = 6)	33.49 (2.74)*
Theoretical	21.71
Karl Fischer (n = 2)	21.41

* R.S.D. (%)

TABLE VII

SPIKE RECOVERIES FROM TRANSITION METAL SALT MATRICES

Matrix compound	*Recovery (%)*
$CoCl_2 \cdot 2H_2O$	102
$CoCl_2$	98
$Cd(CH_3COO)_2$	97
$MnCl_2$	106

TABLE VIII

DETERMINATION OF WATER IN PHARMACEUTICAL PRODUCTS

Pharmaceutical product	*Water content (%)*	
	HSGC (n = 6)	*Karl Fischer (n = 6)*
Cogentin*	1.70	1.49
	(4.85)***	(10.78)
Elavil*	1.72	1.58
(uncoated tablets)	(4.33)	(3.91)
Vasotec*	4.83	4.15
(10 mg enalapril maleate)	(2.75)	(21.08)
Aldomet**	8.68	8.75
(granulation)	(4.35)	(4.01)
Vasotec**	4.06	4.01
(20/50)	(4.91)	(1.93)
Elavil**	1.69	1.66
(coated tablets)	(2.08)	(1.70)
Ivermectin**	5.07	5.08
	(2.67)	(1.74)
Vasotec**	5.04	5.27
(40 mg enalapril)	(2.90)	(1.71
Aldomet**	4.21	4.17
(oral tablets)	(2.12)	(3.91)
Vasotec**	5.32	5.34
(5 mg enalapril) maleate)	(3.49)	(0.76)
Vasotec**	5.15	5.19
(2.5 mg enalapril maleate)	(4.50)	(3.98)

* 30 min extraction time.
** 45 min extraction time.
*** R.S.D. (%)

hydrogens and would have to be considered non-reactive. The alternative to the possibility of the salt itself reacting with the calcium carbide would then be that the presence of the salt is causing one of the other components of the system (*i.e.*, the alcohols) to react.

With the transition metals in the system, the possibility of an oxidation–reduction reaction does exist. Alcohols can be oxidized with a suitable oxidizing agent and

the proper conditions. But the cobalt(II), manganese(II) and cadmium(II) are all in stable oxidation states, and reduction to a lower oxidation level with the conditions used in these experiments would probably not occur. Perhaps a more likely alternative to an oxidation–reduction reaction would be the alcohols being coordinated around the transition metal atoms in solution, with the electronegative oxygen atom of the alcohol moiety drawn in towards the positively charged cation. This, in turn, could make the hydrogen of the alcohol more acidic and more susceptible to reaction with the calcium carbide, resulting in the production of acetylene.

These difficulties encountered with the transition metal compounds indicated that the reliable determination of water in their presence would not be possible with the techniques used in this study.

Determination of water in pharmaceutical products

Several pharmaceutical products were obtained for use as test samples with the HSGC–calcium carbide technique. These products came from the Pharmaceutical Research and Development Section of Merck Sharpe & Dohme's Research Labs., where their water contents are determined routinely by Karl Fischer titration. The water content of the products was determined using both techniques, so that a comparison of the results could be made.

For the investigations, six 1-g samples of the product were weighed to the nearest 0.1 mg and transferred to centrifuge tubes. The water in the samples was extracted with 10.00 ml of methanol and determined in the extract with an automatic coulometric Karl Fischer titrator.

Headspace vials were then prepared, with calcium carbide and 10.0 ml of anhydrous 2-propanol added to each. Aliquots of 200 μl of the methanol extracts were then transferred to the vials. The vials were equilibrated overnight and the HSA completed the following day. When the analyses were complete (Karl Fischer and HSA) the average percent water content of the product was calculated. The results for the analyses are listed in Table VIII.

For the first three analyses, the Karl Fischer results are significantly lower than the results of the headspace technique. The precision of the titration is also unexpectedly poor. The cause of these problems was suspected to be incomplete extraction of the water from the samples, and the order in which the two analyses were performed bears this out. The titrations were always done first, and a substantial amount of time (2 h) elapsed between the titrations and the preparation of the samples for the HSA. Apparently, this additional time was sufficient for the complete extraction of the water, as seen with the higher headspace results. The extraction times were increased (as noted in Table VIII), and the results of the two techniques were in better agreement. In general, the results indicated that the HSGC–calcium carbide technique was a very viable alternative for applications with these sample materials.

CONCLUSIONS

The calcium carbide technique was shown to be effective for the determination of water in certain types of solid sample materials. The water content of several hydrated organic acids and the sodium salts of organic acids was determined with

both the calcium carbide technique and Karl Fischer titration. The results of the determinations with the calcium carbide technique were within ± 5% (a relative value) of the Karl Fischer results. The relatieve standard deviations, obtained from six individual measurements for each of the compounds, were all less than 5%. Eleven commercially available pharmaceutical products were also analyzed by both the calcium carbide technique and Karl Fischer titration. The accuracy and precision of these determinations were also within the range of 5%.

Several compounds were incompatible with the calcium carbide technique. Hydrated transition metal salts and *p*-toluenesulfonic acid yielded results which were significantly higher than expected. The difficulty with these compounds was suspected to be a non-specific reaction of calcium carbide with one of the components (others than water) of the prepared sample, resulting in the formation of additional acetylene. The water content of two transition metal salts was successfully measured after some modifications to the technique. It was concluded, however, that the calcium carbide technique, even with the modifications, was not a very feasible alternative for other techniques which can easily handle these compounds.

From a practical standpoint, there are also several advantages and disadvantages of the calcium carbide technique which should be discussed. The calcium carbide technique can measure levels of water reliably down to the 60-ppm level in liquid samples[1]. There are other techniques which have significantly lower detection limits (*i.e.*, Karl Fischer titration), but most GC techniques are limited to the 60-ppm level or higher. The preparation time needed for six samples was approximately the same for the calcium carbide technique and Karl Fischer titration. For a large number of samples, an automated headspace sampler (capacity of 60–100 samples) could be used with the indirect method. This would mean that an analyst spends time only on the preparation of samples. The acetylene determinations would be completely automated. But for a laboratory which receives only one or two samples for water determinations a week, the calcium carbide technique would not be very practical.

Future investigations with the calcium carbide technique will focus on sample materials which are incompatible with the Karl Fischer titration (*i.e.*, carbonates, bicarbonates, etc.). An automated headspace sampler will be tested with the technique. These samplers demonstrate significantly improved injection reproducibility over that of a manual gas injection. This improved reproducibility would result in lower detection limits for the calcium carbide technique. And finally, some research into the problems associated with the transition metal salts might lead to a modification which would allow these materials, and other to be handled by the calcium carbide technique.

REFERENCES

1 J. M. Loeper and R. L. Grob, *J. Chromatogr.*, 457 (1988) 247.
2 M. Windholz, *The Merck Index*, Merck, Rahway, NJ, 10th ed., 1983.
3 J. Mitchell, Jr. and D. M. Smith, *Aquametry (Part III)*, Vol. 5, New York, 2nd ed., 1980.
4 J. Mitchell, Jr., D. M. Smith, E. C. Ashby and W. M. D. Bryant, *J. Am. Chem. Soc.*, 63 (1941) 2927.
5 J. A. Dean (Editor), *Lange's Handbood of Chemistry*, McGraw-Hill, New York, 12th ed., 1979.
6 C. R. Noller, *Chemistry of Organic Compounds*, W. B. Saunders, Philadelphia, PA, 3rd ed., 1966, p. 504.

Journal of Chromatography, 463 (1989) 375–396
Elsevier Science Publishers B.V., Amsterdam — Printed in The Netherlands

CHROM. 21 077

STUDY OF THE PRIMARY STRUCTURE OF RECOMBINANT TISSUE PLASMINOGEN ACTIVATOR BY REVERSED-PHASE HIGH-PERFORMANCE LIQUID CHROMATOGRAPHIC TRYPTIC MAPPING

R. C. CHLOUPEK*, R. J. HARRIS, C. K. LEONARD, R. G. KECK, B. A. KEYT, M. W. SPELLMAN, A. J. S. JONES and W. S. HANCOCK

Genentech, Inc., 460 Point San Bruno Boulevard, South San Francisco, CA 94080 (U.S.A.)

(Received September 6th, 1988)

SUMMARY

Two high-resolution tryptic maps have been developed for recombinant tissue plasminogen activator (rt-PA) that separate the expected 51 tryptic peptides. The trypsin digestion was performed after reduction and S-carboxymethylation of the protein. The high-performance liquid chromatographic separation of the tryptic peptides used a Nova-Pak C_{18} (5 μm) column with a mobile phase that contained 0.1% aqueous trifluoroacetic acid (TFA) or 50 m*M* sodium phosphate (pH 2.85) and a linear gradient of acetonitrile. A TFA solvent system was also used for re-purification and for characterization of the peptides isolated from the phosphate-based separation. All of the isolated peptides had compositions consistent with the sequence proposed for rt-PA.

The identities of the glycopeptides were confirmed by lectin chromatography on concanavalin A-Sepharose. The mixture of tryptic peptides was also treated with *endo*-β-N-acetylglucosaminidase H and peptide:N-glycosidase F to locate the position of either high mannose or complex oligosaccharides. These studies demonstrated that a high mannose oligosaccharide is attached to Asn-117 while complex carbohydrate side-chains are attached to Asn-184 and Asn-448. The residue Asn-184 is the site of optional glycosylation that results in the formation of two rt-PA variants that contain either two or three oligosaccharides.

INTRODUCTION

Reversed-phase high-performance liquid chromatography (RP-HPLC) has been shown to give a rapid and highly selective separation of tryptic digests of proteins[1] and has been applied to the characterization of several recombinant proteins such as methionyl-human growth hormone[2], bovine growth hormone[3] and interleukin[4]. This analytical technique has become a significant part of quality control procedures for the manufacture of protein pharmaceuticals produced by recombinant-DNA technology[5].

The application of tryptic mapping procedures to recombinant DNA-derived

0021-9673/89/$03.50

tissue plasminogen activator (rt-PA) produced in Chinese hamster ovary cell culture[6] represents a greater challenge. The previous tryptic map applications involved non-glycosylated proteins of molecular weights of up to 22 000 daltons, while rt-PA is a glycoprotein with a polypeptide molecular weight of 59 042 daltons[7] containing glycosylation variants that have either three or two carbohydrate side chains (type I and type II, respectively)[8,9]. This report describes the characterization of the primary structure of rt-PA utilizing two tryptic mapping methods. The tryptic peptides were found to be consistent with the primary sequence derived from the cDNA sequence of rt-PA[7]. The glycopeptides present in the tryptic mixture were further studied by lectin affinity chromatography and by digestion with glycosidases.

EXPERIMENTAL

Materials

HPLC/spectro-grade trifluoroacetic acid (TFA) (Pierce, Rockford, IL, U.S.A.), UV-grade acetonitrile (Burdick & Jackson, Muskegon, MI, U.S.A.), Sephadex G-75 superfine (Pharmacia, Piscataway, NJ, U.S.A.), α-methyl mannoside (Aldrich, Milwaukee, WI, U.S.A.), analytical-grade reagents and distilled, deionized Milli-Q™ water (Millipore, Bedford, MA, U.S.A.) were used. Concanavalin A (Con A) Sepharose, DL-dithiothreitol (DTT) and iodoacetic acid were obtained from Sigma (St. Louis, MO, U.S.A.). The enzymes used were TPCK (L-1-tosylamide-2-phenylethyl chloromethyl ketone) treated trypsin (Cooper Biomedical), peptide:N-glycosidase F (PNGase F) and *endo*-β-N-acetylglucosaminidase H (Endo H) (Genzyme, Boston, MA, U.S.A.). Recombinant tissue plasminogen activator was purified from mammalian cell culture (Chinese hamster ovary cell supernatants)[6] and reconstituted to a concentration of 1 mg/ml.

Sample preparation

A 5 mg-amount of rt-PA was reduced and S-carboxymethylated (RCM) according to a modified method based on Crestfield *et al.*[10]. The rt-PA was first dialyzed into the 8 *M* urea reaction buffer, treated for 4 h at ambient temperature with 10 m*M* DTT, followed by 25 m*M* iodoacetic acid. The resultant RCM rt-PA was then dialyzed into 0.1 *M* ammonium bicarbonate using dialysis tubing with a 3500 molecular weight cut-off.

The two domains of plasmin-treated RCM rt-PA (amino acid residues 1–275 and 276–527) were separated by gel filtration on a Sephadex G-75 superfine column (100 × 1.5 cm I.D.) in 0.1 *M* ammonium bicarbonate as described by Vehar *et al.*[11].

Tryptic digestion

RCM rt-PA was digested in 0.1 *M* ammonium bicarbonate at ambient temperature with an addition of TPCK-trypsin at an enzyme-to-substrate ratio of 1:100 (w/w), followed by a second addition of 1:100 after 8 h. The digestions were stopped after 24 h by freezing (−70°C).

Chromatography

The HPLC separations, unless otherwise indicated, were performed on a Waters gradient liquid chromatograph that included two 6000A pumps, a 720 controller,

a WISP 710B injector and a Nova-Pak 15 × 0.39 cm I.D., 5 μm, C_{-18} reversed-phase column. The elution profile was monitored by combined LKB (2138 UVicord) and Perkin-Elmer (LC75) spectrophotometers for dual-wavelength detection at 214 and 280 nm, respectively. The HPLC separations of glycopeptides were performed on a Hewlett-Packard 1090M liquid chromatograph.

TFA tryptic map

The TFA solvent system used 0.1% aqueous TFA with a linear gradient of 0.08% TFA in acetronitile at a rate of 0.5%/min for 50 min, followed by a 1.0%/min linear gradient for 35 min at a flow-rate of 1.0 ml/min. Tryptic peptide peaks from RCM rt-PA 1–275 and RCM rt-PA 276–527 digests were collected manually from semipreparative separations using the TFA solvent system. Approximately 6.5 nmol of starting material was loaded for each separation.

Sodium phosphate tryptic map

The sodium phosphate solvent system used 50 m*M* sodium phosphate, pH 2.85 with a linear gradient of acetonitrile at a rate of 0.3%/min for 90 min, followed by a 1.0%/min linear gradient for 30 min at a flow-rate of 1.0 ml/min.

Tryptic peptide peaks from the RCM rt-PA digest were manually collected from three semi-preparative separations using the sodium phosphate solvent system totaling 18 nmol of starting material. The peptide peaks were vacuum concentrated and the total sample was rechromatographed in the volatile TFA solvent system using 0.1% TFA with a rapid linear gradient of acentonitrile containing 0.08% TFA at a rate of 10%/min to 60% acetonitrile, followed by isocratic elution at 60% acetonitrile for 20 min.

Peak analysis

Peptide peaks collected from both HPLC solvent systems were characterized by either amino acid analysis after acid hydrolysis or N-terminal sequencing with a Beckman 890C sequencer. Hydrolysis was performed by incubation of the peptides in constant boiling hydrochloric acid for 20 h at 110°C *in vacuo* for the trifluoroacetic acid tryptic map peptide peaks, followed by analysis on an LKB 4400 amino acid analyzer. Phosphate tryptic map peptides were hydrolyzed by the batch method of Waters Assoc. before Pico Tag™amino acid analysis. Amino acids were determined as their phenylthiocarbamyl (PTC) derivatives which were prepared by reaction with phenylisothiocyanate (PITC) at pH 9.5. The PTC-amino acids were chromatographed using an RP-HPLC system with detection at 254 nm. In both cases, identification and quantitation were performed by area comparison with an external standard. Edman degradation methodology was used to sequence peptides for identification in the case of ambiguous amino acid compositional data.

Carbohydrate-containing peptides

Lectin chromatography. Tryptic glycopeptides were isolated by lectin chromatography using a Con A-Sepharose column with a bed volume of 5 ml, equilibrated in 100 m*M* ammonium bicarbonate containing 1 *M* sodium chloride, 1 m*M* calcium chloride and 0.02% sodium azide. Trypsin-digested, RCM rt-PA (10 mg) was applied to the column in 100 m*M* ammonium bicarbonate containing 1 m*M* calcium chloride.

The absorbance at 280 nm was monitored and 0.5-ml fractions were collected. The column was washed with the equilibration buffer until the absorbance at 280 nm returned to baseline. Tryptic glycopeptides were eluted with 100 m*M* ammonium bicarbonate containing 0.2 *M* α-methyl mannoside and 0.02% sodium azide.

Treatment with peptide:N-glycosidase F. A 0.4-mg aliquot of RCM rt-PA was reconstituted in 0.08 ml of 250 m*M* sodium phosphate (pH 8.6) containing 10 m*M* EDTA and 0.02% sodium azide. PNGase F (0.5 manufacturer's units) in 0.018 ml of 50% glycerol was added and the sample was incubated overnight at 37°C. The sample was then diluted to 0.4 ml with water and dialyzed against 100 m*M* ammonium bicarbonate prior to trypsin digestion as described above.

Treatment with endo-β-N-acetylglucosaminidase H. A 0.4-mg aliquot of RCM rt-PA was reconstituted in 0.08 ml of 200 m*M* arginine phosphate (pH 6) containing 0.03 m*M* Polysorbate 80 and 0.02% sodium azide. The sample was treated with Endo H (0.04 manufacturer's units) in 0.02 ml of 50 m*M* sodium phosphate (pH 6) and incubated overnight at 37°C. The sample was then diluted to 0.4 ml with water, dialyzed against 100 m*M* ammonium bicarbonate, and digested with trypsin as described above.

RESULTS

TFA tryptic map

The tryptic map of RCM rt-PA obtained using TFA as the ionic modifier is shown in Fig. 1. The theoretical tryptic peptides are designated by "T"and numerically ordered from amino-terminal (T1) to the carboxy-terminal peptide (T51) (Table I). When a peptide elutes in more than one position in the tryptic map, the minor peak is

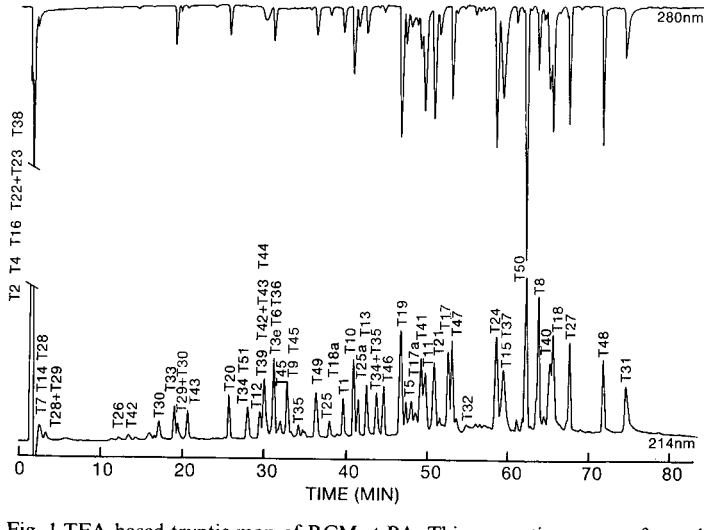

Fig. 1.TFA-based tryptic map of RCM rt-PA. This separation was performed on a 5-μm Nova-Pak C_{18} column (15 × 0.46 cm I.D.). Mobile phase A consisted of aqueous 0.1% TFA and mobile phase B was acetonitrile with 0.08% TFA. A linear gradient of 0–25% mobile phase B was run in 50 min followed by 25–60% mobile phase B in 35 min. The 200-μg sample was loaded in 0.2 ml of 0.1 *M* ammonium bicarbonate and monitored at both 214 and 280 nm.

TABLE I

THEORETICAL TRYPTIC PEPTIDES OF rt-PA

Tryptic Peptide	*Residue No.*		*Sequence**
	Start	*End*	
T1	1	7	SYQVICR
T2	8	10	DEK
T3	11	27	TQMIYQQHQSWLRPVLR
T4	28	30	SNR
T5	31	40	VEYCWCNSGR
T6	41	49	AQCHSVPVK
T7	50	55	SCSEPR
T8	56	82	CFNGGTCQQALYFSDFVCQCPEGFAGK
T9	83	89	CCEIDTR
T10	90	101	ATCYEDQGISYR
T11	102	129	GTWSTAESGAECTNWNSSALAQKPYSGR
T12	130	135	RPDAIR
T13	136	145	LGLGNHNYCR
T14	146	149	NPDR
T15	150	159	DSKPWCYVFK
T16	160	162	AGK
T17	163	189	YSSEFCSTPACSEGNSDCYFGNGSAYR
T18	190	212	GTHSLTESGASCLPWNSMILIGK
T19	213	228	VYTAQNPSAQALGLGK
T20	229	233	HNYCR
T21	234	247	NPDGDAKPWCHVLK
T22	248	249	NR
T23	250	250	R
T24	251	267	LTWEYCDVPSCSTCGLR
T25	268	275	QYSQPQFR
T26	276	277	IK
T27	278	296	GGLFADIASHPWQAAIFAK
T28	297	298	HR
T29	299	299	R
T30	300	304	SPGER
T31	305	327	FLCGGILISSCWILSAAHCFQER
T32	328	339	FPPHHLTVILGR
T33	340	342	TYR
T34	343	351	VVPGEEEQK
T35	352	356	FEVEK
T36	357	361	YIVHK
T37	362	378	EFDDDTYDNDIALLQLK
T38	379	383	SDSSR
T39	384	392	CAQESSVVR
T40	393	416	TVCLPPADLQLPDWTECELSGYGK
T41	417	427	HEALSPFYSER
T42	428	429	LK
T43	430	434	EAHVR
T44	435	440	LYPSSR
T45	441	449	CTSQHLLNR
T46	450	462	TVTDNMLCAGDTR
T47	463	489	SGGPQANLHDACQGDSGGPLVCLNDGR
T48	490	505	MTLVGIISWGLGCGQK
T49	506	513	DVPGVYTK
T50	514	522	VTNYLDWIR
T51	523	527	DNMRP

* Single-letter symbols for amino acids: A = Ala; C = Cys; D = Asp; E = Glu; F = Phe; G = Gly; H = His; I = Ile; K = Lys; L = Leu; M = Met; N = Asn; P = Pro; Q = Gln; R = Arg; S = Ser; T = Thr; V = Val; W = Trp; Y = Tyr.

denoted by the letter of the alphabet in order of relative recovery (T17, T17a, T17b, for example). A peptide generated by an incomplete cleavage is designated by a plus sign, *e.g.*, T29 + T30. The elution profile was monitored at two different wavelengths (214 and 280 nm) and each of the peptides that contained tyrosine and/or tryptophan was observed in the 280-nm profile. Despite the complexity of the mixture of tryptic peptides, the high resolution separation shown in Fig. 1 would suggest minimal co-elutions. This was confirmed by examination of the tryptic maps of the separated domains: RCM 1–275 and RCM 276–527 (Fig. 2).

Peaks were collected for amino acid analysis from both the total TFA tryptic map and the maps of the separated domains. Table II shows the peptide compositions of the peaks collected from the separated domains. If the amino acid analysis was ambiguous, such as in cases of co-elutions, the sample was also sequenced by Edman degradation to establish the identity. The relative contribution of each peptide to the total amino acid analysis of co-eluting peptides was calculated and peptide compositions were then reported separately (for example, T39, T42 + T43 and T44 at 29 min, Fig. 2). In those cases where the observed composition was very close to the deduced

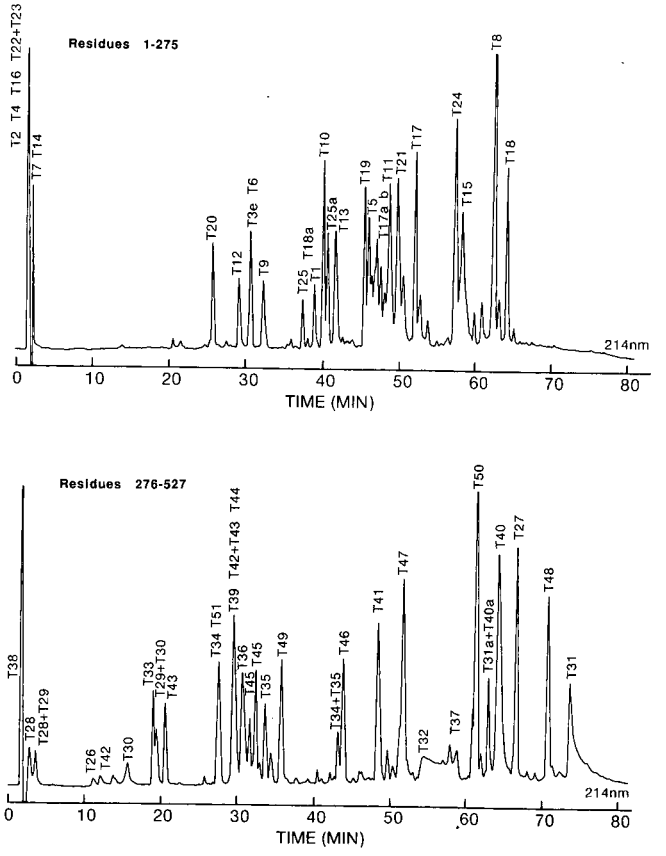

Fig. 2. TFA-based tryptic map comparison of the two separated domains of RCM rt-PA. The 200-μg sample loads were chromatographed as described in Fig. 1.

TABLE II

AMINO ACID COMPOSITIONS OF TFA TRYPTIC PEPTIDE PEAKS
(s) = N-Terminal sequencing; (□) = theoretical values.

	T1	*T3d*	*T5*	*T6(s)*	*T7(s)*	*T8*
Cmc	0.3 (1)	0.0	1.5 (2)	0.6 (1)	0.2 (1)	2.0 (4)
Asx	0.3	0.0	1.1 (1)	0.0	0.0	2.1 (2)
Thr	0.0	0.0	0.0	0.0	0.0	0.9 (1)
Ser	1.1 (1)	0.0	1.0 (1)	0.9 (1)	2.0 (2)	1.0 (1)
Glx	1.2 (1)	0.0	1.0 (1)	1.1 (1)	1.2 (1)	4.0 (4)
Pro	0.0	1.0 (1)	0.0	0.9 (1)	0.8 (1)	1.1 (1)
Gly	0.0	0.0	1.1 (1)	0.0	0.0	4.0 (4)
Ala	0.2	0.0	0.2	1.0 (1)	0.0	2.0 (2)
Cys	0.2	0.0	0.0	0.0	0.0	1.6
Val	0.7 (1)	1.0 (1)	0.8 (1)	2.1 (2)	0.0	1.0 (1)
Met	0.0	0.0	0.0	0.0	0.0	0.0
Ile	0.9 (1)	0.0	0.0	0.0	0.0	0.0
Leu	0.1	1.0 (1)	0.1	0.0	0.0	1.1 (1)
Tyr	1.0 (1)	0.0	0.9 (1)	0.0	0.0	1.0 (1)
Phe	0.0	0.0	0.0	0.0	0.0	4.0 (4)
Lys	0.1	0.0	0.0	1.1 (1)	0.0	1.0 (1)
His	0.0	0.0	0.0	1.0 (1)	0.0	0.0
Arg	1.1 (1)	1.0 (1)	1.0 (1)	0.0	1.1 (1)	0.0

	T9	*T10*	*T11*	*T12*	*T13*	*T14(s)*
Cmc	1.3 (2)	0.8 (1)	0.6 (1)	0.0	0.6 (1)	0.0
Asx	1.0 (1)	1.3 (1)	2.0 (2)	1.0 (1)	2.0 (2)	1.5 (2)
Thr	0.9 (1)	1.0 (1)	2.5 (3)	0.0	0.1	0.0
Ser	0.0	1.5 (1)	4.1 (5)	0.1	0.1	0.0
Glx	1.1 (1)	2.2 (2)	3.4 (3)	0.1	0.4	0.0
Pro	0.0	0.0	1.1 (1)	0.9 (1)	0.1	0.8 (1)
Gly	0.1	1.4 (1)	3.0 (3)	0.0	2.0 (2)	0.0
Ala	0.0	1.2 (1)	3.7 (4)	1.0 (1)	0.0	0.0
Cys	0.0	0.0	0.0	0.0	0.0	0.0
Val	0.0	0.1	0.2	0.0	0.0	0.0
Met	0.6	0.0	0.1	0.0	0.0	0.0
Ile	1.0 (1)	1.0 (1)	0.2	0.9 (1)	0.0	0.0
Leu	0.0	0.2	1.2 (1)	0.0	2.1 (2)	0.0
Tyr	0.0	1.9 (2)	1.5 (1)	0.0	0.9 (1)	0.0
Phe	0.0	0.1	0.2	0.0	0.1	0.0
Lys	0.0	0.4	1.4 (1)	0.0	0.1	0.0
His	0.0	0.0	0.2	0.0	0.9 (1)	0.0
Arg	1.0 (1)	1.0 (1)	1.3 (1)	2.1 (2)	1.0 (1)	1.1 (1)

	T15	*T17*	*T17a*	*T18*	*T18a(s)*
Cmc	0.7 (1)	1.7 (3)	2.6 (3)	1.3 (1)	0.2
Asx	1.0 (1)	2.8 (3)	3.5 (3)	1.2 (1)	0.4
Thr	0.3	1.2 (1)	0.8 (1)	2.0 (2)	0.0
Ser	1.4 (1)	5.1 (6)	5.1 (6)	3.6 (4)	0.1
Glx	0.4	3.5 (2)	2.6 (2)	1.1 (1)	0.0
Pro	1.0 (1)	0.8 (1)	1.1 (1)	0.8 (1)	0.0
Gly	0.4	2.8 (3)	3.2 (3)	3.1 (3)	1.0 (1)
Ala	0.2	1.8 (2)	1.9 (2)	1.0 (1)	0.0

(*Continued on p. 382*)

TABLE II (*continued*)

	T15	*T17*	*T17a*	*T18*	*T18a(s)*	
Cys	0.0	0.0	0.0	0.0	0.0	
Val	0.9 (1)	0.0	0.5	0.0	0.0	
Met	0.1	0.0	0.0	0.3 (1)	0.0	
Ile	0.1	0.0	0.0	1.9 (2)	2.0 (2)	
Leu	0.5	0.0	0.1	3.1 (3)	1.1 (1)	
Tyr	0.9 (1)	2.8 (3)	2.9 (3)	0.0	0.0	
Phe	1.0 (1)	1.7 (2)	1.4 (2)	0.1	0.0	
Lys	2.0 (2)	0.0	0.3	1.1 (1)	0.9 (1)	
His	0.2	0.0	0.0	1.0 (1)	0.0	
Arg	0.1	1.3 (1)	1.6 (1)	0.0	0.0	
	T19	*T20*	*T21*	*T24*	*T25(s)*	*T25a*
Cmc	0.1	0.8 (1)	0.7 (1)	2.5 (3)	0.2	0.1
Asx	1.1 (1)	1.1 (1)	2.7 (3)	1.1 (1)	0.7	0.2
Thr	1.0 (1)	0.1	0.1	1.8 (2)	0.5	0.1
Ser	0.9 (1)	0.0	0.3	1.8 (2)	1.4 (1)	1.0 (1)
Glx	2.1 (2)	0.1	0.2	1.0 (1)	3.0 (3)	3.1 (3)
Pro	0.9 (1)	0.0	1.7 (2)	1.1 (1)	1.1 (1)	0.9 (1)
Gly	2.1 (2)	0.1	1.1 (1)	1.2 (1)	0.8	0.1
Ala	2.9 (3)	0.0	1.2 (1)	0.1	0.9	0.1
Cys	0.0	0.0	0.0	0.0	0.0	0.0
Val	0.8 (1)	0.0	0.8 (1)	0.9 (1)	0.3	0.0
Met	0.0	0.0	0.0	0.0	0.0	0.0
Ile	0.0	0.1	0.0	0.0	0.2	0.2
Leu	2.1 (2)	0.0	1.0 (1)	2.0 (2)	0.5	0.1
Tyr	0.9 (1)	0.8 (1)	0.0	0.9 (1)	0.8 (1)	1.0 (1)
Phe	0.1	0.1	0.0	0.2	0.9 (1)	1.0 (1)
Lys	1.0 (1)	0.1	1.9 (2)	0.3	0.2	0.0
His	0.0	1.0 (1)	0.9 (1)	0.0	0.0	0.0
Arg	0.0	1.1 (1)	0.0	1.2 (1)	1.3 (1)	0.1
	T26	*T27(s)*	*T28(s)*	*T28+T29(s)*	*T29+T30(s)*	*T30*
Cmc	0.0	0.1	0.0	0.0	0.0	0.0
Asx	0.0	1.0 (1)	0.1	0.0	0.0	0.0
Thr	0.0	0.1	0.0	0.0	0.1	0.0
Ser	0.0	0.9 (1)	0.1	0.1	1.0 (1)	0.9 (1)
Glx	0.0	1.1 (1)	0.0	0.1	0.9 (1)	1.0 (1)
Pro	0.0	1.0 (1)	0.0	0.0	0.9 (1)	1.0 (1)
Gly	0.0	2.2 (2)	0.0	0.1	0.9 (1)	1.0 (1)
Ala	0.0	4.7 (5)	0.0	0.0	0.0	0.0
Cys	0.0	0.0	0.0	0.0	0.0	0.0
Val	0.0	0.2	0.0	0.0	0.0	0.0
Met	0.0	0.1	0.0	0.0	0.0	0.0
Ile	1.0 (1)	2.3 (2)	0.0	0.0	0.1	0.0
Leu	0.1	1.2 (1)	0.0	0.0	0.0	0.0
Tyr	0.0	0.1	0.0	0.0	0.4	0.0
Phe	0.0	1.9 (2)	0.0	0.0	0.0	0.0
Lys	1.0 (1)	1.5 (1)	0.0	0.0	0.0	0.0
His	0.0	1.0 (1)	0.9 (1)	1.0 (1)	0.0	0.0
Arg	0.0	0.1	1.1 (1)	2.0 (2)	2.2 (2)	1.0 (1)

TABLE II (*continued*)

	T31	*T31a+T40a (s)*	*T32*	*T33*	*T34*	*T35*
Cmc	2.5 (3)	1.8 (4)	0.0	0.0	0.0	0.0
Asx	0.4	2.6 (2)	1.0	0.0	0.0	0.0
Thr	0.4	1.8 (1)	1.1 (1)	1.0 (1)	0.0	0.1
Ser	2.7 (3)	2.6 (3)	0.6	0.0	0.0	0.1
Glx	2.1 (2)	4.2 (5)	0.5	0.0	3.6 (4)	1.0 (2)
Pro	0.0	2.6 (3)	1.9 (2)	0.0	1.0 (1)	0.1
Gly	2.9 (2)	2.8 (2)	1.8 (1)	0.0	1.0 (1)	0.1
Ala	2.3 (2)	3.4 (3)	0.7	0.0	0.0	0.0
Cys	0.0	0.0	0.0	0.0	0.0	0.0
Val	0.2	0.0	1.0 (1)	0.1	1.4 (2)	1.0 (1)
Met	0.1	0.0	0.0	0.0	0.0	0.0
Ile	3.1 (3)	1.1 (1)	0.9 (1)	0.0	0.0	0.1
Leu	3.3 (3)	3.8 (5)	2.3 (2)	0.0	0.0	0.2
Tyr	0.0	0.6 (1)	0.2	1.0 (1)	0.0	0.0
Phe	1.9 (2)	1.2 (1)	1.1 (1)	0.0	0.0	1.0 (1)
Lys	0.3	1.2 (1)	0.3	0.1	1.0 (1)	1.0 (1)
His	1.0 (1)	0.9 (1)	1.9 (2)	0.1	0.0	0.0
Arg	1.0 (1)	0.9 (1)	1.0 (1)	1.1 (1)	0.0	0.1

	T34+T35	*T36(s)*	*T37*	*T39(s)*	*T40*	*T41*
Cmc	0.0	0.0	0.2	1.1 (1)	1.8 (2)	0.1
Asx	0.0	0.0	6.0 (6)	0.0	1.8 (2)	0.1
Thr	0.0	0.0	1.0 (1)	0.0	1.8 (2)	0.0
Ser	0.0	0.0	0.3	1.9 (2)	1.2 (1)	1.8 (2)
Glx	5.7 (6)	0.0	1.9 (2)	2.0 (2)	2.9 (3)	2.0 (2)
Pro	1.2 (1)	0.0	0.0	0.0	3.2 (3)	1.2 (1)
Gly	1.0 (1)	0.0	0.4	0.0	2.2 (2)	0.2
Ala	0.0	0.0	1.1 (1)	1.0 (1)	1.2 (1)	1.1 (1)
Cys	0.0	0.0	0.0	0.0	0.0	0.0
Val	2.2 (3)	0.5 (1)	0.3	2.0 (2)	0.9 (1)	0.1
Met	0.0	0.0	0.0	0.0	0.1	0.0
Ile	0.0	0.9 (1)	1.2 (1)	0.0	0.3	0.0
Leu	0.0	0.0	2.9 (3)	0.0	4.0 (4)	1.1 (1)
Tyr	0.0	1.0 (1)	1.0 (1)	0.0	0.9 (1)	0.9 (1)
Phe	1.0 (1)	0.0	1.0 (1)	0.0	0.1	1.1 (1)
Lys	2.1 (2)	1.0 (1)	1.0 (1)	0.0	1.1 (1)	0.0
His	0.0	1.1 (1)	0.1	0.0	0.1	1.0 (1)
Arg	0.0	0.0	0.2	1.0 (1)	0.1	1.0 (1)

	T42	*T43*	*T42+T43*	*T44*	*T45*	*T46*
Cmc	0.0	0.1	0.0	0.0	1.0 (1)	1.0 (1)
Asx	0.0	0.1	0.0	0.0	1.1 (1)	2.9 (3)
Thr	0.0	0.0	0.0	0.0	1.0 (1)	2.7 (3)
Ser	0.0	0.2	0.0	1.8 (2)	0.9 (1)	0.0
Glx	0.0	1.1 (1)	1.2 (1)	0.0	1.1 (1)	0.0
Pro	0.0	0.0	0.0	1.2 (1)	0.0	0.0
Gly	0.0	0.1	0.0	0.0	0.2	1.1 (1)
Ala	0.0	1.0 (1)	1.3 (1)	0.0	0.1	1.1 (1)
Cys	0.0	0.0	0.0	0.0	0.0	0.0
Val	0.0	0.9 (1)	0.9 (1)	0.0	0.0	1.1 (1)

(*Continued on p. 384*)

TABLE II (*continued*)

	T42	*T43*	*T42+T43*	*T44*	*T45*	*T46*
Met	0.0	0.0	0.0	0.0	0.0	0.9 (1)
Ile	0.0	0.0	0.0	0.0	0.0	0.0
Leu	1.0 (1)	0.0	1.0 (1)	1.0 (1)	2.0 (2)	1.1 (1)
Tyr	0.0	0.0	0.0	1.0 (1)	0.0	0.0
Phe	0.0	0.0	0.0	0.0	0.0	0.0
Lys	1.0 (1)	0.1	0.7 (1)	0.0	0.0	0.0
His	0.0	1.0 (1)	0.9 (1)	0.0	0.9 (1)	0.0
Arg	0.0	1.1 (1)	1.1 (1)	1.1 (1)	1.0 (1)	1.1 (1)
	T47	*T48*	*T49*	*T50*	*T51*	
Cmc	1.7 (2)	1.0 (1)	0.1	0.0	0.0	
Asx	5.0 (5)	0.2	1.1 (1)	2.0 (2)	2.0 (2)	
Thr	0.1	0.9 (1)	1.0 (1)	0.9 (1)	0.0	
Ser	1.9 (2)	1.0 (1)	0.1	0.0	0.0	
Glx	2.0 (2)	1.0 (1)	0.1	0.0	0.0	
Pro	2.2 (2)	0.3	1.1 (1)	0.0	1.0 (1)	
Gly	6.0 (6)	4.1 (4)	1.0 (1)	0.0	0.0	
Ala	2.1 (2)	1.1 (1)	0.1	0.0	0.0	
Cys	0.0	0.0	0.0	0.0	0.0	
Val	0.9 (1)	0.0	1.9 (2)	1.1 (1)	0.0	
Met	0.0	0.8 (1)	0.0	0.0	0.9 (1)	
Ile	0.1	1.3 (2)	0.0	1.0 (1)	0.0	
Leu	3.0 (3)	2.0 (2)	0.1	1.0 (1)	0.0	
Tyr	0.1	0.0	0.9 (1)	1.0 (1)	0.0	
Phe	0.1	0.0	0.0	0.0	0.0	
Lys	0.1	1.1 (1)	1.0 (1)	0.0	0.0	
His	1.0 (1)	0.0	0.0	0.0	0.0	
Arg	1.0 (1)	0.0	0.1	1.0 (1)	1.0 (1)	

composition no further analysis was performed. Several predicted peptides were sufficiently polar to be unretained by the column and were identified by Edman degradation: Asp-Glu-Lys (T2), Ser-Asn-Arg (T4), Ala-Gly-Lys (T16) and Asn-Arg-Arg (T22 + T23). Peptide T38 was shown to be unretained by the column by chromatography of a synthetic sample (Ser-Asp-Ser-Ser-Arg). All expected peptides were observed in the TFA tryptic maps except the very hydrophobic peptide Gln-Met-Ile-Tyr-Gln-Gln-His-Gln-Ser-Trp-Leu-Arg-Pro-Val-Leu-Arg (T3).

Heterogeneity can be introduced into a tryptic map by the generation of peptides other than those arising directly from the predicted tryptic digestion. In this tryptic map (Fig. 1) additional peptide peaks are the result of various mechanisms such as partial cleavage by trypsin at less favorable sites (adjacent to proline, etc.), chymotrypsin-like cleavages and carbohydrate heterogeneity (Table III). A partial trypsin cleavage product of the arginyl-prolyl bond in peptide T3e was identified at 31.5 min, but the intact peptide T3 was not found in this map. Two chymotryptic-like cleavages were observed: a minor cleavage of the methionyl-isoleucyl bond of peptide T18 at 66 min resulting in peptide T18a (residues 208–212) at 39 min, and cleavage of peptide T25 (38 min) after phenylalanine residue 274 resulting in peptide T25a (residues 268–274) at 41.5 min. A small percentage of peptides T31 and T40 were found

TABLE III

MULTIPLE ELUTION TIMES, NON-TRYPSIN LIKE CLEAVAGES AND INCOMPLETE TRYPSIN CLEAVAGE IN THE rt-PA TRYPTIC DIGEST

Tryptic peptide	*Fragment*	*Sequence*	*TFA map*	*Phosphate map*
T3	11–27	TQMIYQQHQSWLRPVLR		X
T3a	11–23	TQMIYQQHQSWLR		X
T3b	11–22	TQMIYQQHQSWL		X
T3c	22–27	—LRPVLR		X
T3d	24–27	—PVLR	X	X
T11	102–129	GTWSTAESGAECTNWNSSA-LAQKPYSGR	X	X
T11a	102–129	GTWSTAESGAECTNWMSSA-LAQKPYSGR		X
T17	163–189	YSSEFCSTPACSEGNSDCYFGNG-SAYR	X	X
T17a	163–189	YSSEFCSTPACSEGNSDCYFGNG-SAYR	X	X
T18	190–212	GTHSLTESGASCLPWNSMILIGK	X	X
T18a	208–212	—ILIGK	X	X
T25	268–275	QYSQPQFR	X	X
T25a	268–274	QYSQPQF	X	
T27	278–296	GGLFADIASHPWQAAIFAK	X	X
T27a	278–291	GGLFADIASHPWQA		X
T32	328–339	FPPHHLTVILGR	X	X
T32a	328–339	FPPHHLTVILGR		X
T4+T5	28–30+31–40	SNRVEYCWNSGR		X
T23+T24	250+251–267	RLTWEYCDVPSCSTCGLR		X
T28+T29	297–298+299	HRR	X	
T29+T30	299+300–304	RSPGER	X	X
T31a+ T40a	314–327 395–416	SCWILSAAHCFQER CLPPADLQLPDWTECELS-GYGK	X X	
T34+T35	343–351+352–356	VVPGEEEQKFEVEK	X	X
T42+T43	428–429+430–434	LKEAHVR	X	

linked by an intact disulfide and containing chymotryptic-like cleavages (see Fig. 2, T31a + T40a, 63 min). Multiplets of the glycopeptides T11, T17, T45 were found (see carbohydrate-containing peptide analysis section), Five examples of incomplete tryptic digestion were also identified: T22 + T23 (void), T28 + T29 (13 min), T29 + T30 (19 min), T34 + T35 (44 min), T42 + T43 (29 min).

Phosphate tryptic map

Identification of the peaks obtained from the sodium phosphate tryptic map required the removal of the non-volatile salt from the isolated peptides. This was accomplished by rechromatography of the collected peaks in an HPLC solvent system using volatile components. Rechromatography also provided an evaluation of the purity of the peaks in the original phosphate-based map by a second dimension separation of peaks containing multiple components.

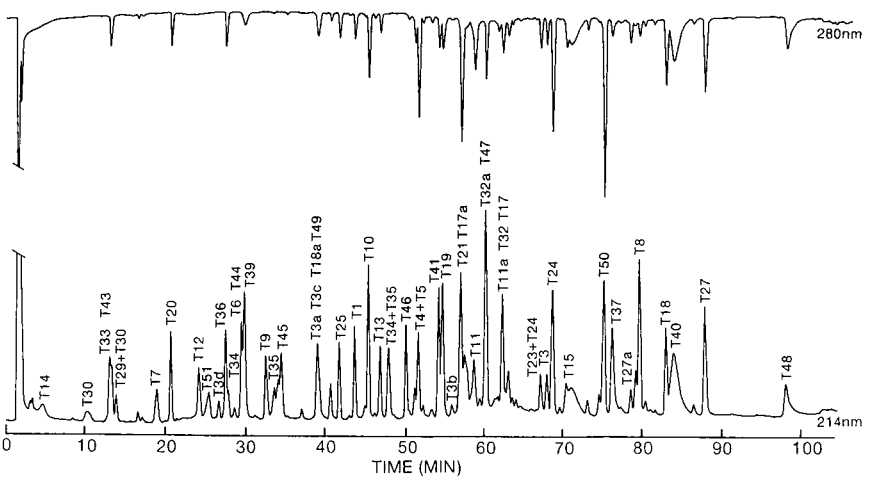

Fig. 3. Sodium phosphate based tryptic map of RCM rt-PA. This separation was performed on a 5-μm Nova-Pak C_{18} column (15 × 0.46 cm I.D.), Mobile phase A consisted of 0.05 *M* sodium phosphate (pH 2.85), and mobile phase B was acetonitrile. A linear gradient of 0–30% mobile phase B was run in 90 min followed by 30–60% mobile phase B in 30 min. The 70-μg sample was loaded in 0.1 ml of 0.1 *M* ammonium bicarbonate and monitored at both 214 and 280 nm.

Fifty-three peaks recovered from the semi-preparative separation of the RCM rt-PA tryptic digest in the sodium phosphate and acetonitrile solvent system (Fig. 3) were rechromatographed in the rapid TFA and acetonitrile system (see Experimental section) then analyzed for amino acid composition (Table IV). The location of the tryptic peptides in the rt-PA sequence was determined from the amino acid analysis, except for very minor peptides and for the polar peptides in the void volume which had been identified in the TFA-based peptide map. In this set of samples, tyrosine recovery was variable while tryptophan was found to be destroyed using the Pico Tag batch hydrolysis system for amino acid analysis. Therefore, the presence of these residues was confirmed by the relative absorbance of each peak monitored at 280 nm. The utility of dual wavelength detection is shown in Fig. 4 where peptide T45 does not contain tyrosine (Cm Cys-Thr-Ser-Gln-His-Leu-Leu-Asn-Arg) and exhibits only 214 nm absorption, whereas peptide T25 (Gln-Tyr-Ser-Gln-Pro-Gln-Phe-Arg) is detected both at 214 and 280 nm. The majority of the peptide peaks eluted as single components in the second dimension chromatography using a TFA–acetonitrile solvent system as in Fig. 4. However, additional purification of some of the fractions isolated from the phosphate-based chromatography was obtained. For example, chromatogram A in Fig. 5 resolved one major peak (T49) and two minor peaks containing the peptides T3a, T3c and T18a. Chromatogram B resolved one major peak (T47) and two minor peaks (T32). Several other peaks clearly contained multiple peptide components in the phosphate tryptic map and peptides were resolved in the TFA-based rechromatography (Fig. 5C, D–F). In most cases, the minor peak represented an insignificant level of peptide by amino acid analysis.

As in the TFA tryptic map, peptide heterogeneity was found by the resolution of other peptides in addition to those arising from the predicted tryptic digestion. Six peptides were found to be reproducibly represented in more than one peak in the

TABLE IV

AMINO ACID COMPOSITIONS OF SODIUM PHOSPHATE TRYPTIC MAP PEPTIDE PEAKS

N.D. = Not detected.

	T1	*T3*	*T3a*	*T3b*	*T3c*	*T3d*
Asp	0.2	0.0	0.2	0.6	0.0	0.0
Glu	1.3 (1)	3.3 (4)	3.7 (4)	3.8 (4)	0.0	0.0
Cm Cys	0.8 (1)	0.0	0.0	0.1	0.0	0.0
Ser	1.1 (1)	0.9 (1)	0.4 (1)	1.2 (1)	0.0	0.0
Gly	0.2	0.2	0.5	0.8	0.0	0.0
His	0.0	1.0 (1)	1.2 (1)	1.0 (1)	0.0	0.0
Arg	1.1 (1)	2.2 (2)	1.1 (1)	0.2	1.9 (2)	0.9 (1)
Thr	0.0	1.1 (1)	1.3 (1)	0.9 (1)	0.0	0.0
Ala	0.0	0.0	0.0	0.4	0.0	0.0
Pro	0.0	1.2 (1)	0.2	0.3	1.0 (1)	1.1 (1)
Tyr	1.0 (1)	N.D (1)	0.1 (1)	0.8 (1)	0.0	0.0
Val	0.8 (1)	1.1 (1)	0.1	0.3	1.1 (1)	1.0 (1)
Met	0.0	0.4 (1)	0.3 (1)	0.2 (1)	0.0	0.0
Cys	0.0	0.0	0.0	0.0	0.0	0.0
Ile	0.8 (1)	0.9 (1)	1.1 (1)	1.2 (1)	0.0	0.0
Leu	0.1	2.2 (2)	0.3 (1)	0.5 (1)	1.5 (2)	1.1 (1)
Phe	0.0	0.1	0.0	0.1	0.0	0.0
Lys	0.0	0.1	0.1	0.3	0.0	0.0

	T4 + T5	*T6*	*T7*	*T8*	*T9*	*T10*
Asp	2.1 (2)	0.0	0.1	2.4 (2)	1.1 (1)	1.1 (1)
Glu	1.3 (1)	1.1 (1)	1.2 (1)	4.0 (4)	1.2 (1)	2.1 (2)
Cm Cys	1.2 (2)	0.9 (1)	0.8 (1)	3.6 (4)	1.8 (2)	0.8 (1)
Ser	1.6 (2)	0.7 (1)	1.9 (2)	0.9 (1)	0.0	1.0 (1)
Gly	1.0 (1)	0.0	0.3	3.8 (4)	0.0	1.1 (1)
His	0.0	1.1 (1)	0.0	0.0	0.0	0.0
Arg	1.6 (2)	0.0	1.0 (1)	0.0	1.0 (1)	1.0 (1)
Thr	0.1	0.0	0.0	1.0 (1)	0.9 (1)	1.0 (1)
Ala	0.1	1.0 (1)	0.0	2.0 (2)	0.0	1.0 (1)
Pro	0.0	0.8 (1)	1.1 (1)	1.0 (1)	0.0	0.0
Tyr	0.8 (1)	0.0	0.0	0.9 (1)	0.0	1.5 (2)
Val	0.9 (1)	1.2 (2)	0.0	0.9 (1)	0.0	0.0
Met	0.0	0.0	0.0	0.0	0.0	0.0
Cys	0.0	0.0	0.0	0.0	0.0	0.0
Ile	0.1	0.0	0.0	0.1	1.0 (1)	1.1 (1)
Leu	0.1	0.0	0.0	1.2 (1)	0.0	0.1
Phe	0.0	0.0	0.0	3.6 (4)	0.0	0.0
Lys	0.0	0.9 (1)	0.0	1.0 (1)	0.0	0.0

	T11	*T11a*	*T12*	*T13*	*T14*	*T15*
Asp	2.3 (2)	2.3 (2)	1.1 (1)	2.6 (2)	2.1 (2)	1.6 (1)
Glu	3.0 (3)	3.5 (3)	0.0	0.0	0.0	0.0
Cm Cys	1.0 (1)	0.7 (1)	0.0	0.7 (1)	0.0	0.8 (1)
Ser	5.1 (5)	4.8 (5)	0.0	0.0	0.0	1.2 (1)
Gly	3.2 (3)	3.3 (3)	0.0	2.0 (2)	0.0	0.2
His	0.0	0.0	0.1	1.0 (1)	0.0	0.1
Arg	0.9 (1)	0.7 (1)	1.9 (2)	1.0 (1)	0.9 (1)	0.0

(*Continued on p. 388*)

TABLE IV (*continued*)

	T11	*T11a*	*T12*	*T13*	*T14*	*T15*
Thr	2.4 (3)	2.8 (3)	0.0	0.0	0.0	0.1
Ala	3.8 (4)	3.7 (4)	1.1 (1)	0.0	0.0	0.1
Pro	1.1 (1)	1.2 (1)	1.0 (1)	0.0	1.0 (1)	1.2 (1)
Tyr	N.D.(1)	0.9 (1)	0.0	0.9 (1)	0.0	0.9 (1)
Val	0.1	0.2	0.1	0.0	0.0	1.0 (1)
Met	0.0	0.1	0.0	0.0	0.0	0.0
Cys	0.0	0.0	0.0	0.0	0.0	0.0
Ile	0.1	0.5	0.8 (1)	0.0	0.0	0.1
Leu	1.2 (1)	1.4 (1)	0.2	2.0 (2)	0.1	0.2
Phe	0.2	0.1	0.0	0.0	0.0	1.1 (1)
Lys	1.0 (1)	0.9 (1)	0.1	0.0	0.1	1.7 (2)
	T17	*T17a*	*T18*	*T18a*	*T19*	*T20*
Asp	3.1 (3)	3.2 (3)	1.1 (1)	0.0	1.2 (1)	1.2 (1)
Glu	2.4 (2)	2.5 (2)	1.1 (1)	0.0	2.1 (2)	0.0
Cm Cys	3.1 (3)	2.6 (3)	0.9 (1)	0.0	0.0	0.8 (1)
Ser	5.6 (6)	4.9 (6)	3.6 (4)	0.0	1.0 (1)	0.0
Gly	3.4 (3)	3.5 (3)	2.9 (3)	1.1 (1)	1.9 (2)	0.0
His	0.1	0.1	1.0 (1)	0.0	0.2	0.9 (1)
Arg	0.9 (1)	1.1 (1)	0.1	0.0	0.4	1.0 (1)
Thr	1.0 (1)	1.1 (1)	1.9 (2)	0.0	1.0 (1)	0.0
Ala	2.3 (2)	2.3 (2)	0.9 (1)	0.0	2.6 (3)	0.0
Pro	1.2 (1)	1.2 (1)	1.0 (1)	0.0	1.0 (1)	0.0
Tyr	N.D.(3)	2.0 (3)	0.0	0.0	0.8 (1)	0.8 (1)
Val	0.1	0.2	0.0	0.0	1.1 (1)	0.0
Met	0.0	0.0	0.9 (1)	0.0	0.0	0.0
Cys	0.0	0.0	0.0	0.0	0.0	0.0
Ile	0.1	0.0	2.1 (2)	1.8 (2)	0.3	0.0
Leu	1.3	0.4	3.4 (3)	1.0 (1)	1.8 (2)	0.0
Phe	2.1 (2)	2.0 (2)	0.0	0.0	0.0	0.0
Lys	0.1	0.1	1.3 (1)	1.2 (1)	1.2 (1)	0.0
	T21	*T23+T24*	*T24*	*T25*	*T27*	
Asp	3.0 (3)	1.2 (1)	1.2 (1)	0.1	1.0 (1)	
Glu		1.3 (1)	1.2 (1)	2.4 (3)	1.0 (1)	
Cm Cys	0.9 (1)	1.5 (3)	2.4 (3)	0.0	0.0	
Ser	0.0	1.8 (2)	1.8 (2)	1.0 (1)	1.0 (1)	
Gly	1.0	1.3 (1)	1.0 (1)	1.0	2.1 (2)	
His	0.8 (1)	0.3	0.0	0.0	1.0 (1)	
Arg	0.0	1.7 (2)	0.9 (1)	1.1 (1)	0.1	
Thr	0.0	1.8 (2)	1.8 (2)	0.0	0.0	
Ala	1.1 (1)	0.3	0.0	0.0	5.1 (5)	
Pro	2.0 (2)	1.2 (1)	1.1 (1)	1.1 (1)	1.0 (1)	
Tyr	0.0	0.7 (1)	1.0 (1)	0.9 (1)	0.0	
Val	0.9 (1)	1.0 (1)	1.0 (1)	0.0	0.0	
Met	0.0	0.0	0.0	0.0	0.0	
Cys	0.0	0.0	0.0	0.0	0.0	
Ile	0.0	0.2	0.0	0.1	2.2 (2)	
Leu	1.0 (1)	2.4 (2)	1.8 (2)	0.1	1.2 (1)	
Phe	0.0	0.2	0.0	1.1 (1)	2.3 (2)	
Lys	2.3 (2)	0.1	0.1	0.0	1.4 (1)	

TABLE IV (*continued*)

	T27a	*T29+T30*	*T30*	*T32*	*T32a*
Asp	0.9 (1)	0.0	0.0	0.1	0.2
Glu	1.0 (1)	1.0 (1)	1.0 (1)	0.2	0.4
Cm Cys	0.0	0.0	0.0	0.0	0.0
Ser	1.0 (1)	1.0 (1)	1.0 (1)	0.3	0.3
Gly	1.9 (2)	1.0 (1)	1.1 (1)	1.2 (1)	1.5 (1)
His	0.9 (1)	0.0	0.0	1.8 (2)	1.7 (2)
Arg	0.1	2.0 (2)	1.0 (1)	1.3 (1)	0.8 (1)
Thr	0.1	0.1	0.0	0.9 (1)	0.8 (1)
Ala	3.1 (3)	0.0	0.0	0.0	0.0
Pro	0.9 (1)	1.0 (1)	1.1 (1)	2.2 (2)	1.9 (2)
Tyr	0.1	0.1	0.0	0.0	0.0
Val	0.1	0.0	0.0	1.0 (1)	0.8 (1)
Met	0.0	0.0	0.0	0.0	0.0
Cys	0.0	0.0	0.0	0.0	0.0
Ile	1.1 (1)	0.0	0.0	0.9 (1)	1.0 (1)
Leu	1.2 (1)	0.0	0.0	2.6 (2)	2.3 (2)
Phe	1.3 (1)	0.0	0.0	1.2 (1)	1.2 (1)
Lys	0.1	0.0	0.0	0.1	0.1

	T33	*T34*	*T34+T35*	*T35*	*T36*	*T37*
Asp	0.0	0.1	0.1	0.1	0.0	4.8 (6)
Glu	0.0	3.2 (4)	5.1 (6)	1.8 (2)	0.1	2.4 (2)
Cm Cys	0.0	0.0	0.1	0.0	0.0	0.0
Ser	0.0	0.1	0.1	0.1	0.0	0.2
Gly	0.0	1.0 (1)	1.1 (1)	0.2	0.1	0.7
His	0.0	0.1	0.0	0.0	1.0 (1)	0.0
Arg	1.0 (1)	0.1	0.1	0.1	0.1	0.1
Thr	1.1 (1)	0.1	0.1	0.0	0.0	1.0 (1)
Ala	0.0	0.2	0.1	0.1	0.0	1.2 (1)
Pro	0.0	1.2 (1)	1.1 (1)	0.0	0.0	0.1
Tyr	1.1 (1)	0.1	0.0	0.0	0.9 (1)	0.8 (1)
Val	0.0	1.2 (2)	2.1 (3)	1.0 (1)	0.7 (1)	0.1
Met	0.0	0.0	0.0	0.0	0.0	0.0
Cys	0.0	0.0	0.1	0.0	0.0	0.0
Ile	0.0	0.2	0.2	0.1	1.7 (1)	1.0 (1)
Leu	0.0	0.1	0.0	0.1	0.0	3.1 (3)
Phe	0.0	0.0	1.2 (1)	1.1 (1)	0.0	1.0 (1)
Lys	0.0	1.1 (1)	2.5 (2)	1.0 (1)	1.1 (1)	1.1 (1)

	T39	*T41*	*T43*	*T44*	*T45*	*T46*
Asp	0.1	0.1	0.1	0.0	1.0 (1)	3.2 (3)
Glu	1.7 (2)	1.8 (2)	1.0 (1)	0.0	1.1 (1)	0.0
Cm Cys	0.9 (1)	0.0	0.0	0.0	1.0 (1)	0.9 (1)
Ser	1.9 (2)	1.5 (2)	0.0	1.5 (2)	2.0 (1)	0.2
Gly	0.0	0.3	0.0	0.0	0.2	1.0 (1)
His	0.1	0.9 (1)	1.0 (1)	0.0	0.9 (1)	0.0
Arg	1.0 (1)	1.0 (1)	1.0 (1)	1.2 (1)	1.0 (1)	1.0 (1)
Thr	0.0	0.1	0.0	0.0	0.9 (1)	2.8 (3)
Ala	1.0 (1)	1.0 (1)	1.1 (1)	0.0	0.0	1.2 (1)
Pro	0.4	1.1 (1)	0.0	0.8 (1)	0.0	0.1
Tyr	0.0	1.0 (1)	0.0	0.8 (1)	0.1	0.0

(*Continued on p. 390*)

TABLE IV (*continued*)

	T39	*T41*	*T43*	*T44*	*T45*	*T46*
Val	1.3 (2)	0.1	1.0 (1)	0.0	0.0	1.1 (1)
Met	0.0	0.1	0.0	0.0	0.0	0.7 (1)
Cys	0.0	0.0	0.0	0.0	0.0	0.0
Ile	0.0	0.0	0.0	0.0	0.0	0.1
Leu	0.2	1.3 (1)	0.0	1.0 (1)	1.5 (2)	1.1 (1)
Phe	0.0	1.0 (1)	0.0	0.0	0.0	0.0
Lys	0.2	0.1	0.0	0.0	0.0	0.1
	T47	*T48*	*T49*	*T50*	*T51*	
Asp	4.9 (5)	0.1	1.1 (1)	1.9 (2)	2.2 (2)	
Glu	2.2 (2)	1.1 (1)	0.2	0.0	0.0	
Cm Cys	1.8 (2)	0.9 (1)	0.0	0.1	0.0	
Ser	1.8 (2)	0.9 (1)	0.0	0.2	0.1	
Gly	5.7 (6)	3.9 (4)	1.1 (1)	0.0	0.1	
His	1.0 (1)	0.0	0.0	0.0	0.0	
Arg	1.1 (1)	0.1	0.1	0.9 (1)	1.3 (1)	
Thr	0.1	1.1 (1)	1.2 (1)	1.0 (1)	0.0	
Ala	2.1 (2)	0.0	0.1	0.2	0.0	
Pro	2.0 (2)	0.0	1.2 (1)	0.0	1.0 (1)	
Tyr	0.0	0.0	0.9 (1)	1.0 (1)	0.0	
Val	1.0 (1)	1.0 (1)	1.2 (2)	1.0 (1)	0.1	
Met	0.0	0.8 (1)	0.0	0.0	0.5 (1)	
Cys	0.0	0.0	0.0	0.0	0.0	
Ile	0.1	0.9 (2)	0.1	0.9 (1)	0.0	
Leu	3.4 (3)	2.1 (2)	0.0	1.3 (1)	0.1	
Phe	0.1	0.0	0.0	0.1	0.0	
Lys	0.0	1.2 (1)	0.9 (1)	0.1	0.1	

phosphate map (Table III). Peptide T3 at 68 min (Fig. 3) was found to have significant cleavage by trypsin between the arginyl-prolyl bond resulting in recovery of peptide T3a (residues 11–23) at 39 min and T3d (residues 24–27) at 26 min. A small amount of chymotryptic-like cleavage at residue 22 (Leu) and residue 21 (Trp) of peptide T3 resulted in the recovery of peptide T3b (residues 11–22) at 60 min and T3c (residues 22–27) at 39 min. Chymotryptic-like cleavage was also found for peptide T18 (83 min) at methionine residue 207, giving rise to peptide T18a (residues 208–212) at 39 min. Peptide T27 (residues 278–296) at 88 min was found to be partially cleaved at alanine residues 291 and 292 (Ala,Ala) resulting in T27a (residues 278–291) at 79 min. Peptide T32 eluting at 63 min was also significantly recovered at 60 min (T32a). The lack of deamidation sites in peptide T32 sequence, and the presence of two prolines suggests conformational effects may play a role in the multiplicity of peaks derived from this peptide[12]. Four examples of incomplete tryptic digestion were identified: T4 + T5 at 52 min, T23 + T24 at 67 min, T29 + T30 at 14 min and T34 + T35 at 48 min. Peptides T29 + T30 and T34 + T35 were also observed in the TFA map of the tryptic digest.

Identification and characterization of carbohydrate containing peptides

Tryptic glycopeptides of RCM rt-PA were isolated by Con A-Sepharose lectin

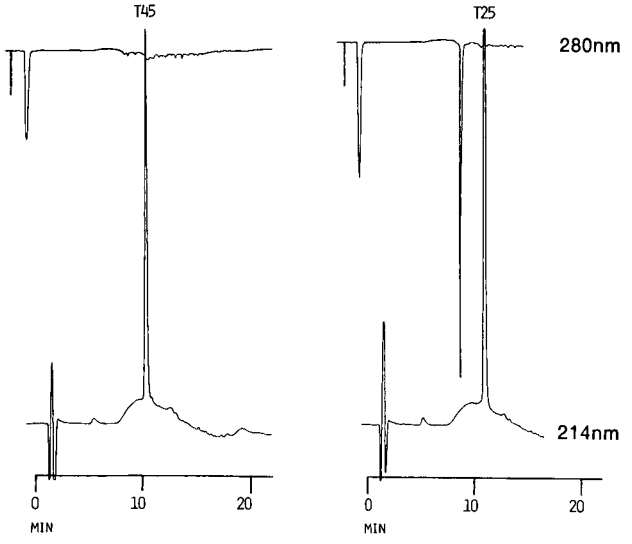

Fig. 4. Rechromatography of peaks from the sodium phosphate tryptic map of RCM rt-PA using the volatile TFA solvent system. Mobile phases A and B were prepared as in Fig. 1. Peaks were eluted by a rapid linear gradient to 60% mobile phase B in 5 min, followed by 20 min of isocratic elution at 60% mobile phase B. The elution profiles at 280 nm demonstrate the presence of aromatic residues tyrosine or tryptophan as in the peptide T25 peak or absence as in the peptide T45 peak.

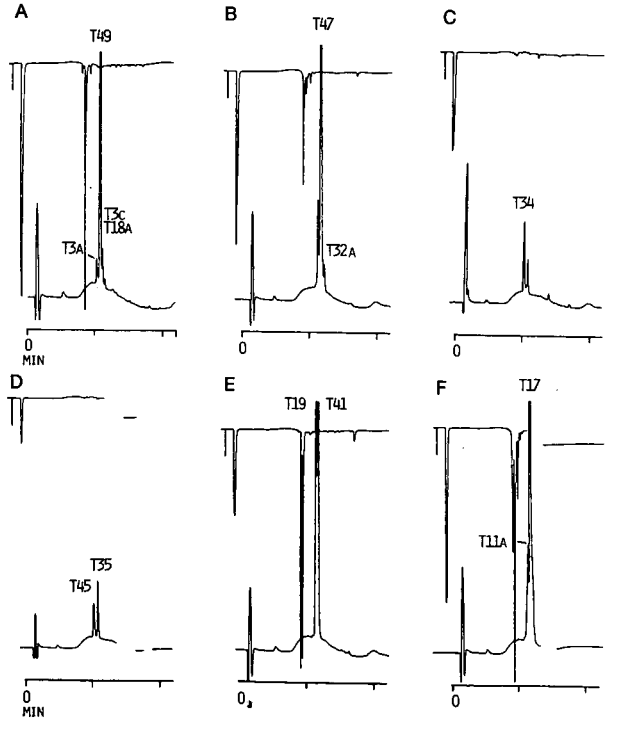

Fig. 5. Examples of the rechromatography of peaks from the sodium phosphate tryptic map of RCM rt-PA using the volatile TFA solvent system described in Fig. 4. For A–F, see text.

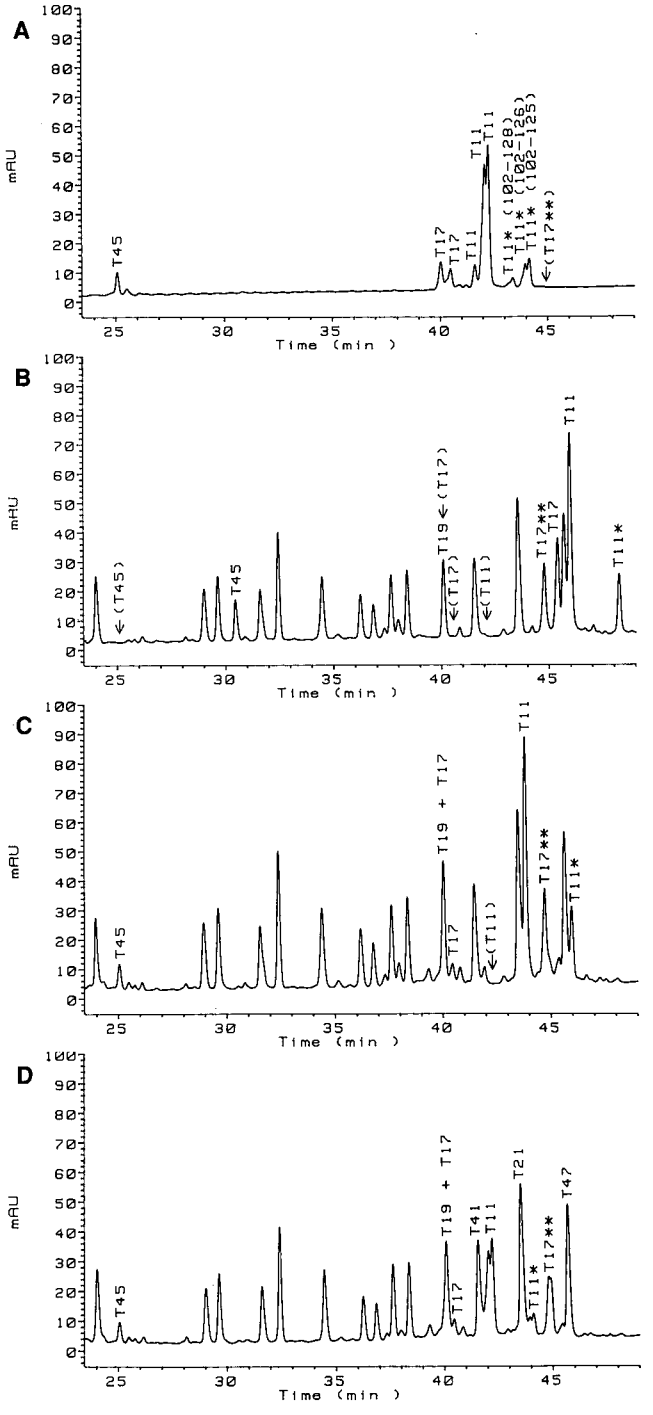

Fig. 6. Comparison of the tryptic peptides of RCM rt-PA recovered from Con A-Sepharose (A), following treatment with PNGase F (B) or following treatment with Endo H (C) to the total RCM rt-PA digest (D). The separation using the TFA solvent system is described in Fig. 1. Approximately 100 μg of sample were loaded for each chromatogram and the eluate was monitored at 220 nm. T11* indicates cleaved forms of peptide T11 as noted on chromatogram (A). T17** indicates the non-glycosylated (Type II) form of peptide T17.

chromatography (Fig. 6A) and compared to a control RCM rt-PA tryptic digest (Fig. 6D) using the TFA tryptic method. Peaks were collected and identified by amino acid analysis. The carbohydrate-containing peptides are T11, T17 and T45, resulting from glycosylations at Asn-117, Asn-184 and Asn-448, respectively. Although peptide T19 contains a potential N-linked glycosylation site, as recognized by the sequence Asn-X-Ser/Thr, it is not glycosylated. These results agree with the earlier report by Pohl *et al.*[9] establishing the identity of the carbohydrate-containing peptides which were further confirmed by mass spectrometry by Carr and Roberts[13]. All of the glycopeptides eluted as multiple peaks, possibly due to carbohydrate microheterogeneity. Peaks labeled T11* arise from carboxy-terminal cleavages of peptide T11. Peaks with amino acid compositions corresponding to T17 are observed at two positions in the control map (40.5 and 44.8 min, Fig. 6D). However, the later-eluting peak (T17**) did not contain detectable amino sugars and was not bound by Con A-Sepharose, indicating that this peptide is probably not glycosylated. Bennet[8] and Pohl *et al.*[9] previously observed that rt-PA can be separated into variants I and II, differing by the optional glycosylation of residue 184 contained in peptide T17.

The type of N-linked oligosaccharide present at each site was determined by TFA tryptic mapping of RCM rt-PA after treatment with Endo H or PNGase F. Endo H removes high-mannose oligosaccharides by cleaving between the two N-acetylglucosamine residues of the core portion[14]. PNGase F hydrolyzes the N-acetylglucosamyl-asparagine bond of both high mannose and complex oligosaccharides[15] resulting in deglycosylation and in conversion of the attachment asparaginyl residue to aspartic acid. Removal of the hydrophilic carbohydrate moiety results in increased retention of a peptide on the RP-HPLC column. Peak identities were confirmed by amino acid analysis.

Fig. 6 shows the portion of the TFA tryptic map that contains the glycopeptide peaks. Digestion with PNGase F (Fig. 6B) caused an increase in the retention time of glycopeptide peaks T11, T17 and T45 consistent with the loss of oligosaccharide side chain. The new peak resulting from deglycosylated peptide T17 does not co-elute with the non-glycosylated peptide T17**, because the former contains aspartic acid while the latter contains asparagine at position 184. The relative elution positions of T17 (Asp-184) and T17** (Asn-184) fits with the observed increase in retention time usually observed with deamidation of a peptide[16]. All of the intact glycopeptides elute as single peaks upon deglycosylation, suggesting that the multiple peaks in the control map are due to carbohydrate microheterogeneity.

Endo H digestion only affected peaks containing glycopeptides T11 and T11* (Fig. 6C). The peaks which result from deglycosylation of peptide T11 by Endo H are of a different retention time than the peaks resulting from PNGase F deglycosylation of peptide T11. This is because Endo H leaves a residue of N-acetylglucosamine attached to asparagine. The altered retention time of glycopeptide peak T11 upon treatment with Endo H demonstrated the presence of a high mannose oligosaccharide at Asn-117. Glycopeptide peaks T17 and T45 were deglycosylated by PNGase F, and not Endo H, further indicating the presence of complex oligosaccharides on Asn-184 and Asn-448.

DISCUSSION

Bacterial clones that contained cDNA sequences corresponding to human tissue plasminogen activator were reported in 1984[6] and from the cDNA data an amino acid sequence of 562 residues was deduced. Amino acid sequencing of purified rt-PA from melanoma cells indicated a protein of 527 amino acids, suggesting post-translational processing that removes a hydrophobic signal peptide and a hydrophilic "pro-peptide" sequence. Pohl *et al.*[9] confirmed the structure of tissue plasminogen activator produced and secreted by a melanoma cell line. These investigators describe an RP-HPLC tryptic map for the N-terminal fragment 1–275 of the protein and of a cyanogen bromide fragment of residues 276–455 both initially formed by plasmin digestion. Subsequently, rt-PA was expressed in Chinese hamster ovary cells and a process was developed for large scale manufacture of the protein for clinical trials as a thrombolytic agent for use in treatment of myocardial infarction[17]. Development of the TFA-based and phosphate-based tryptic maps allowed complete characterization of the protein for FDA submissions for permission to enter clinical trials and for the product licensing application. It was also proposed to use the phosphate-based tryptic map as a release procedure to monitor the consistency of manufactured lots.

The size of rt-PA (66 000 daltons) and the presence of three carbohydrate side chains (including one optional glycosylation site) suggested that the tryptic map would be extremely complex. It was found that other factors such as non-specific cleavages and incomplete tryptic cleavages (Table III) resulted in the formation of more than the expected 51 tryptic peptides (Table I). The presence of 17 disulfide bonds in rt-PA required reduction and S-carboxymethylation of the molecule to achieve satisfactory trypsin digestion, introducing additional concerns for peptide heterogeneity. Under the conditions used for this study, only one example of a small amount of an intact disulfide bond was found (Table III, T31a–T40a) and S-carboxymethylation was otherwise complete as measured by amino acid analysis (Table II and IV).

Because of the complexity of the tryptic map a number of approaches were used to investigate possible co-elutions. Limited digestion of rt-PA with plasmin cleaves the molecule between residue 275 and 276. Two large fragments (1–275 and 276–527) were isolated by gel filtration after reduction and S-carboxymethylation. The TFA tryptic map was optimized using a Nova-Pak C_{18} column with a mobile phase that consisted of 0.1% TFA and a linear gradient of acetonitrile. Comparison of the maps of the separated domains (residues 1–275 and 276–527) with the map of complete molecule (residues 1–527) showed the TFA map contained minimal co-elution. Also, the use of volatile mobile phases allowed direct characterization of the tryptic peptides by amino acid analysis (Table II) and N-terminal sequencing.

A further investigation of potential co-elutions involved the use of 50 m*M* sodium phosphate (pH 2.85) as a mobile phase. It has been shown that the use of different mobile phases produces significant changes in the selectivities of RP-HPLC analyses of peptides[18]. The sodium phosphate tryptic map showed a similar peptide elution order to the TFA tryptic map, as noted for other separations[19]. The peptides that were resolved in the semi-preparative, phosphate-based tryptic map were collected and rechromatographed using a TFA containing mobile phase to allow further characterization. As shown in Fig. 5, some co-elutions were detected by rechromato-

graphy of peaks collected from the phosphate map. Intact peptide T3 and various cleavage products of the peptide were found in the phosphate tryptic map (Table III) whereas only a fragment of T3 was identified in the TFA tryptic map. Peptide T31 (305–327), which contained eight hydrophobic residues and was the last peptide to be eluted in the TFA-based separation, was not found in the phosphate map. The amino acid compositions of all peptides eluted from the two tryptic maps were consistent with the proposed amino acid sequence of rt-PA.

The RCM rt-PA tryptic glycopeptides were characterized by Con A-Sepharose affinity chromatography, specific glycosidases and comparative tryptic mapping. Endo H is specific for high mannose structures, while PNGase F results in removal of all carbohydrate side chains. This combination of techniques confirmed that glycopeptide T11 contained a high mannose oligosaccharide at Asn-177, while T17 and T45 contained complex oligosaccharides at Asn-184 and Asn-448, respectively. Glycosylation of peptide T17 appears to be optional in this expression system and T17 was present in both glycosylated and non-glycosylated forms. Carbohydrate microheterogeneity in the glycopeptides T11, T17 and T45 was demonstrated by the disappearance of multiple peaks for each peptide and the recovery of single peaks after treatment by glycosidases.

In conclusion, these studies have shown that it is possible to develop an RP-HPLC tryptic map for a molecule as complex as rt-PA. The tryptic map has been particularly important in the development of rt-PA as a pharmaceutical product for thrombolytic therapy. The structural information that can be deduced from these high-resolution separations is invaluable in the characterization and quality control of the recombinant DNA-derived product.

ACKNOWLEDGEMENTS

We wish to acknowledge Keri M. Tate, William J. Kohr, Carole Ward and Dr. William F. Bennett for their contributions in many valuable discussions.

REFERENCES

1 W. S. Hancock, C. A. Bishop and M. T. W. Hearn, *Anal. Biochem.*, 92 (1979) 170.
2 W. J. Kohr, R. Keck and R. N. Harkins, *Anal. Biochem.*, 122 (1982) 348.
3 P. A. Hartman, J. D. Stodola, G. C. Harbour and J. G. Hoogerheide, *J. Chromatogr.*, 360 (1986) 385.
4 M. Kunitani, P. Hirtzer, D. Johnson, R. Halenbeck, A. Boosman and K. Koths, *J. Chromatogr.*, 359 (1986) 391.
5 W. S. Hancock. *Chromatogr. Forum*, 1 (1986) 57.
6 D. Collen, J. M. Stassen, B. J. Marifino, Jr., S. E. Builder, F. DeCock, J. Ogez, D. Tagiri, D. Pennica, W. F. Bennett, J. Saliva and C. F. Hoyng, *J. Pharm. Exper. Ther.*, 231 (1984) 146.
7 D. Pennica, W. E. Holmes, W. J. Kohr, R. N. Harkins, G. A. Vehar, C. A. Ward, W. F. Bennett, E. Yelverton, P. H. Seeburg, H. L. Heyneker, D. V. Goeddel and D. Collen, *Nature (London)*, 301 (1983) 214.
8 W. F. Bennett, *Thromb. Res.*, 50 (1983) 106.
9 G. Pohl, M. Kallstrom, N. Bergsdorf, P. Wallen and H. Jornvall. *Biochemistry*, 23 (1984) 3701.
10 A. M. Crestfield, S. Moore and W. H. Stein, *J. Biol. Chem.*, 238 (1963) 622.
11 G. A. Vehar, M. W. Spellman, B. A. Keyt, C. K. Ferguson, R. G. Keck, R. C. Chloupek, R. Harris, W. F. Bennett, S. E. Builder and W. S. Hancock, *Cold Spring Harbor Symp. Quant. Biol.*, 51 (1986) 551.

12 J. Jacobson, W. Melander, G. Vaisnys and Cs. Horváth, *J. Phys. Chem.*, 88 (1984) 4536.
13 S. A. Carr and G. D. Roberts, *Anal. Biochem.*, 157 (1986) 396.
14 A. L. Tarentino and F. Maley, *J. Biol. Chem.*, 249 (1974) 811.
15 A. L. Tarentino, C. M. Gomez and T. H. Plummer, *Biochemistry*, 24 (1985) 4665.
16 D. Guo, C. T. Mant, A. K. Taneja, J. M. R. Parker and R. S. Hodges, *J. Chromatogr.*, 359 (1986) 499.
17 S. E. Builder and E. Grossbard, in *Transfusion Medicine: Recent Technological Advances*, A. R. Liss, New York, NY, 1986, p. 303.
18 W. S. Hancock, C. A. Bishop, J. E. Battersby, D. R. K. Harding and M. T. W. Hearn, *J. Chromatogr.*, 168 (1979) 377.
19 W. S. Hancock and D. R. K. Harding, in W. S. Hancock (Editor), *CRC Handbook of CRC for the Separation of Amino Acids, Peptides and Proteins*, Vol. II, CRC Press, Boca Raton, FL, 1984, p. 3.

Journal of Chromatography, 364 (1989) 397–408
Elsevier Science Publishers B.V., Amsterdam — Printed in The Netherlands

CHROM. 21 055

PREPARATIVE SEPARATION OF ALGAL POLAR LIPIDS AND OF INDIVIDUAL MOLECULAR SPECIES BY HIGH-PERFORMANCE LIQUID CHROMATOGRAPHY AND THEIR IDENTIFICATION BY GAS CHROMATOGRAPHY–MASS SPECTROMETRY

TOMÁŠ ŘEZANKA* and MILOSLAV PODOJIL
Institute of Microbiology, Czechoslovak Academy of Sciences, 142 20 Prague (Czechoslovakia)
(First received August 22nd, 1988; revised manuscript received October 10th, 1988)

SUMMARY

A crude polar lipidic extract of the green fresh-water alga *Chlorella kessleri* cultivated under heterotrophic conditions was separated by high-performance liquid chromatography (HPLC) on a preparative silica gel column into a total of twelve lipid classes, in which the content of fatty acids was determined by means of gas chromatography–mass spectrometry (GC–MS). The separation was by gradient elution from hexane–isopropanol (6:8) to hexane–isopropanol–water (60:80:14) lasting 20 min and then isocratically for 30 min. A total of 17.5 mg of lipids were injected. Individual types of lipid classes were further separated into eighteen molecular species by isocratic HPLC on a reversed-phase C_{18} column using a mixture 20 m*M* choline hydrochloride in methanol–water–acetonitrile (90.5:7:2.5) in the preparative mode (5 mg injected). Phosphatidylcholine and phosphatidylethanolamine were hydrolyzed by phospholipase C and corresponding diglycerides were identified by GC–MS on a polar capillary column. In mono- and digalactosyldiglycerols, fatty acids in position 1 were identified after a specific hydrolysis by lipase. The recovery obtained with an UV detector in HPLC and a mass spectrometer in GC–MS is discussed. It was shown that the relative response of the UV detector decreases with increasing saturation of acids, whereas the relative response of the mass spectrometer increases.

INTRODUCTION

Many organisms, from bacteria to higher plants, contain complex mixtures of polar lipids, phospho- and glycolipids[1]. Hydrolysis of a mixture of total lipids or of individual lipid classes followed by derivatization of fatty acids and their identification and quantification by gas chromatography (GC) or gas chromatography–mass spectrometry (GC–MS) can yield information on the distribution of fatty acids in the mixture. Unfortunately, the method does not provide data concerning the distribution of fatty acids in individual molecular species and it is also impossible to identify them in the native form. For an accurate analysis it is first necessary to separate the total lipids into individual lipid classes, either by thin-layer chromatography (TLC)[2]

0021-9673/89/$03.50

(one- and/or two-dimensional) or by high-performance liquid chromatography (HPLC)[3].

The present progress in instrumentation analysis makes it possible to replace the TLC methods with an HPLC method which is much more "friendly" with respect to the separated compounds and yields a direct detection of individual components in the effluent. However, the HPLC method has mostly been applied to animal lipids[4–6], rarely to plant lipids[7–10]. Polar lipids are separated most frequently on a silica column into individual classes of phospho- and glycolipids, and this is followed by the separation of each separated class into individual molecular species on a reversed-phase column. The method has certain limitations, *e.g.*, it is necessary to detect individual compounds at 200–210 nm, when only the terminal absorption of the molecules in UV light is recorded. It is also impossible to use a refractive index detector as the desirable components are eluted with a gradient. In addition, several molecular species of lipids are eluted in a single peak. The identification of eluted compounds is also difficult unless LC–MS is used[11] and consists primarily in the collection of individual peaks, transesterification and subsequent analysis of the methyl esters by GC or GC–MS. It is also possible to identify individual molecular species by splitting polar moieties of phospholipids by phospholipase C (E.C. 3.1.4.3)[12–14] and after preparation of trimethylsilyl (TMS) or *tert.*-butyldimethylsilyl (t-BDMS) derivatives demonstrate individual diglycerides by means of GC[13,15], GC–MS[16] or LC–MS[12].

In plants, such studies have been concentrated mainly on polar lipids in classical experimental plants, such as spinach[9] or soya[17]. In green algae, particularly in those of the genus Chlorella, galactosyl diglycerides were separated by means of silver ion TLC[18,19], their sugar moieties were investigated[21], polar glyco- and phospholipids were separated[20,22] and the proportions of fatty acids in separated lipid classes were determined[18–20]. MGDGs (monogalactosyldiglycerols) were partially separated according to the number of double bonds and in some simple cases molecular species were demonstrated, *e.g.*, 18:2-16:2 (ref. 19).

In the present work we studied individual lipid classes in the green alga *Chlorella kessleri* and determined the content of fatty acids in these classes. The main polar lipids were further separated into individual molecular species. This work thus extends our previous communications about triglycerides[23] and waxes[24]. However, the use of the given methods is not limited only to algae, they can also be applied to all photosynthesizing organisms containing glyco- and phospholipids.

MATERIALS AND METHODS

The green alga *Chlorella kessleri* was obtained from the Department of Autotrophic Microorganisms of the Institute of Microbiology in Třeboň in the form of centrifuged paste frozen at −25°C. A 10-g amount of fresh biomass (3.7 g dry mass) was extracted with 40 ml of chloroform–methanol (2:1) according to Blight and Dyer[25] and 290 mg of total lipids were obtained. The major part of neutral lipids and pigments was separated from glyco- and phospholipids on a silica gel column (20 g) washed with seven volumes of chloroform. Elution with methanol yielded complex lipids (175 mg) that were further separated by preparative HPLC.

Preparative HPLC was performed in the Gradient LC System G-I (Shimadzu, Japan) with two LC-6A pumps (5 ml/min), a SCL-6A system controller a SPD

ultraviolet detector (208 nm), a SIL-1A sample injector and a C-R3A data processor. Preparative columns 25 m × 21.2 mm I.D. packed with Zorbax SIL or ODS with 5-μm particles were used. After injection of 17.5 mg of polar lipids into the column with Zorbax SIL, it was eluted with a linear gradient from hexane–isopropanol (6:8) to hexane–isopropanol–water (60:80:14) for 20 min and then isocratically for 30 min[9,10]. Individual classes of polar lipids were collected manually and concentrated under reduced pressure and a nitrogen atmosphere. They were identified by comparison of their retention characteristics with those of standard mixtures (Serum lipid mixture; Supelco, Bellefonte, PA, U.S.A.) and by colour reactions after two-dimensional TLC [chloroform–methanol–water (65:25:4) or chloroform–methanol–28%ammonia (65:25:5) in the second direction]. Ten injectons, each of 17.5 mg in 200 μl chloroform, were necessary in order to obtain sufficient quantities of individual lipid classes.

Preparative HPLC of the molecular species of the individual lipids (injection of 5 mg in 100 μl) was performed in the same apparatus on a Zorbax ODS column in the isocratic mode using a mixture of 20 m*M* choline hydrochloride in methanol–water–acetonitrile (90.5:7:2.5)[4,9]. Individual fractions were again collected manually. All fractions were transesterified by sodium methoxide in methanol (except for fraction X_{v1}). The methylesters obtained were then identified and quantified by means of GC–MS.

Enzymatic degradation[14]

PC (phosphatidylcholine) and PE (phosphatidylethanolamine) (1–1.5 mg) were suspended in 3 ml of diethyl ether with 0.1 mg butylated hydroxytoluene (BHT) as an antioxidant and 3 ml of buffer [17.5 m*M* tris(hydroxymethyl)aminomethane (Tris) containing 1.0 m*M* calcium chloride, pH 7.2] with 35 units of phospholipase C (Type XIII from *Bacillus cereus*; Sigma, St. Louis, MO, U.S.A.) were added. After shaking for 3 h, diacylglycerols were extracted with 5 ml of diethylether and the extract was dried with sodium suphate. The enzymatic reaction proceeded with a yield of 98% (TLC; chloroform–methanol–water, 65:25:4). Groups of diacylglycerols from PC or PE were derivatized with TMS[13] for 30 min at room temperature and identified by GC–MS.

Pancreatic lipase (Type II, Sigma) was treated according to Safford and Nichols[19] and impurities were thus removed. The hydrolysis was performed with 1 mg of individual molecular species, *i.e.*, MGDG or DGDG (digalactosyldiglycerol) and with 1 mg of lipase in Tris buffer with calcium chloride at pH 7.6 and 40°C for 3 h under continuous shaking. After hydrolysis, the products were extracted with chloroform, the extract was separated by TLC (hexane–diethyl ether–acetic acid, 70:30:1) and free acids and monoacylgalactosyldiglycerides were methylated with a boiling mixture of methanol–benzene–sulphuric acid (20:10:1) for 1.5 h. Methyl esters were analyzed by GC–MS.

Amide hydrolysis

Fraction X_{v1} (2 mg) containing a lipid with a long base was hydrolyzed under mild conditions (for 1 h at room temperature, 0.6 *M* sodium hydroxide in methanol). After completion of the reaction the mixture was extracted three times with 5 ml of diethyl ether and the methyl esters were separated from the amide by TLC (choroform–methanol–28% ammonia, 65:25:5). The compound with a lower R_F (0.1) was hydrolyzed with boiling 1 *M* potassium hydroxide in methanol for 20 h, the

mixture was then cooled and extracted three times with diethyl ether (secondary aminoalcohol was obtained after evaporation). The acidified aqueous phase (3 *M* hydrochloric acid) was extracted three times with diethyl ether–hexane (1:1) (5 ml), the solvent was evaporated to dryness and methyl esters prepared by reaction with diazomethane were identified by GC–MS.

GC–MS

Methyl esters of fatty acids were separated in an HP 5995 B apparatus (Hewlett-Packard, Avondale, PA, U.S.A.) Chromatographic conditions: splitless injection; temperature, injector 230°C, column 100°C (1 min) then at 20°C/min to 160°C, than at 2°C/min to 270°C; column 30 m × 0.25 mm I.D. × 0.25 μm film, Supelcowax 10; carrier gas helium 30 cm/s; ionization voltage 70 eV; spectra scanned within *m/z* 50–500.

TMS-diglycerides were separated and identified on the same apparatus. Injection temperature: 100°C. Column (15 m × 0.25 mm I.D. × 0.25 μm film, Supelcowax 10) temperature: 100°C (1 min) then at 20°C/min to 230°C and at 2°C/min to 280°C; finally isothermal for 10 min. Carrier gas (helium), flow-rate: 70 cm/s. Spectra were scanned within *m/z* 150–750 at 70 eV.

RESULTS AND DISCUSSION

Lipids and fatty acids in Chlorella kessleri

Tables I–V summarize all the values determined. As far as the qualitative and quantitative occurrence of individual lipid classes in algae is concerned, only Nichols[20] separated but did not quantify individual lipid classes in the green alga *Chlorella* vulgaris. This author found practically all known lipid classes; only CL (cardiolipin) was not detected in our sample, however on the basis of analytical TLC and colour reactions it may be assumed that it is the fraction X_2. Khotimchenko[22] presented known phospholipid types in sea algae. He found common species, such as PG (phosphatidylglycerol), PC, PE and minority PI (phosphatidylinositol), PS (phosphatidylserine) and PA (phosphatidic acid). Brush and Percival[21] analyzed sugar moieties of galactosyllipids, identified MGDG, DGDG and TGDG (trigalactosyldiglyceride) and determined the quantitative order DGDG > MGDG > sulfolipid (SL) which is a characteristic feature of algae; a different order was found in higher plants.

TABLE I
POLAR LIPID COMPOSITION OF THE ALGA *C. KESSLERI* AS DETERMINED BY HPLC

Polar lipid fraction	*%*	*Polar lipid fraction*	*%*
MGDG	19.3	X_2	1.2
DGDG	10.9	PI	3.0
SL	2.3	PA	3.1
X_1	0.7	PS	2.8
PE	9.8	PC	37.2
PG	7.3	X_{v1}	2.4

TABLE II
FATTY ACIDS IDENTIFIED FROM POLAR LIPID CLASSES OF THE ALGA *C. KESSLERI*

*Fatty acid**	*Lipid class*											
	MGDG	*DGDG*	*SL*	X_1	*PE*	*PG*	X_2	*PI*	*PA*	*PS*	*PC*	X_{v1}
12:0	–	–	–	1.4	0.7	1.0	1.1	0.8	1.4	1.0	0.6	–
i-14:0	–	–	–	2.1	–	–	2.5	–	–	–	–	–
14:0	1.5	1.3	2.1	11.4	3.1	1.7	0.7	3.1	3.1	2.2	2.7	–
9-14:1	–	–	–	1.1	0.2	0.8	5.1	0.1	0.3	0.3	0.3	–
ai-15:0	–	–	–	3.0	–	–	7.3	–	–	–	–	–
15:0	1.0	–	1.8	2.1	2.4	1.1	2.4	2.3	2.3	2.8	3.1	–
9-15:1	–	–	–	1.7	1.0	0.7	0.8	1.0	1.3	1.1	1.0	–
i-16:0	–	–	–	8.1	–	–	3.2	–	–	–	–	–
16:0	5.2	7.1	5.4	15.4	13.2	21.3	19.7	16.5	10.8	10.8	25.4	7.2
7-16:1	1.1	1.4	2.1	7.3	4.6	5.2	5.7	5.8	5.2	6.2	4.8	–
9-16:1	2.4	1.2	1.9	1.8	3.2	2.0	0.9	0.8	1.9	4.1	4.9	–
3t-16:1	–	–	–	–	–	7.1	1.3	–	–	–	–	–
7,10-16:2	14.2	18.7	12.7	–	1.4	2.3	0.6	3.4	2.2	3.1	2.8	–
7,10,13-16:3	23.1	14.8	15.7	–	3.1	0.7	–	3.1	0.7	2.5	1.9	–
17:0	1.0	1.0	1.1	7.9	2.5	1.8	4.3	0.9	1.6	0.3	0.5	–
br_2-17:0	–	–	–	5.3	–	–	1.2	–	–	–	–	–
9-17:1	0.5	0.6	1.3	2.3	0.7	2.1	2.7	2.3	1.7	1.1	1.4	–
18:0	2.5	4.5	3.6	13.5	3.4	5.8	16:0	7.2	4.3	22.5	3.8	1.0
9-18:1	5.3	8.1	4.9	14.8	19.8	14.9	22.1	13.1	14.2	17.1	17.4	2.1
9,12-18:2	24.8	25.4	21.4	–	14.1	18.3	1.7	19.6	20.0	14.4	17.1	–
6,9,12-18:3	10.4	5.6	17.8	–	12.2	7.9	–	7.8	2.7	2.7	1.4	–
9,12,15-18:3	7.0	10.3	8.2	–	13.8	5.3	0.7	12.4	15.6	2.1	10.9	–
9-19:1	–	–	–	0.7	–	–	–	–	–	–	–	0.7
20:0	–	–	–	0.1	–	–	–	–	–	0.6	–	3.4
11-20:1	–	–	–	–	0.6	–	–	0.4	3.1	3.1	–	5.1
22:0	–	–	–	–	–	–	–	–	–	–	–	4.8
13-22:1	–	–	–	–	–	–	–	–	–	–	–	7.0
23:0	–	–	–	–	–	–	–	–	–	–	–	2.1
15-24:1	–	–	–	–	–	–	–	–	–	2.0	–	18.3
26:0	–	–	–	–	–	–	–	–	–	–	–	14.2
17-26:1	–	–	–	–	–	–	–	–	–	–	–	17.0
28:0	–	–	–	–	–	–	–	–	–	–	–	3.2
28:1	–	–	–	–	–	–	–	–	–	–	–	4.5
30:0	–	–	–	–	–	–	–	–	–	–	–	4.2
30:1	–	–	–	–	–	–	–	–	–	–	–	5.1

* i = Isoacid; ai = anteisoacid; br_2 = methyl group on C_2; t = trans; numbers before the hyphen = position(s) of double bond(s); first number = number of carbon atoms in the chain, second number = number of double bonds.

In our case the results of quantification of galactosyl-lipids are not in agreement; they can be compared with the order found in higher plants (MGDG > DGDG > SL)[1].

Table II presents the occurrence of individual fatty acids in different phospholipid classes after their hydrolysis. The unidentified class X_{v1}, with very long acids up to C_{30} bound by an amide bond, has the most interesting content of fatty acids. On the basis of preliminary data it may be assumed that an amide with an unidentified aminoalcohol is involved. The content of longer fatty acids (above C_{18}) in PS is also quite interesting; it thus appears that the assumption of Murata *et al.*[26] that PS is a precursor of waxes is substantiated. Branched saturated acids were detected in fractions X_1 and X_2. Nichols[20] was again the only author who determined the qualitative and quantitative contents of individual fatty acids in phospholipid classes. His results are in good agreement with our data.

Table III shows the occurrence of individual molecular species of glycolipids. Fatty acids in positions 1 and 2 of MGDG were studied[19] again. The previous authors detected C_{16} acids in position 2. Our results are not in agreement with theirs. On the contrary, we found more saturated acids in position 1, irrespective of the chain length. The situation in lower and higher plants is quite complicated[1].

Tables IV and V present the percentage occurrence of the molecular species of individual phopholipids and/or of PC and PE. Unfortunately, to the best of our knowledge, literature data are practically absent, so that we have nothing with which to compare our results. Compared with higher plants, *e.g.*, tobacco, potatoes, or soya, no pronounced differences in majority molecular species in PC and other phospholipids were detected, *e.g.*, in tobacco leaves[9] most of the PCs were 18:3-18:3, 18:2-18:3, 16:0-18:3 and 16:0-18:2, whereas in the alga used in the present work most of the PCs were 18:3-18:3, 16:0-16:1 and 16:0-18:1.

This fact can be explained by a close taxonomic relationship between green fresh-water algae with higher plants, as the latter (Telomophyta) can be considered as a section of the tribe Chlorophyta (green algae) from which they are phylogenetically derived.

TABLE III

DISTRIBUTION (%) OF MOLECULAR SPECIES OF ALGAL GALACTOLIPIDS AS DETERMINED BY HPLC

Peak No.	*Molecular species**	*MGDG*	*% FA on C_1*	*DGDG*	*% FA on C_1*	*SL*
1	16:3-18:3**	26.9	79.3	16.1	64.3	22.5
2	16:2-18:3**	10.6	94.5	12.1	86.9	12.2
3	18:3-18:3**	14.4	50.0	10.3	50.0	29.5
4	16:2-18:2	15.1	83.2	26.4	67.8	9.4
5	18:2-18:3**	20.1	47.1	16.4	44.9	20.2
6	16:0-18:3**	1.0	99.7	4.6	98.6	1.7
7	18:1-18:3**	4.3	90.1	5.3	95.4	1.1
8	16:0-18:2	1.4	96.7	7.4	99.0	2.1
9	18:1-18:2	6.2	72.6	1.4	84.3	1.3

* First FA, it's FA on C_1 of glycerol.

** Positional isomer, *e.g.*, 6,9,12-18:3 and 9,12,15-18:3.

TABLE IV

DISTRIBUTION (%) OF MOLECULAR SPECIES OF ALGAL PHOSPHOLIPIDS ACCORDING TO HPLC

Peak No.	*Molecular species*	*Phospholipid*					
		PE	*PG*	*PI*	*PA*	*PS*	*PC*
1	16:3-18:3	2.4	–	2.0	–	0.5	1.0
2	18:3-18:3	10.2	6.0	11.7	17.6	1.0	12.4
3	18:2-18:3	11.0	8.3	13.0	15.0	3.0	5.5
4	16:1-18:2	3.3	4.6	4.5	4.5	6.4	3.5
5	18:2-18:2	5.9	11.6	11.7	12.8	8.9	6.7
6	18:1-18:3	15.4	6.8	8.2	10.6	3.5	9.2
7	16:0-16:1	3.1	7.3	3.5	3.7	4.8	16.8
8	14:0-18:2	–	1.0	2.0	–	–	1.2
9	16:1-18:1	1.3	3.7	2.8	2.0	1.4	1.4
10	16:0-18:2	5.6	13.5	10.3	4.5	6.7	8.2
11	18:1-18:2	18.3	9.4	8.3	9.0	10.6	6.6
12	17:0-18:2	1.1	1.1	0.5	1.0	–	0.8
13	16:0-18:1	7.3	10.9	6.9	7.5	8.0	12.2
14	18:1-18:1	11.7	7.7	5.5	6.4	12.6	7.3
15	18:0-18:2	1.4	3.7	4.5	2.7	14.0	2.0
16	17:1-18:1	–	1.0	1.0	0.8	0.8	1.3
17	17:1-18:0	–	0.4	0.5	–	1.0	0.4
18	18:0-18:1	2.0	3.0	3.1	1.9	16.8	3.5

HPLC separation of polar lipids

In order to separate sufficient amounts for studies of individual classes of polar lipids or even molecular species of respective lipids, it is necessary to apply much larger samples for enzymatic degradation than those used for a bare determination of fatty acids. Therefore, on the basis of literature data, we performed preparative HPLC of polar lipids.

Fig. 1 shows a record of preparative HPLC of total lipids on a silica gel column. We were able to separate twelve lipid classes, of which MGDG, DGDG and PC were the main ones detected. Quantification was on the basis of the UV detector response; individual values are best seen in Table I. Individual lipid classes were separated practically down to the baseline even when 17.5 mg were injected. This amount is some orders of magnitude higher than that applied by Demandre *et al.*[9] (20–50 μg) and Rivnay[10] (2.5 mg). The order of elution was different in the two studies, in spite of the fact that the authors used the same mobile phase. The order of elution of the individual components of our sample is in agreement with that of Rivnay[10].

All fractions were thus completely separated, *i.e.*, residual neutral lipids, triglycerides and residual photosynthetic pigments were separated from polar lipids, and all fractions were separated down to the baseline. In addition, it was possible to separate PC and the fraction X_{v1} (amide resembling sphingomyelin) and to use HPLC in the preparative mode and thus obtain milligram amounts of pure polar lipid classes after a single injection. These facts can also be utilized in further separations and reactions, thus, for instance, for PC it would not be necessary to repeat the HPLC separation as 6.4 mg of PC were obtained after a single injection which is sufficient for

TABLE V
MOLECULAR SPECIES OF ALGAL PC AND PE AS DETERMINED BY POLAR CAPILLARY GC–MS
Determined as TMS ethers after treatment by phospholipase C.

Peak No.	*Molecular species*	*PC*	*PE*	*Peak No.*	*Molecular species*	*PC*	*PE*
1	12:0-16:0	0.4	0.4	27	16:0-18:0	3.8	1.0
2	14:0-16:0 + 15:0-15:0	1.9 + 0.3	0.9	28	16:0-18:1	8.6	5.9
3	14:0-16:1*	0.4	0.3	29	16:1*-18:0	0.6	0.4
4	14:0-16:1	0.4	0.4	30	16:1**-18:0	0.6	0.5
5	15:0-16:0	2.2	0.7	31	16:1*-18:1	1.8	0.0
6	15:0-16:1*	0.4	0.5	32	16:1**-18:1	0.6	1.4
7	15:0-16:1**	0.4	0.3	33	16:0-18:2	4.9	4.2
8	16:0-16:0 + 14:0-18.0	6.5 + 0.3	3.8	34	16:1*-18:2	0.9	1.5
9	16:0-16:1*	8.3	1.4	35	16:1**-18:2	0.9	1.0
10	16:0-16:1**	8.4	0.0	36	16:0-18:3§	1.0	3.6
11	14:0-18:1	0.9	1.4	37	16:0-18:3***	3.8	4.1
12	16:1*-16:1*	0.4	0.5	38	16:1*,**-18:3***,§	1.4	3.3
13	16:1**-16:1*	0.3	0.3	39	17:1-18:1	0.5	0.3
14	16:1**-16:1**	0.4	0.5	40	18:0-18:0	0.4	0.3
15	16:0-16:2	1.9	0.4	41	18:0-18:1	2.3	2.5
16	14:0-18:2	0.6	1.0	42	18:1-18:1	5.4	8.9
17	16:1*-16:2	0.4	0.4	43	18:0-18:2	1.7	2.1
18	16:1**-16:2	0.4	0.5	44	18:1-18:2	3.4	6.3
19	16:0-16:3	1.3	0.9	45	18:0-18:3***	0.6	1.1
20	14:0-18:3***	0.4	1.0	46	18:2-18:2	2.4	6.1
21	16:1*-16:3	0.1	0.3	47	18:1-18:3§	1.3	5.2
22	16:1**-16:3	0.2	0.7	48	18:1-18:3***	3.8	4.0
23	15:0-18:0 + 16:0-17:0	0.3 + 0.3	1.1 + 0.2	49	18:2-18:3§	0.3	3.0
24	15:0-18:1 + 16:0-17:1	1.0 + 1.0	0.8 + 0.7	50	18:2-18:3***	2.0	4.3
25	15:0-18:2	0.6	0.6	51	18:3§-18:3§	1.8	3.2
26	15:0-18:3***	0.5	0.7	52	18:3**-18:3***	3.3	4.2

* 7-16:1.
** 9-16:1.
*** 9,12,15-18:3.
§ 6,9,12-18:3.

both reversed-phase HPLC and enzymatic hydrolysis and other determinations by GC–MS.

HPLC separation of polar lipids into molecular species

A successful separation of polar phospholipids and glycolipids into molecular species depends on the content of fatty acids and also on the polar head group. However, when using the given mobile phase their effect should not be pronounced. For instance, the difference in retention times of the molecular species 18:1-18:3 in PE, PG, PI, PA, PS and PC is negligible, not exceeding ± 7 min with respect to PS, which is in contradiction with Patton *et al.*[4] who reported much larger differences (PI about 40 min, PC and PE up to 100 min). On the contrary, the order of elution of the above molecular species 18:1-18:3 is retained in individual phospholipids, *i.e.*, PI has the shortest retention time (33.5 min), whereas PC, PE and PA have the longest retention

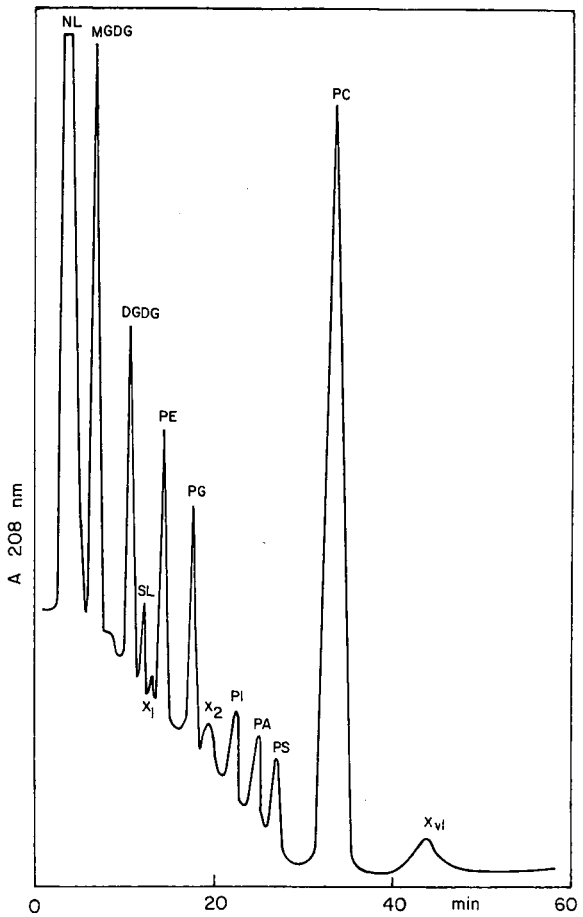

Fig. 1. Preparative HPLC of total polar lipids. For experimental conditions see Materials and Methods.

time (37.5 min). A question thus arises, whether the retention time is determined by the polarity of the given head group or by its polarizability. As a prolongation of the retention time is found in both PC (basic character) and PA (acidic character) it may be assumed that the polarizability plays a role here.

The separation was practically down to the baseline during 30 min when using the isocratic mode (Fig. 2). Thus a total of 9 molecular species of glycolipids were detected, whereas up to 18 molecular species were detected in phospholipids. As compared with Demandre *et al.*[9], we did not detect contamination of MGDG and DGDG by pigments, due probably to a previous separation by column chromatography (see Experimental). The optimum column load was approximately 5 mg. When increasing the injection volume the separation of individual components sharply decreased and the peaks of the molecular species 18:1-18:1 and 18:1-18:2 overlapped when injecting 10 mg of any phospholipid.

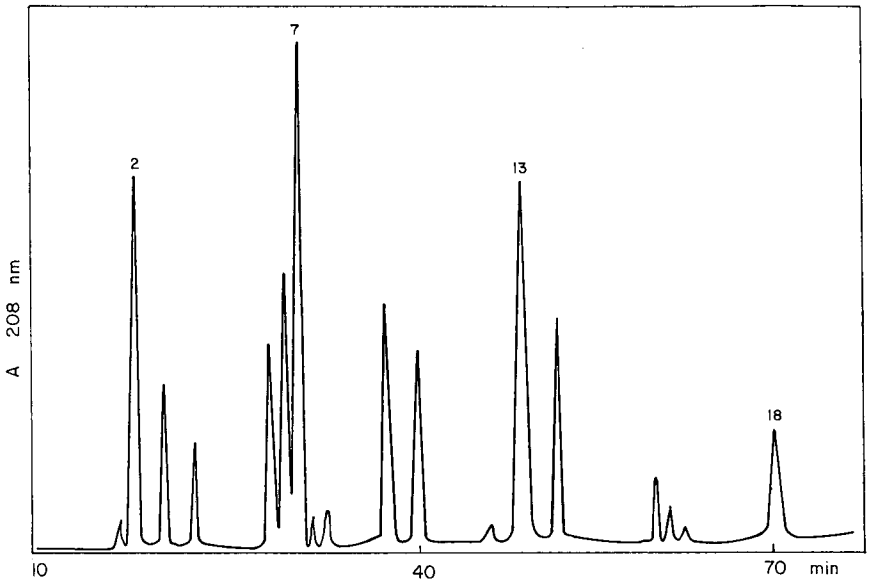

Fig. 2. Preparative reversed-phase HPLC of PCs. For experimental conditions see Materials and Methods; for peak numbers see Table IV. NL = Neutral lipids (mainly triacylglycerols, waxes, sterols, etc.).

GC–MS of TMS-diglycerides

The separation of individual molecular species of TMS-diglycerides on a 30-m capillary column packed with a non-polar phase was described[27]. However, the column efficiency did not permit the separation of even molecular species such as 16:0-18:1 and 16:0-18:2. Odd and even diglycerides including isoacyldiglycerides and diacyldiglycerides were separated on a packed column[16]. Myher and Kuksis[13,15] separated successfully individual molecular species, both TMS- and t-BDMS-diglycerides on a polar capillary column packed with SP-2330. Split and splitless injection and isothermal elution enabled the separation of even positional isomers, *e.g.*, 11-18:1-18:2 from 9-18:1-18:2. Helium was reported to be unsuitable as a carrier gas, however when using this gas we were able to obtain a better separation than that obtained by the above authors. This was primarily due to the injection technique, *i.e.*, on-column injection, and to the use of a less polar and particularly chemically bound and more thermally stable phase of the Supelcowax type which made it possible to use a temperature gradient and thus obtain a better separation (see Fig. 3). We thus separated even a mixture of position isomers, *e.g.*, combination of all 16:1 (see peaks 12–14 in Fig. 3) or diglycerides with 18:3 in combination with other acids (see three peak pairs 47–48, 49–50 and 51–52 in Fig. 3).

Individual peaks in GC–MS can be identified[28] primarily on the basis of $M^+ - 15$ (molecular mass can be determined) and of the ions $M - R_1COO$ and $M - R_2COO$, where R_1COO and R_2COO are acyloxy groups bound to carbon 1 and carbon 2 of TMS-glycerol. In this way it is possible to discriminate even positional isomers, *i.e.*, fatty acids in position 1 and/or 2, on the basis of the intensities of the above ions.

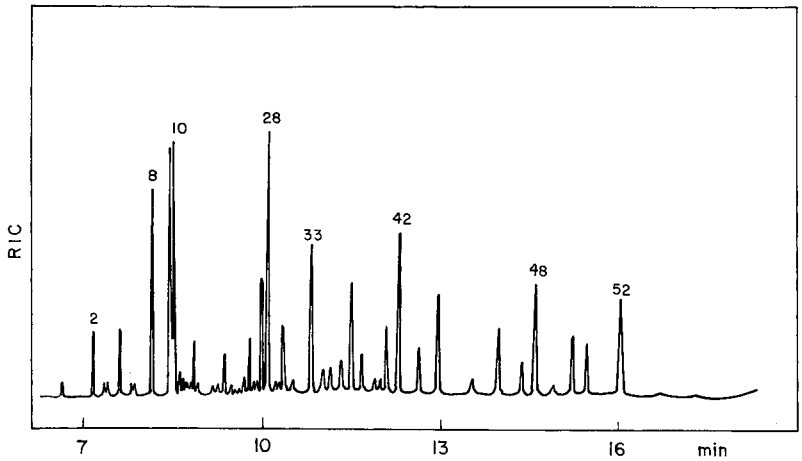

Fig. 3. GC–MS of TMS-diglycerides from PCs after hydrolysis by phospholipase C. For experimental conditions see Materials and Methods; for peak numbers see Table V.

Recovery in HPLC and GC–MS

As pure standards are not available, linearity of the GC–MS and HPLC (UV detector) is quite important for quantification of individual components. Table VI shows the recovery obtained with both detectors (MS an UV) for selected majority peaks in Tables IV and V, the values always being recalculated per 100%. This relationship can be explained by the fact that the terminal absorbancy of the double bond (bonds) is still detected at 208 nm and thus the response of the UV detector is higher than in the case of the saturated chain.

As far as we know, the problem has not yet been discussed in the literature, except in ref. 12. However, as those authors used LC–MS and GC (FID) in which no discrimination occurred, we cannot compare the data obtained. Baty *et al.*[29] when

TABLE VI

RELATIVE RESPONSES TO PCs AS THEIR TMS-DIGLYCERIDES OBTAINED BY HPLC WITH UV DETECTION AND GC–MS WITH TOTAL ION CURRENT DETECTION

*Molecular species**	*Number of C=C bonds*	*HPLC***	*GC–MS***	*Ratio LC/GC*
18:3-18:3	6	14.0	9.1	1.54
18:2-18:3	5	6.2	4.1	1.51
18:2-18:2	4	7.6	6.3	1.21
18:1-18:3	4	10.4	9.0	1.16
18:1-18:2	3	7.5	6.1	1.23
16:0-18:2	2	9.3	8.7	1.07
18:1-18:1	2	8.3	9.6	0.86
16:0-16:1	1	18.9	27.7	0.70
16:0-18:1	1	13.8	15.3	0.90
18:0-18:1	1	4.0	4.1	0.98

* Classified according to the number of double bonds.

** The values were always recalculated per 100% from Tables IV and V.

studying the separation of fatty acid derivatives by HPLC (fluorescence detector) and GC (FID) also did not obtain unambiguous results. These discrepancies can be caused by the chromophore and by the detection method. Pind *et al.*[12] stated that "Theoretically, the polar capillary columns could be connected to the mass spectrometer, but no practical combinations of this type have yet been devised for work with diacylglycerols". On the contrary, we demonstrated that for the analysis of phospholipids the GC–MS method is suitable and more economic than the LC–MS method, due also to the fact that phospholipids are enzymatically hydrolyzed by phospholipase C also for LC–MS and thus the identical substrate can be prepared for both GC–MS and LC–MS.

Hence, it can be concluded that both methods, *i.e.*, GC–MS and HPLC, are mutually complementary and facilitate a better and more efficient separation and quantification of natural mixtures of polar lipids.

REFERENCES

1 P. K. Stumpf, in P. K. Stumpf and E. E. Conn (Editors), *Lipids: Structure and Function*, Vol. 4, Academic Press, New York, 1980.
2 V. P. Skipski and M. Barclay, *Methods Enzymol.*, 14 (1969) 530.
3 N. A. Porter and H. Weenen, *Methods Enzymol.*, 72 (1981) 34.
4 G. M. Patton, J. M. Fasulo and S. J. Robins, *J. Lipid. Res.*, 23 (1982) 190.
5 S. S.-H. Chen and A. Y. Kou, *J. Chromatogr.*, 227 (1982) 25.
6 H. P. Nissen and H. W. Kreysel, *J. Chromatogr.*, 276 (1983) 29.
7 D. V. Lynch, R. E. Gundersen and G. A. Thompson, *Plant Physiol.*, 72 (1983) 903.
8 R. Yamauchi, M. Kojima, M. Isogai, K. Kato and Y. Ueno, *Agric. Biol. Chem.*, 46 (1982) 2847.
9 C. Demandre, A. Tremolieres, A. M. Justin and P. Mazliak, *Phytochemistry*, 24 (1985) 481.
10 B. Rivnay, *J. Chromatogr.*, 294 (1984) 303.
11 A. Kuksis, L. Marai, J. J. Myher and S. Pind, in A. Kuksis (Editor) *Chromatography of Lipids in Biomedical Research and Clinical Diagnosis (Journal of Chromatography Library Series*, Vol. 37), Elsevier, Amsterdam, 1987, p. 403.
12 S. Pind, A. Kuksis, J. J. Myher and L. Marai, *Can. J. Biochem. Cell Biol.*, 62 (1984) 301.
13 J. J. Myher and A. Kuksis, *Can. J. Biochem.*, 60 (1982) 638.
14 W. W. Christie, *Lipid Analysis*, Pergamon Press, Oxford, 2nd ed., 1982.
15 J. J. Myher and A. Kuksis, *Biochim. Biophys. Acta*, 795 (1984) 85.
16 B. F. Dickens, C. S. Ramesha and G. A. Thompson, Jr., *Anal. Biochem.*, 127 (1982) 37.
17 K. Aitzetmüller, *Fette, Seifen, Anstrichm.*, 86 (1984) 318.
18 B. W. Nichols and R. Moorhouse, *Lipids*, 4 (1969) 311.
19 R. Safford and B. W. Nichols, *Biochim. Biophys. Acta*, 210 (1970) 57.
20 B. W. Nichols, *Biochim. Biophys. Acta*, 106 (1965) 274.
21 P. Brush and E. Percival, *Phytochemistry*, 11 (1972) 1847.
22 S. V. Khotimchenko, *Khim. Prir. Soedin.*, (1985) 404.
23 T. Řezanka, P. Mareš, P. Hušek and M. Podojil, *J. Chromatogr.*, 355 (1986) 265.
24 T. Řezanka and M. Podojil, *J. Chromatogr.*, 362 (1986) 399.
25 E. G. Blight and W. J. Dyer, *Can. J. Biochem. Physiol.*, 37 (1959) 911.
26 M. Murata, N. Sato and N. Takahashi, *Biochim. Biophys. Acta*, 795 (1984) 147.
27 S. J. Gaskell and C. J. W. Brooks, *J. Chromatogr.*, 142 (1977) 469.
28 T. Curstedt, *Biochim. Biophys. Acta*, 360 (1974) 12.
29 J. D. Baty, R. G. Wilis and R. Tavendale, *J. Chromatogr.*, 353 (1986) 319.

Journal of Chromatography, 463 (1989) 409–417
Elsevier Science Publishers B.V., Amsterdam — Printed in The Netherlands

CHROM. 21 063

MICROPREPARATIVE SEPARATION OF TRANSFER RIBONUCLEIC ACIDS BY HIGH-PERFORMANCE LIQUID CHROMATOGRAPHY

MILOŠ DOLEŽAL and JAN HRADEC*

Department of Molecular Biology, Research Institute of Tuberculosis and Respiratory Diseases, 180 71 Prague (Czechoslovakia)

(First received May 18th, 1988; revised manuscript received October 20th, 1988)

SUMMARY

A method was developed for the micropreparative separation of individual species of tRNA using reversed-phase high-performance liquid chromatography on large pore spherical silica bonded with C_3 alkyl chains. Columns were eluted with linear gradients of decreasing sodium chloride and increasing methanol concentrations. The decreasing salt gradient gradually abolished hydrophobic interactions and a significantly higher selectivity was thus obtained when compared with increasing gradients of salts usually employed in reversed-phase separations of tRNA. The acceptance of tRNA fractions was tested by charging them with fifteen different amino acids. Significantly different separations were obtained with tRNA from *Escherichia coli* and from rat liver. $tRNA^{Glu}$ and $tRNA^{Tyr}$ from *E. coli* were obtained in a pure form, all other tRNAs were more or less contaminated by adjoining tRNAs for other amino acids. Rechromatography under suitable isocratic conditions was required to obtain pure tRNA species from rat liver. Isoaccepting tRNAs for several amino acids were separated from rat liver. The method described seems suitable for preliminary fractionations of complex mixtures of tRNA and for a simple purification of isoaccepting species if the presence of tRNAs for other amino acids is not an hindrance.

INTRODUCTION

Separation of individual species of tRNA has always been a difficult task because of the close similarity in size and composition of tRNA molecules specific for different amino acids. Chromatography on benzoylated DEAE-cellulose[1] was found useful for tRNAs accepting aromatic amino acids (in particular $tRNA^{Phe}$) which become strongly bound to this carrier. On the other hand, the initiator tRNA ($tRNA_F^{Met}$) is retained only slightly on benzoylated DEAE-cellulose and can thus be relatively simply separated[2]. However, other tRNA species were eluted together without any reasonable resolution. Low-pressure chromatography on reversed phases (RPC)[3] provided better separations of individual tRNAs, however rechromatography was required to obtain tRNA species in a satisfactory purity.

High-performance liquid chromatography (HPLC) was shown to give a promising resolution of RNA molecules of different sizes (as reviewed by McLaughlin[4]).

0021-9673/89/$03.50

Several different stationary phases were used for the separation of individual tRNA species. In earlier attempts, a reversed-phase support consisting of inert poly(chlorotrifluoroethylene) beads to which a pellicular layer of trioctylammonium chloride had been adsorbed was used and a very rapid resolution of isoaccepting tRNAs, *i.e.*, different tRNAs accepting the same amino acid for serine and leucine from bacterial materials was obtained[5]. Alkylated silicas with short-chain chlorosilanes appeared to be a promising support material for the separation of tRNA, employing a gradient elution with decreasing ammonium sulphate concentration at elevated temperatures[6]. Using a Vydac C_4 derivatized silica column, tRNA from *Escherichia coli* B was separated into more than 20 peaks. However, only species accepting phenylalanine, tryptophan and valine have been identified[7]. Microparticulate bonded stationary phases were also employed for the separation of model mixtures of $tRNA^{Glu}$, $tRNA^{Lys}$, $tRNA^{Phe}$ and $tRNA^{Val}$ from *E. coli* and a good and rapid resolution has been demonstrated[8].

Further supports employed for the separation of tRNA by HPLC included polystyrene and reversed-phase anion exchangers as well as affinity columns[9]. A support consisting of an octadecasilyl-bonded phase silica aggregated with the tetraalkylammonium chloride was found to be useful for the separation of isoaccepting tRNAs from baker's yeast and a good resolution of $tRNA^{Val}$, $tRNA^{Ile}$, $tRNA^{Ser}$ and $tRNA^{Phe}$ has been reported[10]. Gel permeation high-performance chromatography appeared to be useful for the separation of small tRNA species but is apparently of minor importance for the resolution of individual tRNA species[11].

With the exception of a single paper[12], only four to eight tRNAs for different amino acids were identified in experiments on the separation of individual tRNA species by HPLC.

For our studies on the interaction of chemical carcinogens with tRNA[13], several species of tRNA specific for different amino acids are required. The method developed for this purpose and described in this paper allows a satisfactory separation of at least thirteen tRNAs for different amino acids not only on an analytical but also on a micropreparative scale.

MATERIALS AND METHODS

Chemicals and radiochemicals

Transfer RNA from *E. coli* B was a product of Calbiochem (San Diego, CA, U.S.A.). Transfer RNA from rat liver was isolated as described by Rogg *et al.*[14] and deacylated[2]. Aminoacyl-tRNA synthetases were partially purified from *E. coli* B or rat liver as described by Stanley[2]. L-[U-^{14}C]alanine (120 mCi/mmol), L-[U-^{14}C]arginine (240 mCi/mmol), L-[U-^{14}C]aspartic acid (160 mCi/mmol), L-[U-^{14}C]glutamic acid (200 mCi/mmol), L-[U-^{14}C]glycine (80 mCi/mmol), L-[U-^{14}C]histidine (240 mCi/mmol), L-[U-^{14}C]isoleucine, L-[U-^{14}C]leucine (240 mCi/mmol), L-[U-^{14}C]lysine (240 mCi/mmol), L-[U-^{14}C]phenylalanine (360 mCi/mmol), L-[U-^{14}C]serine (120 mCi/mmol), L-[U-^{14}C]threonine (160 mCi/mmol), L-[U-^{14}C]tyrosine and L-[U-^{14}C]valine (240 mCi/mmol) were from the Institute for Research, Production and Utilisation of Radioisotopes, Prague, Czechoslovakia. [Methyl-^{3}H]methionine (280 mCi/mmol) was obtained from the Institute of Radioisotopes, Hungarian Academy of Sciences, Budapest, Hungary.

High-performance liquid chromatography

A Beckman 345 HPLC system was used consisting of the 114M solvent delivery module, Type 165 variable wavelength detector and Type 450 data system/controller. Columns containing large pore silica bonded with C_3 alkyl chains (Beckman Ultrapore C_3RPSC) (7.5 cm × 4.6 mm I.D.) were used at a flow-rate of 1 ml/min and the absorbance of the eluate was recorded at 260 nm. A linear gradient of buffer B (10 m*M* Tris–HCl buffer, pH 7.55, 10 m*M* magnesium chloride, 200 m*M* sodium chloride), and 8% (v/v) metanol was added to buffer A (10 m*M* Tris–HCl buffer, pH 7.55, 10 m*M* magnesiumchloride, 1 *M* sodium chloride). Pumps were programmed to deliver 0–50% of buffer B during 100 min after the sample injection and 50–100% of buffer B during the next 50 min. Fractions (each 1.0 ml) were collected. Each fraction was supplemented with 1/10 volume of 2 *M* sodium acetate buffer, pH 5.0, followed by two volumes of chilled (−20°C) ethanol. The solutions were mixed on a vortex mixer and left at −20°C overnight. RNA precipitates were then centrifuged at low speed and −10°C, supernatants were discarded and precipitates were dried under a stream of nitrogen.

Agarose gel electrophoresis

This was performed as described by Maniatis *et al.*[15] in the gel electrophoresis instrument GNA-100 (Pharmacia, Uppsala, Sweden).

Charging of tRNA with amino acids

Transfer RNA in individual fractions was dissolved in 0.1 ml of water and charged with amino acids as described by Hradec[13]. Briefly, mixtures containing tRNA, aminoacyl-tRNA synthetases from *E. coli* or from rat liver, ATP and CTP were incubated with individual labelled amino acids for 20 min at 37°C. Thereafter, aminoacyl-tRNA was precipitated, washed and its radioactivity was assayed by liquid scintillation counting.

RESULTS

The elution profile of fifteen individual tRNA species tested was completely different when comparing tRNA of bacterial origin with that from rat liver. These results are summarized in Table I.

With tRNA from *E. coli* at least two tRNAs ($tRNA^{Glu}$ and $tRNA^{Tyr}$) were obtained in a pure form from a single experiment. With the usual loads, 2.5 mg in 50 µl of buffer A, the yields of these individual tRNAs were in the range of 20–50 µg. Moreover, one isoaccepting species of $tRNA^{Leu}$ was only sparingly contaminated with $tRNA^{Ser}$.

On the other hand, no resolution of $tRNA^{Met}$ from $tRNA^{Thr}$ was obtained. There was also no separation of $tRNA_F^{Met}$ (initiator tRNA) from $tRNA_M^{Met}$ (tRNA inserting L-methionine into the inside of the peptide chain).

The other tRNAs were not isolated in a pure form. Thus $tRNA^{Asp}$ showed overlapping with $tRNA^{Thr}$ and $tRNA^{Lys}$, tRNA accepting arginine was contaminated with $tRNA^{His}$, $tRNA^{Val}$ was partially overlapped with $tRNA^{Gly}$ and $tRNA^{Ser}$ with one isoaccepting species of $tRNA^{Leu}$. The complex of $tRNA^{Met}$ and $tRNA^{Thr}$ was contaminated with the other isoaccepting species of $tRNA^{Leu}$. These overlapping

TABLE I

RETENTION TIMES FOR INDIVIDUAL tRNAs FROM *E. COLI* AND RAT LIVER

The width of a particular peak is indicated in brackets (start to end of the peak).

Amino acid	*Retention time (min)*	
	tRNA from E. coli B	*tRNA from rat liver*
(1) Alanine	95 (94.23–96.50)	5 (4.50–7.07)
	110 (108.97–113.53)	11 (10.20–11.93)
(2) Arginine	66 (65.00–66.23)	53 (52.00–53.20)
		63 (62.33–62.53)
		69 (66.93–70.90)
		77 (75.50–78.50)
(3) Aspartic acid	57 (56.01–57.90)	27 (26.97–27.17)
(4) Glutamic acid	18 (17.00–19.27)	10 (9.20–10.80)
(5) Glycine	32 (31.03–33.20)	8 (7.07–8.97)
(6) Histidine	69 (68.87–69.90)	– –
(7) Isoleucine	50 (46.00–50.53)	41 (39.60–42.80)
		49 (45.63–50.27)
(8) Leucine	43 (42.23–43.30)	24 (23.80–24.37)
	116 (115.03–117.20)	33 (32.63–33.83)
		51 (49.43–53.20)
		75 (74.00–75.90)
(9) Lysine	59 (58.30–62.07)	38 (36.50–39.00)
		56 (55.20–56.93)
		62 (61.23–62.33)
(10) Methionine	48 (46.00–50.53)	36 (34.97–36.50)
(11) Phenylalanine	97 (96.63–97.80)	100 (99.90–100.23)
		112 (108.83–114.07)

TABLE I (*continued*)

Amino acid	*Retention time (min)*	
	tRNA from E. coli B	*tRNA from rat liver*
(12) Serine	108 (105.80–108.93)	37 (36.50–39.00) 94 (93.33–94.87) 109 (108.83–109.53)
(13) Threonine	47 (46.00–50.53)	73 (72.20–73.53) 76 (75.30–76.77) 83 (82.90–83.50)
(14) Tyrosine	144 (140.60–145.87)	16 (15.77–17.53) 33 (32.63–33.83) 40 (39.60–42.80) 88 (87.77–89.43)
(15) Valine	27 (24.63–27.90)	5 (4.50–7.07) 14 (13.57–14.23) 20 (18.53–20.83) 28 (27.17–28.53)

tRNA species were relatively easily purified by rechromatography under isocratic conditions deduced from the appropriate portions of the gradient used for the original separation (results not shown).

In comparison with eukaryotic tRNA, only two isoaccepting species of $tRNA^{Leu}$ and $tRNA^{Ala}$ were separated from bacterial tRNA. The separation of both these species was very good. Results of the resolution of individual bacterial tRNAs are summarized in Fig. 1.

In contrast to bacterial tRNA, not one tRNA species from rat liver was isolated in a pure form during a single experiment.

In spite of this, a good resolution of several isoaccepting tRNAs was obtained. This holds true for $tRNA^{Gly}$, $tRNA^{Ile}$ and $tRNA^{Phe}$, tRNAs for aspartic acid and arginine, for alanine and serine and for glutamic acid and lysine. However, all these tRNA species were contaminated with tRNAs for various other amino acids. In comparison with bacterial tRNA, $tRNA^{Met}$ and $tRNA^{Thr}$ were fully resolved. Moreover, a partial separation of both tRNA species accepting L-methionine was demonstrated.

With the exception of tRNAs for glycine and for aspartic acid, all the other

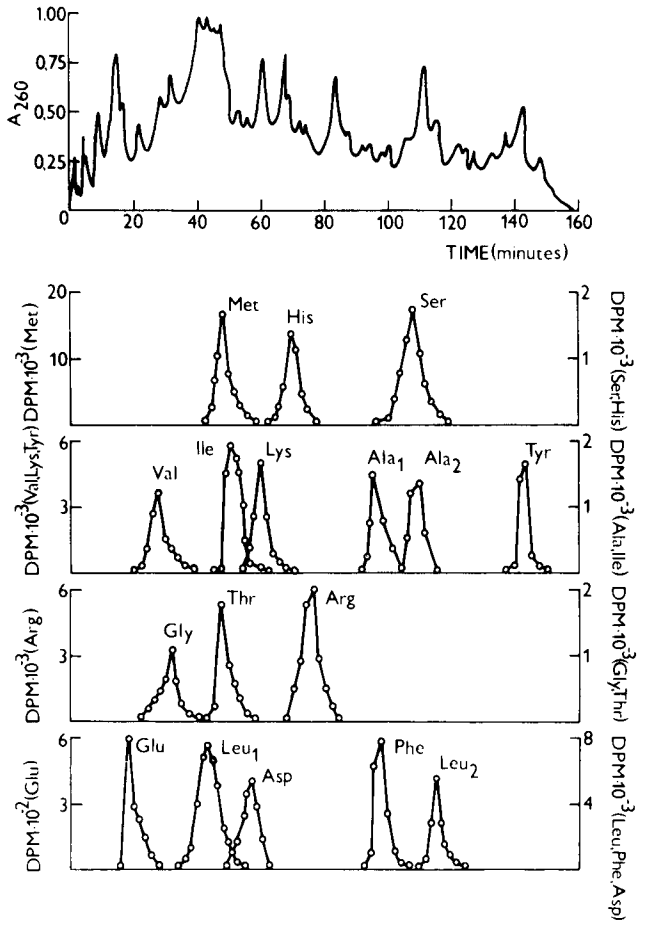

Fig. 1. Separation of total tRNA from *E. coli* by HPLC. A 2.5-mg amount of unfractionated tRNA in 50 μl of the initial buffer (see below) was injected on to a column of large pore silica bonded with C_3 alkyl chains (Beckman Ultrapore C_3RPSC, 75 mm × 4.6 mm I.D.) eluted with a linear gradient of 10 m*M* Tris–HCl buffer, pH 7.55, 10 m*M* magnesium chloride, 200 m*M* sodium chloride and 8% (v/v) methanol added to 10 m*M* Tris–HCl buffer, pH 7.55 containing 10 m*M* magnesium chloride and 1 *M* sodium chloride. 50% of the gradient was delivered during 100 min after the sample injection and the rest during the next 50 min. Details are described in the Materials and Methods section. Top, the A_{260} profile; below, the acceptor activity of fractions for individual amino acids. As described in detail in the Materials and Methods section, tRNA in each third fraction was precipitated with ethanol and after drying it was charged with all fifteen labelled amino acids used in the presence of aminoacyl-tRNA synthetases from *E. coli* and the radioactivity present in aminoacyl-tRNA was assayed. Only amino acids giving a positive charging response are shown.

tRNA species from rat liver were resolved into at least two isoaccepting species. An excellent resolution of at least four isoaccepting tRNAs for tyrosine and serine as well as a partial separation of two species of $tRNA^{Glu}$, $tRNA^{Lys}$, $tRNA^{Phe}$, $tRNA^{Thr}$ and several isoaccepting species of tRNAs for valine, leucine and arginine were obtained. Separations of individual tRNA species from rat liver are demonstrated in Figs. 2 and 3.

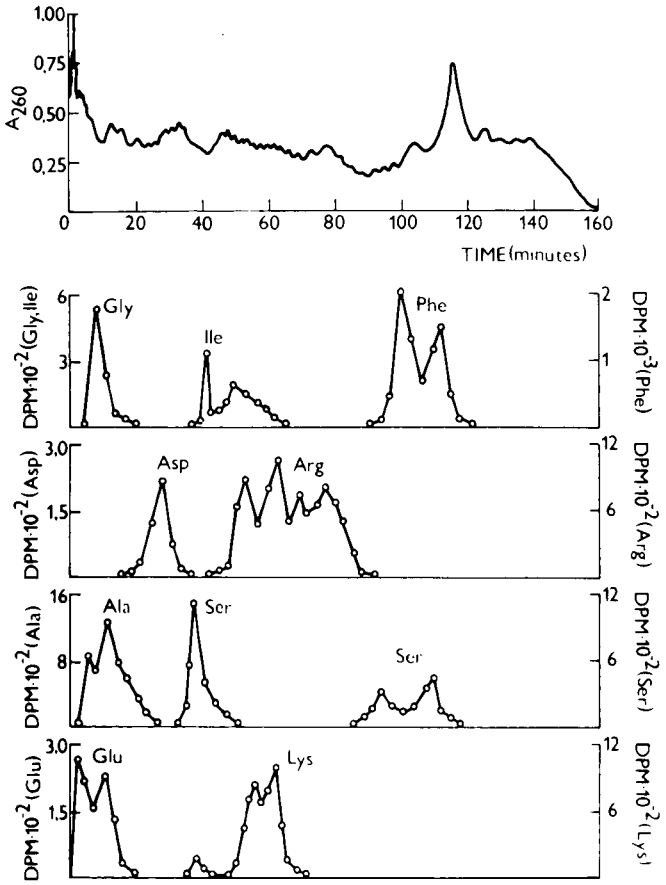

Fig. 2. Separation of unfractionated tRNA from rat liver by HPLC. A 2.5-mg amount of tRNA in 50 μl of the initial buffer was separated on a column of large pore silica bonded with C_3 alkyl chains. See Fig. 1 and the Material and Methods section for experimental details. Fractions were charged with aminoacyl-tRNA synthetases from rat liver.

No charging with any of the amino acids tested was demonstrated in a rather broad range of fractions eluted between 120 and 160 min. Agarose gel electrophoresis revealed that these fractions do not contain tRNA but 5S RNA and further nucleotide impurities of unknown nature (results not shown).

DISCUSSION

Because of an high and rapid resolution of individual RNAs, HPLC is apparently superior to earlier techniques used for the separation of tRNA species. Nevertheless, liquid chromatography at atmospheric pressure may be useful for some special purposes. Thus an excellent separation of isoaccepting tRNA species from *E. coli* was reported using polystyrene anion exchangers[16].

In our present experiments we were able to identify tRNAs for fifteen different

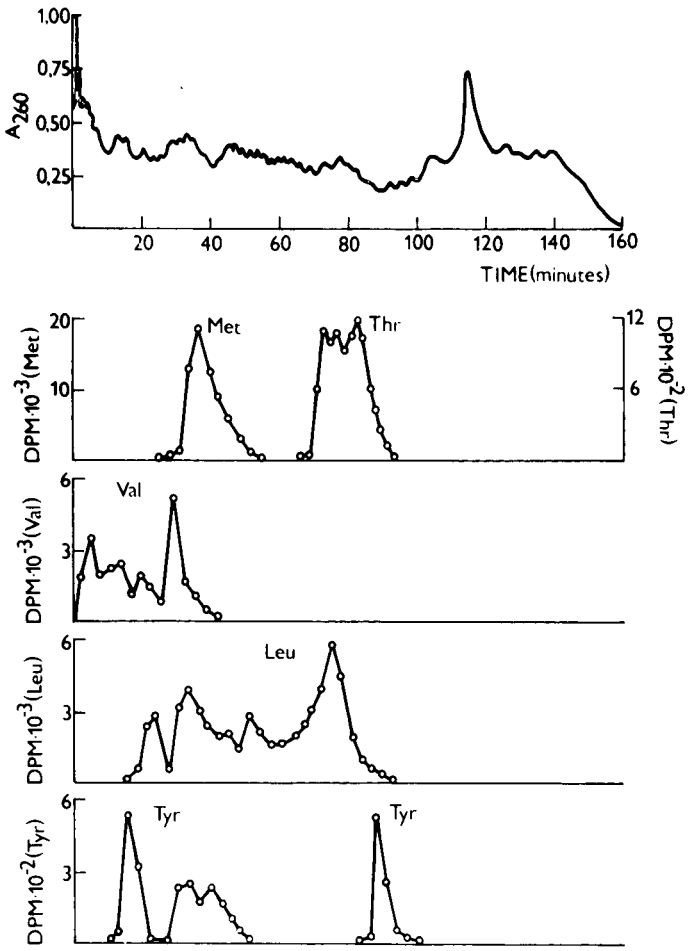

Fig. 3. Separation of unfractionated tRNA from rat liver by HPLC (continued from Fig. 2). Details are given in Fig. 2 and in the Materials and Methods section.

amino acids. This is comparable with the results of Bischoff and McLaughlin[12] who reported the identification of tRNA species for thirteen different amino acids after their separation using an ionic–hydrophobic mixed-mode matrix for HPLC.

The novelty of the method described in this paper lies in the use of short alkyl chains bonded to silica and of a decreasing salt gradient in order gradually to reduce hydrophobic interactions. In our hands, supports containing short alkyl chains were found superior to those with long chains (ODS)[17]. Also, reversed eluting gradients with decreasing concentrations of sodium chloride but increasing contents of methanol were more useful than simpler gradients where only one solvent component was changed.

The procedure described seems to be useful for a micropreparative isolation of tRNA species from *E. coli*. Some species may be isolated pure in a single experiment and several others are purified by rechromatography. On the other hand, it is not

suitable for the purification of tRNA species from eukaryotic cells. Very complex mixtures are obtained in a single experiment and it would be very difficult to use them as a starting material for the purification of individual tRNAs. For the purification of eukaryotic initiator tRNA, a combination of other techniques seems to be more advantageous[18]. However, because of the excellent resolutions of isoaccepting species of tRNA obtained by the present method with tRNA from rat liver, this technique may be useful for the separation of isoaccepting tRNAs for particular amino acids if the presence of tRNAs for other amino acids is not an hindrance. It can also be employed for the removal of 5S RNA and other nucleotide impurities that may be present in preparations of eukaryotic tRNA[14].

REFERENCES

1 I. C. Gillam and G. M. Tener, *Methods Enzymol.* 20 (1971) 55.
2 W. M. Stanley, *Anal. Biochem*, 48 (1972) 202.
3 A. D. Kelmers, G. D. Novelli and M. P. Stulberg, *J. Biol. Chem.*, 240 (1965) 3979.
4 L. W. McLaughlin, *J. Chromatogr.*, 418 (1987) 51.
5 R. Dion and J. Cedergren, *J. Chromatogr.*, 152 (1978) 131.
6 J. D. Pearson, M. Mitchell and F. E. Regnier, *J. Liq. Chromatogr.*, 6 (1983) 1441.
7 S.-B. Zhang, P. M. Bronskill, Q.-S. Wang and J. T.-F. Wong, *J. Chromatogr.*, 360 91986) 282.
8 Z. El Rassi and Cs. Horváth, *J. Chromatogr.*, 326 (1985) 79.
9 R. P. Singhal, *J. Chromatogr.*, 266 (1983) 359.
10 R. Bischoff, E. Graeser and L. W. McLaughlin, *J. Chromatogr.*, 257 (1983) 305.
11 L. Graeve, J. Kruppa and P. Földi, *J. Chromatogr.*, 268 (1983) 506.
12 R. Bischoff and L. W. McLaughlin, *Anal. Biochem.*, 151 (1985) 526.
13 J. Hradec, *Carcinogenesis*, 9 (1988) 837.
14 H. Rogg, W. Wehrli and M. Staehelin, *Biochim. Biophys. Acta*, 195 (1969) 13.
15 T. Maniatis, E. Fritsch and J. Sambrok, *Molecular Cloning: a Laboratory Manual*, Cold Spring Harbor Laboratory, Cold Spring Harbor, NY, 1982, p. 150.
16 R. P. Singhal, G. D. Griffin and G. D. Novelli, *Biochemistry*, 15 (1976) 5083.
17 M. Doležal, unpublished results.
18 M. Doležal and J. Hradec, *Anal. Biochem.*, (1989) in press.

Journal of Chromatography, 463 (1989) 419–428
Elsevier Science Publishers B.V., Amsterdam — Printed in The Netherlands

CHROM. 21 049

DETERMINATION OF NON-VOLATILE N-NITROSAMINES IN BABY BOTTLE RUBBER NIPPLES AND PACIFIERS BY HIGH-PERFORMANCE LIQUID CHROMATOGRAPHY–THERMAL ENERGY ANALYSIS

NRISINHA P. SEN* and STEPHEN W. SEAMAN
Food Research Division, Bureau of Chemical Safety, Food Directorate, Health Protection Branch, Health and Welfare Canada, Ottawa K1A 0L2 (Canada)
and
SANTOSH C. KUSHWAHA
Scientific and Laboratory Services Division, Product Safety Branch, Consumer and Corporate Affairs Canada, Ottawa K1A 0C9 (Canada)
(Received August 12th, 1988)

SUMMARY

A method is described for the determination of non-volatile N-nitrosamines in baby bottle rubber nipples and pacifiers. It consists of extraction of the sample with dichloromethane in the presence of ascorbyl palmitate (an inhibitor of artifactual formation of nitrosamines), clean-up on silica or basic alumina, and final analysis by high-performance liquid chromatography–thermal energy analysis, a technique which is highly specific for N-nitroso compounds. The method worked well for the determination of four rubber-related non-volatile nitrosamines, namely, N-nitrosomethylphenylamine, N-nitrosoethylphenylamine, N-nitrosodicyclohexylamine, and N-nitrosodibenzylamine (recoveries from spiked samples >80%; detection limit, *ca.* 5 μg/kg for each). Eighteen out of twenty four samples analyzed were found to contain varying levels (mean, 41 μg/kg; range, 8–146 μg/kg) of N-nitrosodibenzylamine. The identity of the compound was confirmed by gas chromatography–thermal energy analysis as well as by gas chromatography–mass spectrometry analyses.

INTRODUCTION

Since the initial report of the finding of volatile N-nitrosamines in elastomers and elastomer-based products[1], considerable data have been published on the occurrence of these compounds in various rubber-based consumer products[1,2], especially baby bottle rubber nipples and pacifiers[3–6]. The nitrosamines in these products mainly originate or form from various amine derivatives which are commonly used as accelerators or stabilizers during the rubber vulcanization process. The following volatile nitrosamines have been detected in rubber chemicals and rubber products: N-nitrosodimethylamine (NDMA), N-nitrosodiethylamine (NDEA), N-nitrosodi-*n*-butylamine (NDBA), N-nitrosodi-*sec.*-butylamine (NDSBA), N-nitroso-

0021-9673/89/$03.50

piperidine (NPIP), N-nitrosopyrrolidine (NPYR), and N-nitrosomorpholine (NMOR)[1–6]. All of these nitrosamine are potent carcinogens in laboratory animals[7]. Further details regarding the chemistry of formation of these nitrosamines in rubber, their concentration in rubber factory atmosphere and in various consumer products, and about the significance of the findings can be obtained from several publications[4–6,8,9].

The occurrence of nitrosamines in baby bottle rubber nipples and pacifiers is of special concern because traces of these chemicals may migrate to infant saliva during sucking, and then be ingested. Furthermore, the nitrosamines can also migrate to liquid infant foods which come in contact with rubber nipples during home sterilization or during storage[2–5]. Because of these concerns, various governments in different countries have passed regulations limiting the total volatile nitrosamine content of such products[10,11]. The rubber industry also responded well to this concern, and reformulated the rubber curing formulations which resulted in a significant decline in the levels of volatile nitrosamines in such products. Recent surveys by both the Canadian and U.S.A. government agencies have confirmed this trend[10,11].

Although considerable data are available on the volatile nitrosamine contents of various rubber nipples and pacifiers, corresponding data for the non-volatile N-nitrosamines, which may also occur in such products[2,12], have been lacking. This has been mainly attributed to lack of suitable analytical methodologies for these compounds. Such data are, however, urgently needed for a full assessment of the health hazard to infants that may arise from the use of such products. In this paper, we report a high-performance liquid chromatography–thermal energy analysis (HPLC–TEA) method for the determination of non-volatile N-nitrosamines in baby bottle rubber nipples and pacifers. Some data on the non-volatile nitrosamine contents of such products are also reported.

EXPERIMENTAL*

Materials

Glass-distilled dichloromethane (DCM) was purchased from Burdick & Jackson, (Muskegon, MI, U.S.A.) and was redistilled from an all-glass apparatus and tested for its suitability for nitrosamine analysis as reported previously[13]. Glass-distilled *n*-pentane, *n*-hexane, and acetone were obtained from Caledon Labs. (Georgetown, Canada). The last three solvents were passed through highly activated (<0.1% water content) basic alumina before use. Basic alumina for column chromatography and ascorbyl palmitate were purchased from ICN Biomedicals, K&K Laboratories (Plainview, NY, U.S.A.) and Kieselgel 60 (Si-60) (70–230 mesh) was obtained from Merck (Darmstadt, F.R.G.). Aliquots of alumina and Si-60 were heated in an oven and then deactivated by adding appropriate amounts of water (1.5 and 6%, respectively) as described previously[14]. All other reagents used were of analytical grade.

The nitrosamine standards were purchased or obtained as gifts from various sources as indicated below: N-nitrosodibenzylamine (NDBzA) from W. Fiddler of

* Reference to brand or firm name does not constitute endorsement by the Consumer and Corporate Affairs of Canada or by Health and Welfare Canada over others of a similar nature not mentioned.

USDA (Philadelphia, PA, U.S.A.); N-nitrosoethylphenylamine (NEPhA), N-nitrosomethylphenylamine (NMPhA), N-nitrosodicyclohexylamine (NDChA), from ISCONLAB (Heidelberg, F.R.G.); N-nitroso-4-hydroxybutyl-*n*-butylamine (NHBBA) from M. Okada of Tokyo Biochemical Research Institute (Tokyo, Japan); diphenylnitrosamine (NDPhA) and N-nitrosodiethanolamine (NDELA) from Thermedics, and dinitrosopentamethylenetetramine (NDPMTA) from W. Lijinsky of NCI Frederick Cancer Research Facility (Frederick, MA, U.S.A.).

Apparatus

The HPLC system consisted of two solvent delivery systems (pump Model 6000A, Waters Assoc., Milford, MA, U.S.A.) connected to a solvent programmer (Model 660, Waters Assoc.) and a Rheodyne injector (Model 7125; sample loop 20 or 50 μl). The chromatographic separation was carried out using a Alltech 250 mm × 4.6 mm I.D. stainless-steel column packed with Lichrosorb Si 100 (5 μm) (column 1) or Econosil silica (5 μm) (column 2). The mobile phases and programming conditions were as follows: 1% acetone in *n*-hexane initially, then programmed to 40% acetone in *n*-hexane in 15 min using curve 10 of the solvent programmer. The flow-rate was 2 ml/min. Prior to use, the solvents were passed through basic alumina (to remove nitrosamine contamination) as described under *Materials*.

The tubing from the exit end of the HPLC column was connected via a three-way switching valve to a Model 502 thermal energy analyzer (Thermedics). This switching valve was used to divert the column flow to a waste reservoir, when TEA was not in use. This was also done every time the analyzer was switched to the vent mode or purge mode. (Caution: failure to divert the flow as above would build-up pressure inside the analyzer furnace and also may promote carbon deposition on the pyrolyzer tube causing noise problems with decreased sensitivity). Other TEA operating conditions were as follows: vacuum, 0.8 mm; furnace temperature, 600°C; cold trap-dry ice and ethanol.

In some cases, HPLC–TEA results were confirmed by gas chromatography (GC)–TEA. A Varian gas chromatograph (Model Vista 6000) equipped with a 10 ft. × $\frac{1}{4}$ in. coiled glass column (2 mm I.D.) packed with 10% Carbowax 20M on Chromosorb W, HMDS-treated, 80–100 mesh, or with 3% OV-225 on Chromosorb W-HP, 80–100 mesh, was used for this purpose. The temperature programming mode for both columns was as follows: 2 min at 120°C, then 6°C/min to 150°C with 5 min hold at 150°C, followed by further heating to 220°C at 10°C/min (held at 220°C for 10 min). Injector and transfer line temperatures were 200 and 380°C, respectively.

A VG analytical hybrid mass spectrometer system (Model 7070EQ) was used for mass spectrometric (MS) confirmation. Both selected-ion monitoring at a resolution of 2000 (10% valley definition) and repetitive exponential scanning were used for MS confirmation. The instrument was operated as described before[12,15].

Extraction and clean-up procedure

A 3–5 g aliquot of the sample (cut into small pieces) was mixed with 100 mg ascorbyl palmitate (nitrosation inhibitor), the mixture extracted with DCM by overnight shaking at room temperature and then again by an ambient temperature column extraction procedure as described previously[4,13] for the determination of volatile nitrosamines. The final extract was then carefully concentrated to 1 ml using

a Kuderna–Danish concentrator[13]. A 6–8 μl aliquot of this extract, if desired, could be analyzed by GC–TEA for the presence of volatile nitrosamines[4]. The remaining extract was cleaned-up as described below for the determination of non-volatile nitrosamines.

About 9 ml anhydrous *n*-pentane were mixed with the extract and the mixture was passed through a basic alumina (10 g; 1.5% water content) column (2 cm I.D.) at a flow-rate of 1–2 ml/min. The column was washed with 40 ml anhydrous *n*-pentane and the rinsing discarded. The nitrosamines adsorbed on the column were eluted with 50 ml DCM, the eluate concentrated to 1.0 ml as described previously[13], and a 20–50 μl aliquot analyzed by HPLC–TEA using the conditions mentioned above.

Prior to GC–MS confirmation, the alumina (10 g) clean-up step was repeated using a narrower column (1 cm I.D.) and collecting five successive 10-ml DCM eluates. Each eluate was separately concentrated and analyzed by HPLC–TEA as above. The fraction containing bulk of the nitrosamine (NDBzA) was used for GC–MS confirmation. This procedure provided a cleaner extract because of finer separation of NDBzA from the impurities.

For plastic-based products, a different clean-up step was used. After the overnight extraction of the sample with DCM and the subsequent ambient temperature column extraction, the combined DCM extract was concentrated to *ca.* 10 ml (instead of 1 ml). One-half of the extract was quantitatively transferred into a 250-ml Erlenmeyer flask and mixed with 50 ml *n*-pentane. The flask containing the mixture along with white precipitate, which often formed upon mixing with *n*-pentane, was cooled for 30–45 min inside an insulated box containing dry ice. The mixture was then quickly filtered through a coarse sintered glass funnel containing *ca.* 1 cm layer of granular anhydrous sodium sulfate. Any remaining precipitate was washed with two 10-ml portions of cold *n*-pentane and filtered as above. The combined filtrate was cleaned-up by passing (1–2 ml/min) through a column (2 cm I.D.) of Si-60 (10 g; 6% water content) and washing the column with two 5 ml portions of *n*-pentane. Finally, the column was successively eluted with 50-ml portions of (a) 20% DCM in *n*-pentane, (b) 50% DCM in *n*-pentane, and (c) DCM. The last fraction was concentrated to 1 ml and then analyzed by HPLC–TEA as above.

RESULTS AND DISCUSSION

As previously stated, the method described above is an extention of our earlier method developed for the determination of volatile nitrosamines in baby bottle rubber nipples and pacifiers[4,13]. Since the extraction used in the two methods is the same, aliquots of the same DCM extract can be used for the determination of non-volatile nitrosamines without any additional work except the minor clean-ups on basic alumina or silica as described. The method worked well with all the rubber nipples and pacifiers tested. Since TEA is highly specific for N-nitroso compounds, very little interference was observed (Figs. 1 and 2).

It should be noted, however, that both the resolution and retention times of various nitrosamine peaks may vary depending on the column used for HPLC separation. For example, good resolution of NMPhA and NDChA was obtained with column 1 in Fig. 1 but not with column 2 used to obtain Fig. 2, even though both columns were packed with similar packing materials. Failure to separate the above two

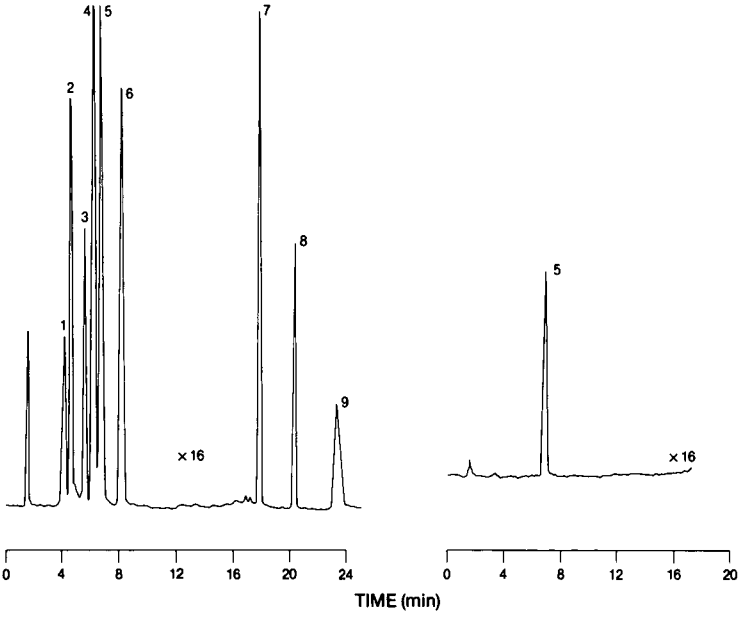

Fig. 1. HPLC–TEA chromatograms of several nitrosamine standards (left) and of NDBzA isolated from a rubber-based pacifier (right). Details of column and mobile phase are given in the Experimental section. Peak identification: 1 = NDPhA, 2 = NEPhA, 3 = NDChA, 4 = NMPhA, 5 = NDBzA, 6 = N-nitrosodi-*n*-propylamine, 7 = NHBBA, 8 = NDPMTA, 9 = NDELA. About 20 ng of each was injected using column 1 for analysis.

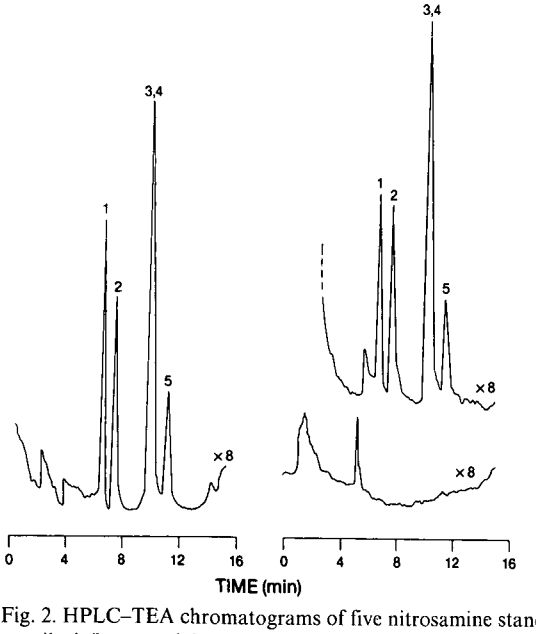

Fig. 2. HPLC–TEA chromatograms of five nitrosamine standards, *ca.* 8 ng each (left); of a rubber nipple, unspiked (bottom-right); and of the same nipple spiked with *ca.* 40 ppb each of the five nitrosamines (top-right). HPLC separation was carried out using column 2. Peak identification: same as in Fig. 1.

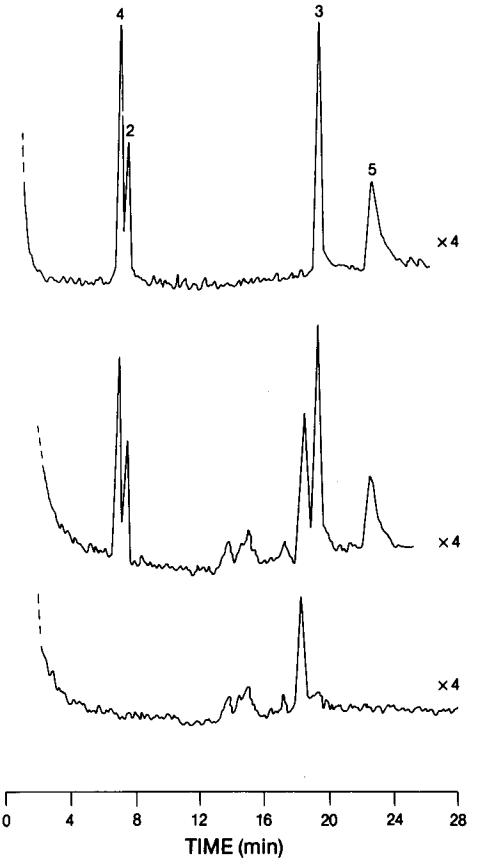

Fig. 3. GC–TEA chromatograms using OV-225 column. Bottom, 10 μl injection of the unspiked rubber nipple extract (from Fig. 2); middle, 10 μl injection of the spiked sample (from Fig. 2); and top, 2 ng each of five standards. GC conditions are described in the Experimental section. Peak identification is the same as in Fig. 1. The sample showed an unidentified peak eluting at *ca.* 18 min.

nitrosamines by HPLC–TEA using column 2 was, however, a minor drawback because these two compounds could easily be separated by GC (Fig. 3). On the other hand, NDPhA could not be measured by GLC–TEA because of its thermal instability[16]; the HPLC–TEA technique had to be used for this purpose. The two techniques were, therefore, complementary to each other.

The recoveries of NMPhA, NEPhA, NDChA, and NDBzA, the four most rubber-associated non-volatile nitrosamines, added in DCM to rubber nipples at 20–50 μg/kg levels at the start of the analysis were highly satisfactory (80–110%). Typical chromatograms from a recovery study experiment are shown in Fig. 2. Similar good recoveries have been observed with the method for the volatile nitrosamines[4,13]. The recovery of a fifth rubber-related non-volatile nitrosamine, NDPhA, was, however, slightly lower (60–70%; also shown in Fig. 2). This was demonstrated to be due to its instability. When standard NDPhA alone (without any rubber nipple) was allowed to stand overnight in DCM and the solution concentrated to 1 ml using

a Kuderna–Danish concentrator, the recovery was still not improved. The N–NO bond in NDPhA is very weak[16] which explains its instability and good transnitrosation property. Because of this, Spiegelhalder and Preussmann[8] recommended discontinuation of its use as rubber curing retarder. Instead, they proposed to replace it with cycohexylthiophthalimide which does not form nitrosamines. Except for NDPhA, the minimum detection limit of the other four nitrosamines was about 5 μg/kg for each compound. For plastic-based products, however, the detection limit was only 30 μg/kg. Such products alway resulted in an oily residue that could not be separated from the above mentioned nitrosamines. Because of this, a less concentrated extract was injected into HPLC–TEA resulting in a lower overall sensitivity.

Fig. 1 also shows HPLC separation of three highly polar N-nitroso compounds, namely, NHBBA (peak 7), NDPMTA (peak 8), and NDELA (peak 9). Although these compounds are not expected to be present in baby bottle rubber nipples and pacifiers, they were included just to demonstrate the usefulness of the technique. If present in the samples, these compounds could be extracted using the described technique but a stronger eluent (*e.g.*, ethyl acetate, ethanol) must be used to elute them from the alumina column[17]. We have developed previously a method for the determination of these compounds in cured meats[17]. Most of the volatile nitrosamines normally detected in such products eluted between peaks 6 and 7 under the HPLC conditions used. Only NDBA eluted between peaks 4 and 5. Therefore, if NDBA is present, as determined by preliminary analysis for volatile nitrosamines[4,13], the result for non-volatile nitrosamines must be confirmed, as was done here, by GC–TEA and/or GC–MS.

The method was used to analyze 24 samples of various rubber nipples and pacifiers. Six were negative for all of the four nitrosamines and the remaining samples contained only NDBzA (Table I). To our knowledge, this is the first reported finding of NDBzA in such products. The same samples were also analyzed for volatile nitrosamines[11]. The data indicated a significant decline in the levels of these compounds in such products when compared to similar monitoring data gathered 3–5 years earlier[4,12]. This reduction was attributed to recent changes in the rubber curing formulations that eliminated or employed only minimal amounts of volatile nitrosamine-forming accelerators. Unfortunately, our older surveys did not include analysis for non-volatile nitrosamines, and one cannot say with certainty whether the older samples also contained NDBzA (in addition to high levels of volatile nitrosamines). However, we have reanalyzed two remaining samples of rubber nipples from our 1985 survey[12]. Both were negative for NDBzA. This suggested that the rubber industry most likely switched to NDBzA-producing accelerators only recently. Similar observations were made by us in the case of elastic rubber nettings used for packaging cured pork products[18].

All the NDBzA-positive samples were confirmed by GC–TEA for confirmation. Although it is a non-volatile nitrosamine, it could be analyzed by GC–TEA provided a high (350–400°C) transfer line (between GC and TEA) temperature and an on-column injection technique was used. Furthermore, the identity of NDBzA in two samples (Table I) was confirmed by GC–MS using the selected-ion monitoring technique as mentioned earlier. Two characteristic fragment ions, namely, m/z 226 $M^{+\cdot}$ and m/z 181 $[M-HN_2O]^+$ were monitored simultaneously for this purpose. The mass spectrum of NDBzA isolated from the samples also matched quite well with that of the authentic standard (Fig. 4).

TABLE I

LEVELS OF N-NITROSODIBENZYLAMINE DETECTED IN DIFFERENT BRANDS OF BABY BOTTLE RUBBER NIPPLES AND PACIFIERS

Type	*Brand*	*Country of origin*	*NDBzA (μg/kg)*
Nipples			
Latex	A	U.S.A.	N*
Latex	B	U.S.A.	86
Latex	C	U.S.A.	20**; 39**
Latex	D	F.R.G.	10
Latex	E	U.S.A.	39
Latex	H	U.S.A.	14
Latex	X	F.R.G.	11
Silicone	II	Thailand	N
Latex	III	F.R.G.	29
Latex	IV	Thailand	N**; 10**
Pacifiers			
Latex	C	U.S.A.	30
Latex	E	U.S.A.	146
Latex	F	F.R.G.	71***
Latex	L	F.R.G.	18
Latex	M	U.K.	N**; N**
Latex	N	F.R.G.	8
Latex	Q	F.R.G.	24
Latex	U	F.R.G.	34
Latex	V	F.R.G.	136***
Plastic	W	U.S.A.	N
Latex	VI	F.R.G.	12

* N = Negative (< 5 μg/kg).
** Two different samples.
*** Confirmed by GC–MS.

Our present investigation suggests that majority of the baby bottle rubber nipples and pacifiers currently available to consumers in Canada contain varying levels (8–146 μg/kg) of NDBzA. The significance of the finding is, however, not clear. NDBzA is reported to be non-carcinogenic in rats[19]. This is one of the reasons that might have prompted the industry to switch from carcinogenic nitrosamine-forming accelerators to one that produces only NDBzA. In a recent study, however, it has been reported that NDBzA can induce DNA single-strand breaks in primary hepatocytes from rat and hamster[20]. Therefore, further research is desirable to fully evaluate the toxicity, if any, of NDBzA.

In summary, the HPLC–TEA method described in this paper offers a simple and rapid method for the determination of non-volatile N-nitrosamines in baby bottle rubber nipples and pacifiers. It is hoped that the method along with the GC–TEA and GC–MS confirmatory techniques will be useful for both regulatory and monitoring purposes.

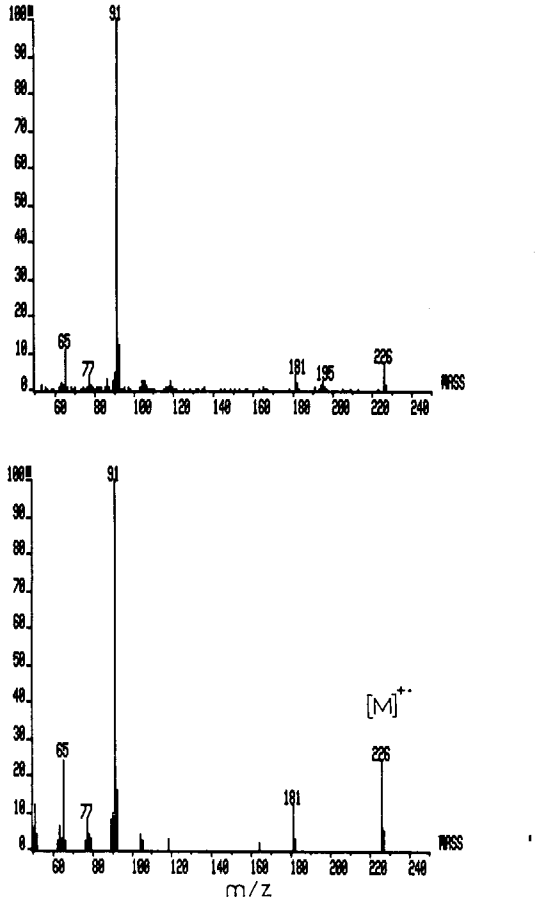

Fig. 4. Electron-impact ionization mass spectra of NDBzA standard (bottom) and that of NDBzA isolated from the pacifier containing 136 μg/kg NDBzA (Table I).

ACKNOWLEDGEMENTS

We wish to thank D. Weber of Food Research Division, HPB, for carrying out the GC–MS confirmation, and W. Fiddler, M. Okada and W. Lijinsky for providing us with the various nitrosamine standards as listed in the Experimental section.

REFERENCES

1 C. B. Ireland, F. P. Hytrek and B. A. Lasoki, *Am. Ind. Hyg. Assoc. J.*, 41 (1980) 895.
2 B. Spiegelhalder and R. Preussmann, *IARC Sci. Publ.*, 41 (1982) 231.
3 D. C. Havery and T. Fazio, *Food Chem. Toxicol.*, 20 (1982) 939.
4 N. P. Sen, S. W. Seaman, S. G. Clarkson, F. Garrod and P. Lalonde, *IARC Sci. Publ.*, 57 (1985) 51.
5 H. C. Thompson, Jr., S. M. Billedeau, B. J. Miller, E. B. Hansen, Jr. and J. P. Freeman, *J. Toxicol. Environ. Health*, 13 (1984) 615.

6 B.-G. Österdahl, *Food Chem. Toxicol.*, 21 (1983) 755.
7 R. Preussmann and B. W. Stewart, in C. E. Searle (Editor), *Chemical Carcinogens (ACS Monograph* 182) Vol. 2, American Chemical Society, Washington, DC, 2nd ed., pp. 643–828.
8 B. Spiegelhalder and R. Preussmann, *Carcinogenesis*, 4 (1983) 1147.
9 International Agency for Research on Cancer, *IARC Monographs on the Evaluation of Carcinogenic Risk of Chemicals to Humans: The Rubber Industry*, IARC, Lyon 1982, pp. 89–120.
10 D. Havery, G. A. Perfetti, B. J. Canas and T. Fazio, *Food Chem. Toxicol.*, 23 (1985) 991.
11 S. C. Kushwaha and N. P. Sen, *Can. J. Public Health*, in press,
12 N. P. Sen, S. C. Kushwaha, S. W. Seaman and S. G. Clarkson, *J. Agric. Food Chem.*, 33 (1985) 428.
13 N. P. Sen, S. W. Seaman and S. C. Kushwaha, *J. Assoc. Off. Anal. Chem.*, 70 (1987) 434.
14 N. P. Sen, *IARC Sci. Publ.*, 18 (1978) 119.
15 D. Weber, N. P. Sen and P.-Y. Lau, *Proc. 36th ASMS Conference on Mass Spectrometry and Allied Topics, San Francisco, CA, June 5–10, 1988*, American Society of Mass Spectrometry, San Francisco, CA, 1988, Abstr. No. MPB 14.
16 D. H. Fine and F. Rufeh, *IARC Sci. Publ.*, 9 (1974) 40.
17 N. P. Sen, S. Seaman and L. Tessier, *IARC Sci. Publ.*, 41 (1982) 185.
18 N. P. Sen, S. W. Seaman, P. A. Baddoo and D. Weber, *J. Food Sci.*, 53 (1988) 731.
19 H. Druckrey, R. Preussmann, S. Ivankovic and D. Schmaehl, *Z. Krebsforsch.*, 69 (1967) 103.
20 P. Schmezer, B. L. Pool, R. Preussmann and D. Schmaehl, *IARC Sci. Publ.*, 84 (1987) 270.

Journal of Chromatography, 463 (1989) 429–440
Elsevier Science Publishers B.V., Amsterdam — Printed in The Netherlands

CHROM. 21 032

QUANTITATIVE THIN-LAYER CHROMATOGRAPHY OF *NICOTIANA TABACUM* LEAF SURFACE COMPONENTS

DAVID R. LAWSON*,* and DAVID A. DANEHOWER
Department of Crop Science, North Carolina State University, Raleigh, NC 27695-7620 (U.S.A.)
(Received September 28th, 1988)

SUMMARY

A thin-layer chromatographic (TLC) method and scanning densitometry technique have been developed for quantitation of major primary and secondary metabolites of *Nicotiana tabacum* L. leaf surface components. These components were resolved after a single development with isopropanol–chloroform–methylene chloride–hexane (7:8:6:79) using laned silica gel G TLC plates. R_F values were reproducible to $\pm$ 0.01 units. Quantitation of all components of interest was accomplished by charring with 30% fuming sulfuric acid followed by densitometry using white light. Overall, charring results were semiquantitative ($\leqslant$ 10% relative error), but were quantitative ($\leqslant$ 6% relative error) for all major secondary metabolites except the sucrose esters. Quantitation of three secondary metabolites was also accomplished by scanning uncharred plates at a wavelength of 200 nm. In general, UV scanning provided semiquantitative results. For both charring and UV quantitation methods, highly correlated, curvilinear responses between mass and integration area were obtained. Advantages and limitations of these procedures *versus* an existing gas chromatographic procedure and their potential implementation are discussed.

INTRODUCTION

The leaf surface of *Nicotiana tabacum* L. and several closely related species is covered with both a cuticular wax and a gummy exudate, which is synthesized and secreted by glandular leaf trichomes[1–3]. This combined cuticular material consists of both primary and secondary metabolites (Fig. 1). Many of these leaf surface compounds contribute to cured leaf quality[4–7] and to the defense or susceptibility to other organisms[8–14].

Previously, thin-layer chromatography (TLC) of *Nicotiana* green leaf surface components has been limited to qualitative identification of selected constituents. Reid[15] used normal- and reversed-phase TLC to selectively separate major cuticular chemical classes and compounds. Zador and Jones[16] separated *N. stocktonii* alkaloids

* Current address: Department of Horticulture, Ohio State University, Columbus, OH 43210-1096, U.S.A.

0021-9673/89/$03.50

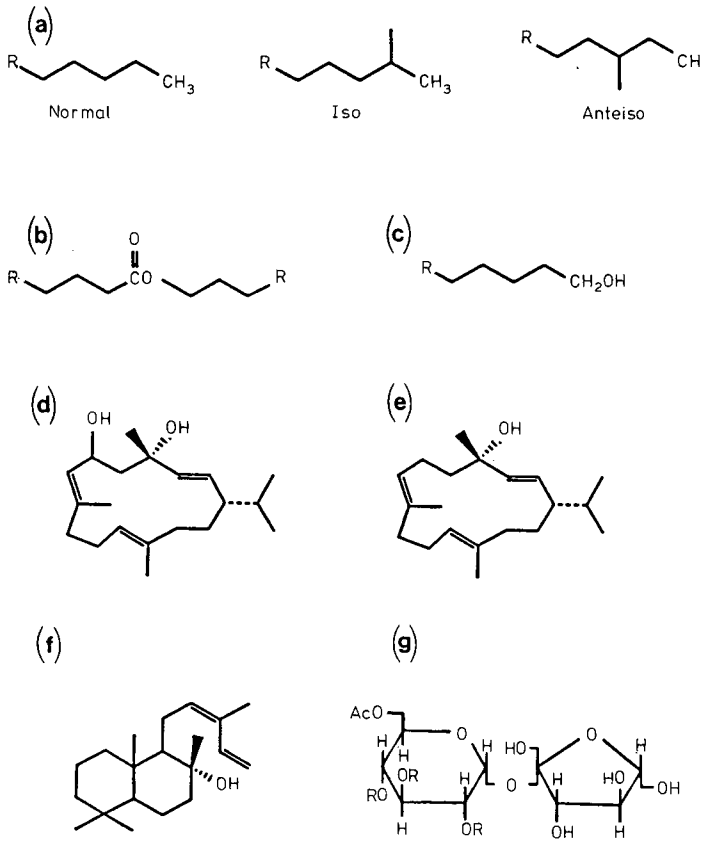

Fig. 1. Major primary and secondary metabolites of *Nicotiana tabacum* leaf surface constituents. (a) Hydrocarbons.; (b) wax esters; (c) fatty alcohols; (d) α- and β-4,8,13-duvatriene-1,3-diol; (e) α- and β-4,8,13-duvatriene-1-ol; (f) *Z*-abienol; (g) sucrose esters (R = C_3–C_8 fatty acids). AC = acetyl.

on Kieselguhr TLC plates using chloroform–methanol (100:40) and chloroform–methanol–ammonium hydroxide (90:10:1). General screening of plants for labdane and duvane diterpenoid production has been performed using Kieselgel TLC plates developed in chloroform–methanol (100:2)[17–19].

To date, no single TLC procedure exists by which the major metabolites of the *Nicotiana* leaf surface (Fig. 1) can be resolved and quantitated. Severson *et al.*[20] has developed an analytical gas chromatographic procedure for quantitation of major cuticular wax components; but this procedure requires sample derivatization before analysis and an analysis time of approximately 1 h. Due to the influence these plant products have on crop quality and the plant's ecology, development of a rapid, high-throughput screening procedure would benefit entomologists, plant pathologists, and plant breeders who are interested in these chemical traits and who require rapid results on large numbers of phenotypes. The purpose of this work was to develop a quantitative TLC (QTLC) procedure to screen leaf surface extracts of *N. tabacum* and related species.

EXPERIMENTAL

Preparation of standards and leaf surface extracts

Isolation of α-4,8,13-duvatriene-1,3-diol (ADVT), β-4,8,13-duvatriene-1,3-diol (BDVT), α- and β-4,8,13-duvatriene-1-ols (DVT-monols), *Z*-abienol (*Z*-AB), and mixtures of 6-O-acetyl-2,3,4-tri-O-acyl-α-D-gluco-pyranosyl-β-D-fructofuranoside, in which the 2, 3, and 4 positions are esterified with C_3–C_8 fatty acids (sucrose esters, SE) was as described elsewhere[21]. *n*-Tetracosane (C_{24} hydrocarbon, HC), octadecyl stearate (wax ester, WE), and *n*-docosanol (fatty alcohol, DOC) were purchased from Analabs/Foxboro (North Haven, CT, U.S.A.). Mixed standard solutions of 1 and 0.1 mg/ml/component were prepared in chloroform immediately prior to analysis.

Preparation and extraction of green bud leaves of field-grown Samsun, greenhouse-grown Burley 21, and greenhouse-grown flue cured [experimental (Coker 209 × NC602) × *N. africana* maternal derived haploids] varieties of *N. tabacum* were as described previously[22]. The resulting volumes (20 ml) from sample workups were quantitatively transferred to calibrated test tubes and reduced to 1 ml under a stream of nitrogen at 40°C on a Pierce Reactitherm® heating block. Samples were stored 1–2 days under nitrogen atmosphere at −80°C until needed.

Plate preparation

Analtech (Newark, DE, U.S.A.) Uniplate silica gel G precoated TLC plates (10 × 20 cm) were predeveloped at least three times in methylene chloride–methanol (1:1). A tight band of contamination concentrated at the top of the plate and was removed. Plates were divided into ten 1-cm wide lanes. The plates were then activated and equilibrated to 52% humidity over a saturated aqueous solution of sodium dichromate[23].

Spotting

Equilibrated plates were removed from the humidity chamber and quickly covered with a clean glass plate to maintain activation[23]. Appropriate volumes of mixed standard solutions and 4 μl of crude leaf surface extract were applied in 1-μl doses 1.5 cm from the bottom of the plate using a Nanomat spotting device (CAMAG Scientific). Complete drying was allowed between applications when multiple doses were required. For establishing calibration curves, sample dosages were randomly assigned to the lanes of individual plates. Each plate represented a replicate, and three replicates were run.

Development

After mixed standard solution or sample applications had completely dried, plates were developed in a rectangular chamber designed to accommodate a 20 × 20 cm thin-layer plate. The mobile phase was isopropanol–chloroform–methylene chloride–hexane (7:8:6:79). The developing tank was lined with a saturation pad and was pre-saturated with the vapor phase of the developing solvent. Development was carried out for 15 cm and allowed to overrun[23] 5 min. Plates were then removed from the developing chamber and dried 5 min using a hand-held hot air gun. Fresh mobile phase was used for each development.

Charring

The charring procedure employed was a slight modification of that developed by Martin and Allen[25]. The charring apparatus consisted of a Corning PC-101 hot plate upon which was placed a 30.5 × 30.5 × 1.3 cm aluminum block. A 25.4 × 25.4 cm Corning pyroceram® plate was used to cover the aluminum block to protect it from liquid acid. A 10 × 20 × 0.16 cm glass plate rested on the pyroceram plate and served as a platform on which the TLC plate was placed in order to prevent liquid acid from contacting the adsorbent layer during charring. To complete the charring chamber, a pyrex® casserole dish lid was used as a cover to secure an atmosphere of sulfur trioxide fumes.

To char the separated components, a glass wool plug was soaked with 30% fuming sulfuric acid (Fisher Scientific, St. Louis, MO, U.S.A.) and spread over the undersurface of the casserole lid using acid resistant tongs. Two glass wool plugs saturated with 30% fuming sulfuric acid were placed on either side of the TLC plate to ensure a continuous supply of sulfur trioxide fumes. Charring began by covering the TLC plate and glass wool plugs with the reagent-coated casserole lid. The hot plate was steadily heated by adjusting a transformer to a setting predetermined to heat the plate from room temperature to 180°C in 30 min. After the 30-min period, charring was terminated by removing the casserole lid.

Quantitation

Plates were scanned and quantitated using a CAMAG TLC Scanner II equipped with a Spectra-Physics SP4290 integrator and accompanying TLC scanning software. A slit width of 0.6 mm, a slit length of 8 mm, and a monochromator bandwidth of 30 nm was employed for scanning. Plates were scanned in reflectance mode with white light at a rate of 1 mm/s. Plates not subjected to charring treatments were scanned at a wavelength of 200 nm in the UV.

RESULTS AND DISCUSSION

Mobile phase selection

Mobile phase composition was optimized using Snyder's solvent classification[26] and its application to TLC as proposed by Heilweil[27]. Because of the chemical complexity and diversity of most tobacco leaf surface extracts, three modifiers were selected (isopropanol, chloroform and methylene chloride), each from a different classification group. Therefore, each modifier contributed different solvent characteristics to the mobile phase.

These three modifiers and hexane were combined in seven different mobile phase mixtures of equal chromatographic strength[27]. All seven were screened for optimum resolution of Galpao Commun (a Brazilian domestic variety of *N. tabacum* L.) leaf surface extracts, as its leaf surface chemistry is one of the most chemically complex. Thus, optimizing resolution of Galpao leaf surface extracts virtually ensured satisfactory resolution of other *N. tabacum* leaf surface extracts (Figs. 2 and 3). Under the described chromatographic conditions, a quaternary mixture of isopropanol–chloroform–methylene chloride–hexane (7:8:6:79) provided resolution of major tobacco leaf surface constituents in both standard mixtures and green leaf surface extracts after just one development. Resolution was sufficient for quantitation. The HC and WE classes were not separated in this system, but codeveloped as a single spot.

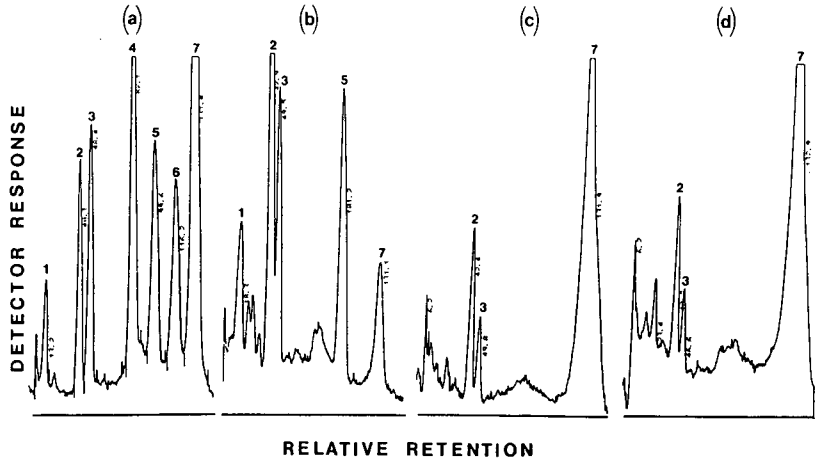

Fig. 2. Scanning densitometry traces of charring treatments. (a) Standard mixture; (b) field-grown Samsun leaf surface extract; (c) greenhouse-grown Burley 21 leaf surface extract; (d) greenhouse-grown experimental flue-cured [(Coker 209 × NC602) × *N. africana* maternally derived haploid]. Peaks: 1 = sucrose esters, 2 = ADVT, 3 = BDVT, 4 = DOC, 5 = Z-AB, 6 = DVT-monols, 7 = HC/WE. TLC plates: silica gel G, 0.25 μm equilibrated to 52% humidity. Mobile phase: isopropanol–chloroform–methylene chloride–hexane (7:8:6:79). Developing distance: 15 cm. Detection: charring with 30% fuming sulfuric acid followed by scanning with white light in reflectance mode.

Reproducibility

R_F values of each compound were reproducible to $\pm$ 0.01 units in comparison between lanes of individual plates and between separate plates (Table I). When R_F values are consistent, one need not run standards alongside samples on the same plate, but only compare sample R_F values to those of a single set of standard runs. Reproducibility also ensures that resolution between components will be constant, and therefore will not affect quantitation of closely developing solutes.

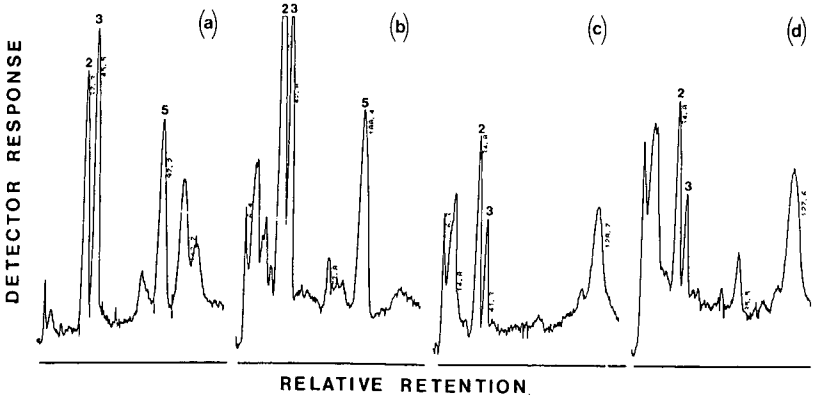

Fig. 3. Scanning densitometry traces of UV scanned plates. Details as for Fig. 2 except detection: scanned without charring at 200 nm in the reflectance mode.

TABLE I

MEAN R_F VALUES ± STANDARD DEVIATION OF *NICOTIANA TABACUM* LEAF SURFACE COMPONENTS

Conditions are as in Fig. 2.

Replication No.	*Compound*						
	SE	*ADVT*	*BDVT*	*DOC*	*Z-AB*	*DVT-monols*	*HC/WE*
1	0.05 ± 0.01	0.21 ± 0.01	0.27 ± 0.01	0.50 ± 0.01	0.62 ± 0.01	0.73 ± 0.01	0.83 ± 0.01
2	0.05 ± 0.01	0.22 ± 0.01	0.28 ± 0.01	0.50 ± 0.01	0.63 ± 0.01	0.74 ± 0.01	0.83 ± 0.01
3	0.05 ± 0.01	0.21 ± 0.00	0.25 ± 0.00	0.48 ± 0.01	0.62 ± 0.01	0.73 ± 0.00	0.83 ± 0.01
Average	0.05 ± 0.01	0.21 ± 0.01	0.27 ± 0.01	0.49 ± 0.01	0.62 ± 0.01	0.73 ± 0.01	0.83 ± 0.01

Reproducibility was accomplished through careful consideration of major parameters which affect TLC. Humidity and plate (adsorbent) activity are two parameters which are closely related and which can be adjusted to optimize resolution[28]. Since laboratory conditions can change daily, humidity must be rigidly controlled in order to maintain reproducible TLC results.

Effects of humidity on plate activation were controlled by equilibrating fully activated plates in a chamber whose atmosphere had been adjusted to 52% relative humidity using a saturated aqueous solution of sodium dichromate[23]. To maintain plate activation, equilibrated plates were covered with clean glass plates during spot application.

Reproducibility was also kept by allowing developments to "overrun"[23]. Dallas[23] noted that if development was stopped immediately after the mobile phase reached the developing distance, upper portions of the plate were less saturated with mobile phase than lower portions. Overrunning until the entire plate was fully saturated with developing solvent produced equal mobile phase to stationary phase ratios across the entire plate. R_F values increased slightly, but were more reproducible.

Equal rates of development between lanes of individual plates were accomplished by using a fully saturated developing chamber. The developing chambers were saturated with solvent vapor of the mobile phase, which was changed routinely after each development. Presumably, differences in rates of development between lanes would suggest different rates of solvent evaporation at the solvent front, as is the case with edge effects[24].

Quantitation: charring

Curvilinear relationships between mass and integration area were observed for each compound (Figs. 4 and 5 and Table III). Curvilinear responses were anticipated based on QTLC theory and on previous reports of quantitative densitometry of lipids. According to QTLC theory, light scattering caused by the thin-layer medium results in a non-linear relationship between substance mass and absorbance (ref. 29, reviewed in ref. 30). Previous work in quantitative densitometry of lipids has reported curvilinear responses at masses $\leqslant 10$ μg[31]. Linear relationships have been reported at masses above 10 μg[32,33].

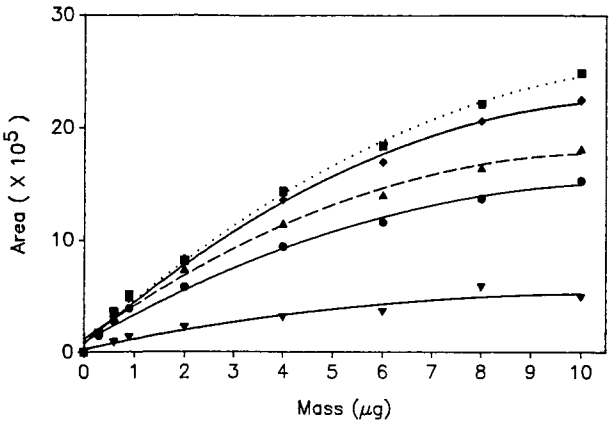

Fig. 4. Relationship between mass and integration area of *N. tabacum* secondary metabolites subjected to charring treatments. Conditions as in Fig. 2. (●) ADVT; (▲) BDVT; (■) DVT-monols; (▼)sucrose esters; (◆) *Z*-AB.

Overall, this technique provided at least semiquantitative results ($\leqslant$ 10% relative error) (Table II). Quantitation was most consistent between 0.6 μg and 2.0 μg. Results were quantitative ($\leqslant$ 6% relative error) in nearly all instances for all major secondary metabolites except the SE.

Quantitation at 0.3 μg was generally not reliable. At this mass, spots of most compounds produced detector responses, but these responses were not sufficient for reliable integration under the described scanning conditions. This is evidenced by the absence of reliable data for the sucrose esters at this mass (Table II).

Nonetheless, quantitation was reliably extended to 0.3 μg for ADVT and BDVT (Table II). These isomers represent two of the more important secondary products on the tobacco leaf surface because of their relative abundance compared to other leaf

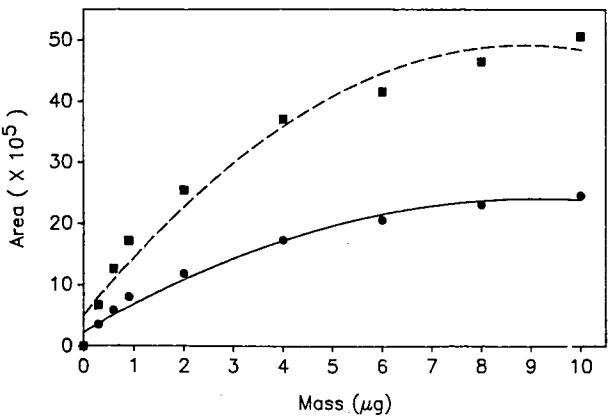

Fig. 5. Relationship between mass and integration area of *N. tabacum* primary metabolites subjected to charring treatments. Conditions as in Fig. 2. (●) DOC; (■) HC/WE.

TABLE II

RELATIVE PERCENT ERRORS OF QUANTITATION OF *NICOTIANA TABACUM* LEAF SURFACE COMPOUNDS

Chemical	*Mass applied (μg)*								
	0.0	*0.3*	*0.6*	*0.9*	*2.0*	*4.0*	*6.0*	*8.0*	*10.0*
Charring technique									
ADVT	0	11	4	11	2	6	5	5	3
BDVT	0	5	3	6	3	6	5	5	4
Z-AB	0	6	3	2	2	9	3	1	2
DVT-monols	0	18	2	6	5	12	3	6	5
SE	0	–	4	3	28	11	0	1	3
DOC	0	8	6	3	5	7	4	8	10
HC/WE	0	11	6	2	6	10	7	8	7
UV absorbance technique									
ADVT	0	4	8	9	3	2	2	4	4
BDVT	0	2	7	5	3	6	4	7	9
Z-AB	0	4	9	17	11	12	7	4	8

surface components[20], their known contribution to the ecology of the plant[8–14], and their eventual contribution to tobacco leaf quality[4–7].

Quantitation of the sucrose esters was not as consistent as other secondary metabolites (Table II). One possible explanation for this is the chemical nature of these these compounds (Fig. 1). The carbohydrate backbone is susceptible to oxidation to carbon dioxide during charring, thus resulting in carbon losses. Even with standardization of charring methods, variations in oxidation may have occurred among replicates.

With the primary metabolites, DOC and HC/WE, semiquantitative results were obtained (Table II). Semiquantitative data would generally be sufficient for HCs and

TABLE III

REGRESSION EQUATIONS AND R^2 VALUES FOR RELATIONSHIP BETWEEN MASS AND INTEGRATION AREA OF LEAF SURFACE CONSTITUENTS DETECTED BY CHARRING TREATMENT OR UV (200 nm) AND DENSITOMETRY

Chemical	*Regression equation*	R^2
Charring		
ADVT	$\text{Area} = -0.11x^2 + 2.52x + 0.91$	0.99
BDVT	$\text{Area} = -0.15x^2 + 3.12x + 1.18$	0.99
Z-AB	$\text{Area} = -0.17x^2 + 3.81x + 0.81$	0.99
DVT-monols	$\text{Area} = -0.16x^2 + 3.94x + 0.85$	0.99
SE	$\text{Area} = -0.04x^2 + 0.93x + 0.28$	0.97
DOC	$\text{Area} = -0.26x^2 + 4.79x + 2.25$	0.99
HC/WE	$\text{Area} = -0.56x^2 + 9.95x + 5.01$	0.99
UV 200 nm		
ADVT	$\text{Area} = -0.12x^2 + 2.59x + 2.07$	0.99
BDVT	$\text{Area} = -0.15x^2 + 3.10x + 2.83$	0.99
Z-AB	$\text{Area} = -0.56x^2 + 3.00x + 0.87$	0.99

WEs in actual screening applications, as interest in their contribution to ecological interactions and quality are small relative to tobacco secondary plant products. Typical of most tobaccos, DOC was below detection limits in tested leaf surface extracts (Fig. 2).

These charring procedures enabled quantitation of all major primary and secondary metabolites of the tobacco leaf surface. While potentially less accurate and less sensitive than the GC procedure developed by Severson *et al.*[20], a more rapid analysis of large numbers of leaf surface extracts can be performed with less sample preparation. Because TLC is a parallel technique rather than a serial technique, such as liquid chromatography (LC) and gas chromatography (GC), many samples can be chromatographed simultaneously. No special sample preparation is required before chromatography as would be necessary for GC analysis of these mixtures[20]. Also, the lack of a UV chromophore in all but one of these compounds would prevent universal detection on LC systems using UV detectors.

Total analysis time for eight samples, including sample application, development, charring, scanning, and integration, was approximately 2 h; using the GC procedure of Severson *et al.*[20], analysis time would be approximately 8 h for eight samples. For twenty samples, charring QTLC analysis time would increase only to approximately 3 h, *versus* 20 h using GC. For the QTLC procedure the most time-consuming steps of the analysis (development and charring) remain constant, whether eight or twenty samples are analyzed. Sample application time for twenty samples would increase approximately 12–15 min over that of eight samples, and scanning and integration time would increase approximately 35–40 min.

The decreased sensitivity of this procedure relative to GC is not necessarily a drawback. The leaf surface products of primary interest are almost exclusively those existing in greatest abundance (*i.e.*, ADVT, BDVT, *Z*-AB and SE)[12,17–20] for which quantitative results were obtained in all but one case.

Quantitation: UV

Detection and quantitation was much more limited using this procedure. Only ADVT, BDVT, and *Z*-AB were reliably detected. Using this procedure, culvilinear responses were obtained between mass and integrator response (Fig. 6 and Table III). High correlations were observed in all three cases. Despite the lack of universality, this procedure represents a rapid means for quantitating these three constituents, as plates were scanned immediately following development without further treatment. Since no modification for detection and quantitation were required, this procedure would be extremely attractive to those researchers who require simple procedures and rapid results.

Overall, semiquantitative results were obtained (Table II). ADVT and BDVT results were most consistent and quantitative in many instances, even in the absence of a strong UV absorbing chromophore. Results of *Z*-AB were less consistent. Scanning at 200 nm in order to quantitate all three components in a single scan decreased sensitivity to *Z*-AB, whose *in situ* absorbance maximum is at a wavelength of 229 nm. More quantitative and consistent results would probably be obtained for *Z*-AB if it were scanned at this wavelength. However scanning at two wavelengths to optimize quantitation of all three metabolites would require two separate scans and would decrease efficiency.

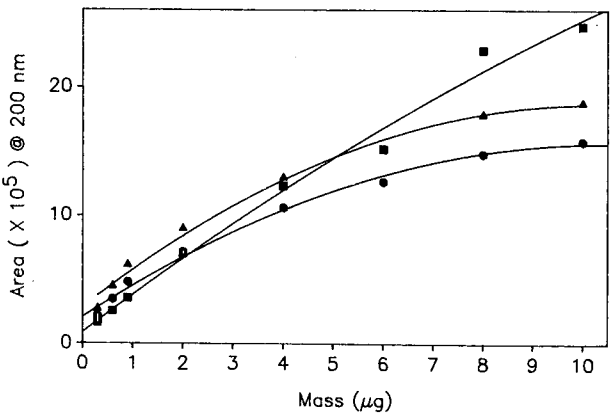

Fig. 6. Relationship between mass and integration area of *N. tabacum* secondary metabolites scanned at a wavelength of 200 nm. Conditions as in Fig. 3. (●) ADVT; (▲) BDVT; (■) *Z*-AB.

For both the charring and the UV procedures, statistical analysis revealed that different TLC plates significantly contributed to variation in quantitation. The contribution of plate effects to variation was small relative to mass, but nonetheless significant. Based on these results, it is recommended that standard curves be produced periodically and routinely to account for variation that may exist between plate lots. Likewise, for most accurate results, replicates of each sample should be run. Replicates of each sample would not be necessary if one requires only "rough" quantitative comparisons, which may be appropriate, for example, in plant breeding selections.

Plate variation may be reduced through use of higher quality high-performance thin-layer chromatography (HPTLC) plates; however organic binders commonly used in their preparation make them incompatible with sulfur trioxide charring procedures. Only one manufacturer was found which produced HPTLC plates without organic binder. In addition, HPTLC plates are more expensive, and thus may be economically prohibitive to some screening programs.

These procedures were tested against crude leaf surface extracts of fresh, green, bud leaf material of field-grown Samsun, greenhouse-grown Burley 21, and a greenhouse-grown experimental flue-curred plant [(Coker 209 × NC602) × *N. africana* maternally derived haploids]. Samsun was selected because of its complex leaf surface chemistry, which includes all the components comprising the mixed standard solutions. Burley 21 was selected because it represented a common tobacco variety, and the experimental flue-cured plant was selected to illustrate the procedure's effectiveness in screening experimental phenotypes. For both charring and UV scanning procedures, peak-to-noise ratios were similar to that of mixed standard scans. Thus, resolution was satisfactory for quantitation of major metabolites of all three crude leaf surface extracts.

Figs. 2 and 3 illustrate the effectiveness of the charring and UV scanning procedures, respectively, to identify differences that exist in the leaf surface chemical compositions of Samsun, Burley 21, and the experimental cross. The charring trace of Samsun (Fig. 2b) confirms the presence of the major tobacco secondary metabolites, SE, ADVT, BDVT, and *Z*-AB, while charring traces of Burley 21 (Fig. 2c) and the

experimental cross (Fig. 2d) properly identify these tobaccos as duvane (*i.e.*, ADVT, BDVT) producers and show no *Z*-AB. Similarly, the UV scanning traces in Fig. 3 confirm the presence of ADVT and BDVT in all three tobaccos (Fig. 3a–d), but the presence of *Z*-AB in Samsun only (Fig. 3b).

CONCLUSION

QTLC procedures have been developed for rapid quantitation of major *N. tabacum* leaf surface metabolites. These procedures should be useful tools in plant breeding and other research programs interested in rapid screening of these chemical traits in large numbers of samples. Utility may also be found in general screening of *Nicotiana* species for taxonomic or other purposes.

ACKNOWLEDGEMENTS

This work was supported by a grant from the N.C. Tobacco Foundation. The authors thank Dr. P. E. Barney Jr. and Mr. Carl Yung for supplying Burley 21 and experimental flue-cured leaf material and Mr. Albert R. Butler, Mr. John C. Weeks, and Ms. Marie Hall for their able technical assistance.

REFERENCES

1 M. J. Michie and W. W. Reid, *Nature (London)*, 218 (1968) 578.
2 C. K. Keene and G. J. Wagner, *Plant Physiol.*, 79 (1985) 1026.
3 A. W. Johnson, R. F. Severson, J. Hudson, G. R. Carner and R. F. Arrendale, *Tob. Sci.*, 29 (1985) 67.
4 A. Colledge, W. W. Reid and R. A. Russell, *Chem. Ind. (London)*, 1975 (1975) 570.
5 C. R. Enzell, *Rec. Adv. Tob. Sci.*, 2 (1976) 32.
6 W. W. Reid, *Ann. Tabac. Sect. 2*, 12 (1975) 33.
7 I. Wahlberg, K. Karlson, D. J. Austin, N. Junker, J. Roeraade, C. R. Enzel and W. H. Johnson, *Phytochemistry*, 16 (1977) 1217.
8 H. G. Cutler, *Science (Washington, D.C.)*, 170 (1970) 856.
9 H. G. Cutler, W. W. Reid and J. Deletang, *Plant Cell Physiol.*, 18 (1977) 711.
10 H. G. Cutler, R. F. Severson, P. D. Cole and D. M. Jackson, in M. B. Green and P. A. Hedin (Editors), *Natural Resistance of Plants to Pests*, Am. Chem. Soc., Washington, DC, 1986, p. 178.
11 A. W. Johnson and R. F. Severson, *Tob. Sci.*, 26 (1982) 98.
12 A. W. Johnson and R. F. Severson, *J. Agric. Entomol.*, 1 (1984) 23.
13 D. M. Jackson, R. F. Severson, A. W. Johnson and G. A. Herzog, *J. Chem. Ecol.*, 12 (1986) 1349.
14 I. A. M. Cruickshank and D. R. Perrin, *Phytopath. Z.*, 90 (1977) 243.
15 W. W. Reid, *Ann. Tabac. Sect. 2*, 11 (1974) 151.
16 E. Zador and D. Jones, *Plant Physiol.*, 82 (1986) 479.
17 H. Tomita, M. Sato and N. Kawashima, *Agric. Biol. Chem.*, 44 (1980) 2517.
18 T. Komari, T. Kuko and M. Sato, *Tob. Sci.*, 30 (1986) 159.
19 T. Kubo, M. Sato, H. Tomita and N. Kawashima, *Tob. Sci.*, 26 (1982) 126.
20 R. F. Severson, R. F. Arrendale, O. T. Chortyk, A. W. Johnson, D. M. Jackson, G. R. Gwynn, J. F. Chaplin and M. G. Stephenson, *J. Agric. Food Chem.*, 32 (1984) 566.
21 D. R. Lawson and D. A. Danehower, in preparation.
22 D. A. Danehower, *Tob. Sci.*, 31 (1987) 32.
23 M. S. J. Dallas, *J. Chromatogr.*, 17 (1965) 267.
24 E. Stahl, in E. Stahl (Editor), *Thin-Layer Chromatography*, Springer Verlag, New York, 2nd ed., 1969, Section C, p. 52.
25 T. T. Martin and M. C. Allen, *J. Am. Oil. Chem. Soc.*, 48 (1971) 752.
26 L. R. Snyder, *J. Chromatogr. Sci.*, 16 (1978) 223.

27 E. Heilweil, in J. C. Touchstone and J. Sherma (Editors), *Techniques and Applications of Thin Layer Chromatography*, Wiley Interscience, New York, 1985, Ch. 3, p. 37.
28 F. Geiss, H. Schlitt, F. J. Ritter and W. M. Weimar, *J. Chromatogr.*, 12 (1963) 469.
29 U. B. Hezel, in A. Zlatkis and R. E. Kaiser (Editors), *HPTLC: High Performance Thin-Layer Chromatography* (*Journal of Chromatography Library*, Vol. 9), Elsevier, Amsterdam, 1987, Ch. 8, p. 149.
30 F. A. Huf, in L. R. Treiber (Editor), *Quantitative Thin-Layer Chromatography and Its Industrial Applications*, Marcel Dekker, New York, 1987, Ch. 2, p. 17.
31 J. Bitman and D. L. Wood, *J. Liq. Chromatogr.*, 5 (1982) 1155.
32 M. L. Blank, J. A. Schmit and O. S. Privett, *J. Am. Oil. Chem. Soc.*, 41 (1964) 371.
33 L. J. Nutter and O. S. Privett, *J. Chromatogr.*, 35 (1968) 519.

Journal of Chromatography, 463 (1989) 441–444
Elsevier Science Publishers B.V., Amsterdam — Printed in The Netherlands

CHROM. 21 066

Note

Heat of solution in a polyethylene glycol stationary phase of several cyclic and bicyclic compounds

A. GARCÍA-RASO*, M. A. VÁZQUEZ, P. BALLESTER and P. M. DEYÁ
Departament de Química, Facultat de Ciències, Universitat de les Illes Balears, 07071 Palma de Mallorca (Spain)
(First received May 2nd, 1988; revised manuscript received October 24th, 1988)

In previous papers[1,2] we reported studies of the heat of solution (ΔH_s) for several acyclic hydrocarbons, aldehydes, esters and alcohols in non-polar (squalane) and polar (Carbowax 20M) stationary phases. It was found that ΔH_s was dependent on the polarity of the functional group. Thus, decreasing in the order alcohols > carbonyls > hydrocarbons. On the other hand, $\Delta(\Delta H_s)$ for an acyclic CH_2 group is 3.3 ± 0.8 kJ/mol, independent of the chemical function present in the compound.

This paper reports ΔH_s values for some bicycloketones (6 and 9), spirolactones (5, 7 and 8) and unsaturated hydroxy esters with a cyclic substituent (1, 2, 3 and 4) that were prepared by a method described previously[3] (Scheme 1). The heat of solution was calculated in order to study the behaviour of different cyclic systems with respect to ΔH_s and the influence of the different compounds on the values of ΔH_s and $\Delta(\Delta H_s)$ for a cyclic CH_2 group.

EXPERIMENTAL

The ΔH_s values were calculated from the slopes of plots of $\ln (V_R^0/T)$ *vs.* $1/T$, where V_R^0, the corrected retention volume, is

$$V_R^0 = t_R^* \varphi$$

t_R^* is the corrected retention time (min), φ is the flow-rate of the carrier gas (ml/min) and ΔH_s represents the sum of ΔH(solution) and ΔH(vaporization).

Retention times were determined with a Hewlett-Packard Model 5834A chromatograph equipped with a Model 18850A integrator and a flame ionization detector. A stainless-steel column (2 m × 1/4 in. I.D.) packed with Carbowax 20M (polyethylene glycol, MW ≈ 20 000) and nitroterephthalic acid ester (free fatty acid phase, FFAP) on Chromosorb P AW DMCS (60–80 mesh), supplied by Teknokroma (Barcelona, Spain), was used. Nitrogen was used as the carrier gas at a flow-rate of 37 ml/min. The determinations were carried out at 220, 230 and 240°C with the injector and flame ionization detector operating at 250°C. Compounds were injected (0.3 μl) as solutions in diethyl ether (3%, w/w). Retention times were measured from the time of sample injection. The dead volume was determined by regression analysis on a series of *n*-alkanes (C_{10}–C_{24}) using the Grobler and Bálisz procedure[4].

0021-9673/89/$03.50

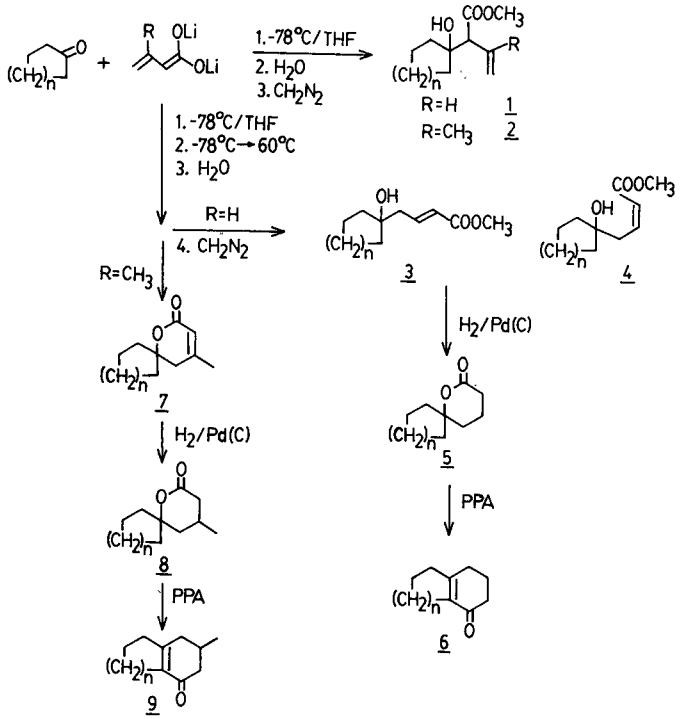

Scheme 1.

TABLE I

ΔH_s VALUES (kJ/mol) FOR THE COMPOUNDS STUDIED

n	*Compound type*								
	*1**	*2**	*3*	*4***	*5*	*6*	*7*	*8*	*9*
1	−41.4	−46.4	−55.6	−53.9	−43.5	−41.4	−68.1	−48.5	−42.6
2	−45.6	−50.2	−59.8	−57.7	−46.8	−44.3	−71.5	−51.8	−45.1
3	−50.2	−53.9	−63.9	−62.3	−50.2	−46.8	−76.1	−55.2	−48.1
4	−53.9	–	−68.1	–	−54.3	−50.2	−79.8	−58.9	−51.4
6	–	–	−76.1	–	−60.2	−55.6	−87.4	−64.8	−56.8
8	−70.6	–	−84.0	−81.9	−66.0	−61.0	−94.9	−71.1	−62.3
$\Delta(\Delta H_s)$	−3.7	−3.8	−4.0	−4.0	−3.2	−2.8	−3.8	−3.2	−2.8
s***	0.50	–	0.18	0.29	0.50	0.21	0.29	0.33	0.25

* Compounds 1 and 2 are very labile substances and most of them decompose totally or partially under chromatographic conditions.

** Compounds 4 are not generally isolated. Retention times were calculated from crude mixtures.

*** Standard deviation.

RESULTS AND DISCUSSION

The ΔH_s values of the compounds studied are given in Table I. In all instances, plots of ΔH_s *vs.* number of cyclic CH_2 groups (n) (see Scheme 1) yield straight lines with high accuracy and low standard deviations (Fig. 1). We consider that the solute–stationary phase interactions depend principally on a number of "active groups" present in the molecule. The "active group" may be described as "the functional group that produces an interaction with the stationary phase more efficiently than an alkane"; for example, see Scheme 2, where a lactone and a double bound would be "active groups".

Compounds 1, 3 and 4 in Scheme 3 have the same number of "active groups" ($COOCH_3$, OH and CH=CH) and hence the different values of ΔH_s will be direct

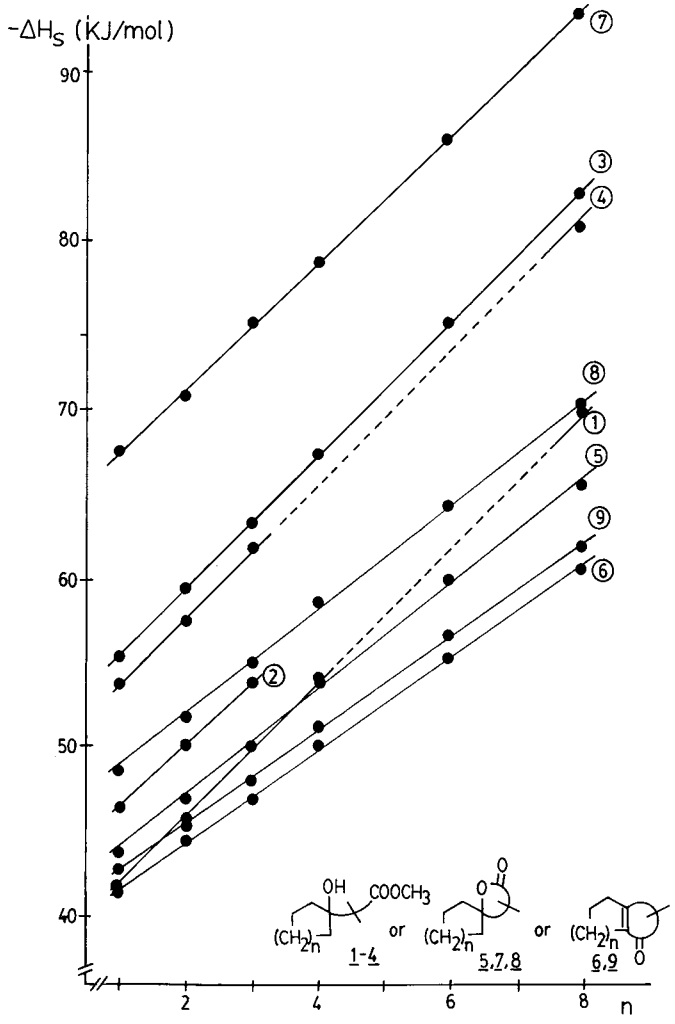

Fig. 1. ΔH_s (kJ/mol) *vs.* n for the compounds studied. The numbers on the lines are the compound types (see text).

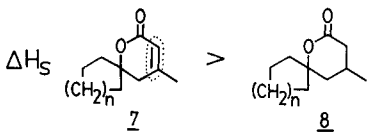

Scheme 2.

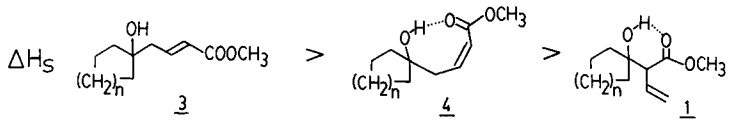

Scheme 3.

functions of the higher or lower molecular interactions between these "active functions", that is, the higher the internal interactions the lower is ΔH_s.

For example, the methyl 4-(1-hydroxy-1-cycloalkyl)-2-(*E*)-butenoates (3) cannot undergo any intramolecular interactions, whereas the corresponding (*Z*)-butenoates (4) can show a slight interaction-type hydrogen bond, although an eight-membered ring is unstable. However, the corresponding methyl 2-(hydroxy-1-cycloalkyl)-3-butenoates (1) can form a stable six-membered ring by hydrogen bonding and therefore ΔH_s decreases. A similar behaviour is shown by spirolactones, where an increase in ΔH_s for 7 *vs.* 8 is produced, owing to the additional double bond in 7 (see Scheme 2).

Although the number of "active groups" is an important parameter determining the sequence of ΔH_s values for closely related compounds, the conformational rigidity of the organic structure can enhance or diminish the ΔH_s values. Thus, the spirolactones (7) show the highest values for the compounds studied and the bicycloalkanones (6) show the lowest values.

On the other hand, in all instances , the ΔH_s value for a cyclic CH_2 group is almost constant at -3.3 ± 0.8 kJ/mol (see Table I), independent of the type of structure. This value is similar to that for the acyclic systems previously reported[2]. The approximate constancy of $\Delta(\Delta H_s)$ for a CH_2 group implies zero excess enthalpies, or at least values no greater than 0–800 J/mol, which would be too small to affect ΔH_s. We conclude that the ΔH_s values are equivalent to enthalpies of condensation (vaporization).

REFERENCES

1 F. Saura-Calixto and P. M. Deyá, *Can. J. Chem.*, 59 (1981) 2243.
2 F. Saura-Calixto, P. M. Deyá and A. Carcía-Raso, *Monatsh. Chem.*, 114 (1983) 385.
3 P. Ballester, A. García-Raso and R. Mestres, *Synthesis*, (1985) 802.
4 A. Grobler and G. Bálizs, *J. Chromatogr. Sci.*, 12 (1974) 57.

Journal of Chromatography, 463 (1989) 445–451
Elsevier Science Publishers B.V., Amsterdam — Printed in The Netherlands

CHROM. 21 068

Note

Analysis of mucin by isotachophoresis

ALEXANDER J. G. EMONDS
Department of Pharmacology, Sylvius Laboratories, University of Leiden, Wassenaarseweg 72, 2333 AL Leiden (The Netherlands)
and
DICK DE VOS*
Medical Department, Pharmachemie B.V., P.O. Box 552, 2003 RN Haarlem (The Netherlands)
(First received July 22nd, 1988; revised manuscript received October 24th, 1988)

The glycoprotein mucin is defined according to ref. 1 as the fraction precipitated by approximately 60% ethyl alcohol from the supernatant liquid after pepsin–hydrochloric acid digestion of hog stomach linings. A number of tests are presented[1] in order to characterize mucin and to guarantee a constant quality when producing porcine mucin.

During a search for a method which could provide a fingerprint of mucin, *cf.*, ref. 2, and a quantitative assay, we selected isotachophoresis as a suitable alternative to the classical methods[1]. This technique has been applied to the analysis of proteins and peptides[3,4]. In our laboratory, isotachophoresis has been used previously for the analysis of methotrexate[5].

MATERIALS AND METHODS

Apparatus

Isotachophoretic experiments were performed in the apparatus provided with UV absorption and conductivity detection as described by Everaerts *et al.*[6]. The separation capillary was approximately 200 mm × 0.2 mm I.D. The electric current was stabilized at 0.06 mA. The electrolyte system used in the isotachophoresis of mucin and other proteins is specified in Table I. The isotachophoretic apparatus was equipped with a Linseis three-channel recorder Type LS34, registering the UV signal (50 mV), the conductivity signal (2.5 mV) and the differentiated conductivity signal. The paper velocity was 20 mm/min. The UV signal was also recorded on a Hewlett-Packard integrator ATT3 (attenuation 3). The paper velocity was 25 mm/min. In order to monitor the whole isotachophoretic separation, use was made of a barrier filter (Longpass 515) and a mercury lamp (HBO 50) with a Shortpass 490 filter. Filters were from Schott (Mainz, F.R.G.).

Reagents

Reagents used were of analytical grade. Water was purified by Millipore ultrafiltration. Mowiol 8-88 was kindly donated by Hoechst-Holland (Amsterdam, The Netherlands) and purified by ion-exchange chromatography (Merck V; Merck, Darmstadt, F.R.G.). Fluorescein isothiocyanate was from Merck.

0021-9673/89/$03.50

TABLE I

OPERATIONAL SYSTEM FOR MUCIN ANALYSIS

Parameter	*Electrolyte*	
	Leading	*Terminator*
Anion	Cl^-	Glycine
Concentration (*M*)	0.01	0.01
Counter ion	Tris	Tris
pH	7.2	8.5
Additive	0.05% Mowiol	
Solvent	Water	Water

Protein preparations

Mucin reference material was freeze-dried batch 315 from A/S Orthana Kemisk Fabrik (Kastrup, Denmark). This batch was characterized by, *inter alia*, UV, IR and ^{13}C Fourier transform (FT)-NMR spectroscopy. Mucin from A/S Orthana is porcine gastric mucin. Further, 3.5% mucin solution from A/S Orthana was batch 230388; pepsin (batch 23326) and peptone 0-24 (batch 4913) were also from A/S Orthana. Bovine albumin was from Sigma (St. Louis, MO, U.S.A.), A-8022, Lot 51F-0320.

Procedure

In order to obtain a qualitative analysis of mucin (or another protein), 1 μl of a 3.5% solution was injected between the leading and terminating electrolytes. The isotachopherogram was compared with that of a 3.5% solution of reference batch 315. For the quantitative analysis, the zone length of the sample solution was compared with that of two reference solutions of batch 315. The beginning and end of a zone can be checked by using the differentiated signal. The percentages indicated below denote g per 100 ml. The isotachophoretic analysis of a mucin sample may take up to 1 h.

RESULTS AND DISCUSSION

Mucin solutions may have a high viscosity while, in general, proteins may adhere to the capillary tube during isotachophoresis[6]. In order to check whether our analysis was in accordance with the isotachophoretic requirement: mobility leading electrolyte > mobility sample > mobility terminating electrolyte, the complete isotachophoretic process was monitored. The mucin was labelled by fluorescein isothiocyanate and the process was inspected visually upon UV irradiation. All proteins participated in the isotachophoresis. Also from the conductometric end signal which was equal to that of the terminator, it became clear that no protein components were migrating in the terminator.

In Fig. 1, isotachopherograms of mucin, pepsin, peptone and albumin are presented as recorded by the Linseis recorder. The protein zones are marked in the figures. Inspection of this figure shows that the isotachopherogram of mucin is quite different from that of pepsin, peptone or albumin. Mucin and pepsin look rather complex protein mixtures. The isotachopherograms of peptone and albumin indicate a limited number of compounds. Compared with the isotachopherograms of possible

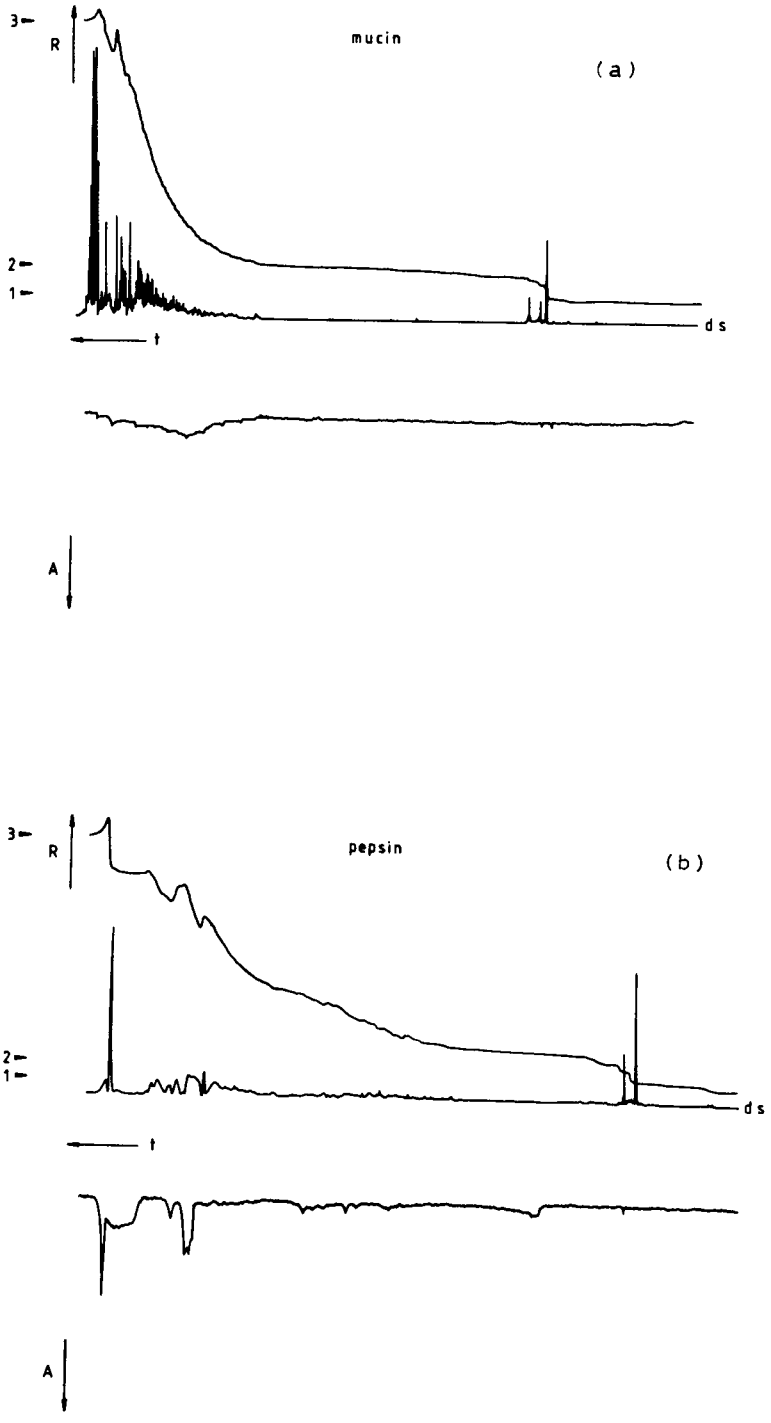

Fig. 1.

(*Continued on p. 448*)

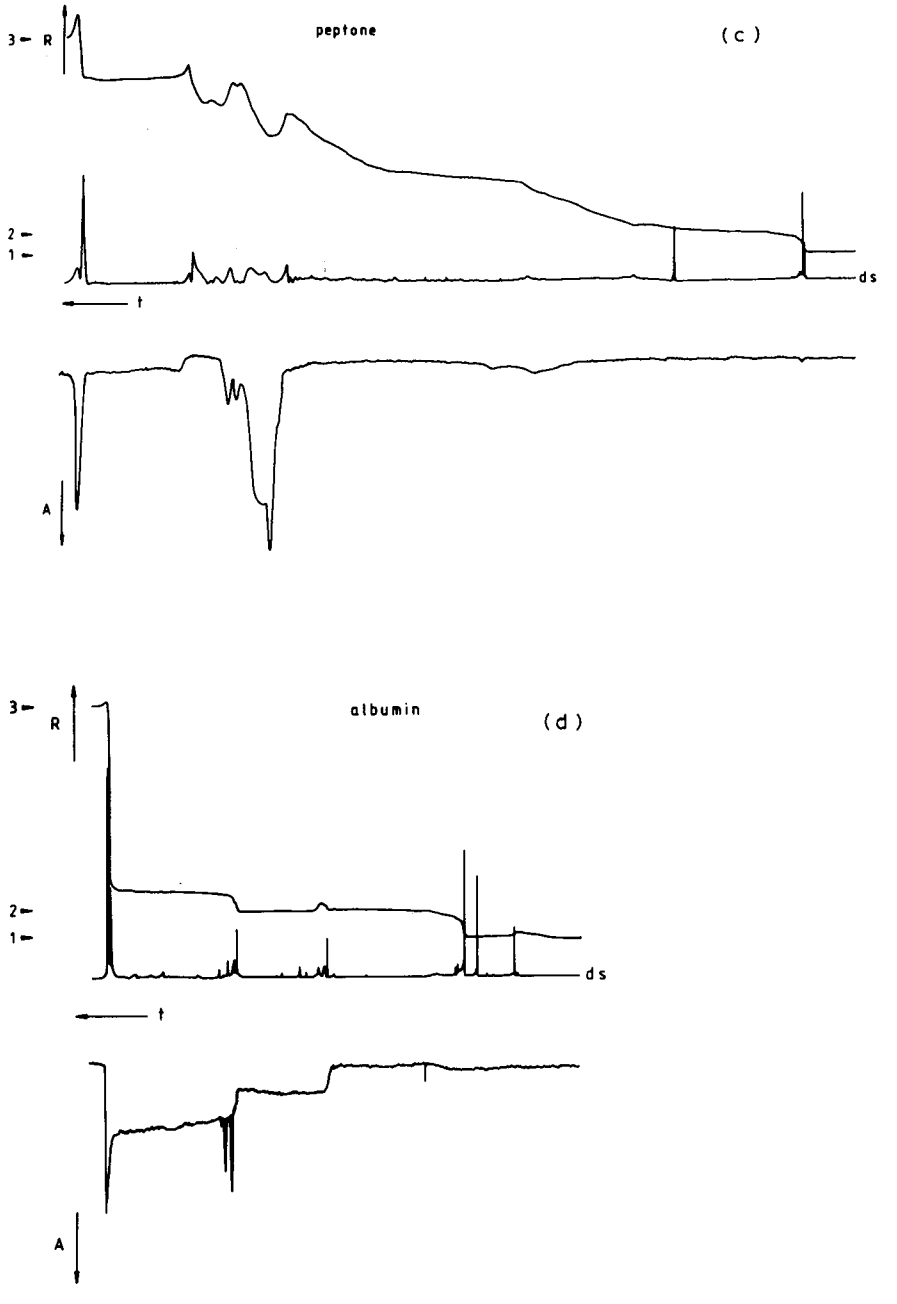

Fig. 1. Isotachopherograms of 3.5% (w/v) solutions of mucin, pepsin, peptone and albumin as recorded by the Linseis recorder. The nature of the anions in the zones is indicated by their resistance level, *R*, or UV absorption, *A*. The zone length indicates the quantity of anion passing the detector. Also shown is the differential signal (ds) of the conductometer, facilitating the determination of the zone length. Time is from right to left. Step heights: 1 = leading electrolyte; 2 = non-UV-absorbing ions from protein sample; 3 = terminating electrolyte; the protein zone is between 2 and 3.

TABLE II

COMPOSITION OF A 3.5% MUCIN SOLUTION

Data from A/S Orthana.

Component	*Content (g/100 ml)*
Mucin	3.5
Na^+	0.080
K^+	0.070
Ca^{2+}	0.025
Mg^{2+}	0.015
HPO_4^{2-}	0.022
Cl^-	0.120

impurities resulting from the manufacturing process (pepsin and peptone) or to a completely unrelated protein (albumin), the isotachopherogram of mucin appears to possess a high specificity.

From Fig. 1 it is clear that non-UV absorbing species are present between the leading zone and the protein zone. This was partly known from the composition of mucin which is presented for a 3.5% solution in Table II. Isotachophoresis may lead to further definition of mucin and related peptides. For a discussion on HCO_3^- which is also present in the system used, see ref. 6. This ion is not shown in the isotachophoretic traces in the figures.

Isotachophoresis was subsequently used to establish the mucin identity of mucin production batches. The isotachopherograms obtained from samples taken during the manufacturing process were identical to that of mucin in Fig. 1.

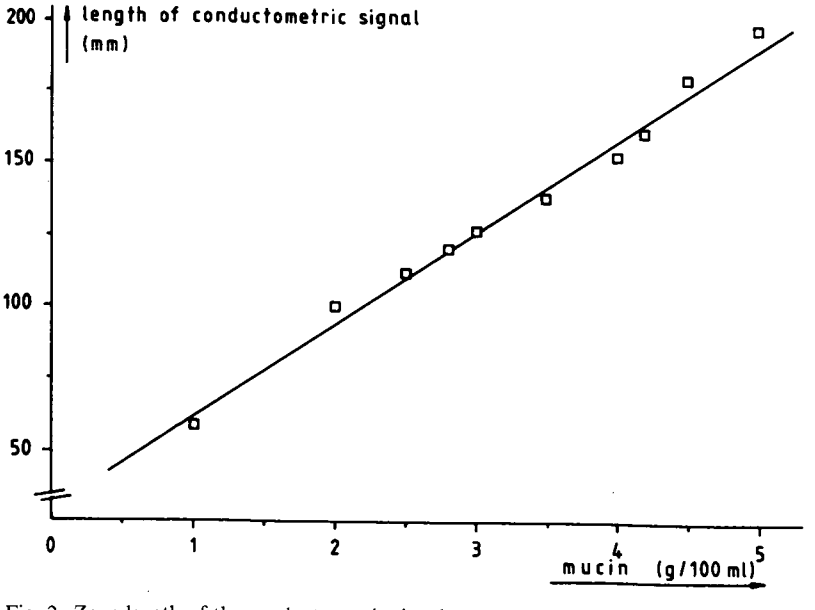

Fig. 2. Zone length of the conductometric signal *versus* concentration for 1–5% mucin solutions.

The zone length found in an isotachopherogram is a measure of the amount of anions in the zone. In the present study, a linear relationship was found between the concentration of mucin and the zone length in the range 1–5% mucin (concentrations 1.0, 2.0, 2.5, 2.8, 3.0, 3.5, 4.0, 4.2, 4.5 and 5.0%; correlation coefficient 0.994). The daily variation was 1.5% ($n = 12$). An example of a calibration graph is presented in Fig. 2. Fig. 3 gives an impression of the UV part of the isotachopherograms from a calibration graph. In this figure only the UV-absorbing protein part of the isotachopherogram is presented as recorded on the HP ATT3.

Using batch 315 (freeze-dried material) as a reference, the mucin content of a production batch of mucin solution (388) was determined. Two reference solutions of 3.5% mucin were prepared. These were measured as well as the sample solution in duplicate on 2 days: batch 388 showed a mucin content of 3.1 $\pm$ 0.1%.

Isotachophoresis has proven to be a suitable method for the qualitative as well as

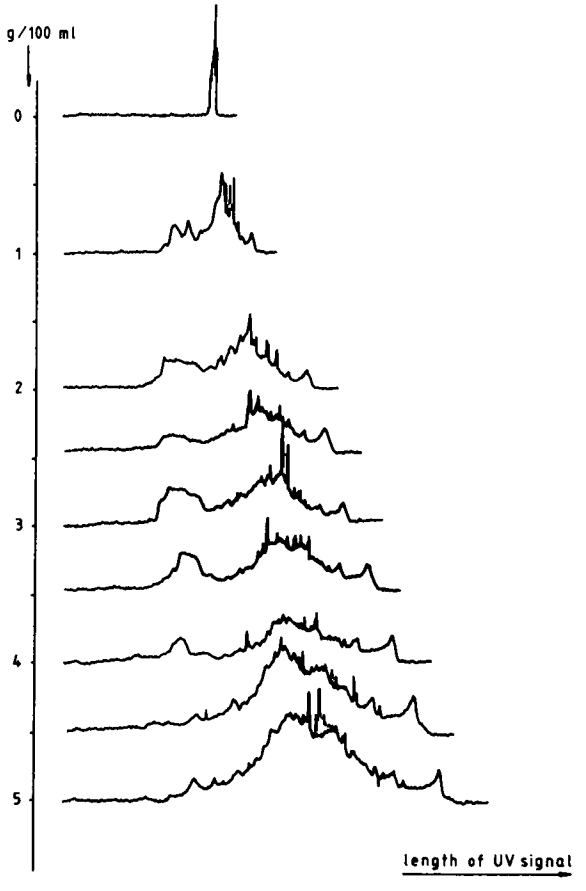

Fig. 3. UV signal of mucin samples from a calibration graph, showing a fingerprint comparison of increasing mucin concentrations. This figure gives the UV-absorbing protein part of the isotachopherogram recorded by the HP ATT3. Zone length was measured by using the differential signal of the conductometer. Time is from left to right.

the quantitative analysis of mucin in solution. It provides a new and independent analytical method to assay mucin and may as such be a modern supplement to the traditional methods[1].

ACKNOWLEDGEMENTS

We thank Mr. E. Balslev of A/S Orthana, Kastrup, Denmark for supporting this study, Ruud van der Geest and Riemer Runia for their technical assistance, Jan Slats for his help during the UV monitoring of the isotachophoretic process and Dr. O. M. J. Driessen for editing the manuscript.

REFERENCES

1 *Tests and Standards for New and Non-official Remedies*, The Chemical Laboratory of the American Medical Association, JB Lippincott Company, Philadelphia, PA, 1953.
2 E. Moczar and D. Waldron-Edward, *J. Chromatogr.*, 181 (1980) 108–114.
3 P. Stehle, H.-P. Bahsitta and P. Fürst, *J. Chromatogr.*, 370 (1986) 131–138.
4 D. Del Principe, *J. Chromatogr.*, 342 (1985) 285–292.
5 O. Driessen, H. Beukers, L. Belfroid and A. Emonds, *J. Chromatogr.*, 181 (1980) 441–448.
6 F. M. Everaerts, J. L. Beckers and T. P. E. M. Verheggen, *Isotachophoresis, Theory, Instrumentation and Application*, Elsevier, Amsterdam, 1976.

Journal of Chromatography, 463 (1989) 452–456
Elsevier Science Publishers B.V., Amsterdam — Printed in The Netherlands

CHROM. 21 075

Note

Thin-layer chromatographic decomposition of the picrates and trinitrobenzolates of polycyclic hydrocarbons and other organic compounds

O. L. TOMBESI*, M. A. TOMÁS and M. A. FRONTERA
Laboratorio de Química Orgánica, Universidad Nacional del Sur, Avda. Alem 253, 8000 Bahia Blanca (Argentina)
(Received October 18th, 1988)

In a previous paper[1], decomposition of picrate, trinitrobenzolate and styphnate derivatives of polycyclic hydrocarbons in a chromatographic column containing basic aluminia, used in the purification of these compounds, was reported to occur. In this paper is described the thin-layer chromatographic decomposition on silica gel (with a fluorescent indicator) of the picrates and trinitrobenzolates of polycyclic hydrocarbons and other representative organic compounds (dibenzofuran, β-naphthol, α-naphthylamine). Such derivatives are used as intermediates in the purification and identification of these compounds. For the identification of the compounds and evaluation of the degree of purification obtained, the melting points and ultraviolet spectra of the products were determined.

EXPERIMENTAL

Apparatus

Melting points were determined on a Kofler hot stage and are uncorrected. UV absorption spectra were measured in ethanol with a Beckman DB instrument. Desaga equipment was used for thin-layer chromatography.

Preparation of derivatives

The picrates and trinitrobenzolates of naphthalene (I), β-methylnaphthalene (II), anthracene (III), phenanthrene (IV), chrysene (V), pyrene (VI), acenaphthene (VII), fluorene (VIII), dibenzofuran (IX), β-naphthol (X) and α-naphthylamine (XI) were prepared by heating for 10 min on a water bath equimolecular solutions of the compounds (I–XI) and either picric acid or trinitrobenzene in solvents or solvent mixtures as indicated in Tables I and II. Subsequent crystallization was carried out at room temperature. The compounds were purified by recrystallization from the same solvents or solvent mixtures. Chrysene picrate is unstable[2] and could not be prepared with the same solvents and procedures as the other compounds. For this preparation an equimolecular mixture of picric acid and V in light petroleum (b.p. 80–100°C) were heated for 10 min, adding the minimum amount of benzene until total dissolution occurred. The solution was allowed to cool and a bright orange crystalline product was obtained (m.p. 160–164°C). On recrystallization from the same solvents mixture it melted at 169–170°C.

TABLE I

PREPARATION AND DECOMPOSITION OF THE PICRATES

Compound	*Picrates*			*Purified compounds*		
	M.p.(°C)	*Solvent**	*Weight (mg)*	*M.p.(°C)*	*Weight (mg)*	*Yield (%)*
I	149–151	E	198	79–80	64	89
II	116–118	E	206	34–35	79	95
III	138–139	B–LP	200	215–216	69	80
IV	142–144	E	148	100–101	58	90
V	169–170	LP**–B	180	255–256	72	81
VI	220–222	E	193	155–156	66	75
VII	160–161	E	200	93–94	64	80
VIII	78–79	B–LP	165	116–117	64	94
IX	98–99	B–LP	252	86–87	79	76
X	160–162	B	274	123–124	82	86
XI	170–172 (decomp.)	B	210	50–51	70	88

* E = ethanol; B = benzene; LP = light petroleum (b.p. 60–80°C).
** LP (80–100)–B.

TABLE II

PREPERATION AND DECOMPOSITION OF THE TRINITROBENZOLATES

Compound	*Trinitrobenzolates*			*Purified compounds*		
	M.p. (°C)	*Solvent**	*Weight (mg)*	*M.p. (°C)*	*Weight (mg)*	*Yield (%)*
I	153–154	E	183	79–80	66	96
II	125–127	E	159	33–34	52	81
III	164–166	B–LP	179	214–215	67	82
IV	159–160	E	200	101–102	70	80
V	187–188	B–LP	220	254–255	107	95
VI	244–246	E	199	156–157	87	92
VII	168–170	B–LP	274	91–92	93	82
VIII	105–106	B–LP	211	114–115	79	86
IX	96–97	B–LP	275	85–86	113	94
X	160–162	B	212	124–125	80	94
XI	218–220	B	219	49–50	73	83

* See Table I.

Chromatographic decomposition

Weighed amounts of the picrates and trinitrobenzolates were dissolved in minimum amounts of solvent (commonly benzene or ethanol). They were spotted on chromatographic plates [20 × 20 cm; silica gel 60 $HF_{254+366}$ (Merck), thickness 0.50 mm] and were developed (at room temperature, 20 ± 2°C) with the solvents indicated in Tables III and IV. Compounds I–XI, products of the decomposition of the derivates, were examined under ultraviolet light. The fluorescence observed varied between violet-brown and bluish-brown, except IX (sky blue) and VI (brilliant yellow). The compounds were extracted from the adsorbent with different solvents (acetone for I,

TABLE III

CHROMATOGRAPHIC DECOMPOSITION OF THE PICRATES

Compound	$R_F \times 100$*			
	LP	*LP–T*	*T*	*T–C–A*
I		53		
II		77		
III	45			
IV	43			
V	28			
VI	42			
VI	53			
VIII	40			
IX	48			
X			14	
XI				53
Picric acid	0	0	0	0

* Eluents: LP = light petroleum (b.p. 60–80°C); LP–T = light petroleum (b.p. 60–80°C)–toluene (98:2); T = toluene; T–C–A = toluene–chloroform–ethyl acetate (7:3:3).

III, IV and IX; benzene for V and VII; ethanol for II, VI, VIII, X and XI), then crystallized from the corresponding solvents (ethanol for I–IV and VI–IX; benzene for V; ethanol–water for X and XI). The melting points and UV spectra of the compounds were then determined.

TABLE IV

CHROMATOGRAPHIC DECOMPOSITION OF THE TRINITROBENZOLATES

Compound	$R_F \times 100$*		
	LP	*LP–T*	*T*
I			84
II		76	
III	49		
IV			87
V		73	
VI	46		
VII		78	
VIII			88
IX		85	
X			14
XI			14
Trinitrobenzene	0	0	60

* Eluents: see Table III.

TABLE V

UV ABSORPTION SPECTRA

Compound	*λ (nm) (log ε)*	λ_{max} *(nm) (log ε)*	
		a	*b*
I	*p* bands: 284 (3.70), 274 (3.86), 264 (3.79), 256 (3.68), 248 (3.44)	274 (3.60)	274 (3.86)
II	*p* bands: 266 (3.65), 274 (3.68), 286 (3.54)	274 (3.45)	274 (3.68)
III	*p* bands: 373 (3.85), 354 (3.87), 340 (3.77), 322 (3.50), 309 (3.17)	354 (3.64)	354 (3.87)
IV	*p* bands: 292 (4.32), 280 (4.22), 272 (4.26)	292 (4.18)	292 (4.32)
V	*p* bands: 320 (4.21), 304 (4.19), 292 (4.14), 280 (4.15)	320 (4.10)	320 (4.21)
VI	*p* bands: 336 (4.75), 320 (4.50), 306 (4.02), 294 (3.66)	336 (4.40)	336 (4.75)
VII	280 (3.80), 288 (3.86), 300 (3.65) 304 (3.34)	288 (3.60)	288 (3.86)
VIII	α–bands: 300 (4.01), 288 (3.76), *p* bands: 262 (4.26)	262 (4.14)	262 (4.26)
IX	300 (3.68), 298 (3.98), 286 (4.22), 278 (4.26), 273 (4.12), 250 (4.30), 242 (4.12)	250 (4.16)	250 (4.30)
X	228 (4.85), 254 (3.40), 260 (3.60), 274 (3.65), 285 (3.50)	228 (4.60)	228 (4.85)
XI	243 (4.30), 320 (3.73)	243 (4.02)	243 (4.30)

RESULTS AND DISCUSSION

The results for the picrates and trinitrobenzolates and the melting points and the yields of the different compounds after the purification procedures are given in Tables I and II. In Tables III and IV the eluents used in the chromatographic decomposition procedure and the $R_F \times 100$ values for the purified compounds and the reactants are given. UV absorption bands, fundamentally *p* bands[3], of the compounds after the purification process are given in Table V, together with $\lambda_{max.}$ (log ε) values of the compounds (a) before and (b) after the purification step. For the trinitrobenzolates, the UV spectra of the compounds do not differ appreciably from those indicated in Table V, and have therefore been omitted.

Compounds I–XI were commercial products with melting points (°C) of 75–77 (I), 29–32 (II), 207–210 (III), 95–98 (IV), 230–234 (V), 150–153 (VI), 88–92 (VII), 107–110 (VIII), 80–83 (IX), 117–120 (X) and 40–43.5°C (XI). The melting points of the compounds after the chromatographic process and after recrystallization are given in Tables I and II. These results and those in Tables III–V indicate the degree of purification attained.

ACKNOWLEDGEMENT

The authors thank the Comisión de Investigaciones Científicas de la Provincia de Buenos Aires, Argentina, for financial support.

REFERENCES

1 A. U. Rahman and O. L. Tombesi, *J. Chromatogr.*, 23 (1966) 312–315.
2 E. H. Rodd, *Chemistry of Carbon Compounds*, Volume III, Part B, Elsevier, Amsterdam, 1956, p. 1481.
3 E. Clar, *Polycyclic Hydrocarbons*, Vol. 1, Academic Press, London, 1964.

Journal of Chromatography, 463 (1989) 457-462
Elsevier Science Publishers B.V., Amsterdam — Printed in The Netherlands

CHROM. 21 112

Note

Bioautographic detection of T-2 and HT-2 toxins

HEATHER KOSHINSKY, SANDRA HONOUR and GEORGE KHACHATOURIANS*
Environmental Toxicology Laboratory, Department of Applied Microbiology and Food Science, University of Saskatchewan, Saskatoon, Saskatchewan S7N 0W0 (Canada)
(First received July 11th, 1988; revised manuscript received November 15th, 1988)

The trichothecenes are a group of mycotoxins produced by numerous fungi that contaminate many agricultural products worldwide. The salient features of these molecules are the 9, 10 double bond and the 12, 13 epoxide ring. Without the presence of these two groups the molecules lose their toxicity[1]. The trichothecene mycotoxins are the causative agents of a large number of animal and human diseases[2]. T-2 toxin is one of the most toxic trichothecenes. In humans[3], cultured chinese hamster ovary cells[4], bovine rumen bacteria[5,6] and soil bacteria[7] the major metabolite resulting from the breakdown of T-2 toxin is HT-2 toxin.

A simple method is described for the detection and quantitative determination of T-2 toxin and its separation from HT-2 toxin on silica gel layers based on growth inhibition of *Kluyveromyces fragilis* and *Saccharomyces cerevisiae* by these mycotoxins. The detection limit for T-2 toxin is 0.2 nmol per spot. The area of growth inhibition corresponds logarithmically to the toxin concentration. T-2 toxin could be quantitatively detected from 0.2 to 160 nmol per spot.

EXPERIMENTAL

Test organism

Cultures of *S. cerevisiae* strain GR 262, *ade 2 ura 1* [ERY^S OLI^R] and *K. fragilis* strain GK 1005 were grown in YPD which consisted of, on a weight per volume basis, 1% yeast extract, 1% peptone and 2% dextrose[8,9]. To keep the number of cells constant in all procedures a standardized culture was prepared by growing cells in YPD at 30°C/200 rpm (3.3 Hz) for *S. cerevisiae* and at 35°C/200 rpm (3.3 Hz) for *K. fragilis* until the optical density at 610 nm was 0.30, as determined with a colorimeter (Chemtrix, Hillsboro, OR, U.S.A.).

Mycotoxins

T-2 toxin (99% pure as supplied by the manufacturer) was purchased from Myco-lab (Chesterfield, MO, U.S.A.). HT-2 toxin was purchased from Sigma (St. Louis, MO, U.S.A.). Tritium-labelled T-2 toxin (1.35 mCi/ml) was from Nuclear Research Centre-Negev (Beer Sheva, Israel). Stock standard solutions of T-2 toxin were prepared at a concentration of 20 nmol/μl in 95% ethanol and stored at −20°C until used. All other chemicals were of analytical-reagent grade.

0021-9673/89/$03.50

Thin-layer chromatography

A 3-μl volume of the stock standard solution was spotted 2 cm from the lower edge of 20 cm glass or plastic-backed pre-coated silica gel 60 thin-layer chromatography (TLC) plates (Merck $60F_{254}$, Merck, Darmstadt, F.R.G.). To equilibriate, without contacting the liquid, dry spotted plates were placed horizontally in a chamber containing chloroform–methanol (9:1, v/v) for 1 h[10]. Following this, the chamber was raised and the TLC plate developed by the ascending technique for approximately 2.5 h until the front reached a height 3 cm from the top of the plate. Plates were removed and dried overnight at 60°C.

Detection

After evaporation of the solvent, divisions of TLC plates containing [^{3}H]T-2 toxin were scraped into fractions which were collected in scintillation vials containing 5 ml of Beckman Ready-Solv GP scintillation cocktail (Beckman Instruments, Irvine, CA, U.S.A.), and counted for radioactivity in a Beckman LS-7500 scintillation counter. For bioautographic detection both sides of TLC plates were sterilized by a 60-s exposure to ultraviolet light (General Electric, germicidal 30-W bulb, G30T8) from 60 cm with a fluence of 24 ergs/s/cm^2. The plastic-backed plates were secured to pieces of glass with double-sided tape. To contain the agar a 3-mm ridge was formed with Tygon® tubing running around the plate. Both glass and plastic-backed plates were placed on a horizontal bench and evenly layered with growth media, either sterile molten (80°C) YPD (1.75% agar) or YPG agar (1% yeast extract, 1% peptone, 4% glycerol, and 1.75% agar). After solidification, the surface of the agar growth medium was swabbed with an inoculum made of a standardized culture of *K. fragilis* or *S. cerevisiae*. These plates were placed in a sterile, tightly sealed plastic container and incubated at 35°C and 24 h for *K. fragilis* and 30°C and 48 h for *S. cerevisiae*. After incubation, the TLC plates swabbed with *K. fragilis* were layered with a 10% (w/v) triphenyltetrazolium chloride agar overlay[11]. Presence of the trichothecenes could be observed as areas where there was no growth. Use of tetrazolium with *K. fragilis* aids the visualization of the zone of growth inhibition as it stains the colonies red. Zones of growth inhibition were measured to the nearest 0.2 mm using calipers.

Densitometry

Following incubation the diameter of the area of no growth was determined with a densitometric scan at 610 nm and a beam slit of 0.5 × 5.0 mm (E-C Apparatus Corp., St. Petersburg, FL, U.S.A.). Scanning was carried out from the origin to the solvent front.

RESULTS AND DISCUSSION

Current TLC methods for trichothecene detection lack sensitivity mainly because type A and B trichothecenes have no absorption bands or fluorescence under ultraviolet or visible light[10]. Visualization of trichothecenes requires the TLC plates to be developed with suitable solvents so that the spots can be detected subsequently by color or fluorescence[12]. Different reagents work best with the different types of trichothecene mycotoxins. Aluminium chloride is relatively specific for type B trichothecenes while type A trichothecenes can be visualized with chromotrophic acid

(CA)[13]. Both these compounds have a poor structural affinity for the 12,13-epoxy group in the trichothecene nucleus[14]. 4-(*p*-Nitrobenzyl)pyridine (NBP) is reported to interact with the trichothecene nucleus and has been used for the detection of types A, B and D. These reagents react with a wide range of extraneous compounds. Unless the samples are put through several cleanup steps these reactions can obscure the toxins[14–16].

Unlike chemical detection bioautography is based on the biological effects of the substance to be detected[17]. As TLC procedures would not alter the chemical structure and hence the biological activity of trichothecenes, bioautography overcomes the visualization problems found when using chemical detection methods and is a suitable alternative. An earlier report[18] of the bioautography of T-2 toxin based on growth inhibition of *Prototheca wickerhamii* indicated a sensitivity range of 0.2 to 5.0 nmol per spot. While satisfactory, the detection range is narrow and there are numerous problems involved in the growth and maintenance of algae.

The study of the toxicity of trichothecene mycotoxins, has shown that several genera of yeast are sensitive[19]. Two of these yeast, *S. cerevisiae and K. fragilis* can be used to bioautographically detect T-2 toxin. Coincident with a single zone of growth

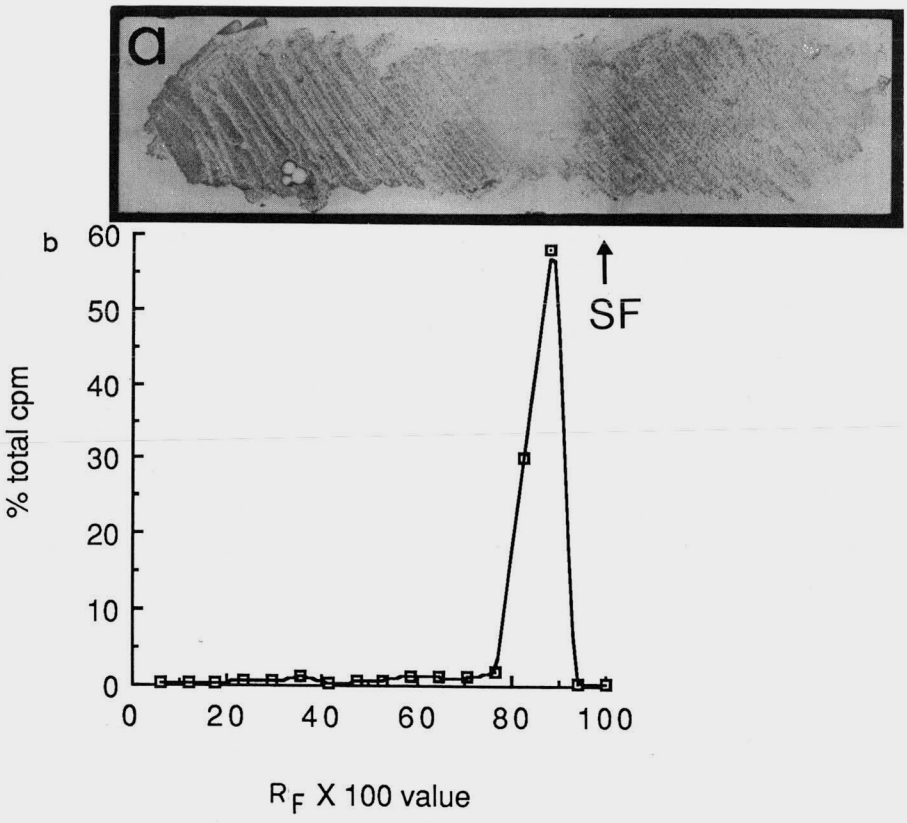

Fig. 1. Thin layer chromatography of T-2 toxin. (a) Detection by bioautography with *S. cerevisiae* on YPG agar (SF = solvent front). Spot contained 20 nmol T-2 toxin. (b) Detection with radioactivity of [^{3}H]T-2 toxin (100% cpm = 8070).

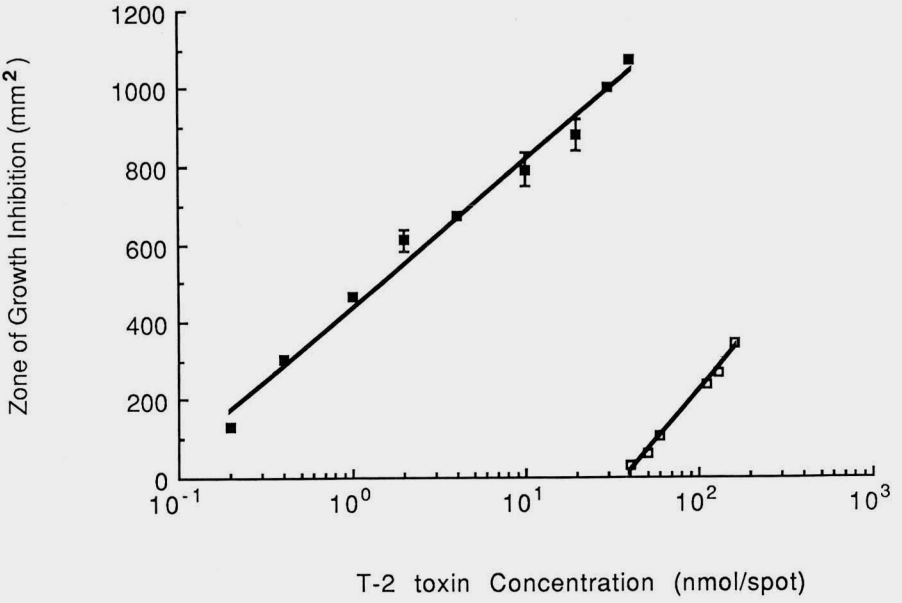

Fig. 2. Calibration graph for T-2 toxin. Bioautographic detection with (□) *S. cerevisiae* or (■) *K. fragilis* on YPD agar. Bars indicate the standard error. Lines represent fitted regression lines: (□) $y = -814.05 + 518.47x$; $r = 1.00$; (■) $y = 442.10 + 377.39x$; $r = 0.99$.

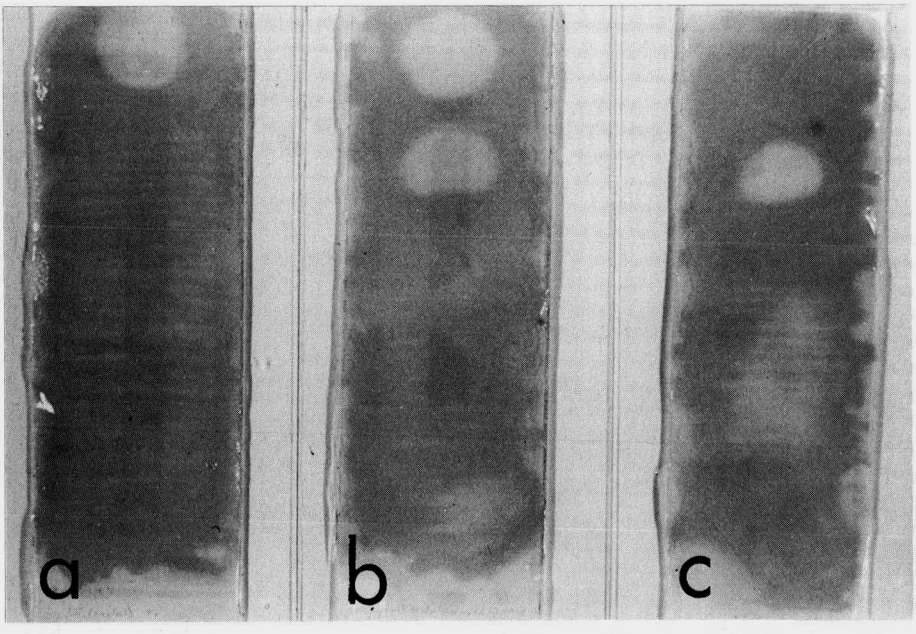

Fig. 3. TLC of trichothecene mycotoxins showing separation of T-2 toxin and HT-2 toxin and bioautographic detection with *K. fragilis* on YPD agar. Spots contained (a) 2.0 nmol T-2 toxin, (b) 2.0 nmol T-2 toxin and 40 nmol HT-2 toxin, (c) 40 nmol HT-2 toxin.

inhibition was a single region of radioactivity from [^{3}H]T-2 toxin (Fig. 1) indicating that growth inhibition is due to T-2 toxin.

A calibration graph (Fig. 2) was constructed for T-2 toxin. The zone of growth inhibition is logarithmically proportional to the toxin concentration in a range from 0.2 to 160 nmol. *K. fragilis* is used as the test organism from 0.2 to 40 nmol, while *S. cerevisiae* is used from 40 to 160 nmol. With both test organisms there was an excellent correlation between log of T-2 toxin concentration and zone of growth inhibition. Values shown in Fig. 2 represent the mean of 3 replicates. The standard error of these values never exceeded 10% of the mean.

To test the calibration curve T-2 toxin and HT-2 toxin were mixed. TLC and bioautography permitted the separation, detection and quantification of T-2 toxin and its major breakdown product, HT-2 toxin (Fig. 3). The larger zone of inhibition is produced by T-2 toxin. The $R_F \times 100$ value of T-2 toxin is 86 while that of HT-2 toxin is 71. In all solvent systems reported T-2 toxin has a larger R_F value than HT-2 toxin[10]. The zone of growth inhibition produced with T-2 toxin is 560 mm^2, corresponding to a T-2 toxin concentration of 1.95 nmol. The calculated concentration is very close to the actual concentration of 2.0 nmol.

At present using visible light T-2 toxin can be detected at levels of 2.0 nmol per spot with cerium(IV) sulphate[20] and 0.2 nmol per spot with CA[13] and NBP[141]. Using ultraviolet light T-2 toxin can be detected at levels of 0.4 nmol per spot with *p*-anisaldehyde[21], 0.1 nmol per spot with CA[13] and 0.05 nmol per spot with nicotinamide-2-pyridine (NAP)[15]. Our bioautographic detection permits visualization at levels comparable to most of these reagents but offers several practical advantages not present in other methods. First, the method of detection is very simple. Unlike the other methods no chemical developing reagents, high temperatures or extensive handling of the plates are required. Second, for reference purposes the TLC plates can be dried and the zone of inhibition remains visible for over 1.5 years. When T-2 toxin is detected with NBP or CA the color remains visible for 3 h[14] and a few weeks[13], respectively. The fluorescence observed when T-2 toxin is detected with NAP is stable for less than 4 h[15]. Third, using bioautography the detection range for T-2 toxin is 0.2–160 nmol per spot, which is an increase over the range of 0.2 to 20 nmol per spot reported for NBP[14] and over the range of 0.2 to 25 nmol per spot reported for bioautographic detection with *P. wickerhamii*[18]. Fourth, the cleanups steps required to avoid reactions with extraneous compounds[16] are eliminated as bioautographic detection identifies the compounds based on toxicity. A final point in considering bioautographic detection of T-2 toxin is that some of the compounds used in other procedures are human health hazards.

Using TLC and bioautography T-2 toxin can be separated from its major breakdown product HT-2 toxin. This coupled with the stability of the plates and the increased detection range makes bioautographic detection especially suited for use in situations demanding the ability to quantify T-2 toxin and detect HT-2 toxin.

ACKNOWLEDGEMENTS

This work was supported by grant 493 from the Natural Sciences and Engeneering Research Council of Canada. H. Koshinsky was the recipient of a University of Saskatchewan Graduate Student Scholarship and the Canadian Pacific Fellowship

in Biotechnology. S. Honour was the recipient of a NSERC Summer Student Fellowship.

REFERENCES

1 Y. Ueno, *Pure Appl. Chem.*, 49 (1977) 1737.
2 C. J. Mirocha, in M. O. Moss and J. E. Smith (Editors), *The Applied Mycology of Fusarium*, British Mycological Society, U.K., 1984, p. 141.
3 S. A. Watson, C. J. Mirocha and A. W. Hayes, *Fundam. Appl. Toxicol.*, 4 (1984) 700.
4 L. R. Trusal, *Toxicon*, 6 (1986) 597.
5 K. Westlake, R. I. Mackie and M. F. Dutton, *Appl. Environ. Microbiol.*, 53 (1987) 587.
6 S. P. Swanson, J. Nicoletti, H. D. Rood Jr., W. B. Buck, L.-M. Cote and T. Yoshizawa, *J. Chromatogr.*, 414 (1987) 335.
7 Y. Ueno, K. Nakayama, K. Ishii, F. Tashiro, Y. Minoda, T. Omori and K. Komagata, *Appl. Environ. Microbiol.*, 46 (1983) 120.
8 K. T. Schappert and G. G. Khachatourians, *Curr. Genet.*, 10 (1986) 671.
9 K. T. Schappert and G. G. Khachatourians, *J. Microbiol. Methods*, 3 (1984) 43.
10 V. Betina, *J. Chromatogr.*, 334 (1985) 211.
11 M. Ogur, R. St. John and S. Nagai, *Science*, 125 (1957) 928.
12 G. V. Rao, P. S. Rao, S. Girisham and S. M. Reddy, *Curr. Sci.*, 54 (1985) 507.
13 J. A. Baxter, S. J. Terhune and S. A. Qureshi, *J. Chromatogr.*, 261 (1983) 130.
14 S. Takitani, Y. Asabe, T. Kato, M. Suzuki and Y. Ueno, *J. Chromatogr.*, 172 (1979) 335.
15 A. Sano, Y. Asabe, S. Takitani, and Y. Ueno, *J. Chromatogr.*, 235 (1982) 257.
16 B. Harrach, C. J. Mirocha, S. V. Pathre and M. Paluysik, *Appl. Environ. Microbiol.*, 41 (1981) 1428.
17 V. Betina, *J. Chromatogr.*, 78 (1973) 41.
18 J. Teren and L. Ferenczy, *Elelmiszervizgalati Kozl.*, 20 (1974) 267.
19 S. Sukroongreung, K.T. Schappert and G. G. Khachatourians, *Appl. Environ. Microbiol.*, 48 (1984) 416.
20 C. P. Gorst-Allman and P. S. Steyn, *J. Chromatogr.*, 175 (1979) 325.
21 P. M. Scott, J. W. Lawrence and W. van Walbeek, *Appl. Microbiol.*, 20 (1970) 839.

Journal of Chromatography, 463 (1989) 463–468
Elsevier Science Publishers B.V., Amsterdam — Printed in The Netherlands

CHROM. 21 111

Note

Analysis of saccharin, acesulfame-K and sodium cyclamate by high-performance ion chromatography

THOMAS A. BIEMER

Warner Lambert Company, Consumer Products Division, 170 Tabor Road, Morris Plains, NJ 07950 (U.S.A.)

(First received August 23rd, 1988; revised manuscript received November 15th, 1988)

Artificial sweeteners are widely used in the food, beverage, confectionary and pharmaceutical industries throughout the world. Some examples of their application include soft drinks, candies, mints, gums, mouthwashes and pharmaceutical dosage forms such as cough syrups. The diversity of products containing artificial sweeteners is therefore quite large, and the sample matrices from which they are to be assayed may be complex. Additionally, the sweeteners may be used singly or in combination with other sweeteners.

Methods have been reported in the literature for the analysis of artificial sweeteners in various sample matrices. The most recent procedures for saccharin and acesulfame K, for example, are represented by high-performance liquid chromatography (HPLC) methods run in reversed-phase mode or reversed-phase mode with an ion pair reagent and using UV detection[1–3].

Analysis of sodium cyclamate is more difficult owing to its poor UV absorbing characteristics. Some of the reported methods for analyzing this sweetener include gas chromatography and colorimetric spectrophotometry[4,5]. These procedures can be time consuming since the compound must be first derivatized prior to analysis. More recently, cylcamate was determined using HPLC with indirect photometric detection[6]. In this technique, the compound's elution is monitored against a UV absorbing mobile phase component.

High-performance ion chromatography offers an attractive alternative to these more traditional methods of analysis. In contrast to organic solvent mediated separations, ion chromatography separations are performed using aqueous buffers. The buffers typically are prepared from inexpensive salts as compared to the expensive organic solvents required for HPLC. In addition, the effluent is usually innocuous since it is comprised of buffer salts and usually can be disposed down laboratory sinks as it is generated. Hydroorganic solvents used in reversed-phase chromatography require costly special handling and disposal.

Typically in ion chromatography, electrochemical detection is employed such as an amperometric or conductivity detector. Compounds having poor UV absorption may be ideal candidates for conductivity detection as in the case of sodium cyclamate, particularly if they readily ionize in solution. On the other hand, UV absorbing excipients such as flavors and dyes, may not give any electrochemical response and can therefore be eliminated as an interferent in quantitation of the

0021-9673/89/$03.50

analyte. Thus ion chromatography offers the opportunity to streamline methods development and increase sample throughput.

This paper describes the development of ion chromatography methods for the analysis of saccharin (or sodium saccharin), acesulfame K and sodium cyclamate. The methods have been tested on various products including gums, mints, boiled and soft confectionary candy, mouthwashes, and cough syrups. The methods have been used as described for the analysis of the sweeteners without any modification of the analytical conditions. It appears that little if any method development work would be required to use the methods on other similar types of products.

EXPERIMENTAL

Apparatus

The entire ion chromatographic system was the Dionex 4000i advanced chromatography module containing the pump, automatic injector and a Model CDM1 conductivity detector (Dionex, Sunnyvale, CA, U.S.A.). The signal from the conductivity detector was passed to a Heath d.c. offset module model EU-200-02 (Heath Schumberger, Benton Harbor, MI, U.S.A.) to reduce the 100-mV baseline signal to 1 mV and be compatible with the Sigma 10 data station (Perkin-Elmer, Norwalk, CT, U.S.A.) used to collect the peak areas. A spectrum 921 high-frequency module set at 0.01 (Spectrum, Newark, DE, U.S.A.) removed any stray high-frequency noise. A Dionex AS4A anion separator column and a AS4G guard column were used at room temperature. The micro membrane suppressor was the Dionex Model AMMS-1.

Reagents

All the reagents used were analytical grade. Water used in the preparation of the mobile phases and regenerate solutions was purified by passing through a Milli-RO4 system (Millipore, Bedford, MA, U.S.A.) and had a resistivity of 16 Ω or greater.

Chromatography conditions

System 1. The mobile phase for analysis of saccharin and acesulfame K consisted of 300 mg sodium carbonate dissolved in 1 l Milli-Q water. The solution was filtered through a 0.45-μm Nylon 66 membrane (Rainin, Woburn, MA, U.S.A.) and degassed using sonication and vacuum prior to use. The conditions used were as follows: flow-rate, 2.0 ml/min; back pressure, *ca.*1000 p.s.i.; injection volume, 50 μl; detector sensitivity, 30 μs; detector compensation temperature, 1.7°C; chart speed, 5 mm/min. The regenerate solution was prepared by diluting 2.4 ml sulfuric acid in 2 l Milli-Q water to give a 0.025 *M* solution.

System 2. The mobile phase for analysis of sodium cyclamate consisted of 140 mg sodium bicarbonate dissolved in 1 l Milli-Q water and filtered and degassed as above. The conditions for cyclamate analysis were as follows: flow-rate, 1.5 ml/min; back pressure, 800 p.s.i.; injection volume, 50 μl; detector sensitivity, 30 μS; detector compensation temperature, 1.7°C; chart speed, 5 mm/min. The regenerate solution was 0.012 *M* sulfuric acid prepared by diluting 1.2 ml sulfuric acid in 2 l Milli-Q water.

For both analyses, the regenerate flow was adjusted to give a background conductivity of 10–18 μS for baseline.

Standard preparation

Stock solutions of saccharin or acesulfame K were prepared by dissolving 100 mg saccharin or acesulfame K in 100 ml of sodium carbonate (300 mg/l) buffer. A 5-ml aliquot was taken into a 50-ml volumetric flask containing 2 ml of a 0.90-mg/ml sodium fumarate internal standard then diluted to volume with buffer. The working standard was prepared by making a final 1:10 dilution of this solution.

A stock solution of sodium cyclamate was prepared by dissolving 90 mg sodium cyclamate in 50 ml of a buffer solution containing 140 mg/l sodium bicarbonate. A 3-ml aliquot was then pipetted into a 50-ml volumetric flask containing 2 ml of potassium bromide (1.5 mg/ml) internal standard then diluted to volume with bicarbonate buffer. A 10-ml aliquot was then diluted to 100 ml to prepare the working standard.

Sample preparation

Gum samples were prepared by placing the sample in a 125-ml erlenmeyer flask and extracting with a mixture of 1 ml glacial acetic acid, 2 ml internal standard, 50 ml water, and 25 ml chloroform. Hard or soft candy samples were shaken with 2 ml internal standard and 50 ml of water until dissolved. An aliquot of the aqueous phase was then taken and diluted to a suitable volume using either the carbonate or bicarbonate buffer. Liquid samples were prepared by diluting aliquots of the sample to an appropriate volume using buffer solution. Samples and standards were filtered through a 0.45-μm Nylon 66 filter prior to injection in the ion chromatograph.

RESULTS AND DISCUSSION

Response was linear for each of the analytes in the following concentration ranges: sodium cyclamate, 0.0508–0.0010 mg/ml; sodium saccharin, 0.0262–0.0022 mg/ml; and acesulfame K, 0.0245–0.0041 mg/ml. The correlation coefficients for the three analytes were 0.994, 0.9998 and 0.9999 respectively.

Chromatographic reproducibility results were obtained by injecting spiked samples of a gum and hard candy eight times throughout the day using the analytical conditions described for each sweetener. The relative standard deviation of area counts for each analyte was: cyclamate, 0.5%; bromide, 1.16%; acesulfame-K, 0.9%; saccharin, 1.1%; and fumarate, 0.5%. Recovery studies were conducted for each analyte by spiking blank gum and candy samples. Recovery of sweeteners from spiked gum is presented in Table I. Similar recovery data was obtained for spiked candy samples.

Table II shows calculated values for plates counts (N), capacity factors (k'), and asymmetry factors (a) for the compounds studied. A typical chromatogram of extracted gum sample spiked with saccharin and acesulfame K is presented in Fig. 1. Fig. 2 shows a typical chromatogram of a gum sample containing sodium cyclamate.

To ascertain the overall usefulness of the procedures, several different types of sugar based fruit flavored candy, and cinnamon, spearmint and peppermint flavored confections were analyzed to ascertain if there were peaks interfering with quantita-

TABLE I

RECOVERY OF ARTIFICIAL SWEETENERS FROM GUM

Added (mg)	*Found (mg)*	*Recovery (%)*
Cyclamate		
29.62	31.28	105.6
24.68	27.00	109.4
21.72	22.22	102.4
19.74	19.74	100.0
17.77	17.77	100.0
9.87	9.37	94.9
4.94	4.75	96.3
Saccharin		
6.55	6.72	102.5
5.46	5.36	98.2
4.32	4.38	100.3
3.28	3.34	101.8
2.18	2.17	99.8
Acesulfame K		
6.12	6.34	103.6
5.09	5.05	99.2
4.08	4.08	100.0
3.06	3.10	101.2
2.04	2.08	102.2

tion of the artificial sweeteners. None of the samples tested contained any extra excipient peaks eluting at the retention times of the sweeteners. Common inorganic anions such as fluoride, chloride, nitrite, phosphate or sulfate, for example, did not interfere in the analysis of saccharin or acesulfame K. The cyclamate analysis is also free from these interferences except for chloride. When analyzing samples containing chloride and cyclamates, the sodium bicarbonate should be reduced to *ca.* 50 mg/l in order to obtain adequate resolution between the chloride and cyclamate peaks. As with any sample, there is always the possibility of an excipient coeluting with the analyte since ingredients can vary from sample to sample and country of origin. One of the distinct advantages is the use of conductivity detection of the artificial sweeteners since exipients may not exhibit an electrochemical response hence not appear in the chromatogram. Additionally, use of ion chromatography can offer considerable savings in the purchase of HPLC grade solvents and subsequent disposal of spent solvents.

TABLE II

PLATE NUMBERS (N), CAPACITY FACTORS (k') AND ASYMETRY FACTORS (a) FOR THE COMPOUNDS STUDIED

	N	k'	a
Cyclamate	1495	4.10	1.17
Acesulfame K	1700	6.98	1.00
Saccharin	1615	10.45	1.23

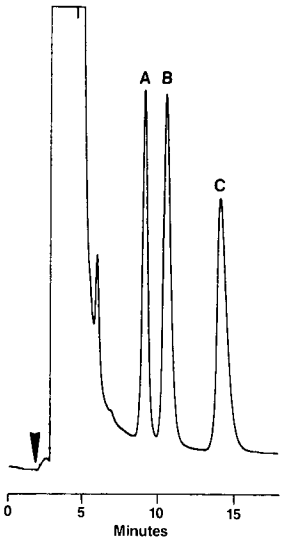

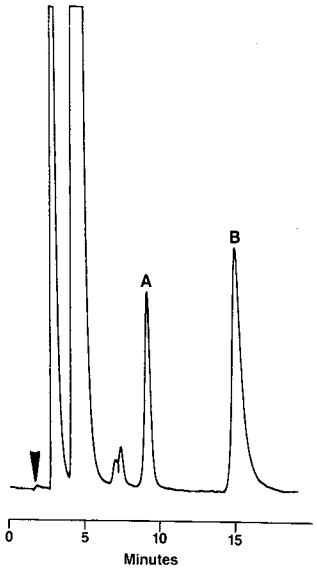

Fig. 1. Chromatogram of gum sample spiked with saccharin and acesulfame K. A = fumarate; B = acesulfame K; C = saccharin; conditions, system 1.

Fig. 2. Chromatogram of gum sample spiked with sodium cyclamate. A = cyclamate; B = bromide; conditions, system 2.

In the method for the analysis of cyclamate, some samples required use of a 'wash injection'. It was observed that after several injections, there was a noticeable decline in retention time for cyclamate and bromide. This situation would probably arise when analyzing products containing species such as phosphate, citrate, or other strongly retained compounds. In a short time, the column began to lose ion-exchange capacity as evidenced by the decreasing retention times of the peaks of interest. In these situations, use of a 0.2 *M* sodium carbonate wash injection during the analysis (*i.e.*, after 6–7 sample injections) helped elute the strongly retained components thus reactivating exchange sites in the resin and regenerating full ion-exchange capacity. The cyclamate analysis required a separate mobile phase because it is a weaker anion than either saccharin or acesulfame K. Therefore, a weak mobile phase was required to retain this compound on the column.

The internal standard methods described above are intended to simplify preparation of solid samples and are not indicative of any imprecision expected in the chromatography or injection of the sample. As a matter of choice, it appeared easier to place samples into wide mouth glassware and pipet small volumes of internal standard than attempting to quantitatively transfer bulky samples to volumetric glassware. In the case of liquid samples, aliquots were taken and diluted to a known volume without adding the internal standard. Using either procedure, the methods are accurate and yield excellent quantitative results.

REFERENCES

1 M. Veerabhadrarao, M. S. Narayan and O. Kapur, *J. Assoc. Off. Anal. Chem.*, 70(3) (1987) 578–82.
2 H. Terada and Y. Sakabe, *J. Chromatogr.*, 346 (1985) 333–340.
3 U. Zache and H. Gruending, *Z. Lebensm.-Unters.-Forsch.*, 184 (1987) 503–509.
4 K. Nagasawa, A. Ogamo and T. Shinozuka, *J. Chromatogr.*, 111 (1975) 51–56.
5 A. J. Shenton and R. M. Johnson, *Analyst (London)*, 98 (1973) 749–754.
6 A. Herrmann, E. Damawandi and M. Wagmann, *J. Chromatogr.*, 280 (1983) 85 90.

Journal of Chromatography, 463 (1989) 469–473
Elsevier Science Publishers B.V., Amsterdam — Printed in The Netherlands

CHROM. 21 076

Note

Identification and purity determination of benzathine and embonate salts of some β-lactam antibiotics by thin-layer chromatography

TARJA SAESMAA

Department of Pharmaceutical Chemistry, University of Helsinki, Fabianinkatu 35, SF-00170 Helsinki (Finland)

(First received February 2nd, 1988; revised manuscript received October 26th, 1988)

The organic salts of both ampholytic β-lactam antibiotics and their prodrug esters are nearly always precipitated from aqueous solutions[1]. In such solutions, penicillins and cephalosporins can decompose in a number of ways[2,3]. Moreover the salt-forming agents and alcoholic solvents, being nucleophiles, may even interact with penicillins and cephalosporins to form amides or esters. However, no thin-layer chromatographic (TLC) or other procedure has yet been proposed for purity tests on the salts in question.

Some of the degradation products of benzathine salts of penicillin G and V have been separated and identified by a TLC system developed for identifying these salts[4]. According to the TLC studies of Fooks and Mattok[5], procaine penicillin G may contain, in addition to procaine and penicillin G, benzylpenicilloic acid, benzylpenillic acid and corresponding alkyl α-D-penicilloate.

The present paper describes a number of TLC systems and spray reagents which are capable of separating and identifying the cation and anion parts of benzathine and embonic acid salts of ampicillin, amoxycillin and cephalexin and talampicillin embonate. Since all of these TLC methods have been described earlier in connection with studies on degradation products of penicillins or cephalexin, they have now been used for assessment of the purity of the synthesized embonate and benzathine salts of β-lactam antibiotics[4,6–11].

EXPERIMENTAL

Materials

Amoxycillin trihydrate (Amphar, Amsterdam, The Netherlands), ampicillin trihydrate (Fermion, Helsinki, Finland) cephalexin monohydrate (Fermion) and talampicillin (Gechim, Milan, Italy) were kindly supplied by Orion Pharmaceutica. Benzathine diacetate (pure) was obtained from Koch-Light Laboratories (Colnbrook, U.K.), and embonic acid (99%) from Ega-Chemie (Steinheim, F.R.G.). All the other chemicals were of commercial analytical grade. The identification of the antibiotics and salt-forming agents and the preparation methods for benzathine and embonate salts of ampicillin, amoxycillin and cephalexin (1:2) and talampicillin embonate (2:1) have been presented elsewhere[12].

0021-9673/89/$03.50

Thin-layer chromatography

Commercially available precoated silica plates (Kieselgel 60 or Kieselgel 60 F_{254}: Merck, Darmstadt, F.R.G.), 20 cm × 20 cm (chromatographic chamber, 22 cm × 22 cm × 10 cm, lined with filter paper) or cut to 10 cm × 10 cm (Camag chamber, 13 cm × 12 cm × 5 cm) were used. The salts and reference substances were rapidly dissolved in methanolic Sörensen phosphate buffers (1/15 *M*, pH 7.0) (7:3, v/v) in an ultrasonic bath at room temperature[13]. A 5-μl aliquot of each of the solutions (0.5, 1 or 2 mg/ml) was applied to the plates (n = 6–10) and the plates were developed in saturated chambers at room temperature. The spots were inspected under UV light (366 nm) and developed with iodine vapour or by uniformly spraying the plate with some of the spray reagents. Mobile phases: (A) 1-butanol–acetic acid–water (4:1:1, v/v/v); (B) ethyl acetate–acetic acid–water (70:15:15, v/v/v); (C) ethyl acetate–acetic acid–water (7:2:1, v/v/v/); (D) ethyl acetate–acetic acid–water (3:1:1, v/v/v); (E) acetic acid–butyl acetate–1/15 *M* Sörensen buffer pH 5.6–1-butanol–absolute ethanol (20:40:12:5:7.5, v/v); (F) 1-butanol–formic acid–water (80:3:1, v/v/v); (G) chloroform–ethanol–acetic acid (9:1:0.2, v/v/v); (H) water–acetic acid–acetone–ethyl acetate (1:2:2:5, v/v). Spray reagents: (1) 0.2% ninhydrin in ethanol and heating at 105°C; (2) modified chloroplatinic reagent: 0.1 ml 1 *M* hydrochloric acid, 300 μl 10% hexachloroplatinate (IV)–acid solution, 20 ml acetone and 0.2 ml 20% potassium iodide–water solution[4,6]; (3) 1% starch solution–acetic acid–0.1 *M* iodine solution (100:8:1, v/v/v)[7].

RESULTS AND DISCUSSION

In order to minimize decomposition of the parent antibiotics, the preparation of the organic salts of β-lactam antibiotics was mainly carried out at low temperatures and at neutral pH region[1]. However, aminopenicillins, and cephalexin can react with water molecules or undergo intra- or intermolecular aminolysis in neutral media[2]. Since no general purity test is available for penicillins, a large number of procedures were used in the present study to determine possible degradation products of the benzathines and embonates synthesized.

A mixture of Sörensen phosphate buffer pH 7.0 and methanol (3:7) was selected for the sampling solvent because it did not give any shadow spots with the samples of the antibiotics and their salts. Moreover, this kind of mixture has been shown to reduce the degradation of penicillin G and V[14].

Methanol proved to be unsuitable as the sampling solvent because aminopenicillins and their salts gave shadow spots when dissolved in methanol. According to an earlier report, decomposition of penicillin G occurs when alcoholic solutions are used for spotting the chromatograms, owing to the formation of the corresponding alkyl α-D-penicilloate[5]. Only penicillin G was detected when freshly prepared aqueous solutions were used. However, no data have been published to indicate that aminopenicillins would behave in the same way as penicillin G.

The best separation and identification of the components of the benzathines were achieved with mobile phases B, E and F (Table I). Mobile phase A separated benzathine and cephalexin completely, but the components of benzathine ampicillin and benzathine amoxycillin were also identified on the basis of the different colours of the benzathine and penicillin spots. Iodine dyes benzathine brown and penicillins and

TABLE I

TLC hR_F VALUES OF BENZATHINE AND EMBONIC ACID SALTS OF AMPICILLIN, AMOXYCILLIN AND CEPHALEXIN AND TALAMPICILLIN EMBONATE AND THEIR REFERENCE SUBSTANCES IN DIFFERENT SOLVENT SYSTEMS

Identification of the impurity spots is explained in the text. – = not sampled.

Sample	*Mobile phase*						
	A	*B*	*C*	*D*	*E*	*F*	*G*
Ampicillin trihydrate	40	14	31	–	34	32	0
Amoxycillin trihydrate	40	11	–	39	32	37	–
Cephalexin monohydrate	29	9	–	34	27	15	–
Talampicillin	69	86	92	–	–	39	55
	53*	38*	58*			32*	24
	39	15	32				19
	32	12					12
		9					0*
Benzathine diacetate	38	19	39	49	39	4	–
Embonic acid	65	83	93	95	–	73	29
Benzathine ampicillin	40	19	42	–	39	32*	–
	38	14	31		34	4.5	
						4	
Benzathine amoxycillin	46	19	–	86	41	37*	–
	40*	16		57	38	9	
	38	11*		52	32*	4	
				48			
				39*			
Benzathine cephalexin	38	19	–	47	39	15	–
	29	9		34	27	4	
Ampicillin embonate	65	83	92	–	–	73	–
	40	15	31			32	
Amoxycillin embonate	65	83	–	95	–	73	–
	40	12		39		37	
Cephalexin embonate	65	83	–	96	–	73	–
	28	10		34		15	
Talampicillin embonate	65	83	90	–	–	73	29
	52	37				32	0

* The main spot of the chromatogram containing additional spots.

cephalexin yellow; ninhydrin dyes benzathine reddish brown and penicillins and cephalexin red. Mobile phase B permits rapid and convenient identification of the benzathines and embonates investigated; it distinguishes them all. The R_F values of embonic acid (UV 366 nm) differ considerably from those of penicillins and cephalexin (Table I, mobile phases B–D); the presence of embonic acid probably does not disturb the determination of the degradation products of embonates.

Ampicillin and its penicilloic acid were separated by five different solvent systems: 1-butanol–formic acid–water (80:3:1), 1-butanol–acetic acid–water (4:1:1), 1-butanol–water–ethanol-acetic acid (5:2:1.5:1.5), acetone–acetic acid (95:5) and 85% aqueous acetone[7,8]. Of these, only the first and second phases (A and F) gave good spots for benzathine and ampicillin; all the others yielded tailing spots.

Mobile phase F, used together with spray reagent 3, gave only one very small

impurity spot for benzathine ampicillin; according to its R_F value, 0.045, this spot may be the penicilloic acid of ampicillin[7]. Spray reagent 3 does not make benzathine visible, but iodine vapour (brown) or ninhydrin (reddish brown) can colour it. In the TLC experiment carried out by Vandamme and Voets[8] the penicilloic acid of ampicillin was dyed red-purple by ninhydrin; this colour was not detected in this experiment although other ninhydrin-positive substances, *e.g.*, aminopenicillins and some impurities of benzathine amoxycillin, were distinguished from benzathine quite clearly according to their different colours.

Some oligomers and the piperazinedione of ampicillin were separated from ampicillin by mobile phases C and F[7,9]. Benzathine ampicillin and ampicillin embonate did not give any spots at the published R_F values of the above-mentioned degradation products. No impurity spot was detected when the samples of benzathine cephalexin (R_F 0.51 and 0.40) or cephalexin embonate (R_F 0.41 and 0.97) were chromatographed by the method published for the determination of the piperazinedione of cephalexin (mobile phase H)[10].

Benzathine amoxycillin gave one impurity spot with mobile phases A (R_F 0.46), B (R_F 0,16), E (R_F 0.41) and F (R_F 0.09) with all the visualization methods. The spots were not identified. Using mobile phase D, benzathine amoxycillin (2 mg/ml) gave four impurity spots with iodine (Table I). In comparison with the published R_F values, these impurities may be piperazine-2,5-dione (R_F 0.86) and oligomers (R_F 0.48, 0.52, and 0.57) of amoxycillin[9]. Ninhydrin solution dyed the spots at R_F 0.48, 0.52 and 0.57 red like the amoxycillin spot; the benzathine spots were brown. The spot at R_F 0.86 was not detected by ninhydrin, only by iodine.

Talampicillin showed traces of impurities with all the methods. The impurity spot with R_F 0.55 (Table I, mobile phase G) may be due to phthalaldehydic acid[11]. One of the impurities of talampicillin may be ampicillin (Table I, mobile phases A–C). Talampicillin embonate samples produced only two intense spots with mobile phases A, B, F and G; the impurities of talampicillin were not detected in talampicillin embonate.

The results of these TLC studies indicate that the synthesized benzathine and embonic acid salts of antibiotics are very pure and homogeneous. The one exception is benzathine amoxycillin, which contains many degradation products. It has been concluded that amoxycillin forms polymers very rapidly, and that these are much more soluble in water than the corresponding ampicillin derivatives[9].

ACKNOWLEDGEMENTS

I thank Mr. John Derome (Lic. For.) for critically reading this manuscript.

REFERENCES

1 T. Saesmaa and J. Halmekoski, *Acta Pharm. Fenn.*, 96 (1987) 65.
2 P. C. Van Krimpen, W. P. Van Bennekom and A. Bult, *Pharm. Weekbl. Sci. Ed.*, 9 (1987) 1.
3 J. P. Hou and J. W. Poole, *J. Pharm. Sci.*, 60 (1971) 503.
4 W. L. Wilson, M. J. Lebelle and K. C. Graham, *Can. J. Pharm. Sci.*, 14 (1979) 27.
5 J. R. Fooks and G. L. Mattok, *J. Pharm. Sci.*, 58 (1969) 1357.
6 M. Pokorny, N. Vitezić and M. Japelj, *J. Chromatogr.*, 77 (1973) 458.
7 C. Larsen and M. Johansen, *J. Chromatogr.*, 246 (1982) 360.

8 E. J. Vandamme and J. P. Voets, *J. Chromatogr.*, 71 (1972) 141.
9 E. Roets, P. De Pourcq, S. Toppet, J. Hoogmartens, H. Vanderhaeghe, D. H. Williams and R. J. Smith, *J. Chromatogr.*, 303 (1984) 117.
10 H. Bundgaard, *Arch. Pharm. Chem. Sci. Ed.*, 5 (1977) 149.
11 Y. Shiobara, A. Tachibana, H. Sasaki, T. Watanabe and T. Sado, *J. Antibiot.*, 27 (1974) 66.
12 T. Saesmaa and J. Halmekoski, *Acta Pharm. Fenn.* 97 (1988) 59.
13 H. M. Rauen, *Biochemisches Taschenbuch*, II Teil, 96, Springer, Berlin, 1964.
14 F. Nachtmann and K. Gstrein, *J. Chromatogr.*, 236 (1982) 461.

Author Index

Errata

J. Chromatogr., 452 (1988) 5–16

Page 6, 11th line from the bottom, "ref. 4" should read "ref. 3", and 9th line from the bottom, "ref. 5" should read "ref. 4".

J. Chromatogr., 457 (1988) 442–445

p. 442, line 6, "and spectrophotometric[7]" should be deleted.
p. 442, line 7, ref. 8 should be ref. 7.
p. 442, line 8, ref. 9 should be ref. 8.
p. 443, first line of the *Preparation of Peumus boldus samples* section, "(1 ml)" should read "(0.2 ml)" and "2 ml" should be deleted.
p. 443, third line of the same section, after "buffer" should be added "–acetonitrile (8:2)".
p. 443, fourth line of the *HPLC* section, "(87:15:0.2, v/v)" should read "(15:87:0.2, v/v)".
p. 444, line 8, ref. 10 should be ref. 9.
p. 445, References section, page number of ref. 4 should be 93 instead of 108; ref. 6 should read *"Farmacopea Italiana, IX*, Vol. II, 1985, p. 268"; ref. 7 should be deleted; refs. 8, 9 and 10 should be refs. 7, 8 and 9, respectively.

PUBLICATION SCHEDULE FOR 1989

Journal of Chromatography and Journal of Chromatography, Biomedical Applications

MONTH	J	F	M	
Journal of Chromatography	461 462 463/1	463/2 464/1	The publication schedule for further issues will be published later	
Bibliography Section		486/1		
Biomedical Applications	487/1	487/2	488/1 488/2	

INFORMATION FOR AUTHORS

(Detailed *Instructions to Authors* were published in Vol. 445, pp. 453–456. A free reprint can be obtained by application to the publisher, Elsevier Science Publishers B.V., P.O. Box 330, 1000 AH Amsterdam, The Netherlands.)

Types of Contributions. The following types of papers are published in the *Journal of Chromatography* and the section on *Biomedical Applications*: Regular research papers (Full-length papers), Notes, Review articles and Letters to the Editor. Notes are usually descriptions of short investigations and reflect the same quality of research as Full-length papers, but should preferably not exceed six printed pages. Letters to the Editor can comment on (parts of) previously published articles, or they can report minor technical improvements of previously published procedures; they should preferably not exceed two printed pages. For review articles, see inside front cover under Submission of Papers.

Submission. Every paper must be accompanied by a letter from the senior author, stating that he is submitting the paper for publication in the *Journal of Chromatography*. Please do not send a letter signed by the director of the institute or the professor unless he is one of the authors.

Manuscripts. Manuscripts should be typed in double spacing on consecutively numbered pages of uniform size. The manuscript should be preceded by a sheet of manuscript paper carrying the title of the paper and the name and full postal address of the person to whom the proofs are to be sent. Authors of papers in French or German are requested to supply an English translation of the title of the paper. As a rule, papers should be divided into sections, headed by a caption (*e.g.*, Summary, Introduction, Experimental, Results, Discussion, etc.). All illustrations, photographs, tables, etc., should be on separate sheets.

Introduction. Every paper must have a concise introduction mentioning what has been done before on the topic described, and stating clearly what is new in the paper now submitted.

Summary. Full-length papers and Review articles should have a summary of 50–100 words which clearly and briefly indicates what is new, different and significant. In the case of French or German articles an additional summary in English, headed by an English translation of the title, should also be provided. (Notes and Letters to the Editor are published without a summary.)

Illustrations. The figures should be submitted in a form suitable for reproduction, drawn in Indian ink on drawing or tracing paper. Each illustration should have a legend, all the *legends* being typed (with double spacing) together on a *separate sheet*. If structures are given in the text, the original drawings should be supplied. Coloured illustrations are reproduced at the author's expense, the cost being determined by the number of pages and by the number of colours needed. The written permission of the author and publisher must be obtained for the use of any figure already published. Its source must be indicated in the legend.

References. References should be numbered in the order in which they are cited in the text, and listed in numerical sequence on a separate sheet at the end of the article. Please check a recent issue for the layout of the reference list. Abbreviations for the titles of journals should follow the system used by *Chemical Abstracts*. Articles not yet published should be given as "in press" (journal should be specified), "submitted for publication" (journal should be specified), "in preparation" or "personal communication".

Dispatch. Before sending the manuscript to the Editor please check that the envelope contains three copies of the paper complete with references, legends and figures. One of the sets of figures must be the originals suitable for direct reproduction. Please also ensure that permission to publish has been obtained from your institute.

Proofs. One set of proofs will be sent to the author to be carefully checked for printer's errors. Corrections must be restricted to instances in which the proof is at variance with the manuscript. "Extra corrections" will be inserted at the author's expense.

Reprints. Fifty reprints of Full-length papers, Notes and Letters to the Editor will be supplied free of charge. Additional reprints can be ordered by the authors. An order form containing price quotations will be sent to the authors together with the proofs of their article.

Advertisements. Advertisement rates are available from the publisher on request. The Editors of the journal accept no responsibility for the contents of the advertisements.

For Superior Chiral Separation

CHIRALCEL, CHIRALPAK and CROWNPAK are now available from DAICEL and include 15types of HPLC columns which provide superior resolution of racemic compounds.

Drugs directly resolved on our DAICEL columns are given as follows;

SUBSTANCE	α	column	SUBSTANCE	α	column	SUBSTANCE	α	column
Alprenolol	3.87	OD	Gauifenesin	2.40	OD	Oxapadol	complete resolution	CA-1
Amphetamine	1.2	CR	Hexobarbital	1.7	CA-1			
Atenoloi	1.58	OD	Homatropine	3.13	OD	Oxazepan	4.36	OC
Atropine	1.62	OD	Hydroxyzine	1.17	OD	Oxazolam	1.67	OF
Baclofen	1.39	CR	Indapamide	1.58	OJ	Oxprenolol	6.03	OD
Carbinoxamine	1.39	OD	Ketamine	complete resolution	CA-1	Perisoxal	1.33	OF
Carteolol	1.86	OD					1.27	OD
Chlophedianol	2.82	OJ	Ketoprofen	1.46	OJ	Pindolol	5.07	OD
Chlormezanone	1.47	OJ	Mephobarbital	5.9	OJ	Piprozolin	1.7	CA-1
Cyclopentolate	2.47	OJ		2.3	CA-1	Praziquantal	complete resolution	CA-1
Diltiazem	1.46	OD	Methaqualone	2.8	CA-1			
	2.36	OF		7.3	OJ	Propranolol	2.29	OD
	1.75	OG	Methsuximide	2.68	OJ	Rolipram	complete resolution	CA-1
Disopyramide	2.46	OF	Metoprolol	complete resolution	OD			
Ethiazide	1.54	OF				Sulconazole	1.68	OJ
Ethotoin	1.40	OJ	Mianserin	1.75	OJ	Suprofen	1.6	OJ
Fenoprofen	1.35	OJ	Nilvadipine	complete resolution	OT	Trimebutine	1.81	OJ
Glutethimide	2.48	OJ				Warfarin	1.96	OC

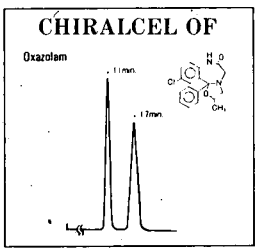

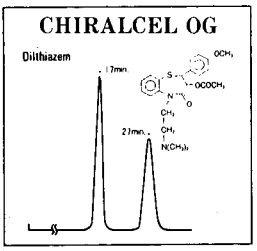

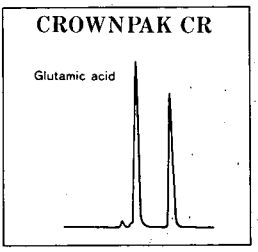

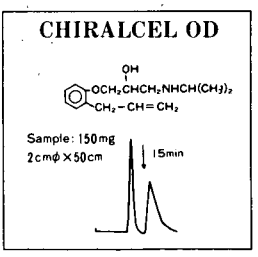

In addition to the drugs listed above, our chiral columns permit resolution also of the following: FMOC amino acids and Carboxylic acids, and Pesticides, for example Isofenfos, EPN and Acephate, and Synthetic intermediate 4-hydroxy cyclophentenone etc, Many other compounds besides these can be readily resolved.

▷ *Separation Service*

- A pure enantiomer separation in the amount of 100g~10kg is now available.
- Please contact us for additional information regarding the manner of use and application of our chiral columns and how to procure our separation service.

For more information about our Chiral Separation Service and Columns, please contact us!

DAICEL CHEMICAL INDUSTRIES, LTD.

Tokyo
8-1, Kasumigaseki 3-chome,
Chiyoda-ku, Tokyo 100, Japan
Phone: 03(507)3151, 3189
Telex: 222-4632 DAICEL J
FAX: 03(507)3193

New York
Pan-Am Bldg. 200 Park Avenue,
New York, N.Y. 10166-0130, U.S.A.
Phone: (212)878-6765, 6766
Telex: (23)236154 DCC UR
FAX: (212)983-8190

DAICEL (U.S.A.) INC.
611 west 6th Street, Room 2152
Los Angeles California 90017, U.S.A.
Phone: (213)629-3656
Telex: 215515 DCIL UR
FAX: (213)629-2109

DAICEL (EUROPA) GmbH
Königsallee 92a
4000 Düsseldorf 1, F.R. Germany
Phone: (0211) 134158
Telex: (41)8588042 DCEL D
FAX: (0211)879-8329